ARTD1 and Poly-ADP-Ribosylation Enhance PPARγ-Dependent Adipogenesis *In Vitro* and *In Vivo*

Dissertation

zur

Erlangung der naturwissenschaftlichen Doktorwürde

(Dr. sc. nat.)

vorgelegt der

Mathematisch-naturwissenschaftlichen Fakultät

der

Universität Zürich

von

Mareike Katharina Gwendolyn Lehmann

aus

Deutschland

Promotionskomitee

Prof. Dr. Dr. Michael O. Hottiger

(Vorsitz und Leitung der Dissertation)

Prof. Dr. Alex Hajnal

Prof. Dr. Christoph Handschin

Prof. Dr. Christian Wolfrum

Zürich 2014

Summary

The ADP-ribosyltransferase Diphtheria toxin like (ARTD; formerly called PARP) enzyme family consists of 18 members that can either mono- or poly-ADP-ribosylate acceptor proteins. ADP-ribosyltransferase D-type 1 (ARTD1, PARP1) synthesizes poly-ADP-ribose (PAR) and is a chromatin-associated enzyme that regulates chromatin compaction and transcription during various cellular processes. Adipocyte differentiation goes along with a dynamic modulation of the chromatin landscape and fundamental changes in the transcriptome, which are mainly controlled by the transcription factor PPARγ. It was the aim of this thesis to study the role of ARTD1 and PAR formation during adipogenesis, with a focus on PPARγ-dependent gene expression, and to elucidate the molecular mechanism by which ARTD1 regulates transcription in this context.

The results presented in this thesis reveal an involvement of ARTD1 and its enzymatic activity during the late phase of adipocyte differentiation. Knockdown of ARTD1 as well as inhibition of PAR formation hampered adipogenesis. Moreover, adipose stem cells derived from ARTD1$^{-/-}$ mice failed to differentiate into adipocytes. Mechanistic studies provided evidence that ARTD1 and PPARγ are recruited to the promoters of PPARγ-dependent genes. PPARγ ligand was able to enhance the interaction of PPARγ with ARTD1 in cells as well as *in vitro*. Topoisomerase IIβ site-specific double strand-DNA breaks induced PAR formation, which was important for the decrease of the NCoR co-repressor and for the increased p300 co-activator recruitment to PPARγ target genes. This co-factor exchange was prevented by PARP inhibitors, but an excess of PPARγ ligand could overcome this inhibition. In addition, mice treated with PARP inhibitor showed significantly reduced bodyweight, smaller adipocytes and fat depots on high fat diet (HFD). Interestingly, ARTD1$^{-/-}$ mice showed a similar phenotype as the inhibitor-treated mice, but additionally accumulated triglycerides in the liver.

Together, the results presented in this thesis define the role of ARTD1 for the maintenance of PPARγ2-dependent gene expression in the late phase of adipocyte differentiation and in adipocyte function.

Zusammenfassung

Die intrazellulären ADP-Ribosyltransferasen mit Ähnlichkeit zum Diphtheria Toxin (ARTDs) bilden eine Enzymfamilie, welche aus 18 Mitgliedern besteht, die Akzeptorproteine entweder mono- oder poly-ADP-ribosylieren können. ARTD1 ist ein Chromatin-assoziiertes Enzym, welches poly-ADP-Ribose (PAR) synthetisiert und dadurch die Transkription von Genen reguliert, welche in vielen unterschiedlichen zellulären Prozessen beteiligt sind. Die Differenzierung von Adipozyten wird von massiven Veränderung auf Chromatin- und Transkriptionsebene begleitet, die hauptsächlich durch den Transkriptionsfaktor PPARγ kontrolliert werden. Es war das Ziel dieser Arbeit, die Rolle von ARTD1 und PAR während der Adipozytendifferenzierung, insbesondere den Effekt auf die PPARγ-abhängige Genexpression, zu charakterisieren und den molekularen Mechanismus zu entschlüsseln, der dieser transkriptionellen Regulation durch ARTD1 zugrunde liegt.

Die hier präsentierten Ergebnisse beschreiben den Einfluss von ARTD1 und seiner enzymatischen Aktivität auf die Adipozytendifferenzierung. Die Reduktion der ARTD1 Proteinmenge oder die Inhibierung der PAR Bildung hemmten die Differenzierung. Stammzellen, die aus dem Fettgewebe von ARTD1$^{-/-}$ Mäusen gewonnen wurden, konnten nicht mehr zu Adipozyten differenzieren. Mechanistische Analysen zeigten eine gemeinsame Bindung von ARTD1 und PPARγ an die Promotoren PPARγ-abhängiger Gene. PPARγ Liganden verstärkten die Interaktion von PPARγ mit ARTD1 in Zellen sowie *in vitro*. Topoisomerase IIβ generierte Doppelstrangbrüche induzierten PAR Bildung, welche für die Reduktion des Corepressors NCoR und die Zunahme des Coaktivators p300 an PPARγ-abhängigen Genen wichtig war. Dieser Cofaktor-Austausch wurde durch PARP Inhibitoren verhindert, was aber durch einen Überschuss an PPARγ Liganden kompensiert werden konnte. Zusätzlich zeigten wildtyp Mäuse auf Hochfettdiät unter PARP Inhibitor Behandlung reduziertes Gewicht, kleinere Fettpolster und kleinere Adipozyten. Intereressanterweise zeigten ARTD1$^{-/-}$ Mäuse unter gleichen Bedingungen einen ähnlichen Effekt, hatten aber zusätzliche Fetteinlagerungen in der Leber.

Zusammengefasst zeigen unsere Ergebnisse eine neue Funktion von ARTD1 in der Aufrechterhaltung der PPARγ-abhängigen Genexpression und Adipozytenfunktion.

Table of Contents

Abbreviations

aa	Amino acid
ADP	Adenosine diphosphate
AID	Activation-induced deaminase
ARH3	ADP-ribosyl hydrolase 3
ART	ADP-ribosyltransferase
ARTD	ADP-ribosyltransferase diphtheria toxin-like
ARTC	ADP-ribosyltransferase cholera toxin-like
ATGL	Adipose triglyceride lipase
ATM	Ataxia telangiectasia mutated
ATP	Adenosine triphosphate
BAT	Brown adipose tissue
BER	Base excision repair
bp	Base pair
BRCT	BRCA1 carboxy-terminal domain
CBP	CREB-binding protein
cAMP	Cyclic adenosine monophosphate
Cat	Catalytic
Cdk	Cyclin-dependent kinase
C/EBP	CCAAT/enhancer binding protein
ChIP	Chromatin immunoprecipitation
CLOCK	Circadian locomotor *output* cycles kaput
CLS	Centriole localization signal
CRBP	cold-inducible RNA-binding protein
DAPI	4',6-diamidino-2-phenylindole
DBD	DNA binding domain
Dbp	AlbuminD-element binding protein
DDR	DNA damage response
DNA	Deoxyribonucleic acid
DNMT	DNA methyltransferase
DSB	Double-strand break

dsDNA	Double-stranded DNA
FCS	Fetal calf serum
Flp	Flippase
Frt	Flp-recombinase target
GTT	Glucose tolerance test
GTP	Guanosintriphosphat
γH2AX	gamma-histone 2A variant X (phosphorylated)
HDAC	Histone deacteylase
HIF	Hypoxia-inducible factor
HMGB	High mobility-group box
HSL	Hormone sensitive lipase
H_2O_2	Hydrogen peroxide
IBMX	3-Isobutyl-1-methylxanthin
IL6	Interleukin 6
iNOS	Inducible nitric oxide synthase
IR	Ionizing radiation
KLF	Krüppel-like factor
LBD	Ligand binding domain
LPS	Lipopolysaccharide
MEF	Mouse embryonic fibroblasts
MPTP	1-Methyl-4-phenyl-1,2,3,6-tetrahydropyridin
NAD	Nicotinamide adenine dinucleotide
NAFLD	Non alcoholic fatty liver disease
NAM	Nicotinamide
NCOR	Nuclear Receptor Corepressor
NF-κB	Nuclear factor of kappa light polypeptide gene enhancer in B-cells 1
NLS	Nuclear localization signal
PAR	Poly-ADP-ribose
PARG	Poly-(ADP-ribose)-glycohydrolase
PARP	Poly-(ADP-ribose)-polymerase
PARylation	Poly-ADP-ribosylation
PBS	Phosphate buffered saline
PCNA	Proliferating cell nuclear antigen

Pol II	Polymerase II
PPAR	Peroxisome proliferator-activated receptor
PPRE	PPARγ response elements
PRC	Polycomb repressive complex
PTM	Post-translational modification
rDNA	Ribosomal DNA
RNA	Ribonucleic acid
rRNA	Ribosomal RNA
RXR	Retinoid-X receptor
SREBP	sterol regulatory element-binding protein
SMRT	silencing mediator of retinoic acid and thyroid hormone receptor
SSB	Single-strand break
SUMO	Small ubiquitin-like modifier
T2D	Type II diabetes
TDG	Thymine DNA glycosylases
TdT	Terminal deoxynucleotidyl transferase
Tip60	HIV-Tat-Interactive protein 60
TNFα	Tumor necrosis factor α
TopoII	Topoisomerase II
UCP-1	Uncoupling protein 1
UTR	Untranslated region
WAT	White adipose tissue
XRCC1/4	X-ray repair cross-complementing protein 1/4
ZF	Zinc finger
5mc	5-methyl-cytosine
5hmc	5-hydroxymethyl-cytosine

1 Introduction

Intracellular signaling pathways control the processes of differentiation and cell determination. Often these pathways are induced by external or internal signals and are tightly controlled within the cell by proteins regulating different cascades. These proteins are often enzymes modifying targets in a precise manner by posttranslational modifications (PTMs). PTMs include acetylation, phosphorylation, ubiquitylation, sumoylation, methylation or ADP-ribosylation of target proteins [1].

1.1 ADP-ribosylation

An emerging PTM is the enzymatic attachment of ADP-ribose to target proteins by members of the ADP-ribosyltransferase (ART) family that use NAD^+ as substrate [2]. Protein ADP-ribosylation can affect the enzymatic activity of the modified protein or the interaction with DNA or other proteins. Consequently, ADP-ribosylation is implicated in a variety of processes, including genomic stability, transcriptional control, energy metabolism, and cell death [2-6]. The process of ADP-ribosylation encompasses the attachment of one or more ADP-ribose units to proteins, resulting in the formation of poly- or mono-ADP-ribosylated proteins.

1.1.1 Mono-ADP-ribosylation

Mono-ADP-ribosylation was first discovered as a pathogenic mechanism used by bacterial toxins such as *cholera, pertussis, diphtheria* or *clostridia* toxins [7]. Once they enter the host cell, the ADP-ribsoylation activity of these toxins causes various pathological changes by modifying host proteins such as tubulin, actin, alpha and beta subunits of GTP-binding proteins, and histones [8-10]. ADP-ribosylation exerts its pathological function mainly by inhibiting the function of the host proteins. Mono-ADP-ribosylation is however also found in bacteriophages or in eukaryotic cells. Intracellular mono-ADP-ribosylation is implicated in the regulation of cellular processes such as signal transduction, gene expression, proliferation, inflammation and differentiation [3,7,11-14].

1.1.2 Poly-ADP-ribosylation

Poly-ADP-ribosylation (PARylation) was first described in 1963 in the laboratory of P. Mandel [15]. The modification occurs most likely on lysines, arginines and glutamates, but other acceptor sites have been discussed as well [2,16-19]. Within the polymer of ADP-ribose (PAR), the ADP-ribose units are linked to each other via glycosidic ribose-ribose bonds. The resulting polymer can be linear or branched and comprise the considerable length of up to 400 moieties when generated *in vitro* [2,16,20]. The PARylation reaction can be divided into three different steps (Fig. 1) [2,21]. After the cleavage of NAD^+, the first ADP-ribose moiety is transferred during the initiation step to an acceptor amino acid. Subsequently, this mono-ADP-ribose can be elongated to oligo- and ultimately poly-ADP-ribose. Finally, the polymers can be branched in an irregular manner with one branching point every 20-50 units of linear ADP-ribose [2,22,23].

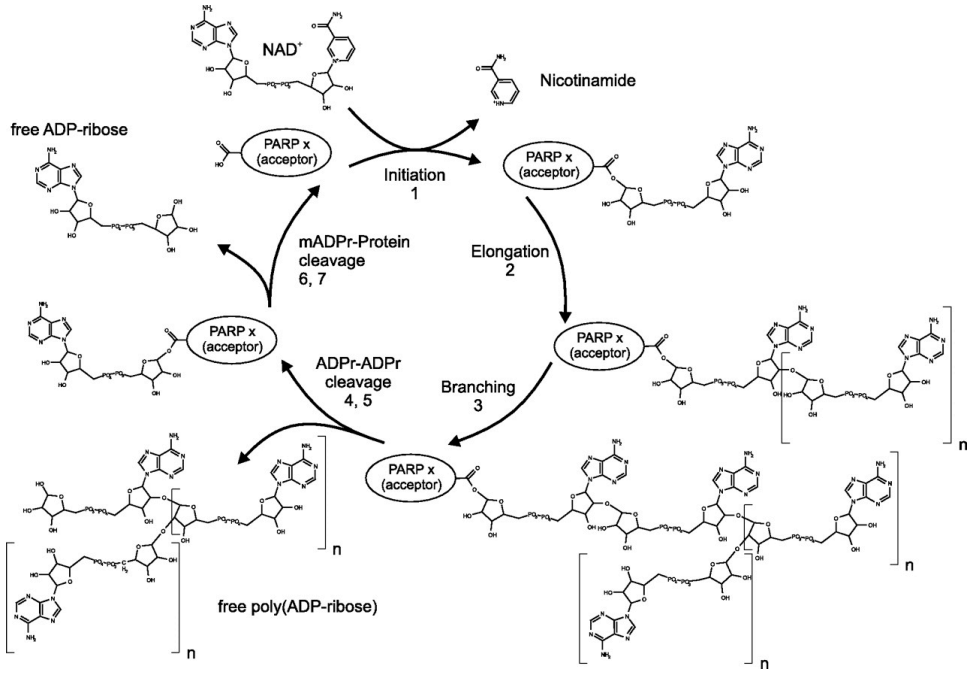

Figure 1: PAR metabolism

Different steps in the formation and catabolism of poly-ADP-ribose are shown. Modified from Hassa and Hottiger [2].

The functional consequences of PARylation on different target proteins are often unknown and depend on the nature of the modified protein. The methods for analyzing the cellular APD-ribosylome are up to now very limited due to lack of good antibodies especially against mono-ADP-ribose. In addition, the modification seems to be unstable during extraction which makes it extremely difficult to detect it by mass spectrometry. However, recently two publications using different approaches

identified several hundred modified or PAR interacting proteins after treatment of cells with genotoxic compounds [24-26]. However, most of these studies are biased, since they are performed in absence or knockdown of PARG (see chapter 1.5) and it is thus of great importance to establish new methods to analyse the ADP-ribosylome. Among the identified proteins are a large number of chromatin-associated proteins such as topoisomerases, histones, PCNA and ARTs of the diphtheria toxin-like (ARTD) subgroup [27-32]. The endogenous cellular PAR levels are usually very low, but upon mitogenic or genotoxic stress these levels can increase up to 50-100 fold within only a few minutes, which is accompanied by a reduction of the cellular NAD^+ pool to 10-20% of the normal levels [2]. *In vivo,* the majority of PAR formed upon genotoxic stress is rapidly degraded with a half-life of less than 40s [2,33,34]. This is in contrast to the much longer half-life (7 hours) of the PAR that is supposed to be continuously formed in the absence of genotoxic stress [33,34]. The fast degradation of PAR is mediated by the cellular activities of enzymes capable of hydrolyzing the protein-ADP-ribose or the ADP-ribose-ADP-ribose bonds. Among these, poly-ADP-ribose-glycohydrolase (PARG) or ADP-ribosylhydrolase 3 (ARH3) are the most important members [35-38]. Earlier studies suggest that PARG is unable to remove the first, protein-bound ADP-ribose unit [39]. Recently, we and others reported that some macrodomains are able to hydrolyze mono-ADP-ribose modifications [13,40,41]. This supports the view that there are ADP-ribose writers and erasers and that PARylation is indeed a highly dynamic and reversible PTM.

1.2 The ARTD family

The enzymes responsible for ADP-ribosylation are the ADP-ribosyltransferases (ARTs). Previously, these enzymes were called poly-ADP-ribosylpolymerases (PARPs). To acknowledge the fact that not all members possess ADP-ribosylation activity and that ADP-ribosylation does not constitute a template driven polymerization reaction, these enzymes have been renamed [11]. The ARTs are further divided into ARTDs (ARTs of the diphtheria toxin family) and ARTCs (ARTs of the cholera toxin family). ARTCs are ecto-enzymes or secreted proteins, whereas ARTDs are all localized within the cell [11]. ARTD1 (PARP1) is estimated to contribute around 85% of the PAR formation [42,43] and for many years it was believed to be the only ARTD capable of synthesizing PAR. However, residual PAR formation was observed

in ARTD1$^{-/-}$ cells, which led to the discovery of other ARTD family members. Among these members, ARTD2 is responsible for the majority of the residual PAR formation and shows high sequence homology to the catalytic domain of ARTD1 [44,45]. To date, the ARTD family contains 18 members in human. ARTD 1-6 share a catalytic domain with a conserved glutamic acid (i.e. E988 of ARTD1). The other ARTD members share a characteristic homology to ARTD1 but lack the conserved E988 residue of ARTD1, which is implicated in chain branching and elongation. It was therefore suggested that these members only possess mono-ADP-ribosylation activity.

1.3 ARTD1

ARTD1 is the founding member of the ARTD family. Human ARTD1 has a molecular weight of 113 kDa, is a chromatin-associated protein and consists of three main domains with distinct functions [2] (Fig. 2):

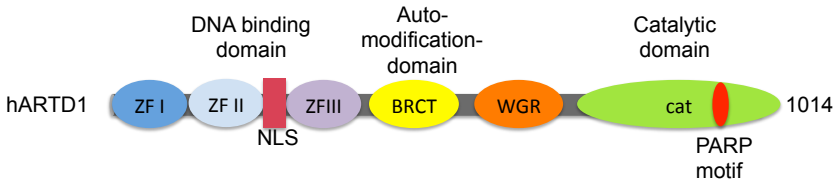

Figure 2: Domain structure of ARTD1

Different domains of ARTD1 are shown. ZFI-III= Zincfinger I-III, NLS=Nuclear localization signal, BRCT=BRCA1 carboxy-terminal domain, cat=catalytic domain WGR=domain containing central W/G/R motif.

The N-terminal DNA binding domain, the auto-modification domain in the middle and the C-terminal catalytic domain. The two structurally and functionally unique N-terminal Zinc fingers I and II (ZFI and ZFII) convey the DNA binding activity of ARTD1. Recently, a third zinc-binding motif (ZFIII), which is structurally completely unrelated to ZF I and II, was discovered [46,47]. ZFIII is not required for DNA binding, but rather for the ADP-ribosyltransferase activity of ARTD1, as well as for its ability to compact chromatin [46-48]. The auto-modification domain contains a BRCT domain, which is supposed to mediate protein-protein interactions. The auto-modification domain also contains most of the amino acids that are auto-ADP-ribosylated. The WGR domain is named after the most conserved central motif (W/G/R) of the domain. This domain was suggested to be involved in DNA binding, but no detailed

analysis has been performed yet and its function remains largely unknown [2]. The catalytic domain is located at the C-terminus of the protein and conveys NAD^+ binding and hydrolysis. It contains the "PARP-signature" that comprises the amino acids required for initiation, elongation and branching of PAR. Several studies indicate that ARTD1 forms a dimer and is catalytically active in a dimer form [49,50]. Therefore, dimerization of ARTD1 seems to be an important step in DNA-dependent activation [18,51]. Several studies have provided evidence that ARTD1 can bind to and its activity is induced by single and double stranded DNA lesions as well as various physiologically relevant structural discontinuities in DNA duplexes in the absence of DNA strand breaks [2]. These include DNA hairpin and cruciform structures [52-54]. To address ARTD1 functions *in vivo,* $ARTD1^{-/-}$ mice were established in three different laboratories by targeting different exons [55-59]. Surprisingly, ARTD1 knockout mice are fertile and healthy. However, they show increased sensitivity to ionizing radiation and alkylating agents [55,57-60]. On the other hand, these mice are protected from tissue injury in various oxidative stress-related disease models including stroke, Lipopolysaccharide (LPS) induced septic shock, streptozotocin induced diabetes, arthritis, colitis and 1-Methyl-4-phenyl-1,2,3,6-tetrahydropyridin (MPTP)-induced parkinsonism [3,55,61]. Interestingly, knockout of ARTD2 also produces only a mild phenotype, while the double knockout of ARTD1 and ARTD2 is embryonically lethal [62].

ARTD1 plays a role in various nuclear processes such as the maintenance of genomic integrity, regulation of chromatin structure and transcription, cell death pathways and the establishment of DNA methylation which will be subsequently discussed [2,3,16,17] (Fig.3).

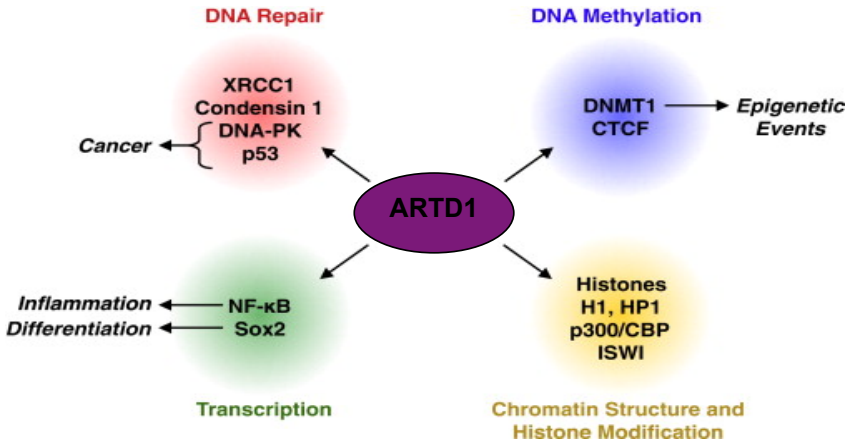

Figure 3. ARTD1 interacts with and modifies different nuclear proteins

Interaction with ARTD1 or modification influence different nuclear processes Modified from Krishnakumar and colleagues [17]

1.3.1 ARTD1 in genomic integrity

The finding that ARTD1 can recognize and bind to DNA lesions led to the idea that ARTD1 can act as a DNA nick sensor. ARTD1 has been described to play a role in different DNA repair pathways including base excision repair (BER), single-strand break (SSB), repair and double strand break (DSB) repair [63,64]. Cellular ARTD1 is activated by genotoxic stress including oxidative stress (e.g. H_2O_2), ionizing radiation, and alkylating reagents [63-68] and is readily recruited to sites of microlaser-induced damage [69,70]. Furthermore, many proteins involved in DNA damage repair, including XRCCI, DNA polymerase β or PCNA, interact with ARTD1 and are in some cases direct targets of ARTD1 [71-74]. Ample data suggest that ARTD1 is involved in DNA damage signaling and genomic integrity [6]. However, at the molecular level the function of ARTD1 in these processes is still under debate. ARTD1$^{-/-}$ mice show no tumor formation under physiological conditions and cells lacking ARTD1 have a normal capacity to repair DNA lesions [56,60]. Thus, the exact contribution of ARTD1 in these processes remains to be elucidated.

1.3.2 ARTD in the regulation of chromatin structure

ARTD1 was also described to act as a structural component of chromatin [2]. Decades ago, it has been described that PARylated chromatin is more relaxed than unmodified chromatin [75,76]. This led to the assumption that ARTD1 acts as a compactor of chromatin, which is released upon auto-modification. It was also proposed, that

ARTD1 can dissociate nucleosomes/histones from the DNA to render it more accessible for the transcription or repair machinery [77,78]. Although histones can be ADP-ribosylated, only a small fraction (1%) is modified *in vivo* [79,80]. Histone H1 is the main ADP-ribose acceptor in native chromatin, whereas in H1-depleted chromatin (open status), H2B is the preferential target of ARTD1 [81]. ARTD1 and H1 bind mutually exclusive to promoters of some genes, possibly by competing for binding to nucleosomes or by modification of H1 by ARTD1 [17]. In addition, ARTD1 activity increases the amount of chromatin-bound HMGB1, a chromatin structural protein that enhances transcription in certain chromatin context [4,82]. Another level of chromatin regulation is mediated by the association of the insulator protein CTCF with PAR, which may regulate even higher order chromatin structures [83,84].

1.3.3 ARTD1 in the control of transcription

A recent study has shown that ARTD1 binds to the promoters of most actively transcribed genes [85]. This binding correlates with the binding of polymerase II (PolII) and the presence of trimethylated lysine 4 on H3 (H3K4me3). This suggests a role of ARTD1 in transcriptional control. Indeed, ARTD1 has been described to influence transcription under various conditions. ARTD1 interacts with and modifies various transcription factors and thereby co-regulates their function [2,3]. During NF-κB-dependent gene expression, ARTD1 can synergistically co-activate transcription by physically interacting with the Mediator complex, p300/CBP and with the p50 and p65 subunits of NF-κB [86-90]. ARTD1 has also been described as a negative co-factor for SMADs [91] and to interact with histone modifying enzymes such as histone deacetylases (HDACs) 1-3 [87]. This led to the hypothesis that ARTD1 can function as a promoter-specific exchange factor that promotes the release of inhibitory cofactors and subsequently the recruitment of stimulatory factors [87,92,93]. Retinoic acid signaling, for example, has been described to depend on ARTD1 as well [93]. In this model, ARTD1, but not its catalytic activity, is required to switch Mediator to its transcriptionally active form and to activate gene transcription. However, there are also scenarios where ARTD1 catalytic activity is important for the induction of such a co-factor switch [82,92,94]. This has been described for neuronal differentiation, where ARTD1 is a component of the co-repressor complex, but upon induction of differentiation it is activated and in turn required for co-activator recruitment and de-

repression [92]. In line with this, Ju and coworkers described a role of ARTD1 in estrogen-dependent gene expression [82,94]. Estrogen-induced Topoisomerase II (TopoII) β-dependent dsDNA break formation on the promoter leads to the recruitment of a co-activator complex, and the release of a co-repressor complex. ARTD1 activity leads to the exchange of H1 for HMGB1 and subsequently transcriptional activation of estrogen-dependent target genes.

1.3.4 ARTD1 and DNA methylation

DNA methylation is established by *de novo* methyltransferases DNMT3a and DNMT3b, while after DNA replication, DNMT1 maintains the methylation status of the cells [95-97]. ARTD1 was described to influence DNA methylation through different mechanisms [98-104]. On one hand, ARTD1 co-regulates the activity and expression of DNA methyltransferase 1 (DNMT1) by binding to its promoter and protecting the DNA from methylation in a PAR-dependent manner [98,99,102]. On the other hand, the DNMT1 protein itself forms a complex with PAR, which inhibits DNMT1 activity [103]. A functional crosstalk of ARTD1 and DNMT3 has not been described yet.

1.4 ARTD3

ARTD3 is the smallest and least studied of the "bona fide" ARTD enzymes. It exists in two splice variants containing 540 or 533 amino acids, respectively [105]. The longer isoform contains the centriole localization signal that targets it to the centrosomes. ARTD3 is thus a much smaller protein than ARTD1 and its domain structure resembles rather the structure of ARTD2. It contains a small DBD of only 54 residues and a targeting motif that can localize the longer isoform to the centrosome whereas the shorter isoform is rather located in the cytoplasm (Fig. 4) [105,106].

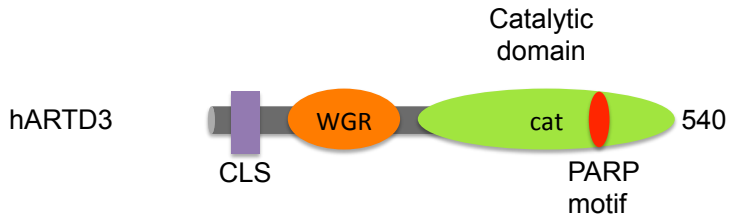

Figure 4: Domain structure of ARTD3

Different domains of ARTD3 are shown. CLS= Centriole localization signal, cat=catalytic domain.

Although the catalytic domain of ARTD3 shows sequence similarity to ARTD1 and ARTD2 and also contains the critical glutamic acid residue (i.e. E988 in ARTD1), PARylation activity could not be demonstrated. Some studies detected short ADP-ribose oligomer formation, while other reported only mono-ADP-ribosylation activity [107,108]. Both reports agreed, that in comparison to ARTD1 and ARTD2 the *in vitro* activity of ARTD3 is significantly lower [18]. In addition, ARTD1 is strongly stimulated by DNA, while the regulation of ARTD3 by DNA is controversial. While some groups state that ARTD3 is not activated by DNA, there are reports claiming the contrary as well [18,107,108]. Unlike ARTD1 and ARTD2, ARTD3 shows a tissue specific distribution and the highest expression levels were recorded in lung, liver, spleen, kidney, ovary and heart [109]. Particularly low ARTD3 expression was observed in thymus, small intestine and colon tissue. While ARTD2 partially compensates for ARTD1 deficiency, ARTD3 cannot compensate for the absence of ARTD1 or ARTD2 [62,110,111]. These results suggest that ARTD3 has a function that is distinct from ARTD1 and ARTD2, despite significant structural similarities. Endogenous ARTD3 shows a widespread nuclear distribution and appears in small, but also larger foci [112]. Experiments with overexpressed ARTD3 describe a change in its cellular localization during cell cycle. ARTD3 was enriched in the centrosomal and nuclear region during the G0/G1 phase and detected in the cytoplasm during S-phase [113]. Knockdown of ARTD3 neither affected cell viability nor induced any obvious morphological phenotype. Stable complexes between ARTD3 and ARTD1 at the centromeres have been implicated in DNA damage surveillance at the mitotic fidelity checkpoint [2,106]. Knockdown of ARTD3 significantly delayed the removal of ionizing radiation (IR)-induced γH2AX foci and led to an increase in the formation of IR-induced DSBs [107,114]. This effect is possibly mediated by ATM-dependent phosphorylation of APLF at Ser^{116} that is important for association of APLF with chromatin and is dependent on ARTD3 [115]. In addition, ARTD3 was described to influence microtubule organization and to stabilize and promote telomere integrity and to thereby interfere with the progression through mitosis, which is impaired in cells lacking ARTD3 [107,114]. ARTD3-mediated PAR formation was proposed to regulate PRC2 and PRC3 mediated silencing and it was shown to interact with DNA-PK and Ku70/80 [112]. In addition, ARTD3 plays a role in ectodermal specification and neural crest development in zebrafish [111]. ARTD3 was shown to activate ARTD1 in a

DNA-independent manner [108]. However, the underlying mechanism for this remains elusive and further experiments are needed to confirm this hypothesis. In summary, ARTD3 seems to be important for physiological processes, but a detailed description of its biochemical properties and cellular functions is still missing.

1.5 Poly-ADP-ribose glycohydrolase (PARG)

PARG is the main PAR-degrading enzyme that shows both endo- and exo-glycosidase activity [39,116]. The enzyme has been first described in 1986 as a 59 kDa protein, but since then differential splicing resulting in PARG proteins that vary considerably in size and cellular localization have been discovered [116-123]. The mammalian PARG gene encodes at least four isoforms: The full length PARG-110 isoform is found in the nucleus because of a nuclear localization signal encoded in exon 1. This isoform shows a lower abundance than the three cytosolic forms PARG-102, -99 and -59, which arise through alternative splicing and differential translation start sites [38,124,125]. Transgenic mice carrying a PARG that lacks exon 2 and 3 (thereby inactivating PARG-110/102 and 99 and thus abrogating the presence of nuclear PARG) are viable and phenotypically normal, but show an increased sensitivity to alkylating agents and ionizing radiation [126]. However, mice carrying a deletion of exons 3 and 4, which leads to a depletion of all PARG isoforms, display embryonic lethality, suggesting an important role for PARG-59 in embryonic development [127]. PARG activity was described to generate a large amount of free PAR that can function as signal transduction molecules [16]. But recent reports suggest that PARG mainly acts as exo-glycohydrolase and is unable to remove the initial protein-bound ADP-ribose unit [39]. To remove mono-ADP-ribose modifications and to completely reverse ADP-ribosylation, a second enzyme, an ADP-ribosyllyase, is required [128-130]. Comparable to ARTD1, PARG has been implicated in pathophysiological conditions such as shock, reperfusion and ischemia [131]. The importance of PAR catabolic activities for cell survival and homeostasis is underlined by experiments in yeast, which does not have any ARTDs or PARG [130,132,133]. The detrimental effect of an over-abundance of PAR is illustrated by the observation that the overexpression of human ARTD1 cDNA in yeast is toxic unless PARG cDNA is co-expressed or PARP inhibitors are included in the experiments. This suggests that the anabolism and catabolism of PAR are essential for the cell's function and required for cell survival.

1.6 Adipose tissue

At the beginning of the 20th century, adipose tissue was regarded as a depot with only one function, namely the storage and release of lipids [134,135]. However, already in the middle of the 20th century, the view of adipose tissue changed drastically [136]. It was acknowledged already then that the adipose tissue is an active tissue that can influence whole body homeostasis. Today, we know that adipose tissue is a complex, organ-like, multifunctional compartment [137]. Pioneering studies in the Spiegelman laboratory in the 80s, the discovery of leptin, and the finding that recombinant leptin can lower bodyweight in mice, proved that adipose tissue can secrete physiologically important molecules [138-145]. To date, adipose tissue is seen as a central player in the control of energy and whole-body lipid homeostasis. Deregulation of adipose tissue is associated with many pathophysiological changes such as obesity, type II diabetes, cancer and artherosclerosis [146-149]. Adipose tissue can be divided into two types with different morphology and function: White and brown adipose tissue (WAT and BAT, respectively)[135].

1.6.1 Brown adipose tissue

Brown adipose tissue consists of brown adipocytes, which are adipocytes that contain many small lipid droplets (multilocular) and feature a characteristic dark brownish color due to the large number of mitochondria [150,151]. The functionality of these brown adipocytes is to produce heat by a process called non-shivering thermogenesis [152]. The protein *uncoupling protein 1* (UCP-1) uncouples oxidative phosphorylation and thereby leads to increased substrate oxidation in the absence of ATP production, which in turn generates heat [150,153]. This helps the organism maintain a stable body temperature, especially in hibernators and newborns. To date, UCP-1 is the only marker known for BAT [150,154]. Whereas in human and mammals BAT dominates in newborns, these pure BAT depots disappear quickly after birth [155-158]. Nonetheless, there have been studies showing that individuals exposed to cold, or patients suffering from pheochromocytoma, show "nests" of BAT within their white adipose tissue [159,160]. Recent studies, however, provide strong evidence for the presence of metabolically active BAT in healthy adult humans [161-165]. Interestingly, the amount of BAT negatively correlates with obesity [162]. Mice possess a life-long classical BAT depot between their shoulder blades. In addition to this, brown adipocytes can be found in WAT depots in response to stimuli such as cold exposure, chronic β3-adrenergic receptor activators or PPARγ-agonists [166-168]. These brown adipocytes, however, differ from those cells arising early during development [167] (Fig. 5). Classical brown adipocytes and myocytes share a common precursor that expresses the myogenic lineage marker Myf5 [169,170]. Brown adipocytes that arise by "browning" of white adipose tissue are typically called beige or brite (brown in white) adipocytes [167], but their origin is controversial. Some groups suggest that beige adipocytes develop from Myf5 negative (Myf5-) precursors that reside in the WAT. It was also suggested that white adipocytes have the potential to interconvert to brown adipocytes by a process called transdifferentiation [168,171-173].

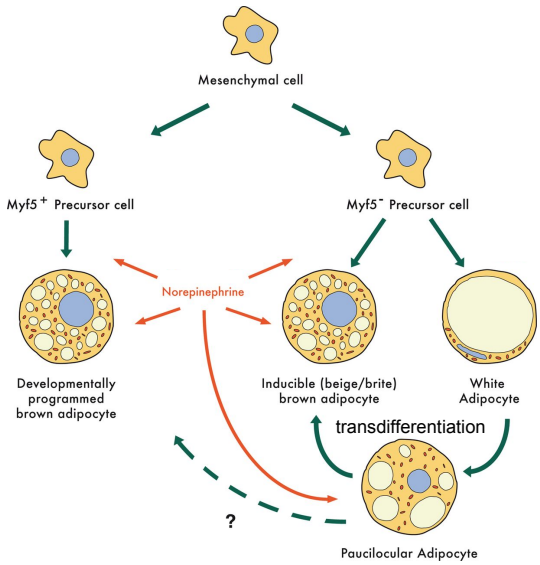

Figure 5: Schematic representation of the main pathways of adipocyte differentiation.
White adipocytes arise from Myf5- precursor cells, classical brown adipocytes from Myf5+ precursors. Inducible (beige/brite) adipocytes can arise through differentiation of a subset of Myf5- precursors or through transdifferentiation via an intermediate state (paucilocular adipocyte). Whether these cells can give rise to cells comparable to classical brown adipocytes is unknown. Norephinephrine can influence the formation of brown adipocytes. Modified from Giralt and Villaroya[167].

1.6.2 White adipose tissue

Although it forms later during development, in adult humans WAT dominates in size over BAT [167]. WAT is important for energy storage, adipokine secretion, as an insulator for the body, and as a mechanical buffer for the organs [135]. WAT is composed of different cell types, including fibroblasts, endothelial cells, immune cells, adipocyte precursors and mature, lipid-laden adipocytes. White adipocytes are unilocular, containing only one large lipid droplet. They differentiate from Myf5- precursor cells (Fig. 5). WAT secretes diverse adipokines such as adiponectin, IL-6 and TNFα that regulate blood pressure, immune function and energy balance [174]. Disturbances in the production of these factors may contribute to diseases such as insulin resistance or impaired insulin secretion in patients with type 2 diabetes or atherosclerosis and cancer [146,147,175,176]. WAT is one of the largest organs of the body; even lean men have a fat mass of 3.5-4 kg [177]. It is located either subcutaneously or viscerally at several locations in the body where it protects the inner organs. Epidemiological studies have shown that only central obesity (visceral fat) is associated with health risks such as artherosclerosis, cancer or overall mortality [178-183]. WAT can dynamically respond with shrinking or expanding to different types of stimuli such as food intake and temperature [184]. As increased levels of fatty acids

circulate in the blood, more triglycerides are taken up and incorporated into the lipid droplet of the adipocyte, thereby increasing in size. Upon starvation, these triglycerides can be broken down through lipolysis and fatty acids are released as energy source. In humans, increased fat cell storage and consequently enlarged fat cells is the most important mechanism of increased fat depots [185-188]. However, there is also a difference in adipocyte cell number of lean and obese individuals [188]. Interestingly, this number only increases during childhood and adolescence, leading to a stable cell number in adulthood, in both lean and obese individuals. There is a constant turnover of adipocytes, which is tightly controlled and thus leads to a stable number of adipocytes in adults. Since adipocytes are postmitotic, there has to be a reservoir of stem cells that can differentiate into new adipocytes. There is strong evidence, that these adipocyte stem cells reside within the adipose tissue close to the vasculature [184,189,190]. Interestingly, these cells are not committed to the adipocyte phenotype, but can also differentiate into bone, cartilage and muscle and thus need to be determinated by stimuli [189].

1.6.3 The 3T3-L1 model system

The most widely used model to study adipogenesis *in vitro* is the 3T3-L1 cell line [191-193]. Most of our understanding of the molecular mechanism of adipogenesis was obtained from studies with these cells [191-193]. The 3T3 cell line was isolated and established from disaggregated Swiss mouse embryos [194]. From this cell line, two clones with lipid accumulating potential were isolated (3T3-L1 and L-2). During differentiation, these cells acquire multilocular lipid droplets and therefore resemble brown adipocytes [195,196]. However, after the completion of differentiation they appear like mature white adipose cells. 3T3-L1 cells were used to establish the protocols that were commonly used today for the differentiation to adipocytes. 1975 Green and colleagues could show that Insulin is beneficial for differentiation [195]. Glucocorticoids and cAMP elevating agent (IBMX) further increase the differentiation of 3T3-L1 cells *in vitro*. The differentiation of 3T3-L1 can be divided into three phases: growth arrest, mitotic clonal expansion and terminal differentiation (Fig. 6) [192].

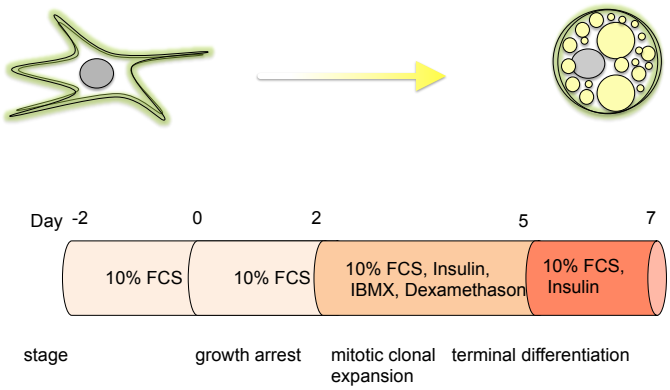

Figure 6: Differentiation of 3T3-L1 cells
Shown is the protocol for differentiation of 3T3-L1 cells and the corresponding stages that are explained in the text.

In the first phase, the cells in the culture plate reach confluency and arrest growth due to contact inhibition. Upon hormonal induction the arrested cells reenter the cell cycle and undergo one or two rounds of cell division, which is described as mitotic clonal expansion. The expression of the transcription factor peroxisome proliferator-activated receptor γ (PPARγ) and of the CCAAT/enhancer binding protein (C/EBP) coincides with a permanent growth arrest and the terminal differentiation into lipid-laden adipocytes that express adipocyte specific genes.

1.7 Transcriptional network in adipogenesis

The process of adipocyte differentiation is controlled by a variety of different transcription factors [191]. It involves a massive chromatin remodeling and the establishment of so called *hotspots*, where multiple transcription factors bind to open chromatin regions and promote transcription of adipogenic genes [197-199]. Adipogenesis involves two different stages that are characterized by specific sets of transcription factors (Fig.7). The early phase of adipogenesis is characterized by the expression of C/EBPβ and C/EBPδ. These transcription factors in turn induce in a later phase the expression of PPARγ and C/EBPα, which consecutively activate the transcription of adipocyte specific genes.

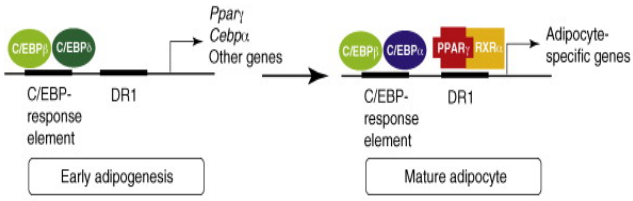

Figure 7: Different phases of differentiation
During the early phase of adipogenesis, C/EBPβ and C/EBPδ induce the expression of PPARγ that in turn induces the expression of adipocyte specific genes during the late phase of adipogenesis. Picture from Lefterova and coworkers. [200].

1.7.1 C/EBPs

Three members of the CCAAT/enhancer-binding protein (C/EBP) family play important roles in adipogenesis [191,201,202]. Within few hours after the induction of differentiation in 3T3-L1 cells, the transcription of C/EBPβ and -δ is induced, which in turn activates transcription of PPARγ and C/EBPα [191,201,203,204] (Fig. 8).

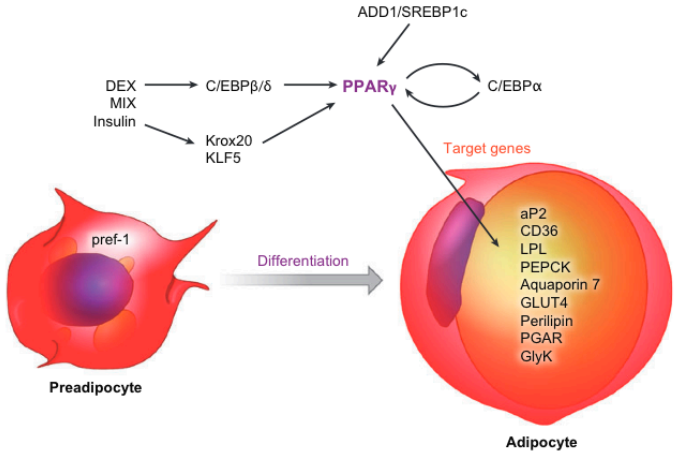

Figure 8: Overview of the transcriptional network in adipogenesis
PPARγ is the master regulator of adipogenesis. The picture shows how PPARγ is influenced by and influences other factors. In addition, it is shown how the hormonal cocktail used for induction of differentiation influences this network. Dex: dexamethasone, MIX:methylisobutylxanthine, GlyK:Glycerol kinase Picture modified from Tontonoz and Spiegelman [202].

Consistently, ectopic expression of C/EBPβ and -δ induces expression of PPARγ and C/EBPα [203,205-207]. In line with these findings, double knockout mice for C/EBPβ and -δ show reduced adipose tissue, whereas single knockouts only show mild phenotypes [208]. As mentioned above, C/EBPβ and -δ activity induces C/EBPα expression. This member of the C/EBP family is expressed together with PPARγ in the late phase of adipogenesis. *In vitro* and *in vivo* studies showed that C/EBPα is able to induce

adipogenesis when ectopically expressed and is required for the formation of WAT, but not of BAT [56,209,210]. PPARγ can induce adipogenesis in C/EBPα deficient MEFs, whereas C/EBPα is not sufficient to induce adipogenesis in cells lacking PPARγ [211]. C/EBPα expression is not only dependent on C/EBPβ and -δ, but also on PPARγ [212]. In addition, a positive feedback loop between PPARγ and C/EBPα expression is well described [211,213]. PPARγ and C/EBPα are able to sustain each other's expression and thereby maintain the phenotype of the mature adipocyte.

1.7.2 PPARγ

PPARγ is the master regulator of adipogenesis [191,192,200,202,214]. Early evidence from Spiegelman and collaborators showed that the nuclear factor first named ARF6, was able to bind an enhancer element in the 5' flanking region of the *aP2* gene and to induce *aP2* expression [215]. ARF6 was later shown to be PPARγ and to interact with its heterodimeric partner RXR [216]. The PPARγ domain structure resembles the composition of many nuclear receptors (Fig. 9) [202].

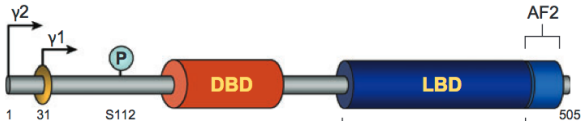

Figure 9: Structure of PPARγ
The domain structure of PPARγ 1 and 2 is shown. Picture modified from Tontonoz and Spiegelman [202]

The N-terminal region contains a non-conserved A/B domain, followed by a DNA binding domain (DBD) and the C-terminal ligand-binding domain (LBD) with the activating fragment 2 (AF-2). The C-terminal domain is required for the interaction with RXRs, the AF2 domain is important for ligand-dependent interactions with cofactors. The ligand binding is conveyed by the LBD that harbors multiple hydrophobic residues in its pocket. The N-terminal domain of PPARγ comprises important regulatory functions. Upon its deletion, the transcriptional activity of PPARγ is increased [217]. This inhibitory function is partially conveyed through phosphorylation of Ser112 by members of the MAP kinase family, which strongly hampers transcriptional activity [218,219]. In addition, the N-terminal domain was shown to interact with cofactors such as p300, HIV-Tat-Interactive protein 60 (Tip60) and

MED14 in a ligand-independent manner [220-222]. Recently, it was shown that this domain is required for the transactivation of only a subset of PPARγ target genes [223]. High affinity binding to DNA is mediated by the two zinc-fingers in the DBD together with RXR to direct hexanucleotide repeats spaced by 1 nucleotide (DR1) named PPARγ response elements (PPREs) that are located in upstream enhancer regions of PPARγ-target genes [202,216,224]. Thiazolidinediones (TZDs), such as rosiglitazone or troglitazone, are synthetic ligands of PPARγ that increase insulin sensitivity in rodents and humans and are used for the treatment of type 2 diabetes (T2D) [225]. The identity of the biological ligand of PPARγ remains controversial and is actively investigated. During adipogenesis in 3T3-L1 cells, a PPARγ activating substance is produced, but its identity remains elusive [226]. Several groups have shown that polyunsaturated fatty acids and related molecules can activate PPARγ in micromolar concentrations [227-230]. Free fatty acids are present at these concentrations in the blood, however, the concentration inside the cell and near the receptor is unknown [231]. Certain prostaglandins such as 15-deoxy-1 12,14prostaglandin J2 (15-dPGJ2) are strong activators of PPARγ *in vitro*, although it is not clear whether these substances are present in the cell in significant amounts [202,232,233]. In addition, other lipids such as oxidized fatty acids, nitrated fatty acids, or lysophosphatic acids seem able to activate PPARγ [234-236]. Especially oxidized fatty acids can be found in low-density lipoprotein and might play a role in artherosclerotic lesions, where they reach a considerable local concentration. In addition, during adipogenesis, the cells acquire a high lipogenic capacitiy[237-239]. Both the expression of enzymes important for *de novo* fatty acid synthesis as well as for triacylglycerol synthesis is tremendously increased. These fatty acids are stored in form of triglycerides in lipid droplets [240]. It is currently unknown if fatty acids can activate PPARs before being incorporated into lipid droplets or if rehydrolysis of the triglycerides by hormone sensitive lipase (HSL) or adipose triglyceride lipase (ATGL) is required before they can signal through PPARγ [241]. Both ATGL and HSL deficient mice show decreased PPAR activity indicating the requirement of lipases for the activation of PPAR [241-243]. However, it is currently unclear how this process is regulated and how PPAR activity is maintained during adipogenesis.

Since the discovery of PPARγ, a series of *in vitro* and *in vivo* experiments have proven PPARγ's role in adipogenesis. Ectopical expression of only PPARγ in

non-adipogenic fibroblasts can initiate the differentiation into functional adipocytes [217]. PPARγ null mice die during embryogenesis due to placental insufficiency (E 10.5) [244]. Different strategies were used to circumvent this problem and to confirm the role of PPARγ in adipose tissue formation [244,245]. The generation of tetraploid embryos partially rescued the lethality [244]. The only mouse that was born died shortly after birth, but the investigators observed a failure in adipose tissue formation in this animal. Embryonic stem cells devoid of PPARγ fail to differentiate into adipocytes *in vitro* [245]. Heterozygous mice with a ubiquitous reduction of PPARγ in all tissues have normal body weight and fat depots [246,247]. However, these mice are insulin sensitive and resistant to diet induced obesity. Deletion of PPARγ2 leads to severe lipodystrophy [248]. Only the development of tissue specific knockout mice allowed to properly assess the contribution of PPARγ to adipogenesis *in vivo*. Deletion of PPARγ in adipose tissues of mice protects the animals from high fat diet–induced obesity and insulin resistance [249-251]. Interestingly, these mice display increased lipid deposition in muscle and liver. Similar results were obtained in mice with pharmacological inhibition of PPARγ by antagonist treatment [252,253]. In addition, the ablation of PPARγ2 in ob/ob mice results in decreased fat mass, severe insulin resistance, β-cell failure and dyslipidemia [254]. PPARγ is a nuclear receptor and belongs to the family of PPARs. This family consists of three subtypes, namely PPAR α, γ, ∂ which are encoded by three different genes but are all important regulators of glucose and lipid metabolism in different tissues [201,255-257]. PPARγ is induced during the differentiation of pre-adipocytes into adipocytes and is highly expressed in white and brown adipose tissue (WAT and BAT) [216]. It exists in two different protein isoforms, PPARγ1 and PPARγ2 that arise through alternative promoter usage of the same gene and the generation of four different mRNAs. The mRNAs PPARγ1, 3 and 4 encode the PPARγ1 protein, while PPARγ2 encodes isoform 2 [216,258-260]. This isoform contains 30 additional amino acids at the N-terminus [216,258-260]. PPARγ1 is expressed in many tissues, whereas the expression of PPARγ2 under normal physiological conditions is restricted to adipose tissue. *In vitro,* PPARγ1 can compensate for PPARγ2 deficiency and adipose-selective PPARγ2 depletion results in mice that still contain considerable amounts of fat [261,262]. However, these mice are insulin-resistant, suggesting that PPARγ2 may play a selective role in regulating insulin sensitivity.

1.7.3 PPAR γ co-repressors and co-activators

PPARγ is a ligand gated transcription factor that is activated by cofactors that are also used by other nuclear receptors [202]. Following dissociation of corepressors, PPARγ exerts its influence on transcription by binding to PPREs, where it recruits coactivators in a ligand-dependent manner. The LXXLL motif that is present in most coactivators is responsible for the interaction with nuclear receptors in a ligand-dependent manner [263]. Binding of a ligand to PPARγ triggers a conformational switch in PPARγ that induces change in confirmation of the AF2 domain and exposes a surface that can interact with LXXLL-containing coactivator domains [264,265]. Prior to activation of PPARγ by the ligand, co-repressors that suppress transcription of target genes bind PPARγ. Important corepressors that are dislodged from PPARγ upon ligand binding are SMRT and NCOR-1. Knockdown of both increases expression of PPARγ-target genes [266]. HDAC-1 and -3 are also part of the corepressor complex and repress C/EBPβ and PPARγ expression through their deacetylating activity [267]. Upon ligand binding, cofactors of the p160 family, usually TIF2 or SRC-1, are recruited. In addition, acetyltransferases p300/CBP can be recruited. Interaction with p300/CBP is mediated in two different ways [220]. They interact with the N-terminus of PPARγ2 independently of the ligand whereas binding of p300/CBP to the C-terminus is ligand-dependent.

1.7.4 Other transcription factors that control adipogenesis

Recent genome/proteome wide studies have identified many additional transcription factors that are required for adipocyte differentiation [268]. Krox20, for example, is induced immediately after induction of differentiation and stimulates the expression of C/EBPβ [269]. Krüppel-like factor 5 (KLF5) is one of the target genes that is induced by C/EBPβ and in turn supports the transcription of PPARγ [270]. In addition to the C/EBPβ/-δ axis, other pathways are initiated early and converge upstream of PPARγ. ADD1/SREBP1 is induced during adipogenesis and can be regulated by sterol levels [271,272]. The exact mechanism of activation in fat remains unknown, but it can stimulate a variety of genes involved in fatty acid and triglyceride metabolism. Additional studies have shown that ADD1/SREBP1 contributes to the production of an endogenous ligand for PPARγ as well as to the induction of PPARγ [272-274].

1.7.5 Transcription factor hot spots during adipogenesis

Although PPARγ is the master regulator of adipogenesis, a multitude of different transcription factors and their exact regulation is required for correct differentiation and adipocyte function [199,275]. Already within 4 hours after induction of differentiation, a massive chromatin remodeling takes place in the pre-adipocytes and so called hotspots are established [199,276,277]. These hotspots are characterized by DNAse-I hypersensitivity, which represents open chromatin regions. In addition, hotspots display enriched binding of a variety of transcription factors. Interestingly, the number of hotspots is biggest shortly after induction of differentiation and decreases again when cells are fully differentiated. Also, these hotspots are enriched mostly in early transcription factors such as C/EBPs, GRs and STAT5A and in transient histone acetylation. The establishment of hotspots correlated with changes in gene expression of nearby genes. However, numerous of these loci seemed to prepare the binding of the later transcription factors. Especially binding of complexes containing C/EBPs act as pioneering factors for later PPARγ-binding. However, not all PPARγ binding sites lie within these early enhanceosomes. It is an interesting model that the early establishment of early enhanceosomes primes the chromatin in a way that allows late enhanceosomes to bind and to increase transcription. However, various PPARγ binding sites do not lie within these early enhanceosomes and are unmarked as defined by Siersbaek and colleagues [199,276,277]. Various other chromatin factors or histone marks as well as three-dimensional structures could however mark these sites. It will need further genome-wide studies to answer these remaining questions.

1.8 Role of ARTDs in metabolism

ARTD1 and ARTD2 have been described to play a role in metabolic homeostasis [278]. ARTD1 is important for food entrainment of circadian clocks in mice [279-281]. Moreover, ARTD $1^{-/-}$ and $ARTD2^{-/-}$ mice display increased energy expenditure [280,282]. Interestingly, several studies provide evidence that deficiency of ARTD1 or ARTD2 protects mice from an age- or diet-induced increase of bodyweight and that these mice display less fat mass deposition [57,280,282,283]. In agreement with these results, mice with ectopic expression of ARTD1 display increased body weight and adiposity with fat deposition in the liver and other organs [284]. However, there are also reports

describing higher body weight for ARTD1$^{-/-}$ mice, although one of these studies used mice of the 129 background instead of C57 BL/6, which could account for the observed differences [56,281]. ARTD1 knockout mice, but not animals lacking ARTD2, also show an increased mitochondrial content, demonstrating that BAT is also influenced [280,282]. *In vitro* experiments suggest a role of ARTD2 in PPARγ-dependent gene expression [283]. Bai and colleagues have shown that ARTD2$^{-/-}$ cells fail to differentiate into adipocytes and identified ARTD2 as a cofactor for PPARγ. Recently, a role of ARTD1-dependent PAR formation in PPARγ-dependent 5-hydroxymethylation of PPREs was described [285]. This model suggests that a PPARγ-co-activator complex is PARylated, which leads to recruitment of Tet proteins that can induce region-specific demethylation by converting 5-methyl-cytosine (5mC) to 5-hydroxymethyl-cytosine. However, it is unclear which component of the co-activator complex is PARylated.

2 Aim of the thesis

In humans, there are 18 ADP ribosyltransferases belonging to the Diphtheria toxin-like types (ARTD) family, which are located within the cell. Some of these enzymes were described to synthesize poly-ADP-ribose, while others can only form mono-ADP-ribose or are enzymatically inactive. ARTD1 is the best-studied member of this family and capable of generating long, branched polymers of ADP–ribose. ARTD1 is a chromatin-associated enzyme that affects chromatin compaction and transcription. Recent studies suggested a dynamic modulation of the chromatin landscape during adipocyte differentiation, which is controlled by the transcription factor PPARγ. ARTD1 has been recently described to play a role in metabolic homeostasis, although a molecular mechanism was not identified.

The aim of this thesis was to investigate the functional role of ARTD1 and ARTD1-induced poly-ADP-ribosylation during adipocyte differentiation. Since the transcription factor PPARγ is the master regulator of adipogenesis, these studies focused mainly on the regulation of PPARγ-dependent gene expression by ARTD1 and on the molecular mechanism that underlies this regulation.

Standard and recently developed molecular and cell biology techniques as well as animal studies were included in these studies.

3 Results

3.1 Published results

3.1.1 Poly(ADP-ribose)polymerase-1 (PARP1) controls adipogenic gene expression and adipocyte function

Authors: Erener, S., **Hesse, M**., Kostadinova, R., and Hottiger, M.O.
Journal: Molecular Endocrinology, 2012
Contribution: Planning, performing and evaluating the experiments for Fig.2B, D; Fig. 4 A,B,C,D; S1A; S2;S3 Preparation of the figures, revision of manuscript.

3.1.2 ARTD1 deletion causes increased hepatic lipid accumulation in mice fed a high-fat diet and impairs adipocyte function and differentiation.

Authors: Erener, S., Mirsaidi, A., **Hesse, M**., Tiaden, A.N., Ellingsgaard, H., Kostadinova, R., Donath, M.Y., Richards, P.J., and Hottiger, M.O.
Journal: FASEB, 2012
Contribution: Planning, performing and evaluating the qRT-PCRs for Figure 4A.

3.1.3 PARP inhibitor with selectivity toward ADP-ribosyltransferase ARTD3/PARP3

Authors: Lindgren, A.E., Karlberg, T., Thorsell, A.G., **Hesse, M**., Spjut, S., Ekblad, T., Andersson, C.D., Pinto, A.F., Weigelt, J., Hottiger, M.O., Linusson, A., Elofsson, M., Schüler, H.
Journal: ACS chemical biology, 2013
Contribution: Planning, performing and evaluating of cellculture experiments (Fig. 3C, D and E and S 6)

ORIGINAL RESEARCH

Poly(ADP-Ribose)Polymerase-1 (PARP1) Controls Adipogenic Gene Expression and Adipocyte Function

Süheda Erener, Mareike Hesse, Radina Kostadinova, and Michael O. Hottiger

Institute of Veterinary Biochemistry and Molecular Biology (S.E., M.H., R.K., M.O.H.), and Life Science Zurich Graduate School (S.E., M.H.), Molecular Life Science Program, University of Zurich, 8057 Zurich, Switzerland

Poly(ADP-ribose)polymerase-1 (PARP1) is a chromatin-associated enzyme that was described to affect chromatin compaction. Previous reports suggested a dynamic modulation of the chromatin landscape during adipocyte differentiation. We thus hypothesized that PARP1 plays an important transcriptional role in adipogenesis and metabolism and therefore used adipocyte development and function as a model to elucidate the molecular action of PARP1 in obesity-related diseases. Our results show that PARP1-dependent ADP-ribose polymer (PAR) formation increases during adipocyte development and, at late time points of adipogenesis, is involved in the sustained expression of *PPARγ2* and of *PPARγ2* target genes. During adipogenesis, PARP1 was recruited to *PPARγ2* target genes such as *CD36* or *aP2* in a PAR-dependent manner. Our results also reveal a PAR-dependent decrease in repressory histone marks (*e.g.* H3K9me3) and an increase in stimulatory marks (*e.g.* H3K4me3) at the *PPARγ2* promoter, suggesting that PARP1 may exert its regulatory function during adipogenesis by altering histone marks. Interestingly, activation of PARP1 enzymatic activity was prevented with a topoisomerase II inhibitor. These data hint at topoisomerase II-dependent, transient, site-specific double-strand DNA breaks as the cause for poly(ADP)-ribose formation, adipogenic gene expression, and adipocyte function. Together, our study identifies PARP1 as a critical regulator of *PPARγ2*-dependent gene expression with implications in adipocyte function and obesity-related disease models. **(*Molecular Endocrinology* 26: 79–86, 2012)**

Obesity is a complex metabolic disorder characterized by an excess of body fat that is closely associated with other serious health conditions, such as heart disease and diabetes. White adipose tissue, which is the predominant type of fat in adult humans, serves as a storage depot for excess energy. Adipose tissue secretes diverse adipokines, such as leptin, *Adiponectin*, IL-6, TNFα, and others, that regulate blood pressure, immune function, and energy balance (1, 2). Disturbed production of these factors may contribute to the development of insulin resistance or impaired insulin secretion resulting in type 2 diabetes.

During adipogenesis, fibroblast-like preadipocytes differentiate into lipid-laden and insulin-responsive adipocytes, which requires a coordinate up-regulation of many enzymes involved in fatty acid metabolism and pyridine nucleotides as coenzymes (3). The murine 3T3-L1 cell line (4) has been broadly used as a model system to study adipogenesis. 3T3-L1 cells undergo a synchronous differentiation process upon addition of an adipogenic cocktail and have been influential for the understanding of the complex regulatory networks during adipogenesis. Adipocyte differentiation is accompanied by large-scale chromatin changes and by the establishment of transcription factor "hotspots" (5). This process occurs in several stages and involves a cascade of transcription factors, among which the CCAAT/enhancer-binding proteins (C/EBP) C/EBP-β and C/EBP-δ are considered crucial determinants for the expression of the key factor peroxisome proliferator-activated receptor γ (PPARγ) and of C/EBP-α (6, 7). A positive feedback loop between PPARγ and C/EBP-α mutually regulates

ISSN Print 0888-8809 ISSN Online 1944-9917
Printed in U.S.A.

doi: 10.1210/me.2011-1163 Received June 28, 2011. Accepted October 11, 2011.
First Published Online November 3, 2011

Abbreviations: C/EBP, CCAAT/enhancer-binding protein; ChIP, chromatin immunoprecipitation; NAD^+, nicotinamide adenine dinucleotide; PAR, polymers of ADP-ribose; PARP1, poly(ADP-ribose)polymerase-1; PPARγ, peroxisome proliferator-activated receptor γ; shRNA, short hairpin RNA.

their expression, and together, these two proteins coordinate adipocyte function (7, 8). In contrast to PPARγ1, PPARγ2 expression is mainly restricted to adipocytes (9). PPARγ2, together with several coactivators, regulates an array of target genes, of which *aP2*, *CD36*, and *Adiponectin* have crucial roles for adipocyte function by regulating fatty acid binding, translocation, and catabolism, respectively (5). Deletion of *PPARγ2* in mouse adipose tissues protects against high-fat diet-induced obesity and insulin resistance, but these mice display increased lipid deposition in muscle and liver (10). Similarly, ablation of *PPARγ2* in mice of the ob/ob background results in decreased fat mass, severe insulin resistance, β-cell failure, and dyslipidemia (11).

Poly(ADP-ribose)polymerase-1 (PARP1) (recently renamed ADP-ribosyltransferase diphtheria toxin-like 1) (12) is an abundant, ubiquitous chromatin-associated enzyme that catalyzes the nicotinamide adenine dinucleotide (NAD^+)-dependent addition of polymers of ADP-ribose (PAR) onto a variety of target proteins (13). PAR is a large, negatively charged polymer that functions as posttranslational protein modification. Most PAR in the cell is produced by the catalytic activity of PARP1, which is the main ADP-ribosyltransferase in the nucleus (14). *In vitro*, PARP1 enzymatic activity is strongly activated upon binding to various interaction partners, such as nucleosomes or certain forms of DNA (15). *In vivo*, polymer formation by PARP1 is undetectable by immunofluorescence under basal (unstimulated) conditions but can be detected upon treatment of cells with DNA-damaging compounds (13). Lack of PARP1 in cells was reported to affect the gene expression profile in a genome-wide manner (15). Besides restructuring the chromatin and influencing transcription indirectly (16, 17), PARP1 can additionally act as a transcriptional cofactor during transcription by directly interacting with a variety of transcription factors (18).

Previous studies reported the body weight of adult *PARP1*−/− mice in diverse genetic backgrounds to be different than the corresponding controls (19, 20). Here, we extend these studies to the molecular level and show with different experimental approaches that PARP1-dependent PAR formation increases during adipocyte development and is involved in regulating adipocyte development and function.

Results

ADP-ribosylation is required for sustained PPARγ2-dependent gene expression

To investigate whether PARP1 and its enzymatic activity have an effect on adipogenesis, 3T3-L1 preadipocytes were differentiated into adipocytes by addition of an adipogenic cocktail (21). Western blot analysis from the differentiated 3T3-L1 cell extracts revealed a shift of PARP1 at d 7, suggesting auto-ADP-ribosylation of PARP1 (Fig. 1A). Further Western blot analysis using an antibody against the PAR confirmed that PAR formation was indeed activated after d 3 of adipocyte differentiation. Moreover, PAR formation was strongly reduced in differentiating 3T3-L1 cells that were treated with the PARP inhibitor PJ34 (or Olaparib, data not shown), providing further evidence that ADP-ribosylation was indeed induced in 3T3-L1 extracts (Fig. 1A). A detailed kinetic analysis detected PAR formation already at d 4 after induction of adipocyte differentiation, which remained elevated until d 10 (Supplemental Fig. 1A, published on The Endocrine Society's Journals Online web site at http://mend.endojournals.org).

Interestingly, PJ34 treatment also inhibited storage of free fatty acids in the adipocytes as judged by Oil-Red O staining (Fig. 1B and Supplemental Fig. 1B), suggesting that adipocyte function might require PAR formation. Next, we evaluated the functional contribution of PAR formation for the transcriptional activation of the main

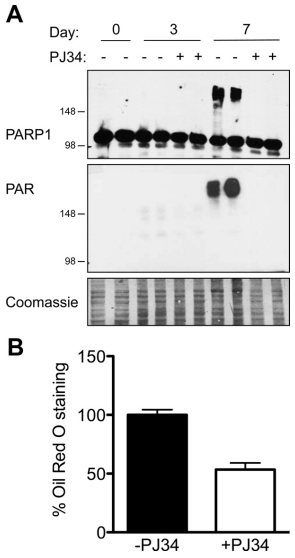

FIG. 1. PAR formation is important during adipogenesis. 3T3-L1 preadipocytes were subjected to adipocyte differentiation during 7 d in the absence or presence of PARP inhibitor PJ34 (10 μM). Inhibitor was supplemented daily. A, Total-cell extracts were prepared and analyzed by Western blotting. An experiment done in duplicates is shown. B, Cells were stained with Oil-Red O, bound Oil-Red O was extracted, and quantified colorimetrically. Result show the mean ± SEM, n = 3.

Mol Endocrinol, January 2012, 26(1):79–86 mend.endojournals.org 81

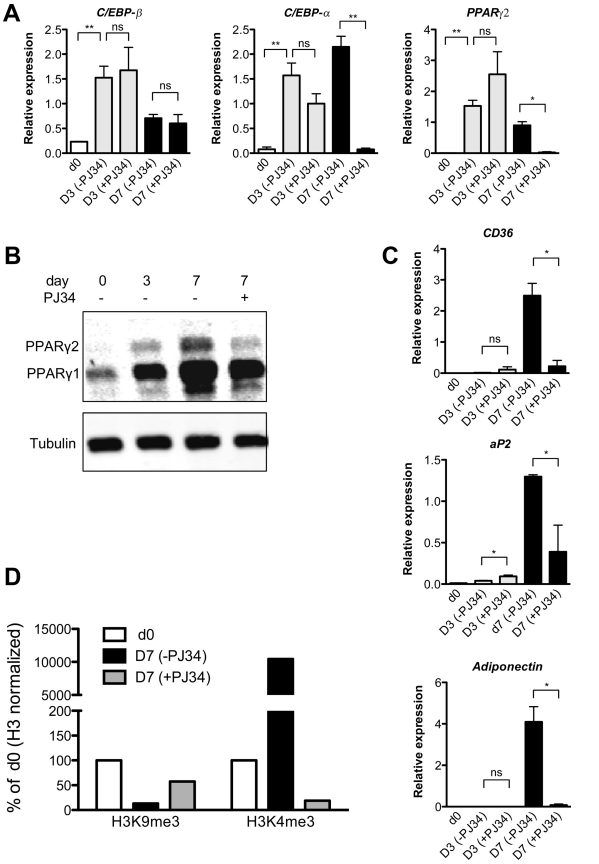

FIG. 2. PAR formation is required for sustained PPARγ2-dependent gene expression. 3T3-L1 preadipocytes were subjected to adipocyte differentiation for 7 d in the absence or presence of PARP inhibitor PJ34 (10 μM). Inhibitor was supplemented daily. A, Real-time RT-PCR analysis for *C/EBP-β*, *C/EBP-α*, and *PPARγ2* is shown. mRNA levels were normalized with *Cyclophilin A*. Results show the mean ± SEM, n = 3. ns, $P > 0.05$; *, $P < 0.05$; **, $P < 001$. B, Total-cell extracts were prepared and analyzed by Western blotting. C, Relative expression levels of the PPARγ2-dependent genes *CD36*, *aP2*, and *Adiponectin* were determined as in A. D, ChIP analysis with H3K9me3 and H3K4me3 antibodies on the *PPARγ2* promoter. The experiment was performed twice with similar results, and one experiment is shown.

drivers of adipogenesis by quantitative PCR. The expression of *C/EBP-β*, the main transcriptional regulator of initial *PPARγ2* expression, as well as of *C/EBP-α* and *PPARγ2*, was significantly induced upon initiation of adipogenesis and not affected by the PARP inhibitor PJ34 (at d 3) (Fig. 2A). In contrast, although the sustained expression level of *C/EBP-β* at d 7 was not affected by PARP inhibition, the *C/EBP-α* and *PPARγ2* mRNA levels at this later time point were significantly reduced by the presence of PJ34 for 6 d (Fig. 2A). The reduction in *PPARγ2* mRNA levels was also manifested in PPARγ2 protein levels, although a residual amount of PPARγ2 was still observed after 6 d of PJ34 treatment (Fig. 2B). Thus, the sustained expression (after d 3 of adipogenesis) of *C/EBP-α* and *PPARγ2* requires the formation and presence of PAR. To elucidate whether the expression of PPARγ2 target genes might consequently also be affected by ADP-ribosylation, we analyzed the expression of *aP2*, *CD36*, and *Adiponectin*. Although *aP2* expression was detected at d 3 and then increased substantially until the late phase of adipogenesis (d 7), *CD36* or *Adiponectin* were significantly expressed only at d 7 (Fig. 2C). Remarkably, the expression of all three genes was abrogated by the PARP inhibitor PJ34 (Fig. 2C), suggesting that PPARγ2-dependent gene expression is indeed regulated by PAR formation.

To investigate whether known histone modifications (22, 23) were affected by PJ34 treatment, repressory (H3K9me3) and stimulatory marks (H3K4me3) were assessed at the *PPARγ2* promoter. Chromatin immunoprecipitation (ChIP) experiments revealed that the repressory histone mark H3K9me3 decreased during differentiation (d 7), whereas PJ34 treatment blocked the release of this repressory histone mark at the *PPARγ2* promoter (Fig. 2D). In contrast, the stimulatory histone mark H3K4me3 increased at the same promoter during adipocyte differentiation (d 7), and PJ34 treatment blocked its accumulation, which is in agreement with the effects that were observed at the gene expression level (Fig. 2D).

3T3-L1 adipocyte differentiation is inhibited by PARP1 depletion

To further assess a specific involvement of PARP1 (but not other PARP family members) and its enzymatic activity in PPARγ2-dependent gene expression, undifferentiated 3T3-L1 preadipocytes were transduced with a lentivirus expressing short hairpin RNA (shRNA) against *PARP1* (to stably knockdown PARP1) or a scrambled

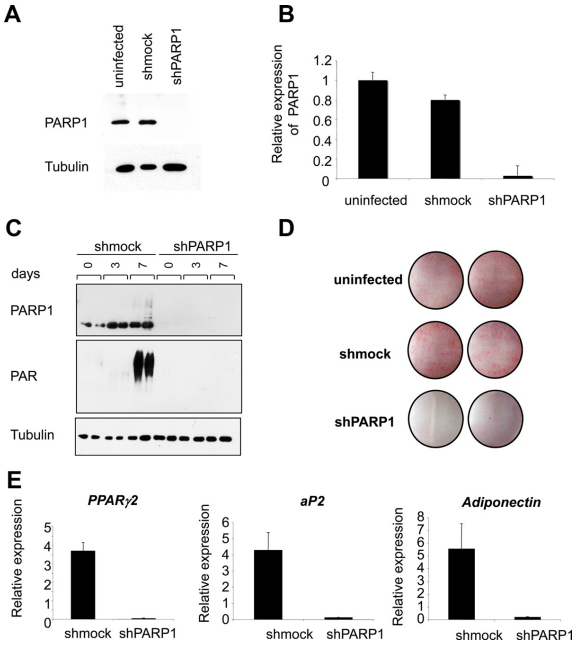

FIG. 3. Depletion of PARP1 retards 3T3-L1 differentiation into adipocytes. Knockdown of PARP1 was confirmed by (A) Western blot and (B) quantitative-PCR analyses. C, shmock or shPARP1 3T3-L1 preadipocytes were differentiated into adipocytes for 7 d. Western blot analysis with total-cell extracts shows PARP1 and PAR levels in shmock and shPARP1 cells during adipogenesis (d 0, 3, and 7 of differentiation). D, Oil-Red O staining of shmock and shPARP1 cultures that were subjected to 7 d of adipocyte differentiation. E, Real-time RT-PCR analysis of *PPARγ2*, *aP2*, and *Adiponectin* in shmock and shPARP1 cells after 7 d of adipocyte differentiation. mRNA levels were normalized with *Cyclophilin A*. Results show the mean ± SEM, n = 3.

control RNA (Fig. 3, A and B). As compared to uninfected cells, *PARP1* mRNA levels decreased slightly in mock-treated cells, whereas in shPARP1 3T3-L1 cells, PARP1 mRNA and protein expression were below 1% of the levels observed in shmock cells (Fig. 3, A and B). Furthermore, no PAR formation was detected in the extracts of differentiated shPARP1 cells (Fig. 3C), suggesting that the observed PAR formation during adipogenesis was indeed dependent on PARP1. Next, we investigated whether depletion of PARP1 affects adipocyte differentiation. As judged by Oil-Red O staining, cells efficiently depleted of PARP1 were strongly hampered in their development to mature adipocytes (Fig. 3D). Moreover, the expression of *PPARγ2* itself and the expression of PPARγ2 target genes such as *aP2* and *Adiponectin* was strongly reduced after 7 d of induced differentiation in shPARP1 3T3-L1 cells (Fig. 3E). These results suggest that PARP1 and PARP1-induced PAR formation are required for *PPARγ2* expression and subsequent adipocyte differentiation and that other PARP family members cannot compensate for the lack of PARP1 during adipocyte differentiation.

Topoisomerase II inhibitor merbarone inhibits PAR formation and PPARγ2-dependent gene expression

Activation of PARP1 and subsequent induction of transcription can be caused by topoisomerase II-mediated, transient, site-specific DNA double-strand breaks (24). We therefore sought to test whether the upstream event that activates PARP1 enzymatic activity requires topoisomerase II-dependent double-strand DNA break formation. To investigate this possibility, 3T3-L1 cells were treated during the last 2 or 3 d of differentiation (treatment at d 5–6 or 4–6, respectively) with PARP inhibitor (PJ34) or topoisomerase II inhibitor (merbarone). PJ34 efficiently inhibited PAR formation even when added only in the later stages of differentiation (d 5 and 6) (Fig. 4A) and could still strongly affect PPARγ2-dependent gene expression, whereas PPARγ2, once expressed, was minimally changed (Fig. 4B and Supplemental Fig. 2, A and B). Interestingly, merbarone also reduced PAR formation significantly, indicating that topoisomerase II activity may be at least partly responsible for PARP1 activation.

In addition, the expression of *PPARγ2*, *aP2*, *Adiponectin*, and *CD36* was strongly reduced in cells treated with merbarone during d 5 and 6 (Fig. 4C). To rule out that merbarone directly inhibits PARP1 enzymatic activity, we performed *in vitro* auto-ribosylation assays (Supplemental Fig. 2C). Although PJ34 efficiently blocked PAR formation, merbarone did not have an *in vitro* inhibitory effect on PAR formation, even at concentrations as high as 80 μM (Supplemental Fig. 2C). These results suggest that topoisomerase II is responsible for the observed activation of PARP1 during the later phase of adipogenesis. Unfortunately, we were not able to demonstrate recruitment of topoisomerase II to the *CD36* and *aP2* promoters in adipocytes with the available antibodies.

PAR formation enhances PARP1 chromatin recruitment

To further address the direct functional link between PARP1 and PAR formation for PPARγ2-dependent gene

Mol Endocrinol, January 2012, 26(1):79–86

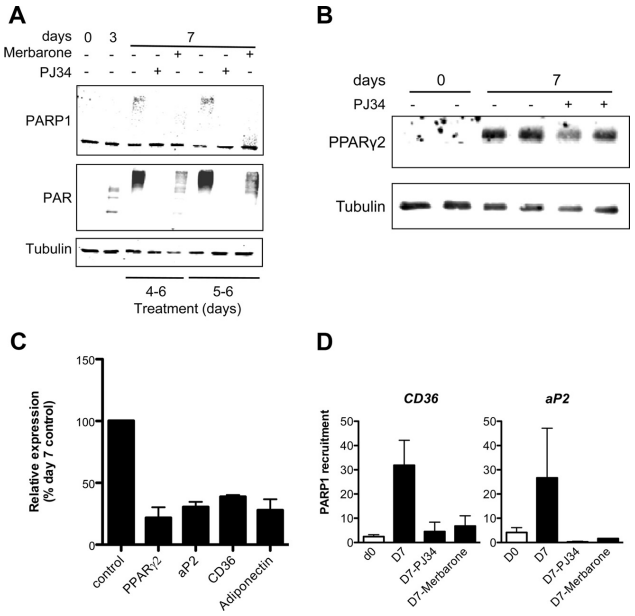

FIG. 4. PAR formation is dependent on topoisomerase II activity and required for PARP1 chromatin recruitment. A, 3T3-L1 preadipocytes were differentiated for 7 d. At d 4–6 or 5–6, 10 μM PJ34 or 40 μM merbarone was added to the medium. Total-cell extracts were prepared and analyzed by Western blotting. B, 3T3-L1 preadipocytes were subjected to adipocyte differentiation. 10 μM PJ34 was supplemented at d 5 and 6. Total-cell extracts from the indicated days were analyzed for PPARγ2 protein expression. C, Real-time RT-PCR analysis on d 7 from differentiated 3T3-L1 cells that were treated at d 5 and 6 of differentiation with dimethyl sulfoxide control or 40 μM merbarone. mRNA levels were normalized with *Cyclophilin A*. Results are from three independent experiments, mean ± SEM. D, ChIP analysis with the PARP1 antibody on *CD36* and *aP2* promoter. Negative control (beads from d 0 samples) was set as 1. Results are from five independent experiments, mean ± SEM.

expression, we investigated the recruitment of PARP1 to PPARγ2 target promoters by ChIP. ChIP analysis revealed that PARP1 was already present at the *CD36* and *aP2* promoters in undifferentiated cells, but this association was substantially increased at d 7 (Fig. 4D). Interestingly, PARP1 recruitment was abrogated when the cells were treated either with PJ34 or with merbarone, suggesting that the association of PARP1 with the tested promoters was dependent on PAR formation, which is induced by topoisomerase II activity.

Discussion

In this study, we provide evidence that PARP1 controls adipocyte function *in vitro*. Our results show that PARP1 is activated after the initial phase of adipogenesis and that either depletion of PARP1 or inhibition of ADP-ribosylation strongly retard the functional differentiation of 3T3-L1 cells. These findings are in agreement with earlier results showing that PAR formation during adipogenesis is increased, although an initial decrease at the beginning of adipocyte differentiation was observed (25). Furthermore, inhibition of topoisomerase II strongly reduced PARP1 activation and adipocyte function.

Recent genome-wide analyses revealed a dramatic and dynamic modulation of the chromatin landscape during the first hours of adipocyte differentiation that coincides with cooperative binding of multiple early transcription factors (including glucocorticoid receptor, retinoid X receptor, *Stat5a*, C/EBP-β, and C/EBP-δ) to transcription factor hotspots (5). C/EBP-β marks a large number of these transcription factor hotspots before induction of differentiation and chromatin remodeling and is required for their establishment. Because the expression of *C/EBP-β* was independent of PAR formation during the whole differentiation period (Fig. 2A), our experiments suggest that PAR formation is not required for the formation of the transcription factor hotspots. In contrast, although the initial induced gene expression of *PPARγ2* and *C/EBP-α* (at d 3) was not affected by PJ34 treatment, the sustained expression of both genes was reduced upon inhibition of PAR formation. Therefore, PAR appears to be necessary for the positive feedback loop that brings about the mutual stimulation of *PPARγ2* and *C/EBP-α* expression. Sustained PPARγ2-dependent gene expression was abrogated even after inhibition of PAR formation only for the last 2 d (d 5 and 6), whereas PPARγ2 protein levels were affected minimally (Fig. 4B). These results provide convincing evidence that the induction of PAR formation and its maintenance are important for sustained PPARγ2-dependent gene expression and adipocyte function. Moreover, this indicates that the reduced PPARγ2 target gene expression is not caused by a lack of cellular PPARγ2 but likely due to an additional function of PAR in PPARγ2-dependent gene expression. Even though the genetic experiments and inhibitor studies demonstrate a strong correlation between PAR formation and adipo-

genic gene expression, additional off-target effects of the PJ34 inhibitor cannot be excluded (*e.g.* on other NAD^+ consuming enzymes). However, given that most of the observed PAR formation at d 7 was associated with PARP1 and that PARP1 knockdown hampered adipogenesis, it is very likely that PARP1 enzymatic activity is required for this process, although we can currently not completely rule out that other ADP-ribosyltransferases, such as PARP2, also contribute to the observed effect (26).

PAR formation by PARP1 could affect adipogenesis in multiple ways: 1) by excluding or retaining transcription factors from a special chromatin site (7); 2) by dissociating corepressors that occupy *PPARγ2* and PPARγ2 target promoters during adipocyte differentiation, allowing the recruitment of transcription coactivators; and finally 3) by regulating histone modifying enzymes and subsequently altering histone modifications (27).

Along this line, mechanistically, our data implicate that topoisomerase II-induced DNA strand breaks as an upstream event preceding PAR formation, whereas altered histone modifications may represent the downstream effect of PARP1 activation. The reduced H3K4 trimethylation (Fig. 2D) upon PJ34 treatment is in agreement with the finding that PARP1 prevents H3K4me3 demethylation (27). In addition, our data further suggest an effect of PARP1 on the H3K9me3 modification (Fig. 2D). PAR could affect H3 marks either via histone demethylases (*e.g.* lysine demethylases) or through specific methyltransferases (*e.g. EHMT1/2*, *GLP*, *SETDB1*, or Suv39h1). Consequently, PAR formation may cause a shift from repressory to activatory histone marks and thereby affect adipogenesis. PARP1 itself is activated by DNA damage, which could be brought about by topoisomerase II activity. Topoisomerase II cuts DNA strands during replication (separation of DNA supercoils). However, the later stages of adipocyte differentiation are accompanied by an exit from the cell cycle (28), thereby excluding this replication-dependent phenomenon as an explanation for the regulation by topoisomerase II. The induction of PARP1 by topoisomerase II in differentiating adipocytes is therefore likely to be mediated by a transient, site-specific double-strand DNA break at the promoters of PPARγ2-dependent target genes, as described for nuclear receptors (29).

PARP1 recruitment to the promoters of different PPARγ-dependent target genes was strongly enhanced upon PAR formation. This observation is in contrast to earlier *in vitro* studies, suggesting that automodified PARP1 is released from chromatin (17) or that PJ34 treatment does not affect PARP1 binding to target gene promoters (27). However, in *Drosophila*, the presence and activity of PARP1 is also required to maintain a transcription compartment by retaining transcription factors (30), which also suggests a function for PARP1 enzyme activity at the promoters of active genes as our findings in this study.

The cellular PAR levels are determined by the synthesizing activities of PARP and the degradation by poly-(ADP-ribose)glycohydrolase, the main cellular enzyme required for PAR degradation. The fact that PAR levels were reduced upon the inhibition of PARP1 shortly before the extraction (data not shown) suggests that these PAR polymers are not stable but rather constantly formed and degraded. Consequently, the strong PAR formation during adipocyte differentiation (as compared with the PAR formation as a response to genotoxic stress such as H_2O_2 treatment) must be due to constant synthesis, which has been documented for the late stages of adipogenesis (25). However, activation of ADP-ribosyltransferases and of PAR formation can drastically affect cellular metabolite levels, such as NAD^+, nicotinamide adenine dinucleotide phosphate, ATP, or glucose-6-phosphate and thereby even indirectly impair cell viability (31). Interestingly, NAD^+ levels during adipogenesis were slightly elevated (Supplemental Fig. 3) or even drastically increased during adipocyte differentiation of 3T3-L1 cells as described by others (3). This explains why the differentiated cells are not dying upon extensive PAR formation (due to the extended NAD^+ and subsequent ATP depletion) as suggested earlier (32). Thus, high NAD^+ levels may maintain PAR formation due to increased substrate availability in a DNA damage-independent manner. In summary, these data suggest that increased NAD^+ synthesis fuels the substantial PAR synthesis and thus allows a constant PAR turnover during adipogenesis.

In conclusion, our data reveal a novel metabolic function of PARP1 in adipose tissue and provide evidence that PARP1 and topoisomerase II regulate the adipogenic gene expression program. These observations additionally provide insight into the link between cellular metabolism (*e.g.* production of NAD^+), gene expression, and differentiation. It will be interesting to investigate whether the inhibition of ADP-ribose formation by PARP inhibitors affects the pathological conditions, such as metabolic disorders.

Materials and Methods

3T3-L1 cell culture and differentiation

3T3-L1 preadipocytes were cultured in DMEM containing 10% (vol/vol) fetal calf serum. On d 2 (2 d after 3T3-L1 prea-

dipocytes reached confluence), cells were induced to differentiate by insulin (5 μg/ml), 3-isobutyl-1-methylxanthine (0.5 mmol/liter), and dexamethasone (1 μmol/liter). On d 4, regular DMEM containing insulin (5 μg/ml) was substituted until d 7. Cells were differentiated in the presence or absence of PJ34 (10 μM), which was supplemented to cells every 24 h. Differentiation was monitored by morphological assessment and Oil-Red O staining. For Oil-Red O staining, cells were washed twice with PBS, fixed in 10% formaldehyde for 1 h, and stained for 10 min with 0.2% (wt/vol) Oil-Red O solution in 60% (vol/vol) isopropanol. Cells were then washed several times with water, and excess water was evaporated by placing the stained cultures at approximately 32 C. For the quantification of the staining, the Oil-Red O was extracted with 100% isopropanol from the cells and measured at 500 nm.

Reagents

Dexamethasone (D-4902), 3-isobutyl-1-methylxanthine (I-5879), insulin (I-9278), Oil-Red O (00625), and merbarone (M2070) were obtained from Sigma-Aldrich (St. Louis, MO). Anti-PARP (sc-7150) antibody was purchased from Santa Cruz Biotechnology, Inc. (Santa Cruz, CA), anti-PAR (51-8114KC) from BD Pharmingen (San Diego, CA), anti-H3 (1791-100) from Abcam (Cambridge, MA), anti-H3K9me3 (07-442) from Millipore (Bedford, MA), anti-H3K4me3 (07-473) from Millipore, and antitubulin (T6199) antibody from Sigma-Aldrich. PJ34 was purchased from Alexis Biochemicals (San Diego, CA) (ALX-270-289-0000).

Whole-cell extraction

Whole-cell extracts were prepared by lysing the cells for 20 min in radioimmunoprecipitation assay buffer [50 mM Tris (pH 8), 400 mM NaCl, 0.5% Nonidet P-40, 1% deoxycholate, 0.1% sodium dodecyl sulfate, 1 μg/ml pepstatin, 1 μg/ml bestatin, 2 μg/ml leupeptin, 2 mM phenylmethylsulfony lfluoride, 10 mM β-glycerophosphate, 1 mM NaF, and 1 mM dithiothreitol] at 4 C rotating on the wheels. Lysate was centrifuged for 20 min at 4 C at 14,000 rpm. Total proteins were loaded on 7.5% sodium dodecyl sulfate gels and blotted with anti-PAR, anti-PARP, anti-PPARγ, and antitubulin antibodies.

In vitro ADP-ribosylation assay

ADP-ribosylation assays were performed as earlier described (33). Briefly, 400 nM PARP1 was incubated with 100 nM ^{32}P-NAD$^+$ and 200 nM DNA in PARP reaction buffer in the presence or absence of PJ34 (20 μM) or merbarone (20, 60, or 80 μM).

NAD measurements

For NAD$^+$ measurements, 0.5×10^{-6} cells of differentiated or undifferentiated 3T3-L1 cells were pelleted, and total NAD$^+$ was measured using the EnzyChrom NAD$^+$/NADH Assay kit (E2ND-100) from BioAssay Systems (Hayward, CA) according to the manufacturers' instructions.

RNA extraction and real-time PCR analysis

Total RNA from 3T3-L1 cells was extracted using TRIzol (Invitrogen, Carlsbad, CA) with a deoxyribonuclease step. Equal amount of RNA were reverse transcribed using the High-Capacity cDNA Reverse Transcription kit (Applied Biosystems, Foster City, CA). Real-time PCR was performed using the Rotor-Gene 3000 (Corbett Life Science, now QIAGEN, Valencia, CA). *Cyclophilin* was chosen as the internal control for normalization after screening several candidate genes.

Chromatin immunoprecipitation

ChIP experiments were performed as described earlier (34).

Stable PARP1 knockdown in 3T3-L1 cells

Generation of viruses and transduction of cells was done as described earlier (35). Briefly, pRDI vector expressing PARP1 shRNA was used to transduce 3T3-L1 cells. The shRNA was directed against the sequence encoding the catalytic region of PARP1, which was amplified with the following primers: 5′-GATCCCCAAGAGCGACGCTTATTACTGTTTCAAGAGAACAGTAATAAGCGTCGCTCTTTTTTTGGAAA-3′ (sense) and 5′-AGCTTTTCCAAAAAAAGAGCGACGCTTATTACTGTTCTCTTGAAACAGTAATAAGCGTCGCTCTTGGG-3′ (antisense). Transduced cells were selected through puromycin-resistance gene.

Acknowledgments

We thank F. Freimoser for revisions during the preparation of this manuscript.

Address all correspondence and requests for reprints to: Michael O. Hottiger, Winterthurerstrasse 190, 8057 Zurich, Switzerland. E-mail: hottiger@vetbio.uzh.ch.

This work was supported by the Swiss National Science Foundation Grant 31-122421 and by the Kanton of Zurich (M.O.H.).

Disclosure Summary: The authors have nothing to disclose.

References

1. **Hotamisligil GS, Shargill NS, Spiegelman BM** 1993 Adipose expression of tumor necrosis factor-α: direct role in obesity-linked insulin resistance. Science 259:87–91
2. **Havel PJ** 2002 Control of energy homeostasis and insulin action by adipocyte hormones: leptin, acylation stimulating protein, and adiponectin. Curr Opin Lipidol 13:51–59
3. **Fukuwatari T, Doi M, Sugimoto E, Kawada T, Shibata K** 2001 Changes of pyridine nucleotide levels during adipocyte differentiation of mouse 3T3-L1 cells. Biosci Biotechnol Biochem 65:2565–2568
4. **Green H, Meuth M** 1974 An established pre-adipose cell line and its differentiation in culture. Cell 3:127–133
5. **Siersbæk R, Nielsen R, John S, Sung MH, Baek S, Loft A, Hager GL, Mandrup S** 2011 Extensive chromatin remodelling and establishment of transcription factor 'hotspots' during early adipogenesis. EMBO J 30:1459–1472
6. **Tontonoz P, Spiegelman BM** 2008 Fat and beyond: the diverse biology of PPARγ. Annu Rev Biochem 77:289–312
7. **Rosen ED, Hsu CH, Wang X, Sakai S, Freeman MW, Gonzalez FJ, Spiegelman BM** 2002 C/EBPα induces adipogenesis through PPARγ: a unified pathway. Genes Dev 16:22–26
8. **Lefterova MI, Zhang Y, Steger DJ, Schupp M, Schug J, Cristancho A, Feng D, Zhuo D, Stoeckert Jr CJ, Liu XS, Lazar MA** 2008 PPARγ

and C/EBP factors orchestrate adipocyte biology via adjacent binding on a genome-wide scale. Genes Dev 22:2941–2952
9. **Vidal-Puig AJ, Considine RV, Jimenez-Liñan M, Werman A, Pories WJ, Caro JF, Flier JS** 1997 Peroxisome proliferator-activated receptor gene expression in human tissues. Effects of obesity, weight loss, and regulation by insulin and glucocorticoids. J Clin Invest 99: 2416–2422
10. **Jones JR, Barrick C, Kim KA, Lindner J, Blondeau B, Fujimoto Y, Shiota M, Kesterson RA, Kahn BB, Magnuson MA** 2005 Deletion of PPARγ in adipose tissues of mice protects against high fat diet-induced obesity and insulin resistance. Proc Natl Acad Sci USA 102:6207–6212
11. **Medina-Gomez G, Gray SL, Yetukuri L, Shimomura K, Virtue S, Campbell M, Curtis RK, Jimenez-Linan M, Blount M, Yeo GS, Lopez M, Seppänen-Laakso T, Ashcroft FM, Oresic M, Vidal-Puig A** 2007 A PPAR γ 2 prevents lipotoxicity by controlling adipose tissue expandability and peripheral lipid metabolism. PLoS Genet 3:e64
12. **Hottiger MO, Hassa PO, Lüscher B, Schüler H, Koch-Nolte F** 2010 Toward a unified nomenclature for mammalian ADP-ribosyltransferases. Trends Biochem Sci 35:208–219
13. **Hassa PO, Haenni SS, Elser M, Hottiger MO** 2006 Nuclear ADP-ribosylation reactions in mammalian cells: where are we today and where are we going? Microbiol Mol Biol Rev 70:789–829
14. **D'Amours D, Desnoyers S, D'Silva I, Poirier GG** 1999 Poly(ADP-ribosyl)ation reactions in the regulation of nuclear functions. Biochem J 342(Pt 2):249–268
15. **Ogino H, Nozaki T, Gunji A, Maeda M, Suzuki H, Ohta T, Murakami Y, Nakagama H, Sugimura T, Masutani M** 2007 Loss of Parp-1 affects gene expression profile in a genome-wide manner in ES cells and liver cells. BMC Genomics 8:41
16. **Tulin A, Spradling A** 2003 Chromatin loosening by poly(ADP)-ribose polymerase (PARP) at *Drosophila* puff loci. Science 299: 560–562
17. **Kim MY, Mauro S, Gévry N, Lis JT, Kraus WL** 2004 NAD+-dependent modulation of chromatin structure and transcription by nucleosome binding properties of PARP-1. Cell 119:803–814
18. **Krishnakumar R, Kraus WL** 2010 The PARP side of the nucleus: molecular actions, physiological outcomes, and clinical targets. Mol Cell 39:8–24
19. **de Murcia JM, Niedergang C, Trucco C, Ricoul M, Dutrillaux B, Mark M, Oliver FJ, Masson M, Dierich A, LeMeur M, Walztinger C, Chambon P, de Murcia G** 1997 Requirement of poly(ADP-ribose) polymerase in recovery from DNA damage in mice and in cells. Proc Natl Acad Sci USA 94:7303–7307
20. **Wang ZQ, Auer B, Stingl L, Berghammer H, Haidacher D, Schweiger M, Wagner EF** 1995 Mice lacking ADPRT and poly-(ADP-ribosyl)ation develop normally but are susceptible to skin disease. Genes Dev 9:509–520
21. **Ntambi JM, Young-Cheul K** 2000 Adipocyte differentiation and gene expression. J Nutr 130:3122S–3126S
22. **Kouzarides T** 2007 Chromatin modifications and their function. Cell 128:693–705
23. **Okamura M, Inagaki T, Tanaka T, Sakai J** 2010 Role of histone methylation and demethylation in adipogenesis and obesity. Organogenesis 6:24–32
24. **Ju BG, Lunyak VV, Perissi V, Garcia-Bassets I, Rose DW, Glass CK, Rosenfeld MG** 2006 A topoisomerase IIβ-mediated dsDNA break required for regulated transcription. Science 312:1798–1802
25. **Pekala PH, Lane MD, Watkins PA, Moss J** 1981 On the mechanism of preadipocyte differentiation. Masking of poly(ADP-ribose) synthetase activity during differentiation of 3T3-L1 preadipocytes. J Biol Chem 256:4871–4876
26. **Bai P, Houten SM, Huber A, Schreiber V, Watanabe M, Kiss B, de Murcia G, Auwerx J, Ménissier-de Murcia J** 2007 Poly(ADP-ribose) polymerase-2 [corrected] controls adipocyte differentiation and adipose tissue function through the regulation of the activity of the retinoid X receptor/peroxisome proliferator-activated receptor-γ [corrected] heterodimer. J Biol Chem 282:37738–37746
27. **Krishnakumar R, Kraus WL** 2010 PARP-1 regulates chromatin structure and transcription through a KDM5B-dependent pathway. Mol Cell 39:736–749
28. **Shao D, Lazar MA** 1997 Peroxisome proliferator activated receptor γ, CCAAT/enhancer-binding protein α, and cell cycle status regulate the commitment to adipocyte differentiation. J Biol Chem 272: 21473–21478
29. **Lin C, Yang L, Tanasa B, Hutt K, Ju BG, Ohgi K, Zhang J, Rose DW, Fu XD, Glass CK, Rosenfeld MG** 2009 Nuclear receptor-induced chromosomal proximity and DNA breaks underlie specific translocations in cancer. Cell 139:1069–1083
30. **Zobeck KL, Buckley MS, Zipfel WR, Lis JT** 2010 Recruitment timing and dynamics of transcription factors at the Hsp70 loci in living cells. Mol Cell 40:965–975
31. **Berger SJ, Sudar DC, Berger NA** 1986 Metabolic consequences of DNA damage: DNA damage induces alterations in glucose metabolism by activation of poly (ADP-ribose) polymerase. Biochem Biophys Res Commun 134:227–232
32. **Berger NA, Sims JL, Catino DM, Berger SJ** 1983 Poly(ADP-ribose) polymerase mediates the suicide response to massive DNA damage: studies in normal and DNA-repair defective cells. Princess Takamatsu Symp 13:219–226
33. **Messner S, Altmeyer M, Zhao H, Pozivil A, Roschitzki B, Gehrig P, Rutishauser D, Huang D, Caflisch A, Hottiger MO** 2010 PARP1 ADP-ribosylates lysine residues of the core histone tails. Nucleic Acids Res 38:6350–6362
34. **Santoro R, Li J, Grummt I** 2002 The nucleolar remodeling complex NoRC mediates heterochromatin formation and silencing of ribosomal gene transcription. Nat Genet 32:393–396
35. **Ariumi Y, Turelli P, Masutani M, Trono D** 2005 DNA damage sensors ATM, ATR, DNA-PKcs, and PARP-1 are dispensable for human immunodeficiency virus type 1 integration. J Virol 79: 2973–2978

Supplemental Figures

Figure S1. PJ34 inhibits lipid accumulation in 3T3-L1 cells.

(A) 3T3-L1 pre-adipocytes were subjected to adipocyte differentiation. Total cell extracts from the indicated days and PAR formation were analyzed by Western blotting. **(B)** Oil-Red O staining of 3T3-L1 cells that are subjected to 7 days of adipocyte differentiation protocol in the presence of PJ34.

Figure S2. Effect of PJ34 treatment at day 6 and 7 on PPARγ2-dependent gene expression and Merbarone doe not influence PARP1's enzymatic activity

(A) Real-time RT-PCR analysis on day 7 from differentiated 3T3-L1 cells that were treated at days 5 and 6 of differentiation with DMSO control or 10μM PJ34. mRNA levels were normalized with *Cyclophilin.* Results are from three independent experiments, mean ± SEM. **(B)** 3T3-L1 pre-adipocytes were subjected to adipocyte differentiation during 7 days in the absence or presence of PARP inhibitor PJ34 (10 μM). Inhibitor was supplemented daily. Real-time RT-PCR analysis is shown. Presented values are not normalized. Results are from 3 independent experiments mean ±SEM. **(C)** 400nM PARP1 was incubated with 100nM ^{32}P-NAD and 200nM DNA in PARP reaction buffer in the presence of 20μM PJ34 or 20μM, 60μM and 80μM Merbarone (M). For each condition a solvent control was carried out. The mixture was incubated for 10 min at 30°C. Proteins were separated by SDS-PAGE and ADP-ribosylation was analyzed by autoradiography.

S3. NAD^+ concentration in undifferentiated and differentiated adipocytes

3T3-L1 pre-adipocytes were subjected to adipocyte differentiation during 7 days. NAD^+ levels of differentiated or undifferentiated cells were measured. Results show NAD^+ levels per mg protein. Results are from 3 independent experiments, mean ± SEM.

Erener *et al*., Figure S1

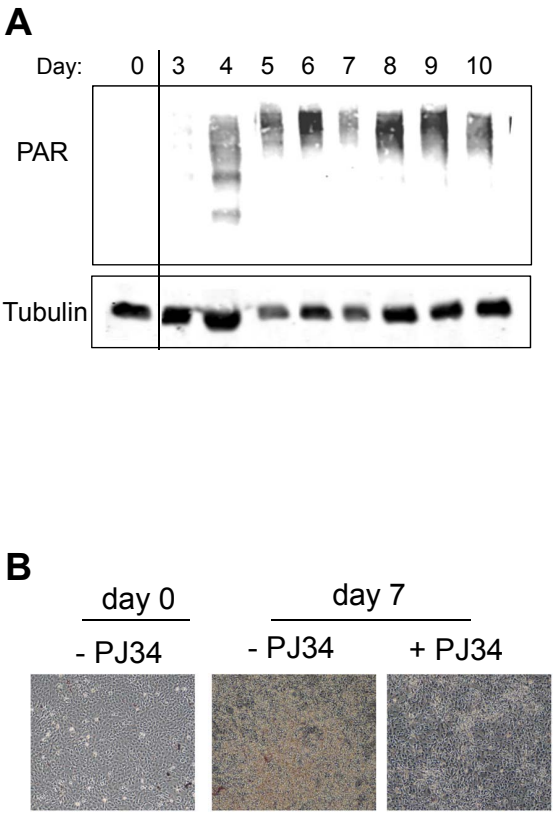

Erener *et al*., Figure S2

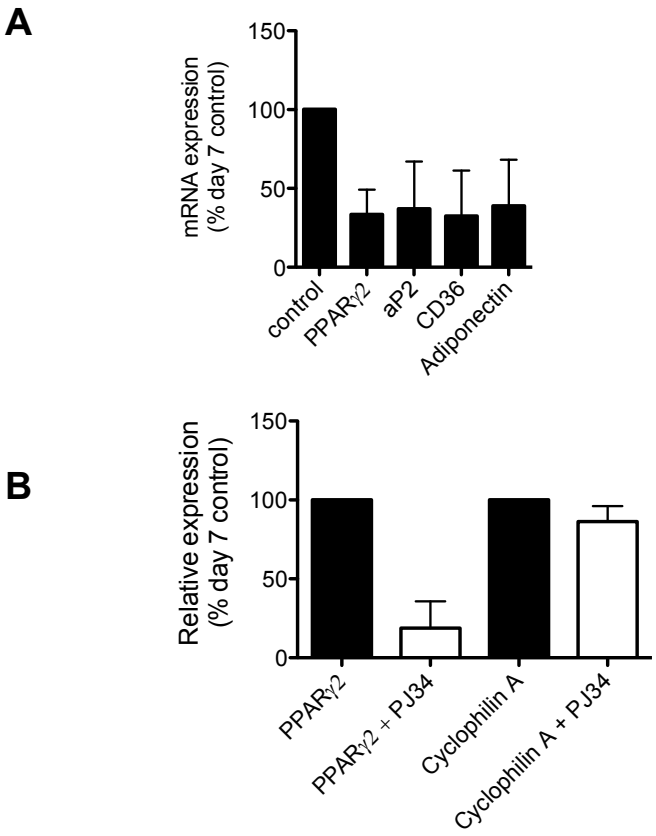

Erener *et al*., Figure S3

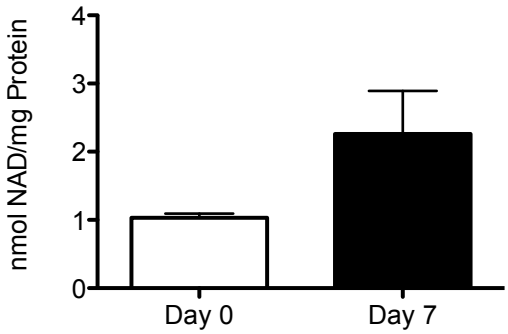

The FASEB Journal • Research Communication

ARTD1 deletion causes increased hepatic lipid accumulation in mice fed a high-fat diet and impairs adipocyte function and differentiation

Süheda Erener,[*,†] Ali Mirsaidi,[‡,§] Mareike Hesse,[*,†] André N. Tiaden,[‡] Helga Ellingsgaard,[‖] Radina Kostadinova,[*] Marc Y. Donath,[‖] Peter J. Richards,[‡,§] and Michael O. Hottiger[*,§,1]

[*]Institute of Veterinary Biochemistry and Molecular Biology, [†]Life Science Zurich Graduate School, Molecular Life Science Program, [‡]Competence Centre for Applied Biotechnology and Molecular Medicine, Bone and Stem Cell Research Group, and [§]Zurich Centre for Integrative Human Physiology (ZIHP), Institute of Physiology, University of Zürich, Zurich, Switzerland; and [‖]Clinic for Endocrinology, Diabetes and Metabolism, University Hospital Basel, Basel, Switzerland

ABSTRACT **ADP-ribosyltransferase *Diphtheria* toxin-like 1 [ARTD1; formerly called poly-ADP-ribose polymerase 1 (PARP1)] is a chromatin-associated enzyme involved in regulating metabolic homeostasis. The liver is at the core of glucose and lipid metabolism and is significantly affected by obesity and the metabolic syndrome. Here, we show that when fed a high-fat diet (HFD), mice lacking *ARTD1* developed exacerbated hepatic steatosis. *ARTD1*$^{-/-}$ mice had a 19% higher liver weight than wild-type (*WT*) animals and exhibited a significantly increased serum concentration of cholesterol (38%) and impaired glucose tolerance. In addition, adipocyte function and size were significantly reduced in *ARTD1*$^{-/-}$ mice fed an HFD (7794 μm^2 for *WT* and 5579 μm^2 for *ARTD1*$^{-/-}$ mice). The significantly reduced adipogenic differentiation of adipose-derived stromal cells (ASCs) isolated from *ARTD1*$^{-/-}$ mice (28 *vs.* 11% Oil red O-positive cells in *WT* and *ARTD1*$^{-/-}$ ASCs, respectively) suggested that impaired adipogenesis as the underlying cause for this adipose tissue malfunction. This function of ARTD1 was specific for adipogenesis, since osteogenic differentiation was not affected by the *ARTD1* deletion. In summary, we show that *ARTD1*$^{-/-}$ mice fed an HFD display impaired adipogenesis and show exacerbated hepatic steatosis, which can have important implications for nonalcoholic fatty liver disease.—Erener, S., Mirsaidi, A., Hesse, M., Tiaden, A. N., Ellingsgaard, H., Kostadinova, R., Donath, M. Y., Richards, P. J., Hottiger, M. O. *ARTD1* deletion causes increased hepatic lipid accumulation in mice fed a high-fat diet and impairs adipocyte function and differentiation. *FASEB J.* 26, 2631–2638 (2012). www.fasebj.org**

Key Words: adipogenesis · ADP-ribosylation · liver · PARP-1

Obesity is a complex metabolic disorder characterized by an excess of body fat that is closely associated with other serious health conditions, such as heart disease and diabetes (1). White adipose tissue (WAT) is the predominant storage site for excess energy in the form of fat in adult humans, but also functions as an important endocrine organ (2, 3). However, it appears that low-grade chronic inflammation (metaflammation) in metabolic tissues is the underlying mechanism leading to the disruption of nutrient and energy metabolism (4, 5).

ADP-ribosyltransferase *Diphtheria* toxin-like 1 [ARTD1; formerly called poly-ADP-ribose polymerase 1 (PARP1); ref. 6] is a chromatin-associated enzyme that modifies itself and target proteins by transferring the ADP-ribose moieties from nicotinamide adenine dinucleotide (NAD^+) to specific acceptor residues on target proteins (7). ARTD1 is thus able to regulate protein function, chromatin compaction, and gene expression (7, 8) and is subsequently involved in numerous biological phenomena, such as stress response, inflammation, and differentiation or cell cycle regulation, as well as in infectious diseases and cancer (9). Mice lacking *ARTD1* also exhibit metabolic phenotypes, such as

Abbreviations: aP2, adipocyte protein 2; ARTD, ADP-ribosltransferase *Diphtheria* toxin-like; ASC, adipocyte-derived stromal cell; ATGL, adipose triglyceride lipase; CD36, cluster of differentiation 36; DMEM, Dulbecco's modified eagle medium; FBS, fetal bovine serum; FFA, free fatty acid; Glut4, glucose transporter type 4; GTT, glucose tolerance test; H&E, hematoxylin and eosin; HFD, high-fat diet; HSL, hormone sensitive lipase; ITT, insulin tolerance test; NAD^+, nicotinamide adenine dinucleotide; NAFLD, nonalcoholic fatty liver disease; ND, normal diet; PAR, poly-ADP-ribose; PPARγ, peroxisome proliferator-activated receptor γ; PARP, poly-ADP-ribose polymerase; PBS, phosphate-buffered saline; WAT, white adipose tissue; WT, wild type

[1] Correspondence: Institute of Veterinary Biochemistry and Molecular Biology, University of Zürich, Winterthurerstrasse 190, Zürich 8057, Switzerland. E-mail: hottiger@vetbio.uzh.ch

doi: 10.1096/fj.11-200212

This article includes supplemental data. Please visit *http://www.fasebj.org* to obtain this information.

alterations in body weight, WAT formation, and the development of high-fat diet (HFD)-induced obesity, although these vary depending on the strain background (10–12). The deletion of *ARTD1*, a major NAD^+-consuming enzyme, can lead to increased cellular NAD^+ levels (10). Consequently, *ARTD1* deletion can activate NAD^+-dependent enzymes, such as sirtuins, and thereby indirectly induce phenotypes, such as increased mitochondrial biosynthesis and altered energy metabolism (10, 13). Furthermore, the enzymatic activity of ARTD1 also directly partakes in the sustained expression of the key regulator of adipocyte function, peroxisome proliferator-activated receptor γ (PPARγ; ref. 14). In cell culture, ARTD1 modulates PPARγ-dependent gene expression [such as cluster of differentiation 36 (*CD36*) or adipocyte protein 2 (*aP2*)] and adipocyte function (14) and may thus also be involved in adipogenesis *in vivo*.

To identify and characterize such direct *in vivo* functions of ARTD1 in metabolism, we analyzed *ARTD1*$^{-/-}$ and wild-type (*WT*) mice of the C57BL/6 background fed an HFD. Here, we report that deletion of *ARTD1* caused increased hepatic fat accumulation and dyslipidemia in mice exposed to HFD. These effects correlated with increased PPARγ2 target gene expression in liver samples from *ARTD1*$^{-/-}$ mice fed an HFD as well as with elevated serum levels of cholesterol, smaller adipocyte size, and impaired adipocyte differentiation. These results define a novel function for ARTD1 in the development of hepatic steatosis, as well as in the modulation of adipocyte differentiation and in adipose tissue function *in vivo*. These findings may thus provide novel insights into the molecular pathways that govern the onset, development, and progression of prevalent human diseases such as nonalcoholic fatty liver disease (NAFLD).

MATERIALS AND METHODS

Animals and animal care

In the *ARTD1*$^{-/-}$ male C57BL/6 mice used in this study and obtained from Zhao-Qi Wang (Leibniz Institute for Age Research–Fritz Lipmann Institute, Jena, Germany), part of the second exon and second intron of the *ARTD1* gene is replaced with the neomycin resistance gene (15). *ARTD1*$^{-/-}$ and *WT* mice were fed an HFD consisting of 60% of calories from fat (S3282; Bio-Serv, Frenchtown, NJ, USA) starting at 6–8 wk of age for 14 wk. Control mice were fed a normal diet (ND) consisting of 4.5% fat. Animals were housed in a specific pathogen-free facility with a 12-h light-dark cycle and given free access to food and water. Animal experiments were performed according to the regulations of the Cantonal Veterinary Office (Zurich, Switzerland).

Culture and analysis of mouse adipocyte-derived stromal cells (ASCs)

ASCs were isolated, cultured, and analyzed as described previously (16). In short, fat pads were removed from male mice and digested with 0.1% collagenase A (Roche Diagnostics, Rotkreuz, Switzerland). Stromal cells were collected by centrifugation and cultured in supplemented Dulbecco's modified eagle medium (DMEM; low glucose with Glutamax; Invitrogen AG, Basel, Switzerland), 10% fetal bovine serum (FBS; Invitrogen), and antibiotics. Supernatant was replaced after 1 d with fresh complete medium and cells were used between passage 3 and 4. Total RNA was isolated and purified using TRIzol reagent (Invitrogen) and reverse transcribed using superscript II (Invitrogen) and random hexanucleotide primers (Promega AG, Dübendorf, Switzerland). mRNA expression analysis was performed with primers specific for *ARTD1* (Mm01321084_m1), *PPARγ2* (Mm00440940_m1), *aP2* (Mm00445878_m1), and glucose transporter type 4 (*GLUT4*; Mm00436615_m1) and by using the StepOnePlus Real-Time PCR System (Applied Biosystems/Life Technologies, Zug, Switzerland). All values were normalized to the *RPS12* ribosomal RNA (Mm00488728_m1).

Adipogenesis

To assess adipogenesis, ASCs were plated at 10,000 cells/cm^2 and incubated in adipogenic medium (DMEM supplemented with 10% FBS and 1 μM dexamethasone; Sigma-Aldrich, Buchs, Switzerland), 10 μg/ml insulin (Sigma-Aldrich), 0.1 mM indomethacin (Sigma-Aldrich), and 0.5 mM isobutyl methylxanthine (IBMX; Sigma-Aldrich). After 2 d, cells were switched to adipogenic medium without IBMX for up to 14 d. Triglyceride content was determined using 0.3% Oil Red O (Sigma-Aldrich), and adipocytes were counted in 30 fields of view by fluorescence microscopy.

Osteogenesis

ASCs were plated at 5000 cells/cm^2 and incubated in α-minimum essential medium (α-MEM; Invitrogen), supplemented with 10% FBS, 50 μM L-ascorbic acid 2-phosphate sesquimagnesium salt hydrate (Sigma-Aldrich), 10 mM β-glycerophosphate (Sigma-Aldrich), and 5 μM retinoic acid (Sigma-Aldrich) for up to 14 d with regular changes of medium. Mineralization in cell colonies was identified using Alizarin Red S (Sigma-Aldrich).

RNA extraction and real-time PCR analysis from WAT

Mouse tissues were isolated, rinsed in phosphate-buffered saline (PBS), frozen in liquid nitrogen and stored at −80°C until extraction. Total RNA was extracted from WAT using the RNeasy Lipid Tissue Kit (Qiagen, Hombrechtikon, Switzerland) according to the manufacturer's instructions, with the inclusion of a DNase digestion step. Total RNA from liver and also from 3T3-L1 cells was extracted using the Total RNA isolation mini kit (Macherey Nagel, Oensingen, Switzerland) with a DNase step. Equal amounts of RNA from 5–8 mice were pooled and reverse-transcribed using the high-capacity cDNA reverse transcription kit (Applied Biosystems/Life Technologies, Zug, Switzerland). Real-time PCR was performed using the Rotor-Gene 3000 (Corbett Life Science, now Qiagen) and SYBR Green using the primers listed in Supplemental Table S1. *Cyclophilin* was chosen as the internal control for normalization and for the relative quantification of gene expression.

Whole-cell extraction

Tissues were lysed in RIPA buffer (50 mM Tris, pH 8; 400 mM NaCl; 0.5% Triton Nonidet P-40; 1% DOC; 0.1% SDS; 1 μg/ml pepstatin; 1 μg/ml bestatin; 2 μg/ml leupeptin; 2 mM

PMSF; 10 mM β-glycerophosphate; 1 mM NaF; and 1 mM DTT), homogenized with a needle and syringe, and rotated for 20 min at 4°C. Lysate was centrifuged for 20 min at 4°C at 14,000 rpm. Total proteins were loaded on 7.5% SDS gels and blotted with anti-PAR and anti-tubulin antibodies.

Serum measurements

Serum insulin concentrations were measured with the insulin ELISA kit (Mercodia Inc., Uppsala, Sweden). Blood glucose was determined by using the FreeStyle Lite glucometer (Abbott, Baar, Switzerland).

Glucose tolerance tests (GTTs) and insulin tolerance tests (ITTs)

For the GTT, mice were unfed overnight (14 h); for the ITT, mice were unfed for 3 h. Glucose (1.2 g/kg body weight) or human recombinant insulin (HFD: 1.4 U/kg; ND: 0.75 U/kg) was injected intraperitoneally. Blood glucose concentrations were determined from tail using the FreeStyle Lite glucometer (Abbott).

Histology and cell-size measurement

Freshly isolated epididymal WAT and liver tissue from mice fed HFD was fixed in 4% formalin and embedded in paraffin. Sections were stained with hematoxylin and eosin (H&E) or Oil Red O. Adipocytes were photographed with a Leica DMR microscope (Leica Microsystems, Glattbrugg, Switzerland) and cell morphology and size were analyzed using the Leica IM 1000 software. Liver photographs were recorded using an Olympus AH-2 microscope (Olympus, Tokyo, Japan) equipped with an Axiocam camera (Carl Zeiss, Oberkochen, Germany).

RESULTS

ARTD1$^{-/-}$ mice fed HFD have increased liver weight and hepatic lipid deposition

To determine the role of ARTD1 in metabolic disorders, we analyzed 6–8 wk old *WT* and *ARTD1*$^{-/-}$ mice in the C57BL/6J background that were fed ND or HFD. *WT* and *ARTD1*$^{-/-}$ mice fed ND had identical body weights (Supplemental Fig. S1*A*). Both *WT* and *ARTD1*$^{-/-}$ mice fed HFD gained significantly more body weight as compared to those fed ND (identified as week 0; **Fig. 1*A***). Furthermore, in comparison to *ARTD1*$^{-/-}$ mice fed HFD, *WT* mice were heavier, which was not attributable to differences in food intake (Supplemental Fig. S1*B*). A pathological analysis revealed that the most apparent phenotype of the *ARTD1*$^{-/-}$ mice fed HFD was the significantly increased liver weight (Fig. 1*B*). Histological examination (H&E and Oil Red O staining) of liver sections revealed markedly increased hepatic lipid deposition in *ARTD1*$^{-/-}$ mice fed HFD, as compared to the *WT* controls (Fig. 1*C*), while no apparent difference was observed in mice fed ND (data not shown). H&E staining of skeletal muscle tissue of *WT* and *ARTD1*$^{-/-}$ mice did not reveal any difference (Fig. 1*C*).

ARTD1$^{-/-}$ mice fed HFD exhibit altered PPARγ2 target gene expression and dyslipidemia

Hepatic lipid accumulation is often associated with an ectopic induction of *PPARγ2* and PPARγ2-dependent gene expression in the liver and muscle (17). We therefore tested whether the increased lipid deposition in livers of *ARTD1*$^{-/-}$ mice correlated with alterations in PPARγ2 target gene expression in the liver. The expression of *PPARγ2* in *ARTD1*$^{-/-}$ livers was increased but not significantly different as compared to *WT* samples (**Fig. 2*A***). However, the PPARγ2 target genes *aP2* (fatty acid binding protein) and *LPL* (lipoprotein lipase) were significantly up-regulated in *ARTD1*$^{-/-}$ livers of mice fed HFD. Significantly increased compensatory expression was also observed for *PPARα*, a key regulator involved in fatty acid catabolism. Lipin, another highly inducible enzyme that is involved in triglyceride metabolism, was unaffected between the two genotypes, indicating that not all factors involved in lipid metabolism were changed in the livers of *ARTD1*$^{-/-}$ mice. These results, and in particular the strongly elevated expression of *aP2*, revealed that livers of *ARTD1*$^{-/-}$ mice fed HFD show gene expression

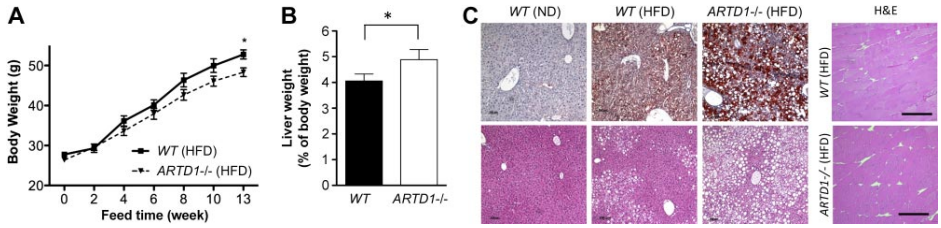

Figure 1. *ARTD1*$^{-/-}$ mice fed HFD display decreased weight gain and have reduced adipocyte size. *A*) Body weight of *WT* and *ARTD1*$^{-/-}$ mice that were fed HFD. HFD feeding started when mice were 6–8 wk old (time point 0; n=8–9 mice/group). *$P < 0.05$. *B*) Liver weight was measured and normalized with body weight (n=8–9 mice/group, means±SE). *$P < 0.05$, 14 wk after HFD. *C*) Representative images of Oil Red O-stained (top panels) or H&E-stained (bottom panels) sections of paraffin-embedded liver tissue from *WT* or *ARTD1*$^{-/-}$ mice fed HFD (n=4). H&E-stained skeletal muscle sections are shown as a control and for comparison (right panel).

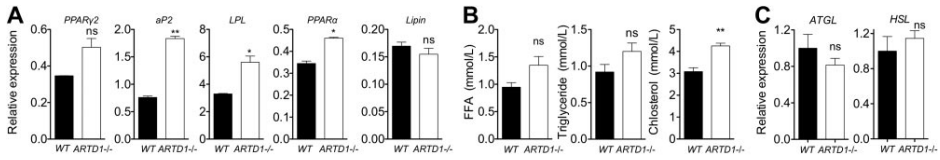

Figure 2. *ARTD1*$^{-/-}$ mice fed HFD exhibit altered PPARγ2 target gene expression and dyslipidemia. *A*) Real-time RT-PCR analysis of *PPARγ2* and PPARγ2 target genes in liver tissue obtained from *WT* and *ARTD1*$^{-/-}$ mice that were fed HFD (RNA of 7 mice pooled, means±SD of technical duplicates, 14 wk after HFD). *B*) Serum free fatty acid (FFA), triglyceride, and cholesterol levels were measured from independent samples of 5 *WT* and 4 *ARTD1*$^{-/-}$ mice. *C*) Real-time RT-PCR analysis of *ATGL* and *HSL* expression in WAT of *WT* and *ARTD1*$^{-/-}$ mice (RNA of 5–6 mice pooled, technical replicates, means±SD).

patterns typically associated with adipocytes and adipogenesis (17).

The hepatic lipid accumulation observed in *ARTD1*$^{-/-}$ mice suggested that the metabolic analytes might be altered in these animals. We therefore measured the plasma levels of free fatty acids (FFAs), triglycerides, and cholesterol. Indeed, *ARTD1*$^{-/-}$ mice displayed a marginal elevation in FFA and triglyceride levels as well as significantly increased cholesterol amounts, which also hinted at a disturbed lipid homeostasis in *ARTD1*$^{-/-}$ mice (Fig. 2*B*). However, lipolysis was likely not the cause for these alterations in lipid levels, since neither adipose triglyceride lipase (*ATGL*) nor hormone sensitive lipase (*HSL*) mRNA levels were significantly affected by the *ARTD1* deletion (Fig. 2*C*).

ARTD1$^{-/-}$ mice fed HFD exhibit defective glucose homeostasis

The increased FFA blood concentration and hepatic lipid accumulation can generate metabolic signals that impair the metabolization of glucose (18). To determine whether the hepatic lipid accumulation and dyslipidemia in *ARTD1*$^{-/-}$ mice is accompanied by abnormalities in glucose homeostasis, we performed GTTs in *WT* and *ARTD1*$^{-/-}$ mice fed HFD. Mice were injected with 1.2 g glucose/kg body weight, and glucose levels were quantified over a period of 2 h. Overall, *ARTD1*$^{-/-}$ mice had an 18% increased glucose content (area under curve) and required more time to clear the injected glucose, although the basal glucose levels were not significantly altered (**Fig. 3*A, B***). Since this analysis was performed with mice that experienced 14 h of food withdrawal, the differences between *WT* and *ARTD1*$^{-/-}$ mice may be underestimated (19). To explore the potential mechanism causing impaired glucose tolerance in *ARTD1*$^{-/-}$ mice, we examined aspects of insulin secretion in mice with and without *ARTD1*. A significant increase in plasma insulin was observed in *ARTD1*$^{-/-}$ mice as compared to *WT* mice following an i.p. glucose injection (Fig. 3*C*), thus indicating that β-cell function is unlikely to be impaired in *ARTD1*$^{-/-}$ mice. This insulin burst, which was not observed in *WT* mice, may hide elevated glucose levels in the *ARTD1*$^{-/-}$ mice at earlier time points. We next asked whether insulin sensitivity contributes to this phenotype. To assess whole-body insulin sensitivity, ITTs were performed in mice after 12 wk of exposure to HFD. Mice were injected with 1.4 U insulin/kg body weight, and glucose levels were determined during 90 min. Serum glucose levels of *ARTD1*$^{-/-}$ mice were 20% higher as compared to the *WT* control (area under curve), which is suggestive of a tendency toward insulin resistance, but this effect was not significant (Fig. 3*D*).

Comparable analysis with animals fed the ND revealed that glucose levels and response to GTTs and ITTs did not significantly change between the two genotypes (Supplemental Fig. S1*C–E*). Furthermore, insulin-stimulated AKT phosphorylation in muscle and WAT tissue from *WT* and *ARTD1*$^{-/-}$ mice fed ND was

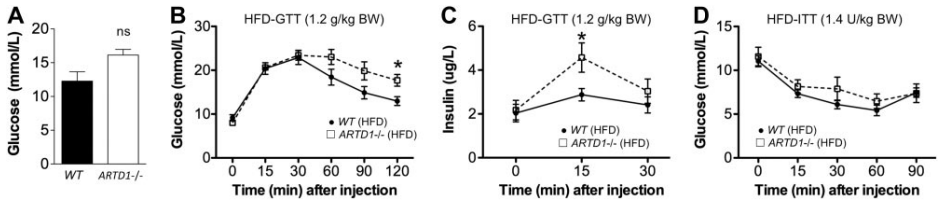

Figure 3. *ARTD1*$^{-/-}$ mice exhibit deteriorated glucose homeostasis. *A*) Serum glucose levels were measured from *WT* and *ARTD1*$^{-/-}$ mice. *B*) GTT: mice were injected with glucose (1.2 g/kg body weight), and glucose levels were quantified over a period of 2 h. *C*) Serum insulin levels during the GTT shown in *B*. *D*) ITT: mice were injected with insulin (1.4 U/kg body weight), and glucose levels were determined over a period of 90 min. Values are means ± SE, $n = 5–6$ mice/group. *$P < 0.05$, 12 wk after HFD.

also comparable (Supplemental Fig. S1*F*) suggesting that ARTD1 does not have a direct role in glucose homeostasis and insulin signaling under ND, but that the changes observed with HFD were rather the consequence of dyslipidemia and excessive lipid accumulation in the liver.

Adipocyte size and poly-ADP-ribose (PAR) formation in *ARTD1*$^{-/-}$ mice

We have recently reported that ARTD1 regulates adipogenesis *in vitro* (14), and PPARγ deletion in mouse adipose tissue was shown to cause increased lipid deposition in the livers (20). Our results on hepatic lipid accumulation and the dyslipidemic phenotype in *ARTD1*$^{-/-}$ mice fed HFD encouraged us to investigate the role of ARTD1 on adipocyte and WAT function *in vivo*. We therefore analyzed WAT from *WT* and *ARTD1*$^{-/-}$ mice. Surprisingly, neither the expression of *PPARγ2* or its target genes *aP2* and *CD36* nor the inflammatory genes *IL-1*β, *IL-13ra*, and *MCP1* differed between the *WT* and *ARTD1*$^{-/-}$ WAT samples from mice fed HFD (**Fig. 4*A***) and Supplemental Fig. S2). However, *ARTD1*$^{-/-}$ WAT tissue from mice fed HFD expressed less *IL-6*, which is a main regulator of inflammation. In addition, relative mRNA levels of the inflammatory genes *IL-10* and *IL-12* and of the macrophage specific genes *Pu.1* and *MPEG 1* were also reduced, while *SAA3* transcription was elevated. These results showed that a subset of the inflammatory genes was affected. Moreover, histological analysis of epididymal WAT from *ARTD1*$^{-/-}$ mice revealed a profound change in adipose tissue morphology, as evidenced by the significant reduction in adipocyte size (Fig. 4*B*, *C*). These results suggest that altered adipose tissue morphology likely impaired the storage of excess lipids in *ARTD1*$^{-/-}$ mice fed HFD and thus caused a pathological lipid accumulation in the liver. This significant effect of *ARTD1* deficiency on lipid metabolism and on the size of adipocytes from *ARTD1*$^{-/-}$ mice fed HFD suggests a fundamental role for ARTD1 in adipocyte function. Since we have recently shown that PAR formation is strongly induced in 3T3-L1 cells after 7 d of adipogenic induction (14), we investigated whether PAR was also formed in mature adipocytes *in vivo*. We could not detect PAR formation in WAT of *WT* mice that were fed ND (data not shown), but a distinct PAR signal was observed in the WAT extracts of *WT* mice (but not in the WAT of *ARTD1*$^{-/-}$ mice) that were maintained on HFD (Fig. 4*D*), suggesting that high energy diet (nutrient availability) induced ADP-ribosylation in WAT *in vivo* and in an ARTD1-dependent manner.

Adipogenic gene expression in differentiating aASCs is dependent on ARTD1

The *in vivo* results obtained from the studies with *ARTD1*$^{-/-}$ mice suggested that ARTD1 and PAR formation are centrally involved in adipose tissue activities. In addition, ARTD1 and PAR formation have been implicated in chromatin regulation (21) and were shown to affect PPARγ2-dependent gene expression and adipocyte function in differentiating 3T3-L1 cells (14, 21). We therefore hypothesized that ARTD1 may also affect the differentiation and development of functional adipocytes *in vivo*.

We tested this hypothesis by using ASCs, which can be easily isolated and expanded and have the ability to differentiate into several types of mesenchymal tissue. Differentiating ASCs are an established experimental system to study adipocyte differentiation (22). To study the role of ARTD1 and poly-ADP-ribosylation in adipogenesis, we compared ASCs from *ARTD1*$^{-/-}$ and from *WT* mice. In uninduced ASCs from *WT* mice, *ARTD1* expression levels were high and increased further at d 10 after the induction of adipogenesis (**Fig. 5*A***). Transcripts of the adipogenesis marker genes *PPARγ2*, *aP2*, and *GLUT4* were not detectable prior to the induction of adipogenesis but increased significantly on adipogenic induction in *WT* mice (Fig. 5*B–D*). In contrast, *PPARγ2*, *aP2*, and *GLUT4* expression remained at significantly lower levels in ASCs from *ARTD1*$^{-/-}$ mice throughout adipogenesis (Fig. 5*B–D*). The marked

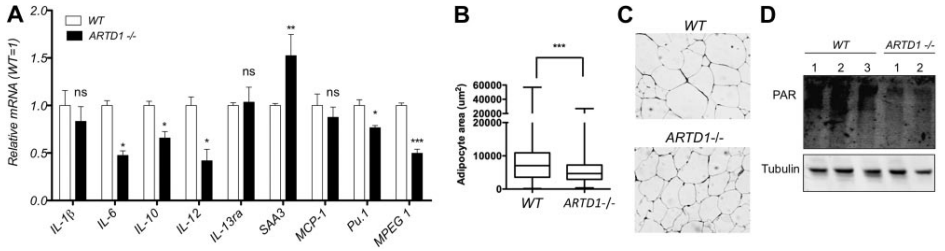

Figure 4. Adipocyte size and PAR formation in *ARTD1*$^{-/-}$ mice. *A*) Real-time RT-PCR analysis in total cell extracts from epididymal WAT of *WT* and *ARTD1*$^{-/-}$ mice that were fed HFD. mRNA levels were normalized with *cyclophilin A*. Results are means of 5–6 pooled mice, means ± SD of technical replicates. ns, not significant. *$P < 0.05$; **$P < 0.01$; ***$P < 0.0001$. *B*) Whisker plot of adipocyte area from evaluation of 450 adipocytes from 4–5 independent mice. ***$P < 0.0001$ comparing mean adipocyte area. *C*) Representative images of H&E-stained epididymal adipose tissue from *WT* and *ARTD1*$^{-/-}$ mice. *D*) PAR detection in total cell extracts from epididymal WAT of *WT* and *ARTD1*$^{-/-}$ mice that were fed HFD. All panels: 14 wk after HFD.

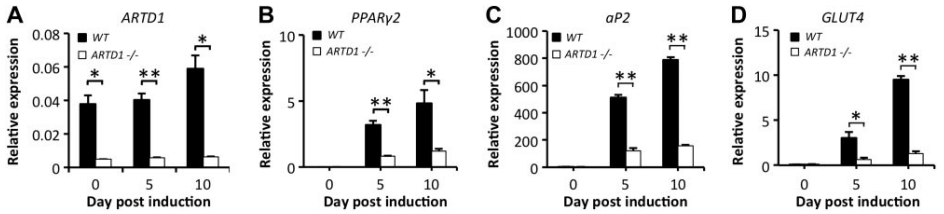

Figure 5. Adipogenesis is impaired in ASCs from *ARTD1*$^{-/-}$ mice. Expression levels of *ARTD1* (*A*) *PPARγ2* (*B*), *aP2* (*C*), and *GLUT4* (*D*) were evaluated by qRT-PCR over 0, 5, and 10 d of adipogenic differentiation. Expression value of each gene was normalized to the amount of ribosomal protein S12 (*RPS12*) RNA in order to calculate relative amounts of mRNA. *$P < 0.05$, **$P < 0.01$.

effect of *ARTD1* deletion on adipogenic gene expression suggests that ARTD1 is a major regulator of normal ASC differentiation.

Functional characterization of adipogenic ASCs isolated from *ARTD1*$^{-/-}$ mice

After 10 d of adipogenic differentiation, Oil Red O staining revealed a significantly higher percentage of mature adipocytes in ASC cultures isolated from *WT* mice as compared to *ARTD1*$^{-/-}$ mice (**Fig. 6*A***). To further study the link between *ARTD1* and adipogenesis, we assessed ASC differentiation in the presence of the three PARP inhibitors (PJ34, olaparib, and nicotinamide) by Oil Red O staining (Fig. 6*B–D*). All three compounds significantly reduced the percentage of Oil Red O-positive cells in a concentration-dependent manner. Interestingly, the detrimental effect of *ARTD1* loss of function on ASC adipogenesis was much less apparent in ASCs undergoing osteogenesis, thus suggestive of a lineage-specific role for ARTD1 in mesenchymal stem cell differentiation (Supplemental Fig. S3). These results are in agreement with the strong and specific influence of the *ARTD1* deletion on PPARγ2-dependent gene expression in adipose tissue and thus further highlight the importance of ADP-ribosylation in adipogenesis.

Taken together, these results demonstrate that *ARTD1*$^{-/-}$ deficiency in mice affects adipocyte function *in vivo*, and lipid deposition in the liver. This correlates with the up-regulated expression of hepatic *PPARγ2* and its target genes involved in fatty acid metabolism in *ARTD1*$^{-/-}$ mice. The effect of ARTD1 and PAR formation on the adipogenic differentiation process may represent the underlying cause for the *in vivo* effects on WAT function and lipid deposition in *ARTD1*$^{-/-}$ mice.

DISCUSSION

In the present study, *ARTD1*$^{-/-}$ mice of the C57BL/6 background were fed HFD, and adipocyte and WAT function were analyzed. Several independent groups have previously reported significant differences in the body weight of adult *WT* and *ARTD1*$^{-/-}$ mice from various backgrounds (15, 23). While we and others (10) have observed a decreased body weight in C57BL/6 *ARTD1*$^{-/-}$ mice fed HFD, *ARTD1*$^{-/-}$ mice of the

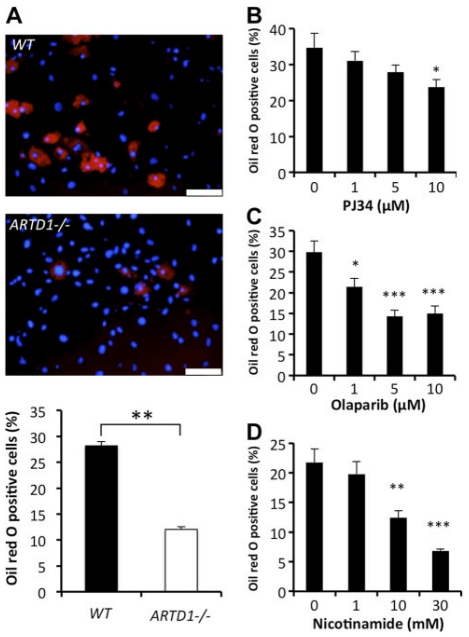

Figure 6. Triglyceride accumulation is decreased in adipogenic ASCs from *ARTD1*$^{-/-}$ mice. *A*) Representative fluorescent images of ASCs stained with Oil Red O (red) and Hoechst 33342 nuclear stain (blue). Scale bars = 150 μm. Percentage of cells demonstrating triglyceride accumulation was quantified in ASCs at d 10. *B–D*) ASCs from *WT* mice were induced to adipogenic differentiation in the presence of the ARTD1 inhibitors PJ34 (*B*), olaparib (*C*), and nicotinamide (*D*), and the percentage of cells demonstrating triglyceride accumulation was quantified at d 10. All differentiation studies were carried out using ASCs at passage 3 to 4 and were performed in triplicate. *$P < 0.05$, **$P < 0.01$, ***$P < 0.01$.

SV129 background have been shown to be more susceptible to HFD-induced obesity (11). However, mice of the C57BL/6 background are readily susceptible to diet-induced obesity, irrespective of the presence or absence of ARTD1 (12). Our findings of lower body weight, increased liver weight, smaller adipocytes, elevated serum cholesterol levels, and impaired glucose tolerance in *ARTD1*$^{-/-}$ mice suggest that lipid allocation is impaired. These results differ from recently published observations with *ARTD1*$^{-/-}$ mice of the same strain background (10), although hepatic lipid accumulation was not assessed in this study. However, it should be noted that the two C57BL/6 *ARTD1*$^{-/-}$ mouse strains were created independently by targeting different *ARTD1* exons (15, 23), and as such, have given rise to certain age-related disparities, as evidenced by alterations in telomere lengths (24, 25). Whether such differences also account for the contradicting effects of the *ARTD1* deletion on lipid metabolism remains to be determined. In addition, the metabolic differences between the two studies using C57BL/6 *ARTD1*$^{-/-}$ mice might also be due to the fact that we started HFD feeding earlier (when the mice were 6–8 wk old), performed our analysis later (after 12 wk of HFD feeding) and used an HFD preparation from a different supplier with slightly different composition (10).

In the present study, PAR formation was only observed in *WT* mice and on HFD feeding. The absence of PAR formation in the WAT of *ARTD1*$^{-/-}$ animals indicated that PAR formation in WAT was dependent on nutrient availability and on ARTD1. Alterations in PAR formation due to *ARTD1* deletion could potentially change NAD^+ metabolism in these animals and thereby cause the activation of sirtuin 1 (SIRT1; ref. 10). Altered sirtuin activity may, in turn, affect adipocyte gene expression and function, metabolism, or number of mitochondria, for example, through the deacetylation of Forkhead box protein O1 (FOXO1; refs. 10, 26–28). Such indirect effects cannot be excluded, but our results describing the effects of *ARTD1* deletion on ASC adipogenesis also point to a direct effect of ARTD1 and ADP-ribosylation. These findings are in agreement with our earlier *in vitro* observation, where ARTD1 activity and ADP-ribosylation were induced at d 7 during adipogenesis and crucial for the sustained expression of PPARγ2 and CCAAT/enhancer-binding protein α (C/EBP-α), but not for the upstream regulator C/EBP-β (14). In the current study, ASCs from *ARTD1*$^{-/-}$ mice differentiated less efficiently into mature adipocytes but were capable of undergoing normal osteogenesis, thus confirming that ARTD1 plays a lineage-specific role in ASC differentiation. Further studies are needed to confirm the involvement of PAR formation in adipogenesis and also its role in the regulation of PPARγ2-dependent gene expression in WAT. The fact that three of the analyzed inflammatory genes (*IL-6*, *IL-10*, and *IL-12*) were affected by the *ARTD1* deletion suggests a limited and specific effect on only a subset of the genes expressed in WAT *in vivo*. Interestingly, two macrophage-specific genes (*Pu.1* and *MPEG 1*) exhibited reduced mRNA levels, alluding to a possible involvement of ARTD1 in macrophage differentiation.

The results presented here point to a direct and specific involvement of ARTD1 in adipogenesis *in vivo*. However, other genes or compensatory mechanisms seem to assure WAT formation in the absence of ARTD1. Apart from this, our results suggest that ARTD1 is required for efficient adipogenesis and that *ARTD1* ablation limits lipid storage in adipocytes, restricts adipocyte size, and causes hepatic lipid deposition. It therefore appears that ARTD1 may regulate adipocyte turnover and thereby indirectly affect adipocyte number and the response to different nutritional schemes. It will be interesting to investigate the metabolism and the long-term effect of HFD on *ARTD1*$^{-/-}$ mice. *ARTD1* deficient mice may thus become a useful model to study how adipocyte differentiation and function affect pathological responses to HFD and lead to diet-induced obesity.

Although the storage of excess energy in the form of triglycerides and the release of FFAs is the principal function of adipocytes (29), the liver is the organ of fatty acid uptake, synthesis, and circulation and can therefore be considered a hub of fatty acid metabolism (30). In humans, components of the metabolic syndrome, such as obesity, insulin resistance or dyslipidemia, are associated with fatty liver syndrome, which is one characteristic of NAFLD (31, 32). One consequence of NAFLD is an excessive release of FFAs into the bloodstream, which exacerbates peripheral insulin resistance. Our findings of significantly increased hepatic lipid accumulation, elevated serum cholesterol levels, and impaired glucose tolerance in *ARTD1*$^{-/-}$ mice, despite the unaffected insulin response, suggests that other lipid mediators or related mechanisms, such as inflammation, may be required for the development insulin resistance. Alternatively, it can be speculated that the hepatic insulin resistance is compensated for during the whole-body insulin resistance test. To explore insulin sensitivity more specifically at the level of the liver, hyperinsulinemic-euglycemic clamp studies could be employed, since the majority of endogenously produced glucose comes from hepatocytes. Currently, it is also not clear whether elevated cholesterol levels are only a consequence of the changes in WAT or whether they are also caused and exacerbated by the *ARTD1* deficiency in liver tissue, which might affect other metabolic processes. Further studies using conditional knockout mice with reduced expression of *ARTD1* either in WAT or liver would certainly provide additional insights into this interdependency. FJ

The authors thank I. Mittner and M. Wanner (University of Zurich) for FFA measurements. F. Freimoser (University of Zurich) provided editorial assistance and critical input during the writing. This work was supported in part by the University Research Priority Program, Integrative Human Physiology, at the University of Zurich; a Forschungskredit of the University of Zurich (to M.H.); Swiss National Science Foundation grants 31-122421 and 310030B-138667; and the Kanton of Zurich (to M.O.H.). The authors declare no conflicts of

interest. Author contributions: S.E., A.M., M.H., P.J.R., R.K., M.Y.D., and M.O.H. designed the experiments; S.E., A.M., M.H., A.N.T., and H.E. performed the experiments; P.J.R. and M.O.H. supervised the study; M.O.H., S.E., and P.J.R. wrote and edited the manuscript.

REFERENCES

1. Bluher, M. (2009) Adipose tissue dysfunction in obesity. *Exp. Clin. Endocrinol. Diabetes* **117,** 241–250
2. Trayhurn, P., and Beattie, J. H. (2001) Physiological role of adipose tissue: white adipose tissue as an endocrine and secretory organ. *Proc. Nutr. Soc.* **60,** 329–339
3. Trayhurn, P., and Wood, I. S. (2004) Adipokines: inflammation and the pleiotropic role of white adipose tissue. *Br. J. Nutr.* **92,** 347–355
4. Gregor, M. F., and Hotamisligil, G. S. (2011) Inflammatory mechanisms in obesity. *Annu. Rev. Immunol.* **29,** 415–445
5. Hotamisligil, G. (2006) Inflammation and metabolic disorders. *Nature* **444,** 860–867
6. Hottiger, M., Hassa, P., Lüscher, B., Schüler, H., and Koch-Nolte, F. (2010) Toward a unified nomenclature for mammalian ADP-ribosyltransferases. *Trends Biochem. Sci.* **35,** 208–219
7. Hassa, P., Haenni, S., Elser, M., and Hottiger, M. (2006) Nuclear ADP-ribosylation reactions in mammalian cells: where are we today and where are we going? *Microbiol. Mol. Biol. Rev.* **70,** 789–829
8. Krishnakumar, R., and Kraus, W. (2010) The PARP side of the nucleus: molecular actions, physiological outcomes, and clinical targets. *Mol. Cell* **39,** 8–24
9. Hassa, P., and Hottiger, M. (2008) The diverse biological roles of mammalian PARPS, a small but powerful family of poly-ADP-ribose polymerases. *Front. Biosci.* **13,** 3046–3082
10. Bai, P., Canto, C., Oudart, H., Brunyanszki, A., Cen, Y., Thomas, C., Yamamoto, H., Huber, A., Kiss, B., Houtkooper, R. H., Schoonjans, K., Schreiber, V., Sauve, A. A., Menissier-de Murcia, J., and Auwerx, J. (2011) PARP-1 inhibition increases mitochondrial metabolism through SIRT1 activation. *Cell Metab.* **13,** 461–468
11. Devalaraja-Narashimha, K., and Padanilam, B. (2010) PARP1 deficiency exacerbates diet-induced obesity in mice. *J. Endocrinol.* **205,** 243–252
12. Surwit, R. S., Kuhn, C. M., Cochrane, C., McCubbin, J. A., and Feinglos, M. N. (1988) Diet-induced type II diabetes in C57BL/6J mice. *Diabetes* **37,** 1163–1167
13. Bai, P., Canto, C., Brunyanszki, A., Huber, A., Szanto, M., Cen, Y., Yamamoto, H., Houten, S. M., Kiss, B., Oudart, H., Gergely, P., Menissier-de Murcia, J., Schreiber, V., Sauve, A. A., and Auwerx, J. (2011) PARP-2 Regulates SIRT1 expression and whole-body energy expenditure. *Cell Metab.* **13,** 450–460
14. Erener, S., Hesse, M., Kostadinova, R., and Hottiger, M. O. (2012) Poly(ADP-ribose)polymerase-1 (PARP1) controls adipogenic gene expression and adipocyte function. *Mol. Endocrinol.* **26,** 2011–1163
15. Wang, Z., Auer, B., Stingl, L., Berghammer, H., Haidacher, D., Schweiger, M., and Wagner, E. (1995) Mice lacking ADPRT and poly(ADP-ribosyl)ation develop normally but are susceptible to skin disease. *Genes Dev.* **9,** 509–520
16. Mirsaidi, A., Kleinhans, K. N., Rimann, M., Tiaden, A. N., Stauber, M., Rudolph, K. L., and Richards, P. J. (2011) Telomere length, telomerase activity and osteogenic differentiation are maintained in adipose-derived stromal cells from senile osteoporotic SAMP6 mice. [E-pub ahead of print] *J. Tissue Eng. Regen. Med.* doi: 10.1002/term.440
17. Vidal-Puig, A., Jimenez-Linan, M., Lowell, B. B., Hamann, A., Hu, E., Spiegelman, B., Flier, J. S., and Moller, D. E. (1996) Regulation of PPAR gamma gene expression by nutrition and obesity in rodents. *J. Clin. Invest.* **97,** 2553–2561
18. Samuel, V. T., Petersen, K. F., and Shulman, G. I. (2010) Lipid-induced insulin resistance: unravelling the mechanism. *Lancet* **375,** 2267–2277
19. Andrikopoulos, S., Blair, A. R., Deluca, N., Fam, B. C., and Proietto, J. (2008) Evaluating the glucose tolerance test in mice. *Am. J. Physiol. Endocrinol. Metab.* **295,** E1323–1332
20. Jones, J. R., Barrick, C., Kim, K. A., Lindner, J., Blondeau, B., Fujimoto, Y., Shiota, M., Kesterson, R. A., Kahn, B. B., and Magnuson, M. A. (2005) Deletion of PPARgamma in adipose tissues of mice protects against high fat diet-induced obesity and insulin resistance. *Proc. Natl. Acad. Sci. U. S. A.* **102,** 6207–6212
21. Messner, S., and Hottiger, M. O. (2011) Histone ADP-ribosylation in DNA repair, replication and transcription. *Trends Cell Biol.* **21,** 534–542
22. Zuk, P. A., Zhu, M., Ashjian, P., De Ugarte, D. A., Huang, J. I., Mizuno, H., Alfonso, Z. C., Fraser, J. K., Benhaim, P., and Hedrick, M. H. (2002) Human adipose tissue is a source of multipotent stem cells. *Mol. Biol. Cell* **13,** 4279–4295
23. Ménissier de Murcia, J., Niedergang, C., Trucco, C., Ricoul, M., Dutrillaux, B., Mark, M., Oliver, F. J., Masson, M., Dierich, A., LeMeur, M., Walztinger, C., Chambon, P., and de Murcia, G. (1997) Requirement of poly(ADP-ribose) polymerase in recovery from DNA damage in mice and in cells. *Proc. Natl. Acad. Sci. U.S.A.* **94,** 7303–7307
24. D'Adda di Fagagna, F., Hande, M. P., Tong, W. M., Lansdorp, P. M., Wang, Z. Q., and Jackson, S. P. (1999) Functions of poly(ADP-ribose) polymerase in controlling telomere length and chromosomal stability. *Nat. Genet.* **23,** 76–80
25. Samper, E., Goytisolo, F. A., Menissier-de Murcia, J., Gonzalez-Suarez, E., Cigudosa, J. C., de Murcia, G., and Blasco, M. A. (2001) Normal telomere length and chromosomal end capping in poly(ADP-ribose) polymerase-deficient mice and primary cells despite increased chromosomal instability. *J. Cell Biol.* **154,** 49–60
26. Picard, F., Kurtev, M., Chung, N., Topark-Ngarm, A., Senawong, T., Machado De Oliveira, R., Leid, M., McBurney, M. W., and Guarente, L. (2004) Sirt1 promotes fat mobilization in white adipocytes by repressing PPAR-gamma. *Nature* **429,** 771–776
27. Qiao, L., and Shao, J. (2006) SIRT1 regulates adiponectin gene expression through Foxo1-C/enhancer-binding protein alpha transcriptional complex. *J. Biol. Chem.* **281,** 39915–39924
28. Wang, F., and Tong, Q. (2009) SIRT2 suppresses adipocyte differentiation by deacetylating FOXO1 and enhancing FOXO1's repressive interaction with PPARgamma. *Mol. Biol. Cell* **20,** 801–808
29. Sethi, J. K., and Vidal-Puig, A. J. (2007) Thematic review series: adipocyte biology. Adipose tissue function and plasticity orchestrate nutritional adaptation. *J. Lipid Res.* **48,** 1253–1262
30. Nguyen, P., Leray, V., Diez, M., Serisier, S., Le Bloc'h, J., Siliart, B., and Dumon, H. (2008) Liver lipid metabolism. *J. Anim. Physiol. Anim. Nutr. (Berl.)* **92,** 272–283
31. Cortez-Pinto, H., Camilo, M. E., Baptista, A., De Oliveira, A. G., and De Moura, M. C. (1999) Non-alcoholic fatty liver: another feature of the metabolic syndrome? *Clin. Nutr.* **18,** 353–358
32. Marchesini, G., Brizi, M., Bianchi, G., Tomassetti, S., Bugianesi, E., Lenzi, M., McCullough, A. J., Natale, S., Forlani, G., and Melchionda, N. (2001) Nonalcoholic fatty liver disease: a feature of the metabolic syndrome. *Diabetes* **50,** 1844–1850

Received for publication November 11, 2011.
Accepted for publication February 28, 2012.

Supplementary Material

Supplementary Figure S1

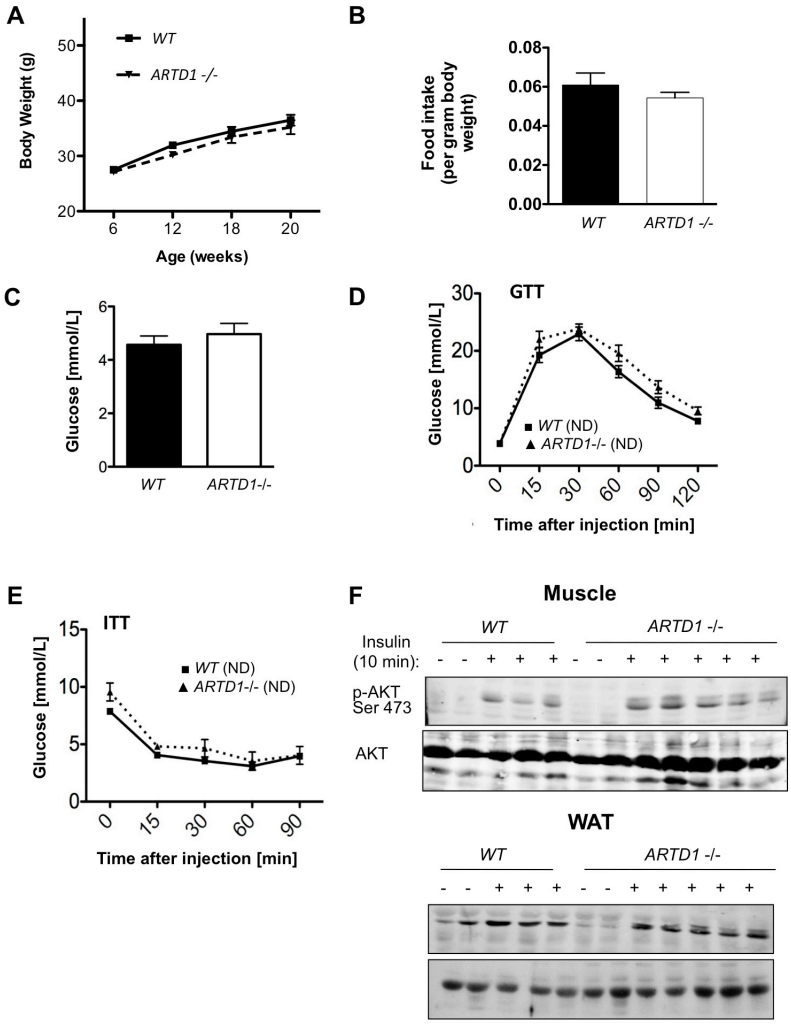

Supplementary Figure S2

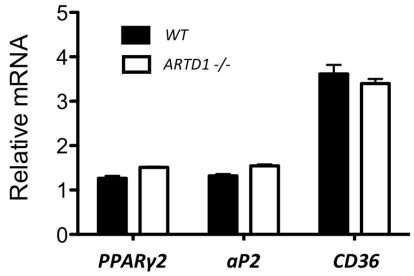

Supplementary Figure S3

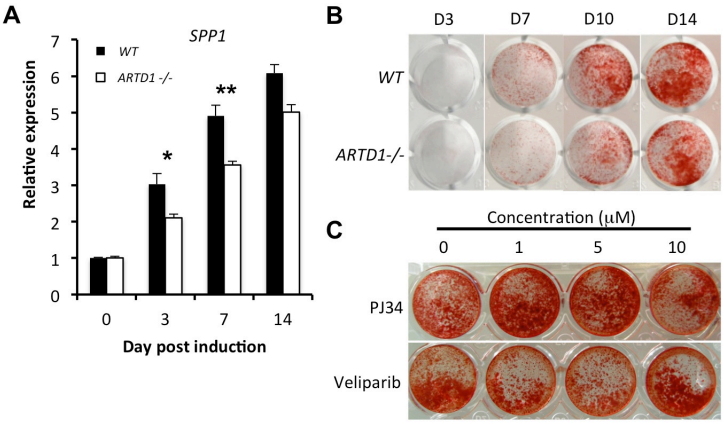

Suppl. Figure S1. *ARTD1 -/-* mice on ND exhibit reduced expression of adipogenic gene markers in WAT. (A-E) *ARTD1 -/-* mice display comparable sensitivity with *WT* mice to GTT and ITTs. **(A)** Body weight **(B)** Food intake (**C)** Starving glucose levels of *WT* and *ARTD1 -/-* mice. n=6 mice per group, mean ±SE. **(D)** Glucose tolerance test (GTT) measured after 14 h fasting *WT* and *ARTD1 -/-* mice. 6 weeks old mice were injected 0.75 g glucose per kg body weight. n = 5 mice per group, mean ±SE. **(E)** Insulin tolerance test (ITT) measured after 3 hr fasting *WT* and *ARTD1 -/-* mice. Mice were injected 0.75 U insulin per kg body weight n = 5 mice per group, mean ±SE. **(F)** Western blot analysis of phosphorylated Akt (p-Akt) from muscle and WAT of insulin (0.75 U/kg, 10 min) injected *WT* and *ARTD1 -/-* mice (14 h fast).

Suppl. Figure S2. PPARγ and PPARγ - dependent gene expression in WAT from *ARTD1 -/- mice on HFD*. Real-time RT-PCR analysis in total cell extracts from epididymal WAT of *WT* and *ARTD1 -/-* mice that were fed with HFD. mRNA levels were normalized with *Cyclophilin A.* Results represent mean ±SD of technical replicates.

Suppl. Figure S3. Osteogenic differentiation of ASCs is not adversely affected by *ARTD1* deletion. Analysis of osteogenic differentiation in ASCs isolated from wild type (*WT*) and *ARTD1*$^{-/-}$ mice. **(A)** The expression level of osteopontin (*Spp1*) was evaluated by qRT-PCR over 0, 3, 7 and 14 days of osteogenic differentiation. The expression value of each gene was normalized to the amount of ribosomal protein S12 (*RPS12*) RNA in order to calculate relative amounts of mRNA. **(B)** Mineral deposition was identified in mouse ASCs by Alizarin red S staining (red) at various stages during osteogenic differentiation. **(C)** The effect of ARTD1 inhibition on the osteogenic differentiation of ASCs isolated from *WT* mice was evaluated after 14 days using Alizarin red S staining. *$P < 0.05$, **$P < 0.01$.

Supplemental table S1. Primers used for real-time RT-PCR analyses.

The sequences of forward (F) and reverse (R) primers used for PCR are given in 5`-3`direction.

Gene	Sequence (F, R; 5`-3`)
aP2	F: ATGGGTGAAACTCTGGGAGATTCT R: CTTGGAGCTTCAGGTCATATTTGTA
Arginase 1	F: CAGAAGAATGGAAGAGTCAG R: CAGATATGCAGGGAGTCACC
ATGL	F: TGTGGCCTCATTCCTCCTAC R: TCGTGGATGTTGGTGGAGCT
CD36	F: ACAACAGGGTTTCAGCAGAAAGAGG R: GGTCTCTGACACCTGAGCCAAATG
Cyclophilin A	F: TCACCATTTCCGACTGTGGA R: AATGCCCGCAAGTCAAAAGA
HSL	F: GCTGGGCTGTCAAGCACTGT R: GTAACTGGGTAGGCTGCCAT
IL-10	F: GCTCTTACTGACTGGCATGAG R: CGCAGCTCTAGGAGCATGTG
IL-12	F: GAAGTTCAACATCAAGAGCAGTAG R: AGGGAGAAGTAGGAATGGGG
IL-13ra	F: TGCTGCTACTGTGGACCGCCA R: CCTTCAGGAGGACTCCACGTCCA
IL-1β	F: AAGGAGAACCAAGCAACGACAAAA R: TGGGGAACTCTGCAGACTCAAACT
IL-6	F: CTGCAAGAGACTTCCATCCAGTT R: GAAGTAGGGAAGGCCGTGG
IP-10	F: GCACGAACTTAACCACCATCTTCC R: CTACCCATTGATACATACTTGATGACAC
Lipin	F: AGCGCCAAAGAATAACCTGG R: TGAAGACTCGCTGTGAATGG
LPL	F: AGGACCCCTGAAGACAC R: GGCACCCAACTCTCATA
MCP-1	F: TTAAAAACCTGGATCGAACCAA R: GCATTAGCTTCAGATTTACGGGT
MPEG-1	F: GTGAAACAAAAGCCAGACAGAGCCT R: TCATGGCGCAGATGGTTTTGGC
PPARα	F: CGGGAAAGACCAGCAACAAC R: TGGCAGCAGTGGAAGAATCG
PPARγ2	F: ATGGGTGAAACTCTGGGAGATTCT R: CTTGGAGCTTCAGGTCATATTTGTA
Pu.1	F: GATCCGCCTTGATCCCCACCG R: TCTCCATCGCTGCCCACGAA
SAA3	F: TGCCATCATTCTTTGCATCTTGA R: CCGTGAACTTCTGAACAGCCT
aP2	Mm00445878_m1
ARTD1	Mm01321084_m1
GLUT4	Mm00436615_m1
PPARγ2	Mm00440940_m1
RPS12	Mm00488728_m1

ACS chemical biology

Letters

pubs.acs.org/acschemicalbiology

PARP Inhibitor with Selectivity Toward ADP-Ribosyltransferase ARTD3/PARP3

Anders E. G. Lindgren,[†,⊥] Tobias Karlberg,[‡,⊥] Ann-Gerd Thorsell,[‡] Mareike Hesse,[§] Sara Spjut,[†] Torun Ekblad,[‡] C. David Andersson,[†] Ana Filipa Pinto,[‡] Johan Weigelt,[‡,∥] Michael O. Hottiger,[§] Anna Linusson,[†] Mikael Elofsson,[†,*] and Herwig Schüler[‡,*]

[†]Department of Chemistry, Umeå University, Umeå, Sweden

[‡]Department of Medical Biochemistry and Biophysics, Karolinska Institutet, Stockholm, Sweden

[§]Institute of Veterinary Biochemistry and Molecular Biology, University of Zurich, Zurich, Switzerland

Supporting Information

ABSTRACT: Inhibiting ADP-ribosyl transferases with PARP-inhibitors is considered a promising strategy for the treatment of many cancers and ischemia, but most of the cellular targets are poorly characterized. Here, we describe an inhibitor of ADP-ribosyltransferase-3/poly(ADP-ribose) polymerase-3 (ARTD3), a regulator of DNA repair and mitotic progression. *In vitro* profiling against 12 members of the enzyme family suggests selectivity for ARTD3, and crystal structures illustrate the molecular basis for inhibitor selectivity. The compound is active in cells, where it elicits ARTD3-specific effects at submicromolar concentration. Our results show that by targeting the nicotinamide binding site, selective inhibition can be achieved among the closest relatives of the validated clinical target, ADP-ribosyltransferase-1/poly(ADP-ribose) polymerase-1.

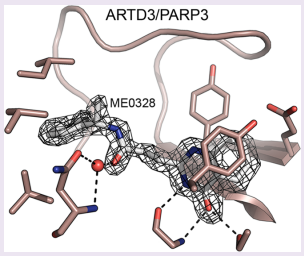

The 17 human ADP-ribosyltransferases with diphtheria toxin homology (ARTD) catalyze substrate protein ADP-ribosylation to regulate multiple processes including chromatin remodeling, transcription, DNA repair, and protein degradation. Poly(ADP-ribose) polymerase-1 (ARTD1/PARP1) is a pivotal regulator of DNA base excision repair. As such, it is a target for cancer and ischemia drug development, as its inhibition enhances DNA damage during cytotoxic chemo- or radiotherapy treatment for cancer and reduces ARTD1 overactivation due to ischemia, respectively.[1−3] However, selective inhibitors of individual ARTD family members are not available, and new inhibitors are generally profiled against a limited subset of ARTD enzymes. This makes evaluation of the clinical benefits of broad range vs. selective inhibition impossible. This also hampers research into ADP-ribosylation dependent signaling mechanisms, where selective inhibitors would be a valuable complement to genetic methods. Thus, there is a critical need for selective inhibitors of ADP-ribosyltransferases, both for probing the functions of individual ARTD enzymes and for evaluating their potential as therapeutic targets.

To address this need, we recently profiled a focused library of 185 compounds for their ability to bind to the active sites of 13 human ARTDs.[4] We found that 3-(4-oxo-3,4-dihydroquinazolin-2-yl)-N-[1-pyridin-2-yl)ethyl]propanamide (STO1131; Figure 1a) preferentially bound ARTD3/PARP3,[5] a family member that is similar to ARTD1 in the active site[6] and also functions in DNA repair.[7−11] To further investigate the STO1131−ARTD3 interaction and to improve the qualities of the compound as a selective ARTD3 inhibitor, we performed differential scanning fluorimetry during thermal unfolding, melting temperature (T_m) shift assays. The results confirmed that STO1131 significantly stabilized ARTD3 and that it only slightly stabilized the closely related homologues ARTD1 and ARTD2/PARP2 (Figure 1b and Supporting Information Table 1). The individual enantiomers ME0354 and ME0355 of the racemic STO1131 were prepared (Figure 1c, the Supporting Information text, and Supporting Information Figures 1 and 2). ME0354 had a moderate effect (ΔT_m 4.8 °C) whereas ME0355 displayed strong thermal stabilization of ARTD3 (ΔT_m 9.7 °C; Table 1). Next, we established an *in vitro* activity assay in which histone protein H1.0 modification by ARTD3 was measured (Supporting Information Figure 3) and confirmed that ME0355 inhibited ARTD3 transferase activity (IC_{50} 1.3 μM) while ME0354 had only weak inhibitory activity (Table 1).

In order to understand these interactions at a molecular level, we determined crystal structures of the transferase domain of ARTD3 in complex with these compounds. When crystals were grown in presence of the racemic STO1131, only one enantiomer was found in the active site, namely, ME0355. Crystallization of ARTD3 in the presence of ME0355 resulted in an identical structure (Figure 2a and b and Supplementary

Received: March 24, 2013
Accepted: June 6, 2013
Published: June 6, 2013

dx.doi.org/10.1021/cb4002014 | *ACS Chem. Biol.* 2013, 8, 1698−1703

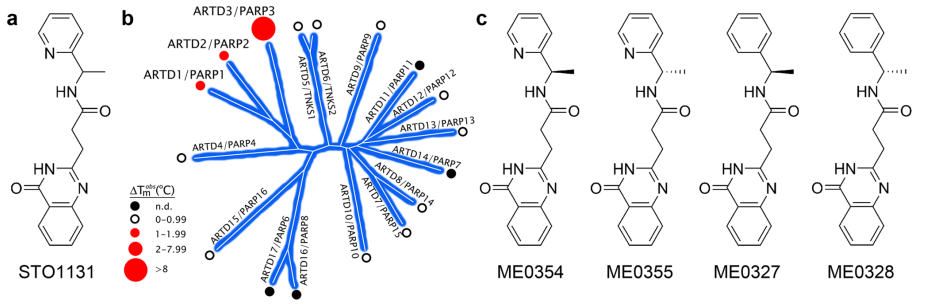

Figure 1. 4-Oxo-3H-quinazolin-2-yl derivatives bind and stabilize a subset of the 17 human PARP-family ADP-ribosyltransferases. (a) Chemical structure of the racemic compound STO1131, a recently identified ARTD binder.[4] (b) In T_m shift assays, STO1131 strongly stabilized ARTD3, and displayed weak stabilization of ARTD1 and ARTD2 (see Supporting Information Table 1 for details). N.d., not determined. (c) Chemical structures of ME0354 and ME0355, the individual enantiomers of STO1131, as well as the two analogs ME0327 and ME0328.

Table 1. Compound Effects on ARTD3/PARP3 Thermal Stability and Enzymatic Activity *In Vitro*

	ARTD3/PARP3		ARTD1/PARP1	
compd.	T_m shift (°C)[a]	IC_{50} (μM)[b]	T_m shift (°C)[a]	IC_{50} (μM)[b]
STO1131	8.5 ± 0.2	6.0 ± 2.2	2.0 ± 0.1	n.d.[c]
ME0354	4.8 ± 0.2	>100	2.4 ± 0.1	0.9 ± 0.1
ME0355	9.7 ± 0.4	1.3 ± 0.2	2.0 ± 0.2	9.1 ± 2.6
ME0327	6.0 ± 0.5	15.3 ± 10.0	3.1 ± 0.03	1.0 ± 0.1
ME0328	8.5 ± 0.6	0.89 ± 0.28	1.8 ± 0.1	6.3 ± 0.6

[a] T_m shift data: Values represent means ± SD of three independent experiments [b] IC_{50} data: Values represent means ± SE of the fitted parameter (based on duplicate or triplicate experiments, each using three replicates). [c] n.d., not determined.

Table 2). This was consistent with the inability of ME0354 to stabilize and inhibit ARTD3.

The 4-oxo-dihydroquinazolinyl moiety anchors ME0355 in the nicotinamide binding cleft of the ARTD3 active site. Therefore, the anchoring moiety was not modified in effort to synthesize close analogs with improved binding affinity and selectivity. Two analogs, ME0327 and ME0328, which contain a phenyl group instead of the 2-pyridinyl moiety, were synthesized (Figure 1c, Supporting Information, and Supporting Information Figures 4 and 5). In the histone H1 ADP-ribosylation assay, ME0327 (ΔT_m 6.0 °C, IC_{50} ~15 μM), similar to ME0354, was a weak inhibitor of ARTD3 activity. In contrast, ME0328 (ΔT_m 8.5 °C) inhibited ARTD3 with an IC_{50} of 0.89 μM (Figure 3a and Table 1), which was a slight improvement in IC_{50} over ME0355.

Crystal structures of ARTD3 compound complexes explain the differential potencies of the respective enantiomers (Figure 2b and c): whereas the carbonyl oxygens in the linker amides of ME0328 and ME0355 form water mediated hydrogen bonds with the Asn387 side chain, the corresponding carbonyl oxygen in the ARTD3-ME0354 complex (and, thus, the ARTD3-ME0327 complex) is rotated away from Asn387. The different conformations of the enantiomers also affect the angles between the distal 2-pyridinyls and phenyls of ME0354/ME0355 and ME0327/ME0328, respectively, and the hydrophobic side chains Leu287, Val288 and Val390 in the α-helical regulatory domain.

Next, the selectivity of ME0328 for ARTD3 over the closest ARTD3 homologues was investigated. To obtain a comparable measure for the potency of ME0328, we established ADP-ribosyltransferase activity assays for 11 ARTD enzymes. The results show that ME0328 selectively inhibits ARTD3 (IC50 0.89 μM, Figure 3a), with weaker activity against ARTD1 and ARTD2 (IC_{50} 6.3 and 10.8 μM, respectively), and no significant activity (IC_{50} >30 μM) against any other ARTD enzyme for which we could measure transferase activity (Figure 3b, Table 1, and Supporting Information Table 3).

The crystal structures of ARTD3 and ARTD1, each in complex with ME0328, illustrate the structural basis for selective ARTD3 inhibition (Figure 2). In ARTD3, ME0328 is clearly visible in the electron density, stretching from the nicotinamide anchoring pocket to the amino-terminal end of the donor loop and making contacts with the α-helical regulatory domain, similar as ME0355. In contrast, in ARTD1, density was only observed for the 4-oxo-dihydroquinazolinyl moiety and the remainder of the compound could not be modeled (Figure 2e); a similar observation was made for the complex of ARTD1 with ME0355 (results not shown). The underlying reason is likely the higher polarity of the region as compared to ARTD3, dominated by the ARTD1 side chains Asp766, Asn767, and Asn868 near the ME0328 phenyl group. This is consistent with the lower potency of the compounds as ARTD1 inhibitors.

Finally, we investigated whether ME0328 could inhibit ARTD3 in cells. Depletion of ARTD3 by RNA interference results in a delay of DNA repair, which can be quantified by measuring the retention of γH2AX protein containing foci in cells after induced DNA damage.[9,10] The retention of γH2AX foci in human alveolar basal epithelial (A549) cells was measured after preincubation for 1 h with ME0328 or ME0355 (10 μM), followed by γ-irradiation (2 Gy). Both compounds resulted in a significant delay of γH2AX-foci resolution, showing that both compounds were able to affect ARTD3 in cells (Figure 3c). In A549 cells a concentration dependent delay of γH2AX-foci resolution was observed 4 h after irradiation (Figure 3d). The effects were significant, even at concentrations below 1 μM. γH2AX foci retention upon ARTD3 inhibitor treatment was also observed in primary human fetal lung fibroblast (MRC5) cells. Importantly, these effects were specific for the two compounds that inhibited

dx.doi.org/10.1021/cb4002014 | ACS Chem. Biol. 2013, 8, 1698–1703

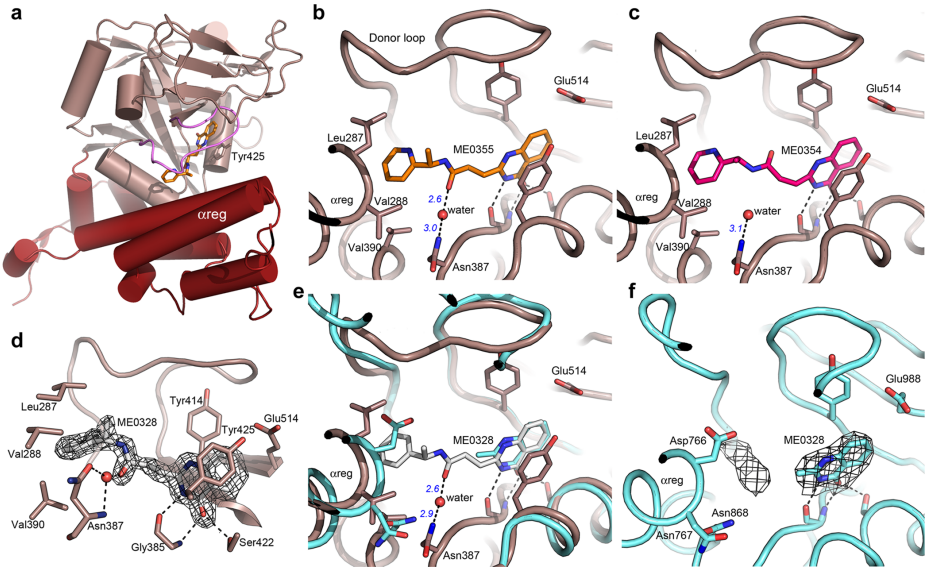

Figure 2. Structural basis of ARTD3 inhibition by ME0328 and related compounds. (a) Overview of ARTD3 in the ARTD3−ME0355 crystal complex (PDB entry 4GV0). The α-helical regulatory domain (αreg) is shown in a darker shade. The donor loop is shown in pink, and the bound inhibitor is shown in orange. The Tyr425 side chain is shown for orientation. (b) Close-up of the active site in the ARTD3−ME0355 complex. Notable interactions outside the nicotinamide pocket are the hydrogen bond with the Asn387 side chain mediated by water (hydrogen bonding distances indicated in Ångstrom), and hydrophobic interactions with side chains in the α-helical regulatory domain. (c) In the ARTD3−ME0354 complex (4GV2), the weak inhibitor does not form a hydrogen bond with Asn387. (d) Crystal structure, at 1.80 Å resolution, of ARTD3 in complex with ME0328 (4GV4). The quinazolinyl moiety anchors the compound in the nicotinamide binding pocket, while the elongated tail of the compound makes extensive interactions with side chains lining the active site. The electron density for the ligand, rendered at 1.5 σ, is indicated as mesh. In ARTD3−ME0328, the conformation of the inhibitor is similar to that of ME0355 (panel b), but the proximity of a phenyl (as compared to 2-pyridinyl) to the hydrophobic environment around Val288 might explain its slightly higher potency over ME0355. (e) Superposition of the ARTD3−ME0328 complex (chocolate; compound in gray) with the ARTD1−ME0328 complex (cyan; compound in cyan; 4GV7) to illustrate the overall structural conservation in the active sites and the different environments (hydrophobic in ARTD3 vs polar in ARTD1) contributed by side chains in the α-helical regulatory domain. Side chain labels and hydrogen bonding distances in this panel refer to ARTD3. (f) In the ARTD1−ME0328 complex, only partial electron density was observed for the ligand (shown as mesh, rendered at 1 σ), consistent with low potency of ME0328 against ARTD1. A section of the donor loop was omitted for clarity.

ARTD3 catalytic activity *in vitro*; their enantiomers, which lack ARTD3 inhibitory activity, did not elicit γH2AX-foci retention (Figure 3e). Thus, ME0327 and ME0354, which differ from ME0328 and ME0355, respectively, only in the stereochemistry of a single methyl group, fail to inhibit ARTD3 in biochemical and cellular assays and can serve as negative controls in the study of ARTD3 functions.

In silico and *in vitro* physicochemical and metabolic profiling indicated that ME0328 is soluble, cell permeable, and metabolically stable in human liver microsomes and rat hepatocytes (Supporting Information Table 4). Cell proliferation assays conducted with nonirradiated human A549 and mouse MRC5 cells cultured in the presence of ME0328 or ME0355 (10 μM) did not reveal any signs of compound toxicity after 72 h; similar assays conducted with U2OS, 3T3, and Hek293T cells cultured in the presence of compounds (50 μM) did not indicate compound toxicity after 96 h. Control experiments using mouse 3T3 and MRC5 cells showed that neither ME0328 nor ME0355 (20 μM) affected ARTD1/PARP1 activity after H_2O_2-induced DNA damage (Supporting Information Figure 6). Database searches on similarity and substructures using ME0328/ME0355 did not yield any hits that imply off-target biological effects (Supporting Information Table 5).

This is the first report of a nicotinamide pocket anchored PARP inhibitor with documented selectivity over a wide range of ARTD enzyme family members. Recently, selective inhibition of the tankyrases (ARTD5 and ARTD6) has been achieved by targeting compounds at the putative binding site for the NAD^+ adenine moiety, a site that is poorly conserved in other PARP-family members.[12] Our results are in support of development of selective PARP inhibitors using nicotinamide mimetics, possibly based on existing compounds.

In summary, we describe a cell-permeable, selective inhibitor of ARTD3/PARP3; this compound inhibits ARTD3 ADP-ribosyltransferase activity and displays >7-fold selectivity over ARTD1 and its nearest homologues. The cellular effects of ME0328 are likely to be ARTD3 specific based on several

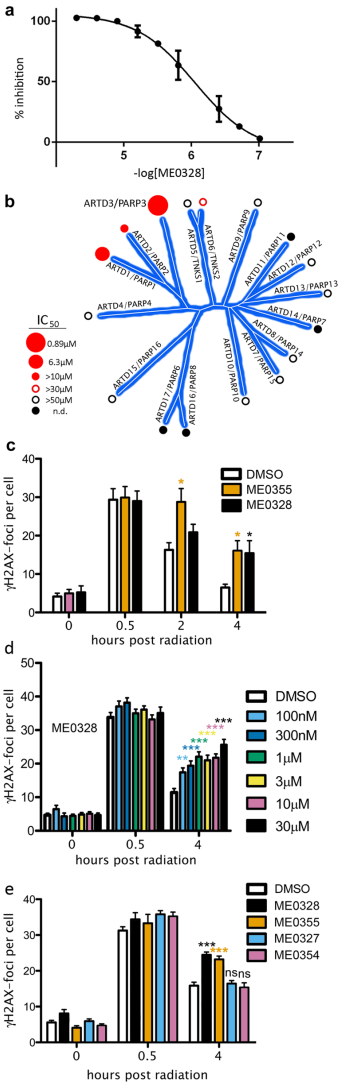

Figure 3. ME0328 is a potent and selective inhibitor of ARTD3/PARP3 that is active in cells. (a) In *in vitro* histone H1 modification assay, ME0328 inhibits the transferase activity of ARTD3 with an IC50 of 0.89 ± 0.28 μM. (b) *In vitro* IC50-values for ME0328 against 11 human PARP-family ADP-ribose transferases illustrated as circles in the dendrogram, as indicated (see Supporting Information Table 3 for details). (c) In human A549 cells, ME0328 and ME0355 (at 10 μM) delay the resolution of γH2AX-containing foci that serve as markers for DNA double strand break repair following γ-irradiation (2 Gy). These compounds cause effects similar to those of ARTD3 depletion by RNA interference.[9,10] (d) Treatment of A549 cells with ME0238 at varying concentrations resulted in a concentration dependent retention of γH2AX-containing foci. (e) After γ-irradiation, foci retention could be observed only in response to treatment with ME0328 or ME0355, but not with their respective enantiomers ME0327 and ME0354, which also did not inhibit ARTD3 enzymatic activity *in vitro*. Data from two (panel c) and three biological replicates (panels d and e) were analyzed, and statistical significance was evaluated using a two-tailed *t*-test (*$p < 0.01$; **$p < 0.001$) using DMSO treatment as control.

observations: (i) Neither ME0328 nor ME0355 inhibited ARTD1 (Supporting Information Figure 6). (ii) The enantiomers ME0327 and ME0354, which inhibit ARTD1 but not ARTD3 (Table 1), did not elicit γH2AX-foci retention in cells after γ-irradiation (Figure 3). (iii) Depletion of ARTD1 by RNA interference did not result in a delay of γH2AX foci resolution after DNA damage.[9] Given these results, we expect that ME0328 will be useful for research into the specific functions of ARTD3 vis-à-vis ARTD1 and ARTD2, which is important for understanding the cellular functions of ADP-ribosylation, the basic mechanisms of DNA repair, and, in the long term, PARP-inhibitor based therapeutics development.

METHODS

Molecular Cloning, Protein Expression, and Protein Purification. Molecular cloning and protein production was carried out as described before.[4] Briefly, the sequences encoding residues ARTD1$^{654-1013}$, ARTD2$^{186-530}$, full-length ARTD3, ARTD3$^{178-532}$, ARTD4$^{241-600}$, ARTD5$^{1017-1325}$, ARTD6$^{952-1166}$, ARTD7$^{459-656}$, ARTD8$^{1611-1810}$, ARTD12$^{480-688}$, ARTD15$^{1-274}$, and full-length histone H1.0 were inserted into pNIC28-Bsa4, and ARTD10$^{809-1017}$ was inserted into pNIC28-CH, by ligation independent cloning.[13] Proteins were purified by immobilized metal affinity followed by size exclusion chromatography, concentrated by ultrafiltration, flash frozen in aliquots, and stored at −80 °C. Protein masses were verified by time-of-flight mass spectrometry. Full-length ARTD1 (cat. no. 11040-H08B) was purchased from Sino Biological Inc.

Biophysical and Enzymatic Assays. T_m-shift assays of compound stabilization of ARTD catalytic domain fragments was carried out by differential scanning fluorimetry as described.[4] Reported values represent means ± SD of two to five independent experiments. Protein ADP-ribosylation was measured using hexahistidine-tagged ARTD proteins and recombinant histone proteins captured on 96-well Ni^{2+}-chelating plates (S-PRIME).[14,15] ADP-ribosylation reactions were initiated by addition of NAD^+ (2% biotinylated; Nordic BioSite), and modified reaction products were detected by chemiluminescence. K_m values were estimated using plots of initial rates vs. NAD^+ concentrations and linear curve fitting with GraphPad Prism (GraphPad Software). All compounds were dissolved in dimethyl sulfoxide (DMSO) to a stock concentration of 50 mM. Experiments to determine IC_{50} values were conducted with compound concentrations in the range between 10 nM and 450 μM with a DMSO concentration of 1% (v/v). Measurements were carried out at an NAD^+ concentration below K_m for each transferase. IC_{50} values were estimated using curve fitting with GraphPad Prism. Reported values represent means ± SE of the fits of the curves based on duplicate or triplicate experiments, each determined based on three replicates.

Protein Crystallization. Crystals of the ARTD3 complexes with compounds ME0328, ME0354, and ME0355 were obtained by the sitting drop vapor diffusion method in 96-well plates (Corning) by mixing 2 μL of protein (12 mg mL^{-1}) including 1−2 mM compound dissolved in dimethyl sulfoxide (DMSO) and 0.7 μL of reservoir solution containing 1.7−2.0 M DL-malic acid, 0.1 M bis-tris-propane pH 7.0, and 0.3 μL of crystal seed solution. The crystal seed solution

dx.doi.org/10.1021/cb4002014 | *ACS Chem. Biol.* 2013, 8, 1698−1703

was prepared by crushing needle crystals of ARTD3 and mixing with reservoir solution. The plates were incubated at 20 °C and crystals appeared within a few days. After two weeks, crystals were briefly transferred to a cryo solution consisting of 1.7−2.0 M DL-malic acid, 0.1 M bis-tris-propane pH 7.0, 20−25% (w/v) glycerol, 0.2 M sodium chloride, and 1−2 mM compound and then cooled in liquid nitrogen.

Crystals of the ARTD1−ME0328 complex were obtained by the sitting-drop vapor diffusion method in 96-well plates (Corning) by mixing 0.3 μL of protein at a concentration of 50 mg mL^{-1} including 1 mM compound dissolved in dimethyl sulfoxide (DMSO) and 0.4 μL of reservoir solution containing 20% PEG3350, 0.2 M potassium thiocyanate, 0.1 M bis-tris-propane pH 7.5. The plates were incubated at 4 °C, and crystals appeared after 1 day. The crystals were briefly transferred to a cryo solution consisting of 20% PEG3350, 0.2 M potassium thiocyanate, 0.1 M bis-tris-propane pH 7.5, 20% glycerol, 0.2 M sodium chloride, 1.2 mM ME0328, then cooled in liquid nitrogen.

Diffraction Data Collection, Processing and Refinement. Diffraction data were collected on cryo-cooled crystals at the synchroton beamlines I04 at Diamond Light Source (Didcot, United Kingdom), ID14.4 at ESRF (Grenoble, France), and BL14.1 at BESSY (Berlin, Germany). Data were indexed and integrated using the XDS package[16] or the AutoProc toolbox.[17] Model building was done with Coot[18] and refinement with Refmac5[19] (ARTD3) or Buster[20] (ARTD1). The refinement progress was monitored by decreasing R and R_{free} values.

Cellular Assay of γH2AX-Foci Resolution. Prior to experiments, compound cytotoxicity in A549 and MRC5 cells was evaluated using WST-1 assays (Roche Bioscience). A549 cells were cultured in Dulbecco's Modified Eagle's Medium supplemented with 10% fetal calf serum (FCS), penicillin, and streptomycin. MRC5 cells were cultured in Minimal Essential Medium supplemented with 10% FCS, penicillin, streptomycin, and L-glutamine. Both cell lines were maintained in a humidified incubator at 37 °C and 5% CO_2. Irradiation was done using a Pantak Seifert X-ray system operating at 120 kV and 19 mA at a dose rate of 3.11 Gy/min (total of 2 Gy). Olaparib (AstraZeneca), ME0327, ME0328, ME0354, and ME0355 were dissolved in DMSO at a stock concentration of 10 mM. Compounds were added 1 h prior to irradiation and maintained for the duration of the experiment. Cells were fixed in ice-cold methanol and blocked in PBS buffer containing 10% bovine serum albumin. Cells were subsequently treated with an antibody against γH2AX (Millipore 05-636) and analyzed using a Leica DMI 6000B microscope. Foci were quantified using Imaris software (Bitplane) 7.4.0. All values are represented as means ± s.e.m. Two tailed Student's t-tests were performed using GraphPad Prism.

Synthetic Strategy. The synthetic route to compounds ME0327, ME0328, ME0354, and ME0355 and analytical data (NMR spectroscopy, HRMS, optical rotation measurements, and chiral HPLC) are presented in the Supporting Information.

■ ASSOCIATED CONTENT

Supporting Information

Tables and figures describing crystallographic data, additional selectivity profiling, cellular compound effects, physicochemical stability profiling, results of similarity searches, proof of compound purity, additional materials and methods (chemical procedures). This material is available free of charge via the Internet at http://pubs.acs.org.

Accession Codes

The atomic coordinates and structure factors of ARTD3 in complex with inhibitors have been deposited in the Protein Data Bank with accession codes 4GV4 (ARTD3-ME0328), 4GV2 (ARTD3-ME0354), and 4GV0 (ARTD3-ME0355). The crystal structure of ARTD1 in complex with ME0328 has been deposited with accession code 4GV7.

■ AUTHOR INFORMATION

Corresponding Author

*E-mail: mikael.elofsson@chem.umu.se (M.E.); herwig.schuler@ki.se (H.S.).

Present Address

[‖]The Royal Swedish Academy of Engineering Sciences (IVA), Lilla Frescativägen 4A, 114 18 Stockholm, Sweden

Author Contributions

[⊥]These authors contributed equally to this work.

Notes

The authors declare no competing financial interest.

■ ACKNOWLEDGMENTS

We are grateful to S. Andersson and her team (AstraZeneca R&D, Mölndal, Sweden) for compound *in vitro* pharmacokinetic profiling. We thank the beamline staff at the Berliner Elektronenspeicherring-Gesellschaft für Synchrotronstrahlung (BESSY; Berlin, Germany), the Diamond Light Source (Didcot, U.K.), and European Synchrotron Radiation Facility (ESRF; Grenoble, France) for excellent support, and M. Moche (Protein Science Facility, Karolinska Institutet, Stockholm, Sweden) for assistance with synchrotron data collection. This work was financed by the Swedish Foundation for Strategic Research (RBc08-0014). M.H. and M.O.H. are supported by the Swiss National Foundation (310030B-138667). A.L. thanks the Swedish Research Council and Umeå University for financial support. H.S. is grateful to the Structural Genomics Consortium for additional support.

■ REFERENCES

(1) Moroni, F. (2008) Poly(ADP-ribose)polymerase 1 (PARP-1) and postischemic brain damage. *Curr. Opin. Pharmacol. 8*, 96−103.

(2) Basu, B., Yap, T. A., Molife, L. R., and de Bono, J. S. (2012) Targeting the DNA damage response in oncology: Past, present, and future perspectives. *Curr. Opin. Oncol. 24*, 316−324.

(3) Lord, C. J., and Ashworth, A. (2012) The DNA damage response and cancer therapy. *Nature 481*, 287−294.

(4) Wahlberg, E., Karlberg, T., Kouznetsova, E., Markova, N., Macchiarulo, A., Thorsell, A. G., Pol, E., Frostell, A., Ekblad, T., Oncu, D., Kull, B., Robertson, G. M., Pellicciari, R., Schüler, H., and Weigelt, J. (2012) Family-wide chemical profiling and structural analysis of PARP and tankyrase inhibitors. *Nat. Biotechnol. 30*, 283−288.

(5) Boehler, C., and Dantzer, F. (2011) PARP-3, a DNA-dependent PARP with emerging roles in double-strand break repair and mitotic progression. *Cell Cycle 10*, 1023−1024.

(6) Lehtio, L., Jemth, A. S., Collins, R., Loseva, O., Johansson, A., Markova, N., Hammarstrom, M., Flores, A., Holmberg-Schiavone, L., Weigelt, J., Helleday, T., Schüler, H., and Karlberg, T. (2009) Structural basis for inhibitor specificity in human poly(ADP-ribose) polymerase-3. *J. Med. Chem. 52*, 3108−3111.

(7) Rouleau, M., McDonald, D., Gagné, P., Ouellet, M. E., Droit, A., Hunter, J. M., Dutertre, S., Prigent, C., Hendzel, M. J., and Poirier, G. G. (2007) PARP-3 associates with polycomb group bodies and with components of the DNA damage repair machinery. *J. Cell. Biochem. 100*, 385−401.

(8) Altmeyer, M., Messner, S., Hassa, P. O., Fey, M., and Hottiger, M. O. (2009) Molecular mechanism of poly(ADP-ribosyl)ation by PARP1 and identification of lysine residues as ADP-ribose acceptor sites. *Nucleic Acids Res. 37*, 3723−3738.

(9) Boehler, C., Gauthier, L. R., Mortusewicz, O., Biard, D. S., Saliou, J. M., Bresson, A., Sanglier-Cianferani, S., Smith, S., Schreiber, V., Boussin, F., and Dantzer, F. (2011) Poly(ADP-ribose) polymerase 3 (PARP3), a newcomer in cellular response to DNA damage and mitotic progression. *Proc. Natl. Acad. Sci. U. S. A. 108*, 2783−2788.

(10) Rulten, S. L., Fisher, A. E., Robert, I., Zuma, M. C., Rouleau, M., Ju, L., Poirier, G., Reina-San-Martin, B., and Caldecott, K. W. (2011) PARP-3 and APLF function together to accelerate nonhomologous end-joining. *Mol. Cell 41*, 33−45.
(11) Fenton, A. L., Shirodkar, P., Macrae, C. J., Meng, L., and Koch, C. A. (2013) The PARP3- and ATM-dependent phosphorylation of APLF facilitates DNA double-strand break repair. *Nucleic Acids Res. 41*, 4080−4092.
(12) Ekblad, T., Camaioni, E., Schüler, H., and Macchiarulo, A. (2013) PARP inhibitors: Molecular aspects of polypharmacology vs selective inhibition. *FEBS J.*, DOI: 10.1111/febs.12298.
(13) Gileadi, O., Burgess-Brown, N. A., Colebrook, S. M., Berridge, G., Savitsky, P., Smee, C. E., Loppnau, P., Johansson, C., Salah, E., and Pantic, N. H. (2008) High throughput production of recombinant human proteins for crystallography. *Methods Mol. Biol. 426*, 221−246.
(14) Langelier, M. F., Ruhl, D. D., Planck, J. L., Kraus, W. L., and Pascal, J. M. (2010) The Zn3 domain of human poly(ADP-ribose) polymerase-1 (PARP-1) functions in both DNA-dependent poly(ADP-ribose) synthesis activity and chromatin compaction. *J. Biol. Chem. 285*, 18877−18887.
(15) Karlberg, T., Thorsell, A. G., Kallas, A., and Schüler, H. (2012) Crystal structure of human ADP-ribose transferase ARTD15/PARP16 reveals a novel putative regulatory domain. *J. Biol. Chem. 287*, 24077−24081.
(16) Kabsch, W. (2010) XDS. *Acta Crystallogr., Sect. D: Biol. Crystallogr. 66*, 125−132.
(17) Vonrhein, C., Flensburg, C., Keller, P., Sharff, A., Smart, O., Paciorek, W., Womack, T., and Bricogne, G. (2011) Data processing and analysis with the autoPROC toolbox. *Acta Crystallogr., Sect. D: Biol. Crystallogr. 67*, 293−302.
(18) Emsley, P., Lohkamp, B., Scott, W. G., and Cowtan, K. (2010) Features and development of Coot. *Acta Crystallogr., Sect. D: Biol. Crystallogr. 66*, 486−501.
(19) Murshudov, G. N., Skubak, P., Lebedev, A. A., Pannu, N. S., Steiner, R. A., Nicholls, R. A., Winn, M. D., Long, F., and Vagin, A. A. (2011) REFMAC5 for the refinement of macromolecular crystal structures. *Acta Crystallogr., Sect. D: Biol. Crystallogr. 67*, 355−367.
(20) Bricogne, G., Blanc, E., Brandl, M., Flensburg, C., Keller, P., Paciorek, W., Roversi, P., Smart, O. S., Vonrhein, C. and Womack, T. O. (2011). *BUSTER*, version 2.11.1. Global Phasing Ltd., Cambridge, U.K.

Supporting Information

A PARP inhibitor with selectivity toward ADP-ribosyltransferase ARTD3/PARP3

Anders E. G. Lindgren,[1] Tobias Karlberg,[2] Ann-Gerd Thorsell,[2] Mareike Hesse,[3] Sara Spjut,[1] Torun Ekblad,[2] C. David Andersson,[1] Ana Filipa Pinto,[2] Johan Weigelt,[2,4] Michael O. Hottiger,[3] Anna Linusson,[1] Mikael Elofsson[1]* and Herwig Schüler[2]*

[1]Department of Chemistry, Umeå University, Umeå, Sweden. [2]Department of Medical Biochemistry and Biophysics, Karolinska Institutet, Stockholm, Sweden. [3]Institute of Veterinary Biochemistry and Molecular Biology, University of Zurich, Zurich, Switzerland. [4]Current address: The Royal Swedish Academy of Engineering Sciences (IVA), Stockholm. *e-mail: mikael.elofsson@chem.umu.se or herwig.schuler@ki.se

Supplementary figures 1-6 and supplementary tables 1-5

http://pubs.acs.org/doi/suppl/10.1021/cb4002014

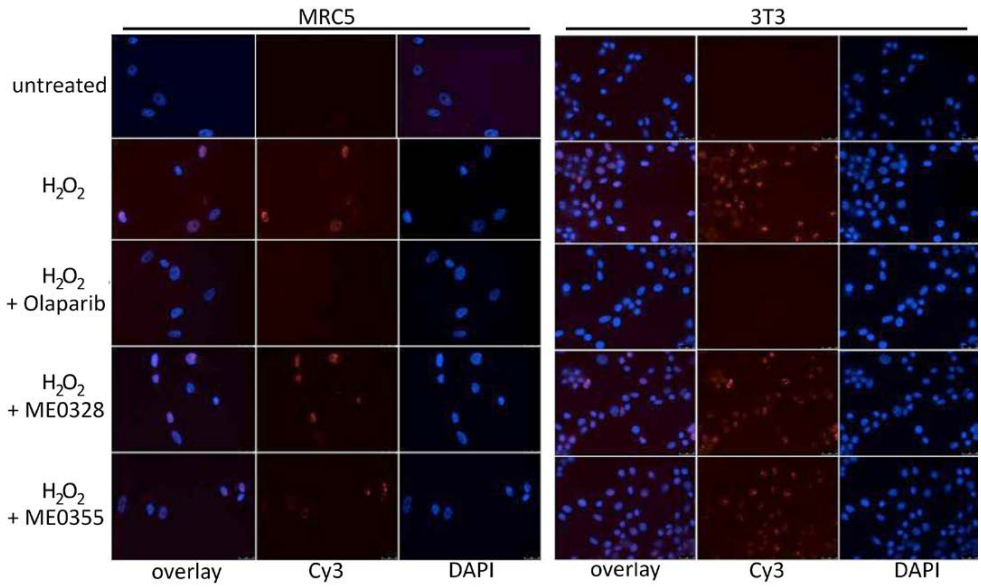

Supplementary Figure 6. ME0328 and ME0355 have no effect on ARTD1/PARP1 activity in cells after H_2O_2-induced DNA damage. MRC5 or 3T3 cells were pretreated for 1 hour with either Olaparib or ME0328 or ME0355 (20 μM) prior to H_2O_2 treatment (1 mM for 10 minutes). Cells were fixed (methanol/acetic acid) and stained with anti-PAR 10H antibody followed by Cy3-coupled anti-mouse antibody. Cells were co-stained with DAPI to visualize nuclei.

3.2 Submitted manuscript

3.2.1 ARTD1-dependent PAR formation facilitates ligand-induced PPARγ co-factor exchange

Authors: **Lehmann, M**., Pirinen, E., Mirsaidi, A., Richards, P., Auwerx, J. and Hottiger, M.O.
Journal: Manuscript submitted
Contribution: Planning, performing and evaluating the all cellculture experiments., isolation of RNA and qRTPCR on mouse tissue, Preparation of figures and revision of manuscript.

ARTD1-dependent PAR formation facilitates ligand-induced PPARγ co-factor exchange

Mareike Lehmann[*,†], Eija Pirinen[2,3], Ali Mirsaidi[‡,§], Peter J. Richards[‡,§], Johan Auwerx[2] and Michael O. Hottiger[*,1]

Running title: PAR formation facilitates PPARγ co-factor exchange

[*]Institute of Veterinary Biochemistry and Molecular Biology, [†]Life Science Zurich Graduate School,Molecular Life Science Program, [‡]Competence Centre for Applied Biotechnology and Molecular Medicine, Bone and Stem Cell Research Group, and [§]Zurich Centre for Integrative Human Physiology (ZIHP), Institute of Physiology, University of Zurich, 8057 Zurich, Switzerland, [2]Laboratory of Integrative and Systems Physiology, Ecole Polytechnique Fédérale de Lausanne, 1015 Lausanne, Switzerland, [3]Biotechnology and Molecular Medicine, A.I. Virtanen Institute for Molecular Sciences, Biocenter Kuopio, University of Eastern Finland, Kuopio, Finland

[1]Corresponding author: Email: hottiger@vetbio.uzh.ch

Key words: Adipogenesis, ADP-ribosylation, ARTD1, NCoR, p300, PARP1, PARP inhibitor, PPARγ

Total number of characters (including spaces): 55216

Abstract

Adipogenesis is accompanied by a dynamic modulation of the chromatin landscape induced by the transcription factor PPARγ. Binding of a ligand to PPARγ induces the exchange of co-repressors with co-activators. How PPARγ-dependent gene expression is maintained remains elusive, since ligands are stored in vacuoles throughout adipogenesis. ADP-ribosyltransferase D-type 1 (ARTD1; PARP1) is a chromatin-associated enzyme that synthesizes poly-ADP-ribose (PAR). Here, we show that on a high-fed diet, a pan-PARP inhibitor reduces white adipose tissue and cell size in mice. PARP inhibition also hampered PPARγ-dependent gene expression *in vitro*, whereas inhibition of PAR degradation stimulated gene expression. ChIP experiments confirmed that ARTD1 and PPARγ are both recruited to PPARγ target genes in a PAR-dependent manner. PPARγ ligand enhanced the PPARγ/ARTD1 interaction and induced ARTD1-dependent PAR formation, which was important for the co-repressor NCoR/co-activator p300 exchange at PPARγ target genes. Our study shows that ARTD1 promotes adipogenesis by fascilitating ligand-induced PPARγ co-factor exchange.

Introduction

Adipocyte formation relies on the adipogenic differentiation of multipotent mesenchymal stromal cells (MSCs), resulting in lipid-laden cells which have the capacity to influence numerous biological processes, including signaling and immune functions (Church et al., 2012). The underlying mechanism of adipogenesis is a broad reorganization of the transcriptional landscape due to large-scale chromatin changes (Siersbaek et al., 2011). Instrumental in this step-wise reorganization is the transcription factor peroxisome proliferator-activated receptor gamma (PPARγ) (Heikkinen et al., 2007; Tontonoz and Spiegelman, 2008) and in particular the adipocyte-specific isoform PPARγ2 (Fajas et al., 1997; Vidal-Puig et al., 1996).

PPARγ is a nuclear receptor of the PPAR family, which functions as an obligate heterodimer with RXRs (Chawla et al., 2001; Escher et al., 2001; Kliewer et al., 1992; Siersbaek et al., 2010). Like many nuclear receptors, PPARγ contains a N-terminal, non-conserved A/B domain, a DNA-binding domain (DBD), and the C-terminal ligand-binding domain (LBD). The C-terminal domain is required for the hetero-dimerization with RXRs, ligand-binding is conveyed by the LBD, which harbors multiple hydrophobic residues and is important for ligand-dependent interactions with cofactors (Gampe et al., 2000; Kallenberger et al., 2003). Binding of a ligand to PPARγ triggers a conformational switch that exposes a surface that can interact with LXXLL-containing co-activators. Prior to the activation of PPARγ by its ligands, PPARγ is bound to co-repressors that suppress transcription of target genes and are dislodged upon ligand binding (Yu et al., 2005). PPARγ is induced during the differentiation of adipocytes and is highly expressed in white and brown adipose tissue (WAT/BAT) (Tontonoz et al., 1994). A series of transcription factors, in particular CCAAT/enhancer-binding proteins β and δ (C/EBP-β and C/EBP-δ,

respectively), establish transcription factor hotspots and regulate PPARγ2 as well as C/EBP-α (Siersbaek et al., 2011; Tontonoz and Spiegelman, 2008). Together with C/EBP-α, PPARγ2 determines adipocyte function and transcriptionally co-regulates target genes such as *adipocyte protein 2* (*aP2*), *cluster of differentiation 36* (*CD36*) and *Adiponectin* (Lefterova et al., 2008; Rosen et al., 2002; Saladin et al., 1999). In previously published work, we have shown that the regulation of PPARγ2-dependent gene expression and adipocyte function depends on the formation of poly-ADP-ribose (PAR) (Erener et al., 2012a; Erener et al., 2012b). The activity of ARTD1, the best-studied ADP-ribosyltransferase so far, is strongly activated during adipogenesis and is absolutely required for adipogenesis (Erener et al., 2012a). Furthermore, PAR formation increases the recruitment of ARTD1 to PPARγ2 target gene promoters. However, the molecular mechanism that leads to PAR-dependent regulation of PPARγ2 target gene expression remains unknown.

PAR is synthesized by proteins belonging to the family of ADP-ribosyltransferases (ARTs), which transfer the ADP-ribose moiety of nicotinamide dinucleotide (NAD^+) to acceptor proteins. This reaction leads to either mono- or poly-ADP-ribosylation of specific residues in the acceptor protein. The family of ADP-ribosyltransferase Diphteria toxin like proteins (ARTD) is currently comprised of eighteen human members (ARTD1-18, of which ARTD1 represents the initially characterized PARP protein) that all function in different cellular compartments and are structurally similar to the bacterial Diphteria toxin (Hottiger et al., 2010). The most abundant and best-studied member is the chromatin-associated ARTD1 (PARP1), which has been implicated in a plethora of important cellular and biological processes. Thus, ARTD1-dependent poly-ADP-ribosylation has been implicated in the regulation of chromatin compaction, the recruitment of proteins to chromatin, the regulation of enzymatic

activities and was described to be involved in biological processes such as stress signaling, cell death, inflammation, as well as differentiation (Hassa and Hottiger, 2008). Furthermore, defects in ADP-ribosylation or in function of ARTs have been linked to diseases such as chronic inflammation, neurodegenerative disorders, cardiovascular diseases and cancer (Graziani and Szabo, 2005). In this report we aim to elucidate the molecular function of ARTD1 and of poly-ADP-ribosylation during adipogenesis and in particular, in the regulation of PPARγ2.

The results presented here indicate that PPARγ-dependent gene expression during adipogenesis *in vitro and in vivo* depends on PAR formation. According to our findings, this regulatory function of poly-ADP-ribosylation is brought about by complex formation between ARTD1 and PPARγ at the promoter regions of target genes and involves the exchange of transcriptional co-repressors such as NCoR with activators such as p300. The lack of co-factor exchange in the presence of PARP inhibitors could be overcome by treating the cells with an excess of PPARγ ligand. In summary, our work elucidates the molecular mechanism by which ADP-ribosylation promotes adipogenesis.

Results

PARP inhibitor treatment reduces body weight, white adipose tissue content and cell size in mice fed with high fat diet

Earlier studies have implicated ADP-ribosylation and in particular ARTD1 in adipogenesis and adipocyte function (Bai and Canto, 2012; Bai et al., 2007; Erener et al., 2012a; Erener et al., 2012b). Based on these results, we hypothesized that the inhibition of poly-ADP-ribosylation may have beneficial effects on the onset and development of obesity. In order to test this hypothesis, we treated male chow and HFD-fed C57BL/6J (WT) mice with for 18 weeks with a pan-PARP inhibitor. To confirm that PARP inhibitor treatment reduced PAR formation, we measured total ARTD activity in adipose tissue. As expected, total ARTD activity was significantly reduced by 35% in mice treated with PARP inhibitor (Figure S1A). Overall, vehicle-treated mice on the HFD presented with significant higher bodyweight compared to equivalently fed PARP inhibitor-treated animals (Figure 1A, B), although their food intake was equal (Figure S1B). In addition, HFD caused a marked increase in the amount of subcutaneous (Sc) fat, while only minor increases were observed in the epididymal (Epi), perirenal (Peri) white adipose tissue (WAT), and the brown adipose tissue (BAT) (Figure 1C, D). However, the increase in HFD-mediated ScWAT observed in PARP inhibitor-treated mice was found to be significantly lower as compared to vehicle-treated mice, while no significant differences were seen between EpiWAT, PeriWAT or BAT (Figure 1D). In order to test if this PARP inhibitor effect on WAT also manifested itself in the epiWAT adipocyte morphology, as it observed in ARTD1$^{-/-}$ mice (Erener et al., 2012b), epiWAT was isolated, fixed, stained and subjected to quantitative microscopic analysis. Adipocytes from PARP inhibitor-treated mice were significantly smaller than corresponding cells from WAT of the

vehicle-treated control animals (Figure 1E). To test if the smaller adipocyte size correlated with adipogenic gene expression, a quantitative RT-PCR analysis was performed. In agreement with earlier studies (Erener et al., 2012b) and the reduced bodyweight gain as well as the reduced expansion of the Sc fat pad after HFD and PARP inhibitor treatment (Figure 1A-E), the expression of the key adipogenesis regulator *PPARγ2* was significantly reduced (Figure 1F). The expression of other adipogenic markers including *aP2, CD36* and *Adiponectin* were also found to be down-regulated in WAT from PARP inhibitor-treated mice, although statistical significance was not reached (Figure S1C).

In summary, these results show that HFD-induced hypertrophy and obesity in mice is dependent on ADP-ribosylation.

PAR formation is required for PPARγ-dependent gene expression

In order to study the mechanistic details of how ADP-ribosylation impacts on adipogenesis (Erener et al., 2012a), we characterized adipocyte differentiation in 3T3-L1 pre-adipocyte cultures in the presence or absence of different inhibitors. Adipogenesis was induced in 3T3-L1 cells following the addition of insulin, 3-isobutyl-1-methylxanthine (IBMX) and dexamethasone (Ntambi and Young-Cheul, 2000), upon which they consistently formed lipid-laden adipocytes (Figure 2A).

In line with our earlier studies (Erener et al., 2012a), where we used PJ34 as PARP inhibitor, the presence of the more specific PARP inhibitor ABT888 during the first seven days of adipogenesis strongly affected the expression of *PPARγ*2 itself and its target genes *aP2*, *CD36* and *Adiponectin* (Figure 2B, S2A). The effect of PARP inhibitors on *PPARγ2* itself can be explained by previous results (Erener et al., 2012a), which showed that PARP inhibition does not inhibit initial *PPARγ2*

expression but rather inhibits the regulatory feedback loop of *C/EBPα* and *PPARγ* expression (Saladin et al., 1999). To confirm that the effect of PARP inhibitors was indeed due to the lack of PAR, we also performed the reverse experiment by inhibiting PAR degradation with the PARG inhibitor RBPI-3, which enhanced PAR formation (Figure S2B). In agreement with the hypothesis, RBPI-3 caused a significant increase in the transcription of *PPARγ2*, *aP2*, *CD36* or *Adiponectin* (Figure 2C). Similarly, the inhibition of nicotinamide phosphoribosyl transferase (NAMPT) by FK866, which decreases cellular NAD^+ levels and thus interferes with PAR formation, strongly reduced PPARγ-dependent gene expression and PPARγ protein levels (Figures S2C, S2D). Finally, mouse embryonic fibroblasts (MEFs) lacking ARTD1 exhibited significantly reduced PAR formation and reduced PPARγ-dependent gene expression (Figures S2E, S2F). To exclude potential effects on early differentiation events (e.g., mitotic clonal expansion), we also treated 3T3-L1 cells with PARP inhibitor only during late stages of adipocyte differentiation, from day 7 to day 21. As expected, the PARP inhibitor significantly reduced expression of the PPARγ-dependent genes *aP2*, *CD36* and *Adiponectin* (Figure 2D). Based on these findings, we conclude that PAR formation is required for the expression of PPARγ and PPARγ-dependent genes during the differentiation of 3T3-L1 cells to functional, lipid-laden adipocytes.

The ligand-dependent interaction between PPARγ and ARTD1 at target genes induces PAR

ARTD1 is the main intracellular ADP-ribosyltransferase and generally responsible for about 90% of the cellular PAR formation under normal conditions (Shieh et al., 1998). The stimulation of PPARγ-dependent gene expression upon PARG inhibitor

treatment thus hints at a role for ARTD1 and PAR in regulating the promoter activity of PPARγ target genes. We first assessed the interaction of ARTD1 with PPARγ by immunoprecipitation (IP) experiments of PPARγ from nuclear extracts of 3T3-L1 cells on day 7 of differentiation. The results show that PARylated ARTD1 was co-precipitated using an anti-PPARγ antibody (Figure 3A). Chromatin-IP (ChIP) experiments with anti-ARTD1 antibodies confirmed the PAR-dependent recruitment of ARTD1 at the PPREs of PPARγ-dependent genes (Figure S3A). To further confirm this interaction and to analyze whether ARTD1 and PPARγ interact at the promoter region of the respective target genes, re-ChIP experiments were performed. Chromatin taken from 3T3-L1 cells 7 days after differentiation induction was first precipitated with an anti-ARTD1 antibody and then with an anti-PPARγ antibody, and the presence of *aP2* and *CD36* promoter sequences, corresponding to the PPARγ response elements (PPREs), were subsequently analyzed by quantitative real-time PCR (qRT-PCR). Both, *aP2* and *CD36* PPREs were enriched by the re-ChIP treatment (Figure 3B). In contrast, the negative control gene keratin 19 (*K19*) was not enriched. These results indicate a direct interaction of ARTD1 with PPARγ at the PPREs of at least a subset of PPARγ target genes.

Nuclear receptors such as PPARs are activated and undergo a conformational switch upon ligand binding (Gampe et al., 2000; Gelman et al., 1999; Kallenberger et al., 2003). It was thus hypothesized that the PPARγ ligand may be involved in the ARTD1-dependent regulation of PPARγ itself and thereby affects the interaction between these two proteins. We therefore performed ChIP experiments with lysates from Rosiglitazone pre-treated 3T3-L1 cells at day 7 days of differentiation. In Rosiglitazone pre-treated cells, ARTD1 was more tightly associated with the PPREs of the PPARγ-dependent genes *aP2*, *CD36* and *Adiponectin* (Figure 3C) compared to

cells that were not treated with Rosiglitazone, suggesting a ligand-induced interaction of ARTD1 with PPARγ at the PPREs of these genes. Similarly, ChIP of PAR with the 10H anti-PAR antibody revealed the association of PAR with the PPREs of PPARγ target genes (Figure S3B). To further confirm the interaction between ARTD1 and PPARγ in the presence of the PPARγ ligand Rosiglitazone, pull-down experiments with recombinant, GST-tagged PPARγ2 and recombinant ARTD1 were performed in the presence or absence of Rosiglitazone. The presence of Rosiglitazone enhanced the affinity of ARTD1 for PPARγ2 (Figure 3D). Interestingly, Rosiglitazone treatment not only stimulated ARTD1-PPARγ2 interaction, but also enhanced PAR formation in 3T3-L1 cells at day 7 of differentiation (Figure 3E). In contrast, HEK 293T cells, which do not express PPARγ, only showed weak PAR formation that was not stimulated by Rosiglitazone (Figure S3C), suggesting that the presence of PPARγ is required for PAR formation induced by Rosiglitazone.

Since we have recently shown, that PAR formation during adipogenesis depends on topoisomerase II (TopoII) (Erener et al., 2012a), we also tested whether Rosiglitazone-induced PAR formation depended on TopoII. Indeed, the TopoII inhibitor Merbarone effectively attenuated Rosiglitazone-induced PAR formation (Figure 3F) and ChIP experiments revealed the enrichment of TopoII at the PPREs of the PPARγ-dependent genes *aP2* and *CD36*, while no significant enrichment at the control gene *K19* was observed (Figure 3G). Finally, the co-localization of TopoII and ARTD1 in 3T3-L1 cells (day 7 of adipogenesis) was confirmed by immunofluorescence confocal microscopy (Figure 3H).

In summary, these experiments suggest that ARTD1 and PPARγ interact at the PPREs of target genes in a ligand-dependent manner, which leads to TopoII-dependent PAR formation at PPARγ-dependent genes.

H_2O_2-induced PAR formation causes upregulation of PPARγ-dependent gene expression

So far, our results have shown that PPARγ ligand Rosiglitazone favours the interaction of ARTD1 with PPARγ at the PPREs of target genes and leads to PAR formation during adipogenesis. We therefore tested if PAR formation could induce markers of adipogenesis independent of Rosiglitazone and the classical differentiation protocol. PPARγ and HA-tagged ARTD1 were overexpressed in HEK293T cells and H_2O_2 treatment was used to induce PAR formation (data not shown). An IP with anti-HA antibody precipitated PPARγ2, but only if the cells were treated with H_2O_2 (Figure 4A). Similarly, IP of PPARγ2 precipitated poly-ADP-ribosylated ARTD1 only when PPARγ2-overexpressing HEK293T cells had been exposed to H_2O_2 (Figure 4B). This result confirms that the induction of PAR formation alone is sufficient to stabilize the interaction between ARTD1 and PPARγ. Next, we tested if H_2O_2 also induces adipogenic gene expression in undifferentiated 3T3-L1 cells that overexpress PPARγ2. For these experiments, PPARγ-dependent gene expression was assessed with a reporter construct following exposure to H_2O_2, and other additional experimental conditions (PARP inhibition, overexpression of wild-type (WT) ARTD1, two enzymatic inactive ARTD1 mutants, or PARG inhibition). Rosiglitazone treatment induced PPARγ-dependent gene expression confirming that this reporter construct permits the detection of PPARγ-dependent gene expression in these cells and under these experimental conditions (Figure S4A). H_2O_2 treatment led to increased Luciferase activity, which was comparable to the effect induced by Rosiglitazone (Figure 4C, S4A). Co-treatment with the PARP inhibitor abolished this stimulation, indicating that ADP-ribose polymers are indeed responsible for the

observed effect. Since overexpression of WT ARTD1 strongly enhanced the RLU Firefly/Renilla signal, while neither the E988K nor the Y907A C908Y enzymatically inactive mutant conferred this effect, PPARγ-dependent gene expression was mediated by ARTD1-dependent PAR formation under these experimental conditions (Figure 4D). Co-treating the cells with PARG inhibitor increased the response to H_2O_2 as compared to an inactive control substance (Figure 4E). A similar result was observed in HEK 293T cells overexpressing PPARγ and either one of the ARTD1 mutants (Figure S4B).

Excess of PPARγ ligand functionally replaces PAR

To confirm the results obtained with the Luciferase reporter assay, the effect of PAR formation on PPARγ-dependent gene expression was studied in the 3T3-L1 cells. At day 3 of differentiation we treated cells with H_2O_2, in the presence or absence of PARP inhibitor. Two hours after treatment with H_2O_2, which coincides with PAR formation, the expression of *aP2*, *CD36* and *Adiponectin* was analyzed by qRT-PCR. H_2O_2 treatment led to increased expression of *Adiponectin* (*AdipoQ*) in PPARγ-overexpressing 3T3-L1 cells, which was inhibited by PARP inhibitor (Figure 4F). Not all PPARγ target genes (e.g *aP2*) were induced upon H_2O_2 stimulation (Figure 4F). These results thus demonstrate that the induction of PAR formation by H_2O_2 alone is sufficient to activate the expression of at least a subset of PPARγ-dependent genes. Finally, we assessed whether the PPARγ ligand Rosiglitazone could functionally replace PAR. We therefore treated differentiating 3T3-L1 cells with PARP inhibitor and supplemented with an excess of Rosiglitazone to compensate for the lack of PAR. Indeed, the Rosiglitazone excess compensated for the effect of PARP inhibitor treatment and robustly induced the expression of *aP2*, *CD36*, *Adiponectin* and

PPARγ$_2$ (Figure 4G). As expected, Rosiglitazone induced the expression of all PPARγ-target genes whereas the activation of ARTD1 as shown in Figure 4F was more selective and only induced the expression of a subset of genes.

In summary, these experiments show that PAR formation is able to induce PPARγ-dependent gene expression independent of the presence of PPARγ ligands.

PAR formation controls PPARγ-dependent gene expression by facilitating ligand induced co-factor exchange

The function of DNA-binding transcription factors is regulated by the dynamic exchange of co-activator and co-repressor complexes at the promoters of the target genes (Rosenfeld et al., 2006). Two of the most important regulators of PPARγ functions are the co-activator complex p300 and the nuclear receptor co-repressor 1(NCoR-1) (Lee et al., 2001). We therefore analyzed if these co-factors also interact with ARTD1 and PPARγ in the presence of PPARγ ligands.

GST pull-down experiments with ARTD1, p300 and PPARγ revealed complex formation in the presence of Rosiglitazone, which was further increased in the presence of ADP-ribosylated ARTD1 (Figure 5A). This result suggests a direct interaction of the PPARγ co-activator p300 with ARTD1 and PPARγ. Next, we tested if H_2O_2-stimulated PAR formation could also induce this complex formation in HEK293T cells. PPARγ, ARTD1 and p300 were overexpressed in H_2O_2-stimulated HEK293T cells, and nuclear extracts were prepared. IP of p300 co-precipitated ARTD1 and PPARγ, and in both cases, more protein was co-precipitated in the H_2O_2-treated samples (Figure 5B). Furthermore, we analyzed if the localization of p300 co-activator to the PPARγ-dependent genes was dependent on PAR formation. In 3T3-L1 cells differentiated for 7 days, the binding of p300 to the PRRE of *aP2* and

Adiponectin was significantly reduced upon PARP inhibitor treatment (Figure 5C). This suggests that the reduction of p300 at the PPRE translates into reduced expression of the corresponding gene. The PPARγ-dependent gene *CD36* showed the same trend. Importantly, p300 was not enriched at the PRRE of the PPARγ-independent control gene *K19*. Interestingly, and in agreement with the respective co-activator and -repressor functions, occupancy of the co-repressor NCoR-1 exhibited the opposite behavior and was increased at the PRREs of PPARγ-dependent genes upon PARP inhibiton (Figure 5D). A similar result was obtained with cells that were treated with PARP inhibitor from day 5 to 8 of differentiation (Figure S5A). These findings thus confirm that maintainance of PAR formation is a regulatory requirement for PPARγ-dependent gene expression throughout the differentiation process.

Our findings thus provide evidence that inhibitoion of PARP at the latter stages of adipogenesis allows PPARγ recruitment to its target genes, but that the co-recruitment of the NCoR-1 repressor inhibits the expression of the target genes. In contrast, the presence of PAR favours the recruitment of p300 and subsequently allows progressive PPARγ-dependent gene expression. Taken together, our findings indicate that PAR formation favours co-activator recruitment and enhances transcription from the promoter of specific genes during adipogenesis.

Discussion

Adipogenesis is driven by changes in gene transcription, being reliant on the reprogramming of the cellular transcription profiles through the activation of specific transcription factors (Rosen et al., 2000). Transcription factors that determine the early phase of adipogenesis such as Stat5a, C/EBP-β, and C/EBP-δ, are also responsible for mediating PPARγ activity (Siersbaek et al., 2011). C/EBP-β is required for the establishment of so-called transcription factor 'hotspots', but not sufficient for the maintenance of PPARγ-dependent gene expression. The activation of transcription not only depends on the presence of the correct transcription factor, but also on a permissive chromatin structure (Siersbaek et al., 2011). Transcriptional cofactors regulate chromatin compaction and recruit elements of the transcription machinery. During the course of adipogenesis, co-repressors, which maintain a condensed and closed chromatin state, are replaced by co-activators, which induce relaxation of the chromatin, thereby rendering the DNA accessible to transcription factors (Rosen et al., 2000; Siersbaek et al., 2011).

We have previously shown that ADP-ribosylation, and in particular that mediated by ARTD1, plays an important role in adipogenesis and adipocyte function (Erener et al., 2012a; Erener et al., 2012b). We have shown that ARTD1 activity is required for normal differentiation of 3T3-L1 cells and is likely dependent on the formation of transient, site-specific double strand DNA breaks at promoters of PPARγ-dependent genes (Erener et al., 2012a). These findings were further corrobated by *in vivo* studies showing that the presence of ARTD1 permits efficient adipogenesis, whereas lack of ARTD1 limits adipocyte function, adipocyte size, and lipid metabolism in the liver (Erener et al., 2012b). Although these studies have established a role for ARTD1 in adipogenesis and adipocyte turnover, the molecular mechanism by which ARTD1 or

of ADP-ribosylation in general co-regulate these processes have not yet been described.

In the work presented here, we build up on these earlier studies and show that ADP-ribosylation is an important mediator of WAT formation and *PPARγ2* expression in mice subjected to HFD. Furthermore, our work demonstrates that PAR formation also influences adipogenic gene expression in cell culture and that ARTD1 and PPARγ interact at the promoters of PPARγ target genes, including *aP2* and *CD36,* in a PAR-dependent manner. Most importantly, PAR formation was necessary to induce an exchange of the NCoR1 co-repressor with the p300 co-activator at PPARγ target gene promoters. Treating cells with an excess of PPARγ ligand could overcome the lack of co-factor exchange in the presence of PARP inhibitors. This study thus defines PAR-induced co-factor exchange in the later phase of adipogenesis as the mechanism by which PAR formation regulates and maintains PPARγ2-dependent gene expression. Our own *in vitro* results (data not shown) indicate that this regulation is not mediated by PARylation of PPARγ itself, suggesting that it is mainly the auto-modification of ARTD1 or the ADP-ribosylation of yet unknown acceptor proteins, that is responsible for the ARTD1-dependent regulation of adipogenesis.

PPARγ is a ligand-dependent transcription factor, but the identity of the physiological ligands remains controversial and is under active investigation. During adipogenesis, 3T3-L1 cells synthesize a PPARγ-activating substance, but its identity remains elusive (Tzameli et al., 2004). Polyunsaturated fatty acids and related molecules can activate PPARγ in micromolar concentrations (Forman et al., 1997; Keller et al., 1993; Kliewer et al., 1997; Krey et al., 1997), but it is not yet known if the concentration inside the cell and in proximity to the receptor is sufficient to activate PPARγ or not (Houseknecht et al., 2002). These fatty acids are stored in the

form of triglycerides in lipid droplets (Ducharme and Bickel, 2008). It is currently unclear if fatty acids can activate PPARs before being incorporated into lipid droplets, if rehydrolysis of the triglycerides is required, or if PPARs can be maintained in an activated state by other co-factors (Haemmerle et al., 2011).

Here, we have demonstrated that the increased presence of PAR activates PPARγ-dependent gene expression and showed direct binding and interaction of auto-modified ARTD1 with PPARγ. However, the PPARγ ligand Rosiglitazone did not compete, but rather stimulated the interaction of modified ARTD1 with PPARγ, thus excluding PAR as a classical PPARγ ligand. These results thus define poly-ADP-ribosylated ARTD1 as a new modulator of PPARγ acitivity. PPARγ antagonists exhibit gene-silencing activity due to their ability to promote the recruitment of co-repressors and the subsequent formation of a condensed chromatin state (Bourguet et al., 2000). Co-repressors, such as SMRT and NCOR-1, are dislodged from PPARγ upon ligand binding and their inhibition has the potential to increase the expression of PPARγ target genes (Li et al., 2011; Yu et al., 2005). In contrast, agonists favor the formation of co-activator complexes which can acetylate histones and thereby induce chromatin de-condensation and transcriptional initiation (Bourguet et al., 2000). An important component of such co-activator complexes are the acetyltransferases p300/CBP, which interact with the N-terminus of PPARγ2 independently of the ligand, whereas binding to the C-terminus is ligand-dependent (Gelman et al., 1999). Based on our results, we postulate that ARTD1 represents a new member of PPARγ2 co-activator complexes that helps maintain PPARγ2-dependent gene expression throughout adipogenesis. Recently, selective activation of PPARγ-target genes by certain PPARγ modulators has been reported (Choi et al., 2010; Houtkooper and Auwerx, 2010; Ohno et al., 2012; Rocchi et al., 2001). Similarly to these reports, we

observed increased expression upon H_2O_2 treatment only for a subset of PPARγ-target genes. Hence, it could be speculated that PAR formation influences PPARγ in a similar way as a modulating ligand.

In the experimental system of adipogenesis studied here, PAR formation favored p300 binding to PPREs and thereby ensured continuous expression of PPARγ target genes. This is consistent with the model of PAR as a platform for the recruitment and binding of chromatin remodeling components and elements of the transcription machinery (Tulin and Spradling, 2003). Different nuclear receptors and transcription factors have been linked to TopoII- and ARTD1-dependent activation of gene expression, supporting the idea that this might be a general regulatory mechanism for different nuclear receptors involved in the regulation of various cellular processes (Ju et al., 2006; Ju and Rosenfeld, 2006; Ju et al., 2004).

PPARγ is also expressed in cells of the immune system, such as macrophages, where it can act as a repressor for inflammatory gene expression through a process called transrepression. It is an intriguing possibility that PAR formation may also be involved in this process as well. Recently, a role for NCoR in systemic insulin resistance upon HFD-induced obesity has been described (Li et al., 2013), raising the question as to whether PAR formation might be important for the cofactor recruitment and thus for the development of insulin resistance in this context.

An interesting and unexpected result of this study was the strong effect of PARP inhibition on ScWAT formation in mice exposed to HFD. Since ScWAT is a potential target for therapies aimed at treating metabolic syndrome (Rodriguez et al., 2007), PARP inhibitors may open up new treatment options for patients suffering from this disorder. Due to their high level of tolerance and anti-inflammatory effects, PARP inhibitors are considered to be promising therapeutic compounds (Giansanti et al.,

2010; Haddad et al., 2006; Hutchinson, 2010). Also, it might be beneficial that PAR has an atypical ligand function and thereby activates only a subset of genes, since this allows for more selective treatment. Previous studies showed hepatic steatosis in ARTD1$^{-/-}$ mice fed with HFD (Erener et al., 2012b), whereas lipid accumulation in the liver was absent in WT mice treated with PARP inhibitor. The differences between the PARP inhibitor experiments reported here and the previously reported phenotypes of ARTD1$^{-/-}$ mice may indicate functions of the ARTD1 protein in WAT and the liver that are independent of its activity, an effect on energy metabolism by PARP inhibitor treatment (not the case for ARTD1$^{-/-}$ mice), qualitative differences in the composition of the diet, or a contribution of ARTD2 or other ARTDs (Bai et al., 2007).

In summary, our results support a model that involves the formation of co-activator complexes by PAR at the promoters of PPARγ-dependent genes (Figure S5B). Most importantly, the presence of PAR molecules correlated with the switch from co-activator to co-repressor complexes at promoters of PPARγ-dependent genes, implying a direct role for PAR in determining the transcriptional outcome at specific loci. These results thus demonstrate that PAR formation is required for the maintenance of PPARγ-dependent gene expression. Together with the beneficial effect observed with PARP inhibition in the mice, our results obtained *in vitro* highlight the therapeutic potential of targeting ADP-ribosylation to modulate adipocyte function under conditions such as obesity.

Methods

Animal experiments

A novel pan-PARP inhibitor MRLB-45696 (IC50 for PARP-1 and -2 <1 nM; Pirinen et al, 2013 manuscript submitted) was kindly provided by Thomas Vogt, from Merck Research Laboratories. Eight weeks old male C57BL/6J mice were fed with in house-made pellets containing vehicle or PARP inhibitor (50 mg/kg/day) for 18 weeks. All animal experiments were carried out according to the Swiss and EU ethical guidelines and have been approved by the local animal experimentation committee of the Canton de Vaud under license #2465.

Cell culture

For differentiation, 3T3-L1 cells were plated at 80% confluence, medium was changed after 2 days, and induction medium containing 1μg/ml insulin (I-9278) 0.25 mM 3-isobutyl-1-methylxanthine (I-5879), and 0.5 μM dexamethasone (D-4902) (Sigma Aldrich, St. Louis, MO, USA) was added after 3 additional days. Starting at day 5, medium was changed every second day to DMEM containing insulin (1 μg/ml). Cells were differentiated in the presence or absence of PARP inhibitors PJ34 or ABT888 (both at 1 μM or 10 μM), PARG inhibitor RBPI-3, Topoisomerase II inhibitor Merbarone (50 μM), or PPARγ agonist Rosiglitazone (1 μM or 10 μM) added to the cells every 24 hours. For differentiation until day 21, ABT888 was added only every second day. H_2O_2 treatment (1 mM, 15 min) was performed in DMEM without FCS (and in the presence of catalase inhibitor 3-AT (30 μM) and in the presence or absence of PJ34 (10 μM)).

GST-pulldown

GST-PPARγ2 was coupled to magnetic GST-Beads (Pierce). 1 µg modified or unmodified ARTD1 (in reaction buffer, 5 pmol 40mer DNA, ±10 mM NAD, 30 mins at 30°C) and 1 µg His-p300 were added to the GST-PPARγ2. Pulldown was performed for 2 h at 4°C in pulldown buffer (50 mM Tris pH 7.5, 150 mM KCl, 5 mM MgCl2, 0.2 mM EDTA, 20% Glycerol, 0.1% NP40) in the presence of 10 µM PJ34. The beads were washed 3x with wash buffer (20 mM Tris pH 7.5, 150 mM KCl, 5 mM MgCl2, 0.2 mM EDTA, 10% Glycerol, 0.1% Tween).

Chromatin immunoprecipitation (ChIP)

ChIP was performed as previously described (Santoro et al., 2002). For Re-ChIP experiments, the first ChIP (anti-ARTD1) was eluted twice in 10 mM DTT (30 mins, at 30°C), diluted in ChIP buffer, and the second ChIP (anti-PPARγ) was performed as previously described (Santoro et al., 2002).

References

Bai, P., and Canto, C. (2012). The Role of PARP-1 and PARP-2 Enzymes in Metabolic Regulation and Disease. Cell Metab *16*, 290-295.

Bai, P., Houten, S.M., Huber, A., Schreiber, V., Watanabe, M., Kiss, B., de Murcia, G., Auwerx, J., and Menissier-de Murcia, J. (2007). Poly(ADP-ribose) polymerase-2 [corrected] controls adipocyte differentiation and adipose tissue function through the regulation of the activity of the retinoid X receptor/peroxisome proliferator-activated receptor-gamma [corrected] heterodimer. J Biol Chem *282*, 37738-37746.

Bourguet, W., Germain, P., and Gronemeyer, H. (2000). Nuclear receptor ligand-binding domains: three-dimensional structures, molecular interactions and pharmacological implications. Trends Pharmacol Sci *21*, 381-388.

Chawla, A., Boisvert, W.A., Lee, C.H., Laffitte, B.A., Barak, Y., Joseph, S.B., Liao, D., Nagy, L., Edwards, P.A., Curtiss, L.K.*, et al.* (2001). A PPAR gamma-LXR-ABCA1 pathway in macrophages is involved in cholesterol efflux and atherogenesis. Mol Cell *7*, 161-171.

Choi, J.H., Banks, A.S., Estall, J.L., Kajimura, S., Bostrom, P., Laznik, D., Ruas, J.L., Chalmers, M.J., Kamenecka, T.M., Bluher, M.*, et al.* (2010). Anti-diabetic drugs inhibit obesity-linked phosphorylation of PPARgamma by Cdk5. Nature *466*, 451-456.

Church, C., Horowitz, M., and Rodeheffer, M. (2012). WAT is a functional adipocyte? Adipocyte *1*, 38-45.

Ducharme, N.A., and Bickel, P.E. (2008). Lipid droplets in lipogenesis and lipolysis. Endocrinology *149*, 942-949.

Erener, S., Hesse, M., Kostadinova, R., and Hottiger, M.O. (2012a). Poly(ADP-ribose)polymerase-1 (PARP1) controls adipogenic gene expression and adipocyte function. Mol Endocrinol *26*, 79-86.

Erener, S., Mirsaidi, A., Hesse, M., Tiaden, A.N., Ellingsgaard, H., Kostadinova, R., Donath, M.Y., Richards, P.J., and Hottiger, M.O. (2012b). ARTD1 deletion causes increased hepatic lipid accumulation in mice fed a high-fat diet and impairs adipocyte function and differentiation. FASEB J *26*, 2631-2638.

Escher, P., Braissant, O., Basu-Modak, S., Michalik, L., Wahli, W., and Desvergne, B. (2001). Rat PPARs: quantitative analysis in adult rat tissues and regulation in fasting and refeeding. Endocrinology *142*, 4195-4202.

Fajas, L., Auboeuf, D., Raspe, E., Schoonjans, K., Lefebvre, A.M., Saladin, R., Najib, J., Laville, M., Fruchart, J.C., Deeb, S.*, et al.* (1997). The organization, promoter analysis, and expression of the human PPARgamma gene. J Biol Chem *272*, 18779-18789.

Forman, B.M., Chen, J., and Evans, R.M. (1997). Hypolipidemic drugs, polyunsaturated fatty acids, and eicosanoids are ligands for peroxisome proliferator-activated receptors alpha and delta. Proc Natl Acad Sci USA *94*, 4312-4317.

Gampe, R.T., Jr., Montana, V.G., Lambert, M.H., Miller, A.B., Bledsoe, R.K., Milburn, M.V., Kliewer, S.A., Willson, T.M., and Xu, H.E. (2000). Asymmetry in the PPARγ/RXRα crystal structure reveals the molecular basis of heterodimerization among nuclear receptors. Mol Cell *5*, 545-555.

Gelman, L., Zhou, G., Fajas, L., Raspe, E., Fruchart, J.C., and Auwerx, J. (1999). p300 interacts with the N- and C-terminal part of PPARgamma2 in a ligand-independent and -dependent manner, respectively. J Biol Chem *274*, 7681-7688.

Giansanti, V., Dona, F., Tillhon, M., and Scovassi, A.I. (2010). PARP inhibitors: new tools to protect from inflammation. Biochem Pharmacol *80*, 1869-1877.

Graziani, G., and Szabo, C. (2005). Clinical perspectives of PARP inhibitors. Pharmacol Res *52*, 109-118.

Haddad, M., Rhinn, H., Bloquel, C., Coqueran, B., Szabo, C., Plotkine, M., Scherman, D., and Margaill, I. (2006). Anti-inflammatory effects of PJ34, a poly(ADP-ribose) polymerase inhibitor, in transient focal cerebral ischemia in mice. Br J Pharmacol *149*, 23-30.

Haemmerle, G., Moustafa, T., Woelkart, G., Buttner, S., Schmidt, A., van de Weijer, T., Hesselink, M., Jaeger, D., Kienesberger, P.C., Zierler, K.*, et al.* (2011). ATGL-mediated fat catabolism regulates cardiac mitochondrial function via PPAR-alpha and PGC-1. Nat Med *17*, 1076-1085.

Hassa, P.O., and Hottiger, M.O. (2008). The diverse biological roles of mammalian PARPs, a small but powerful family of poly-ADP-ribose polymerases. Front Biosci *13*, 3046-3082.

Heikkinen, S., Auwerx, J., and Argmann, C.A. (2007). PPARgamma in human and mouse physiology. Biochim Biophys Acta *1771*, 999-1013.

Hottiger, M.O., Hassa, P.O., Lüscher, B., Schüler, H., and Koch-Nolte, F. (2010). Toward a unified nomenclature for mammalian ADP-ribosyltransferases. Trends Biochem Sci *35*, 208-219.

Houseknecht, K.L., Cole, B.M., and Steele, P.J. (2002). Peroxisome proliferator-activated receptor gamma (PPARγ) and its ligands: a review. Domest Anim Endocrinol *22*, 1-23.

Houtkooper, R.H., and Auwerx, J. (2010). Obesity: New life for antidiabetic drugs. Nature *466*, 443-444.

Hutchinson, L. (2010). Targeted therapies: PARP inhibitor olaparib is safe and effective in patients with BRCA1 and BRCA2 mutations. Nat Rev Clin Oncol *7*, 549.

Ju, B.-G., Lunyak, V., Perissi, V., Garcia-Bassets, I., Rose, D., Glass, C., and Rosenfeld, M. (2006). A topoisomerase IIbeta-mediated dsDNA break required for regulated transcription. Science *312*, 1798-1802.

Ju, B.-G., and Rosenfeld, M. (2006). A breaking strategy for topoisomerase IIbeta/PARP-1-dependent regulated transcription. Cell Cycle *5*, 2557-2560.

Ju, B.-G., Solum, D., Song, E., Lee, K.-J., Rose, D., Glass, C., and Rosenfeld, M. (2004). Activating the PARP-1 sensor component of the groucho/ TLE1 corepressor complex mediates a CaMKinase IIdelta-dependent neurogenic gene activation pathway. Cell *119*, 815-829.

Kallenberger, B.C., Love, J.D., Chatterjee, V.K., and Schwabe, J.W. (2003). A dynamic mechanism of nuclear receptor activation and its perturbation in a human disease. Nat Struct Biol *10*, 136-140.

Keller, H., Dreyer, C., Medin, J., Mahfoudi, A., Ozato, K., and Wahli, W. (1993). Fatty acids and retinoids control lipid metabolism through activation of peroxisome proliferator-activated receptor-retinoid X receptor heterodimers. Proc Natl Acad Sci USA *90*, 2160-2164.

Kliewer, S.A., Sundseth, S.S., Jones, S.A., Brown, P.J., Wisely, G.B., Koble, C.S., Devchand, P., Wahli, W., Willson, T.M., Lenhard, J.M.*, et al.* (1997). Fatty acids and eicosanoids regulate gene expression through direct interactions with peroxisome proliferator-activated receptors alpha and gamma. Proc Natl Acad Sci USA *94*, 4318-4323.

Kliewer, S.A., Umesono, K., Mangelsdorf, D.J., and Evans, R.M. (1992). Retinoid X receptor interacts with nuclear receptors in retinoic acid, thyroid hormone and vitamin D3 signalling. Nature *355*, 446-449.

Krey, G., Braissant, O., L'Horset, F., Kalkhoven, E., Perroud, M., Parker, M.G., and Wahli, W. (1997). Fatty acids, eicosanoids, and hypolipidemic agents identified as

ligands of peroxisome proliferator-activated receptors by coactivator-dependent receptor ligand assay. Mol Endocrinol *11*, 779-791.

Lee, J.W., Lee, Y.C., Na, S.Y., Jung, D.J., and Lee, S.K. (2001). Transcriptional coregulators of the nuclear receptor superfamily: coactivators and corepressors. Cell Mol Life Sci *58*, 289-297.

Lefterova, M.I., Zhang, Y., Steger, D.J., Schupp, M., Schug, J., Cristancho, A., Feng, D., Zhuo, D., Stoeckert, C.J., Jr., Liu, X.S.*, et al.* (2008). PPARγ and C/EBP factors orchestrate adipocyte biology via adjacent binding on a genome-wide scale. Genes Dev *22*, 2941-2952.

Li, P., Fan, W., Xu, J., Lu, M., Yamamoto, H., Auwerx, J., Sears, D.D., Talukdar, S., Oh, D., Chen, A.*, et al.* (2011). Adipocyte NCoR knockout decreases PPARgamma phosphorylation and enhances PPARgamma activity and insulin sensitivity. Cell *147*, 815-826.

Li, P., Spann, N.J., Kaikkonen, M.U., Lu, M., Oh da, Y., Fox, J.N., Bandyopadhyay, G., Talukdar, S., Xu, J., Lagakos, W.S.*, et al.* (2013). NCoR repression of LXRs restricts macrophage biosynthesis of insulin-sensitizing omega 3 fatty acids. Cell *155*, 200-214.

Ntambi, J.M., and Young-Cheul, K. (2000). Adipocyte differentiation and gene expression. J Nutr *130*, 3122S-3126S.

Ohno, H., Shinoda, K., Spiegelman, B.M., and Kajimura, S. (2012). PPARgamma agonists induce a white-to-brown fat conversion through stabilization of PRDM16 protein. Cell Metab *15*, 395-404.

Rocchi, S., Picard, F., Vamecq, J., Gelman, L., Potier, N., Zeyer, D., Dubuquoy, L., Bac, P., Champy, M.F., Plunket, K.D.*, et al.* (2001). A unique PPARgamma ligand with potent insulin-sensitizing yet weak adipogenic activity. Mol Cell *8*, 737-747.

Rodriguez, A., Catalan, V., Gomez-Ambrosi, J., and Fruhbeck, G. (2007). Visceral and subcutaneous adiposity: are both potential therapeutic targets for tackling the metabolic syndrome? Curr Pharm Des *13*, 2169-2175.

Rosen, E.D., Hsu, C.H., Wang, X., Sakai, S., Freeman, M.W., Gonzalez, F.J., and Spiegelman, B.M. (2002). C/EBPalpha induces adipogenesis through PPARgamma: a unified pathway. Genes Dev *16*, 22-26.

Rosen, E.D., Walkey, C.J., Puigserver, P., and Spiegelman, B.M. (2000). Transcriptional regulation of adipogenesis. Genes Dev *14*, 1293-1307.

Rosenfeld, M., Lunyak, V., and Glass, C. (2006). Sensors and signals: a coactivator/corepressor/epigenetic code for integrating signal-dependent programs of transcriptional response. Genes Dev *20*, 1405-1428.

Saladin, R., Fajas, L., Dana, S., Halvorsen, Y.D., Auwerx, J., and Briggs, M. (1999). Differential regulation of peroxisome proliferator activated receptor gamma1 (PPARgamma1) and PPARgamma2 messenger RNA expression in the early stages of adipogenesis. Cell Growth Differ *10*, 43-48.

Santoro, R., Li, J., and Grummt, I. (2002). The nucleolar remodeling complex NoRC mediates heterochromatin formation and silencing of ribosomal gene transcription. Nat Genet *32*, 393-396.

Shieh, W., Amé, J., Wilson, M., Wang, Z., Koh, D., Jacobson, M., and Jacobson, E. (1998). Poly(ADP-ribose) polymerase null mouse cells synthesize ADP-ribose polymers. J Biol Chem *273*, 30069-30072.

Siersbaek, R., Nielsen, R., John, S., Sung, M.H., Baek, S., Loft, A., Hager, G.L., and Mandrup, S. (2011). Extensive chromatin remodelling and establishment of transcription factor 'hotspots' during early adipogenesis. EMBO J *30*, 1459-1472.

Siersbaek, R., Nielsen, R., and Mandrup, S. (2010). PPARγ in adipocyte differentiation and metabolism - novel insights from genome-wide studies. FEBS Lett *584*, 3242-3249.

Tontonoz, P., Hu, E., Graves, R.A., Budavari, A.I., and Spiegelman, B.M. (1994). mPPAR gamma 2: tissue-specific regulator of an adipocyte enhancer. Genes Dev *8*, 1224-1234.

Tontonoz, P., and Spiegelman, B.M. (2008). Fat and beyond: the diverse biology of PPARγ. Annu Rev Biochem *77*, 289-312.

Tulin, A., and Spradling, A. (2003). Chromatin loosening by poly(ADP)-ribose polymerase (PARP) at Drosophila puff loci. Science *299*, 560-562.

Tzameli, I., Fang, H., Ollero, M., Shi, H., Hamm, J.K., Kievit, P., Hollenberg, A.N., and Flier, J.S. (2004). Regulated production of a peroxisome proliferator-activated receptor-gamma ligand during an early phase of adipocyte differentiation in 3T3-L1 adipocytes. J Biol Chem *279*, 36093-36102.

Vidal-Puig, A., Jimenez-Linan, M., Lowell, B.B., Hamann, A., Hu, E., Spiegelman, B., Flier, J.S., and Moller, D.E. (1996). Regulation of PPAR gamma gene expression by nutrition and obesity in rodents. J Clin Invest *97*, 2553-2561.

Yu, C., Markan, K., Temple, K.A., Deplewski, D., Brady, M.J., and Cohen, R.N. (2005). The nuclear receptor corepressors NCoR and SMRT decrease peroxisome proliferator-activated receptor gamma transcriptional activity and repress 3T3-L1 adipogenesis. J Biol Chem *280*, 13600-13605.

Author Contributions

ML planned and performed the experiments, evaluated the data, and wrote the manuscript. AM and PJR performed histological and RNA isolation from mouse tissue. EP organized and performed mouse studies. JA supervised experiments and revised the manuscript. MOH supervised the study and wrote the manuscript.

Johan Auwerx is a founder and SAB member of Mitokyne.

Acknowledgements

The authors thank Laia Morato (EPFL, Switzerland) for measurement of ARTD activity. The RBPI-3 PARG inhibitor was a kind gift of Prof. Dr. Paul J. Hergenrother (University of Illinois, USA). The novel pan-PARP inhibitor MRLB-45696 was kindly provided by Thomas Vogt (Merck Research Laboratories). We thank M. Altmeyer (NNF CPR, Copenhagen) for generating the ARTD1 mutants and C. Wolfrum for the 3T3-L1 cells and for helpful discussions (ETH Zurich, Switzerland). W. Wahli (University of Lausanne) provided the Luciferase and PPARγ expression plasmids. F. Freimoser and all the members of the Institute of Veterinary Biochemistry and Molecular Biology (University of Zurich, Switzerland) for help and discussions during the preparation of this manuscript. Research on ADP-ribosylation in the laboratory of MOH is supported by the Swiss National Science Foundation Grant 310030B_138667 and the Kanton of Zurich. ML was funded by the Forschungskredit of the University of Zurich. EP was funded by the Academy of Finland, the Saastamoinen Foundation, the Finnish Cultural Foundation and the Finnish Diabetes Foundation. JA is the Nestlé Chair in Energy Metabolism and his lab is supported by grants of the Ecole Polytechnique Fédérale de Lausanne, the EU

Ideas program (AdG-23138) “Sirtuins”, and the Swiss National Science Foundation (31003A-124713).

Figure Legends

Figure 1. PARP inhibitor treatment reduces body weight and adipose tissue size in mice.

A-B) Weight development during chow and high-fat diet (HFD) in vehicle- and PARP inhibitor-treated mice. Eight weeks old male C57BL/6J mice were fed with chow or HFD containing vehicle (DMSO) or PARP inhibitor (50 mg/kg/day) for 18 weeks. Body weight gain was monitored at the given time points. Data are mean ± SEM, Anova two-way analysis revealed $p<0.001$ for both HFD and Chow. Data are mean ± SEM. T-test: *$p<0.05$, **$p<0.01$, ***$p<0.001$. n=10 C-D) Fat pad weights on chow and HFD. Animals were sacrificed after overnight fasting using isoflurane inhalation and tissues were collected upon sacrifice and flash-frozen in liquid nitrogen. epiWAT; epididymal white adipose tissue, scWAT; subcutaneous white adipose tissue, periWAT; perirenal white adipose tissue and BAT; brown adipose tissue. Data are mean ± SEM. Anova one way test *$p<0.05$, **$p<0.01$, ***$p<0.001$. n=10 E) Mouse adipose tissue was fixed, dehydrated, and embedded in paraffin wax. Sequential sections (6μm) were cut and morphological changes visualized using H&E staining (scale bar 200μm). Blinded analysis of mean adipocyte area in tissue sections from mice (N= 5-6 per treatment group) was performed F) qRT-PCR analysis of WAT isolated from vehicle- and PARP inhibitor-treated mice. For qRT-PCR analysis of tissue samples, isolated WAT from 8 mice per group was pooled and expression values were normalized against 36BP4. Data are mean ± SEM. T-test: *$p<0.05$, **$p<0.01$, ***$p<0.001$.

Figure 2. PAR formation is required for PPARγ-dependent gene expression. A) Adipogenesis was induced by adding insulin, 3-isobutyl-1-methylxanthine (IBMX)

and dexamethasone for three days and maintaining cells in medium containing 10% fetal calf serum (FCS) and insulin. B) Cells were differentiated in the presence of 10 μM ABT888 (daily treatment) until day 7, at which point RNA was isolated (n=8). C) Differentiating 3T3-L1 cells were treated with 10μM PARG inhibitor RBPI-3 at the days 1-5 and RNA was isolated on day 6 of differentiation (n=5). D) PAR formation is required for maintenance of PPARγ-dependent gene expression. Starting from day 7 of adipogenesis of 3T3-L1 cells, the culture medium containing insulin and 10 μM ABT888 was changed every second day. RNA was isolated at day 21 and gene expression was analyzed by RT-qPCR (n=4). All values represent the mean ± SEM, unteated samples were set as 1. T-test: *p<0.05, **p<0.01, ***p<0.001.

Figure 3. Ligand-dependent interaction of PPARγ and ARTD1 at the PPREs of PPARγ-target genes. A) 3T3-L1 cells were differentiated until day 7, nuclear protein extracts were prepared and PPARγ was immuno-precipitated. To prevent degradation of PAR, extracts were treated with 10 μM PARG inhibitor (RBPI-3). B) At day 7 of differentiation, cells were fixed and the chromatin was first precipitated with an ARTD1 antibody and then with a PPARγ antibody (n=4). C) Cells were differentiated and treated with 10 μM Rosiglitazone at day 2 and 5. At day 7 of differentiation, cells were fixed and the chromatin was immuno-precipitated with an ARTD1 antibody (n=2). D) PPARγ$_2$-GST pull-down of ARTD1 in the presence or absence of a 10 μM Rosiglitazone preincubation. E) At day 7 of differentiation, cells were treated with 10 μM Rosiglitazone for the indicated periods of time. Whole cell extracts were analyzed by Western Blot. F) At day 7 of differentiation, cells were treated for 24 or 2 h with 10 μM Rosiglitazone in the presence or absence of 50μM Merbarone (Mer). Whole cell extracts were analyzed by Western Blot. G) Cells were fixed at day 7 of

differentiation and chromatin was immuno-precipitated with a Topoisomerase II antibody (n=3). H) At day 7 of differentiation, 3T3-L1 cells were fixed with PFA and stained with an antibody against Topoisomerase II (green) and PPARγ (red). DAPI was used to visualize the nuclei (blue). Cells were analyzed by confocal microscopy. All values represent the mean ±SEM. Values were normalized over IgG control. T-test: *p<0.05, **p<0.01, ***p<0.001.

Figure 4: PAR formation enhances PPARγ-dependent gene expression. A) Hek293T cells overexpressing PPARγ2 and HA-ARTD1 were treated with 1 mM H_2O_2 (15 min) in the presence of 30 μM catalase inhibitor (3-AT). IP with an anti-HA antibody was performed with nuclear extracts. B) Hek293T cells overexpressing PPARγ2 were treated with 1 mM H_2O_2 (15 min) in the presence of catalase inhibitor. IP with an anti-PPARγ antibody was performed with nuclear extracts. C) 3T3-L1 cells overexpressing PPARγ2 were treated with 1 mM H_2O_2 (2 h) in the presence of 30 μM catalase inhibitor (3-AT) and in the presence or absence of 10 μM PJ34. Luciferase activity was measured (n=4). D) 3T3-L1 cells co-overexpressing PPARγ2 and ARTD1 (wild-type, n=5), ARTD1 E988K (n=4), ARTD1 Y907A/C908Y (n=3) or GFP (as a negative control, n=5) were treated with 1 mM H_2O_2 (2 h) in the presence of 30 μM catalase inhibitor (3-AT). E) 3T3-L1 cells overexpressing PPARγ2 were pretreated with 10μM PARG inhibitor (RBPI-3) and treated with 1 mM H_2O_2 (2h) in the presence of 30 μM catalase inhibitor (3-AT) (n=5). F) Cells were treated with 1 mM H_2O_2 (2 h) in the presence of 30 μM catalase inhibitor (3-AT) and in the presence or absence of 10 μM PJ34. The medium was then exchanged with medium containing fresh FCS and samples were taken after 2h (n=5). G) PAR formation is required for the maintenance of PPARγ-dependent gene expression. During

differentiation, 3T3-L1 cells were treated with 10 μM Rosiglitazone or 10 μM ABT888 at days 2-6 of adipogenesis (n=4). T-test: *p<0.05, **p<0.01, ***p<0.001.

Figure 5: PAR formation controls PPARγ-dependent gene expression by maintaining ligand induced cofactor exchange. A) PPARγ2-GST pull-down of ARTD1 (nonmodified or automodified, indicated by *, modified ARTD1 has a higher molecular weight (above 130 kDa) than unmodified and p300 in the presence or absence of 10 μM Rosiglitazone pretreatment of PPARγ2-GST. B) Hek293T cells overexpressing PPARγ2, p300 and ARTD1 were treated with 1 mM H_2O_2 (15 min) in the presence of catalase inhibitor. IP with an anti-p300 antibody was performed with nuclear extracts. C) Starting from day 2 of adipogenesis, 3T3-L1 cells were treated daily with 10 μM PJ34. At day 7, the cells were fixed with formaldehyde and the chromatin was immuno-precipitated with an anti-p300 antibody (n=4). D) Same analysis as in C for NCOR-1 (n=3). T-test: *p<0.05, **p<0.01, ***p<0.001.

Lehmann et al. *Figure 1*

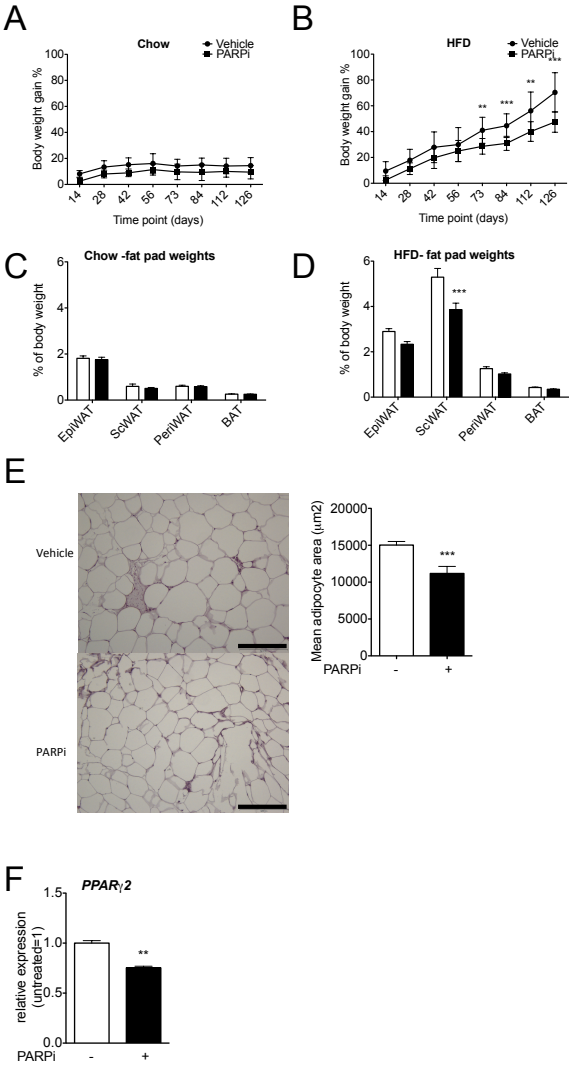

Lehmann et al. *Figure 2*

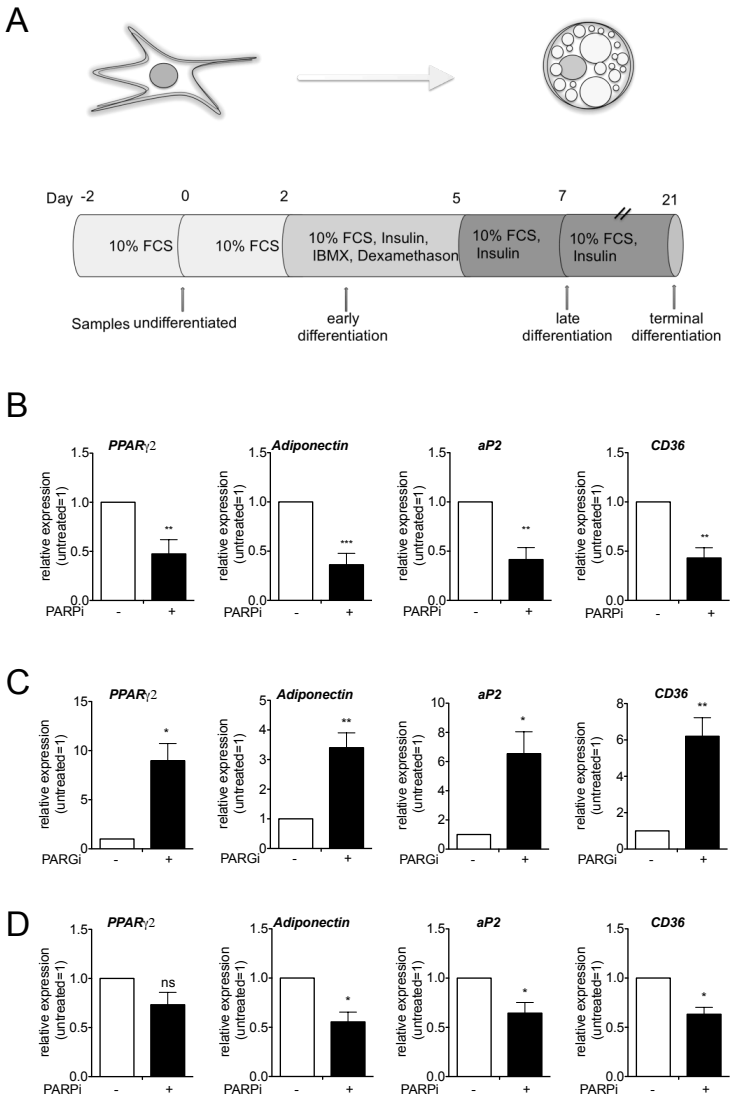

Lehmann et al. *Figure 3*

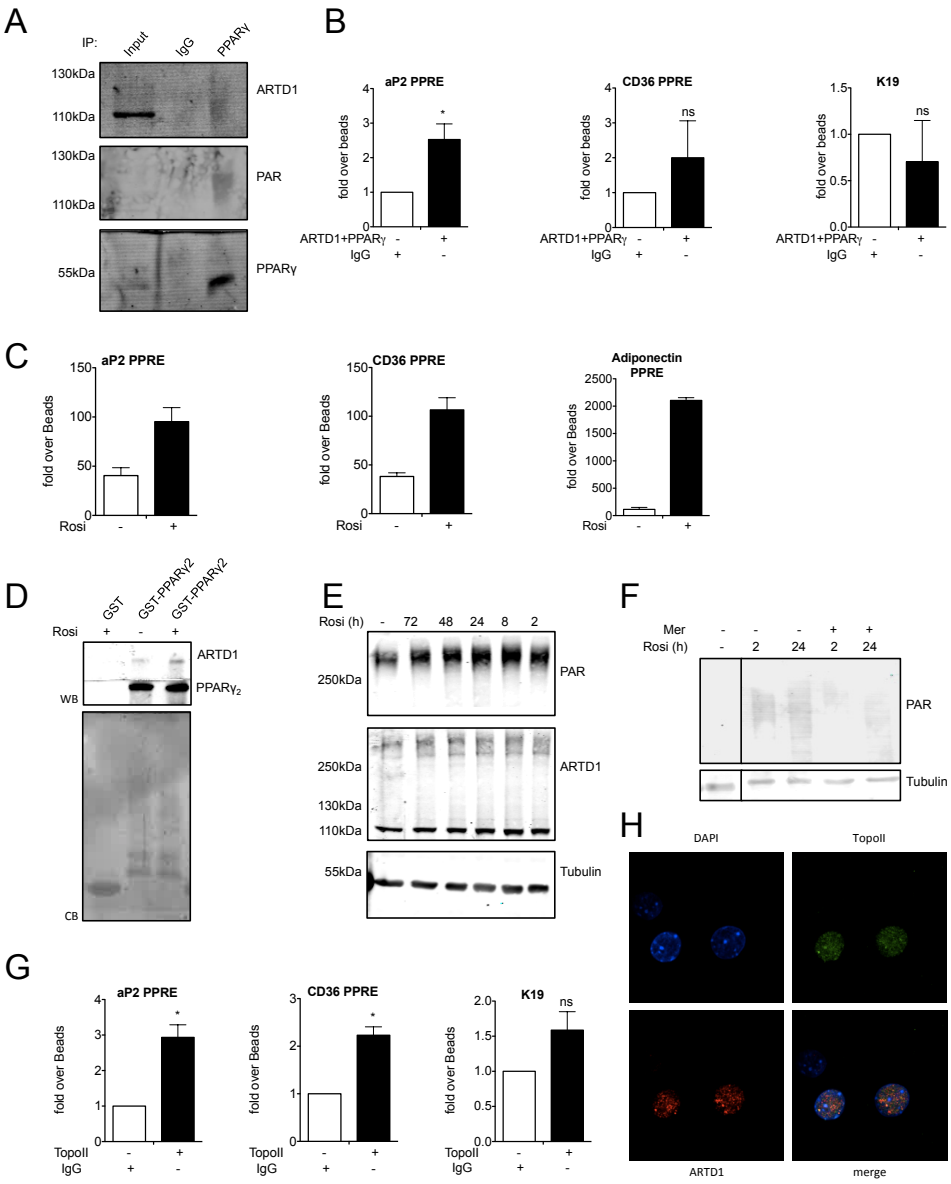

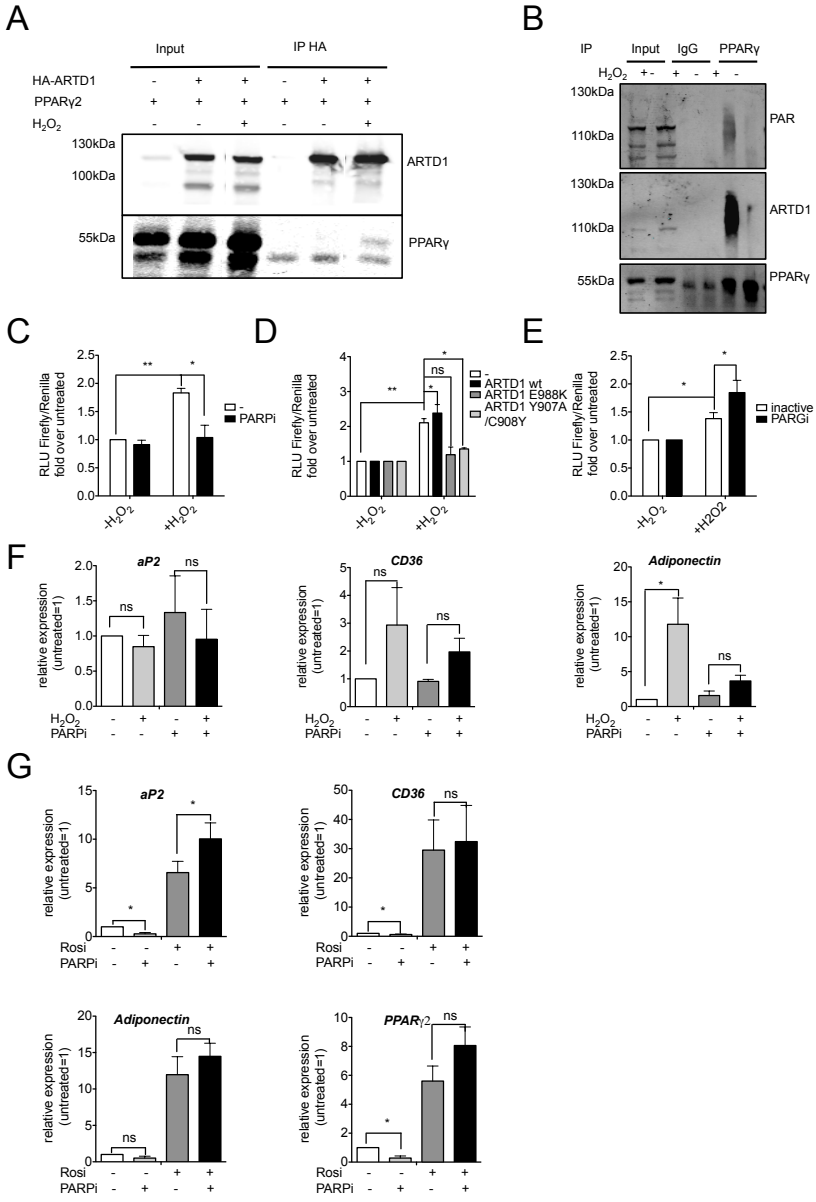
A
Input
IP HA
HA-ARTD1
PPARγ2
H2O2
130kDa
100kDa
55kDa
ARTD1
PPARγ
B
IP
Input
IgG
PPARγ
H2O2
130kDa
110kDa
PAR
ARTD1
PPARγ
C
RLU Firefly/Renilla fold over untreated
PARPi
-H2O2
+H2O2
D
ARTD1 wt
ARTD1 E988K
ARTD1 Y907A /C908Y
E
inactive
PARGi
+H2O2
F
aP2
CD36
Adiponectin
relative expression (untreated=1)
G
Rosi
PARPi
PPARγ2

Lehmann et al. *Figure 5*

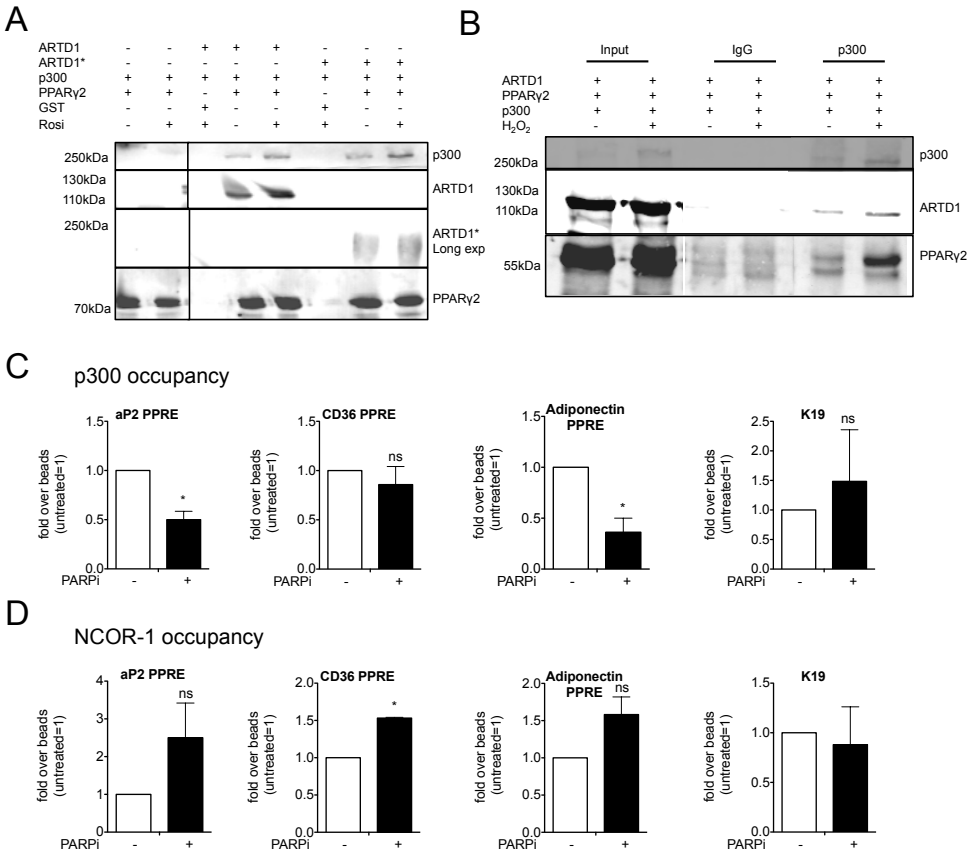

Supplementary Information

Supplemental Experimental Procedures

Reagents

RBPI-3 and inactive substance was a kind gift of Prof. Dr. Paul J. Hergenrother (University of Illinois, USA). Dexamethasone (D-4902), 3-isobutyl-1-methylxanthine (I-5879), insulin (I-9278), rosiglitazone (R-2408) and merbarone (M2070) were obtained from Sigma-Aldrich (St. Louis, MO). Anti-PARP (sc-7150) and anti-Topoisomerase II (sc-8030; used for Immunofluorescence) antibodies were purchased from Santa Cruz Biotechnology, Inc. (Santa Cruz, CA), anti-PPARγ rb (2443S), and anti-PARP (46D11) were from Cell Signaling (Cambridge, UK), anti-p300 (554215) from BD Pharmigen (Franklin Lakes, NJ, USA), anti-PPARγ ms (ab41928), anti-NCOR-1 (ab24552), anti-TopoII (ab58442; used for ChIP) were obtained from Abcam (Cambridge, UK), and anti-tubulin (T6199) antibody was from Sigma-Aldrich. The anti-PAR 10H antibody was homemade. PJ34 and ABT888 were from Enzo Life Sciences (Farmindale, NY, USA)(ALX-270-289; ALX-270-444).

Animal experiments

A novel pan-PARP inhibitor MRLB-45696 (IC50 for PARP-1 and -2 <1 nM; Pirinen et al, 2013 manuscript submitted) was kindly provided by Thomas Vogt, from Merck Research Laboratories. Eight weeks old male C57BL/6J mice were purchased from Charles River and after two weeks of adaptation time, mice were fed with homemade pellets containing vehicle or PARP inhibitor (50 mg/kg/day) for 18 weeks. The pellets were prepared as follows; the powder food and water were mixed with DMSO (vehicle) or with PARP inhibitor dissolved in DMSO and pellets were dried under the hood at least over night. Powder chow (D12450B) and high fat (D12492) diets used

were from Research Diets Inc. Body weights were recorded every second week and food intake was measured by weighting one-week food consumption in the middle of the experiment. Animals were sacrificed after overnight fasting using isoflurane inhalation. Tissues were collected upon sacrifice and flash-frozen in liquid nitrogen. During experiment, mice were housed under a 12h dark-light cycle and they had ad libitum access to water and food.

Cell culture

3T3-L1 and Hek293T cells were cultivated in Dulbecco's Modified Eagle's Medium (DMEM) (PAA, Pasching, Austria, supplemented with 1% (v/v) Penicillin/Streptavidin and 10% (v/v) fetal calf serum (Gibco, Invitrogen, CA, California, USA).

RNA extraction with TRIzol® reagent and qPCR analysis

TRIzol® RNA Isolation Reagent (Life Technologies, CA, California, USA) was applied directly to the plates and the supplier's protocol was followed. DNase treatment was performed using the TURBO DNA-freeTM Kit (Life Technologies, Carlsbad, CA, USA). RNA was quantified with a NanoDrop (ThermoFisherScintific, Waltham, MS, USA) and reverse transcribed according to the supplier's protocol (High Capacity cDNA Reverse Transcription Kit, Applied Biosystems, Foster City, CA, United States). Quantitative-real-time polymerase chain reactions (qPCR) were performed in triplicate with SYBR® green SensiMix SYBR Hi-ROX Kit (Bioline Reagents Ltd, London, UK) in a Rotor-Gene Q 2plex HRM System (Qiagen, Hilden, Germany). For qRT-PCR analysis of tissue samples, isolated WAT from 8 mice per group was pooled and expression values were normalized against *36BP4*.

Immunofluorescence

Cells were seeded in chamber slides and differentiated according to protocol until day 7. Cells were fixed with 4% PFA, washed twice with PBS, permeabilized with 0.2% Triton X-100, and incubated with anti-Topoisomerase II and anti ARTD1 antibody (1:150; 1:500) in PBS (containing 2% BSA and 0.1% Triton X-100, 1 h room temperature). Chamber slides were incubated with secondary ms-Cy3-Antibody and rb-Alexa-488-antibody (1 h room temperature). After washing with PBS, chamber slides were mounted with Vectashield containing DAPI (Vector Laboratories, Burlingame, CA, USA). Confocal laser scanning microscopy was carried out with a Leica SP 5 resonant APD system (Leica microsystems GmbH, Wetzlar, Germany).

Histological assessment of adipose tissue

Mouse adipose tissue (EpiWAT) was fixed in 4% paraformaldehyde overnight at 4^{o}C, and dehydrated prior to embedding in paraffin wax. Sequential sections (6µm) were cut and morphological changes visualized using hematoxylin and eosin (H&E) staining. Blinded analysis of mean adipocyte area in tissue sections from mice (N= 5-6 per treatment group) was performed using Image J-macro software (http://dev.mri.cnrs.fr/projects/imagej-macros/wiki/Adipocytes_Tool).

Whole Cell extracts and SDS-PAGE

Whole-cell extracts (WCE) were prepared by lysing cells for 20 min in radio-immunoprecipitation assay buffer [50 mMTris (pH 8), 400 mM NaCl, 0.5% Nonidet P40, 1% deoxycholate, 0.1% sodium dodecyl sulfate, 1 g/ml pepstatin, 1 g/ml bestatin, 2 g/ml leupeptin, 2 mM phenylmethylsulfonyl fluoride, 10 mM

glycerophosphate, 1 mM NaF, and 1 mM dithiothreitol] at 4°C. Lysate was centrifuged (20 min, 4°C, 14'000 rpm). WCE were loaded on 7.5% sodiumdodecylsulfate gels and blotted with anti-PAR, anti-ARTD1, anti-PPAR, and anti-tubulin antibodies.

Co-immunoprecipitation

Hek293T cells were plated one day prior to calcium phosphate transfection with 12 µg total DNA. 48 h after transfection, cells were treated with H2O2 in DMEM as described above. Cells were harvested in PBS, nuclei were extracted in a buffer containing 85 mM KCl, 0.5% NP40 and 5 mM Hepes (pH 7.4). After centrifugation (10 min, 6000 rpm) cells were resuspended in Buffer D (50 mM Tris pH 7.5, 50 mM KCl, 5 mM MgCl2, 0.2 mM EDTA, 20% Glycerol, 0.1% NP40, 0.1 mM DTT and 1x Proteinase Inhibitor), sonicated, and treated with DNAse I (30 min on ice). After centrifugation (10 min, 6000 rpm), proteins in the supernatant were quantified by Bradford assay. IP was performed at 4°C for 4 h with 2 µg of antibody per 150 µg of extract. Dynabeads G or A beads or Sepharose beads coupled to HA-antibody were added (10 µl/20µl of HA beads per reaction, incubation for 2 hr at 4°C). Beads were washed 4x with washing buffer (20 mM Tris pH 7.5, 50 mM KCl, 5 mM MgCl2, 0.2 mM EDTA, 10% Glycerol, 0.1% Tween), 2x Laemmli buffer (20 µl) was added, the reaction was boiled (5 min, 95°C). SDS-PAGE and western blot analysis were performed as described. For the analysis of p300 the blotting buffer was supplemented with 0.1% SDS.

Luciferase assay

Luciferase assays were performed by overexpressing a 3xPPRE-Firefly Luciferase construct, PPARγ2, (both generous gifts from Prof. Dr. Walter Wahli, Lausanne, Switzerland), a TK-Renilla construct and, when required, ARTD1 wt and mutant constructs. 3T3-L1 cells were transfected using TransIT-3T3 Transfection reagent (Mirus Bio LLC, Madison, WI, USA) according to the manufacturer's instructions. Hek293T cells were transfected with calcium phosphate in 24-well plates using 10 ng Renilla, 100 ng PPRE-Firefly, 200 ng ARTD1, 100 ng PPARγ2 per well. Cells were treated with 10 μM rosiglitazone for 16 h (4 h after transfection). Prior to collection, cells were treated with 1 mM H_2O_2 in DMEM without FCS in the presence of catalase inhibitor 3-AT (30 μM) for 2 h in the presence or absence of 10 μM PJ34. Luciferase was measured using the Dual-Luciferase reporter assay kit (Promega, Madison, WI, USA) according to the manufacturer's instructions.

Chromatin immunoprecipitation (ChIP)

ChIP was performed as previously described (Santoro et al., 2002). Briefly, 3T3-L1 cells were fixed in 1% Formaldehyde in PBS. Chromatin was fragmented with a Bioruptor (Diagenode). Antibodies were incubated with crosslinked chromatin overnight at 4°C and collected with Protein A or G magnetic Dynabeads® (Life Technologies, Carlsbad, CA, USA) for 4 hours. After reversal of the crosslinking and digestion with proteinase K, DNA was extracted and analyzed by real-time PCR using SYBR Green and the Rotor-Gene 3000 (Corbett Life Science, now Qiagen).

Supplementary Figures

Figure S1: PARP inhibitor treatment reduces adipose tissue formation in mice. A) ARTD activity measured in epiWAT isolated from vehicle- and PARP inhibitor-treated mice on HFD after fasting o/n. Data are mean ± SEM. T-test: *p<0.05, **p<0.01, ***p<0.001. n=7 B) Food intake of mice fed during one week on Chow or HFD in the presence or absence of PARP inhibitor. Data are mean ± SEM. C) qRT-PCR analysis of epiWAT isolated from vehicle- and PARP inhibitor-treated mice. For qRT-PCR analysis of tissue samples, isolated WAT from 8 mice per group was pooled and expression values were normalized against 36BP4. Data are mean ± SEM. T-test: *p<0.05, **p<0.01, ***p<0.001.

Figure S2: PAR formation is required for PPARγ-dependent gene expression. A) 3T3-L1 cells were treated during differentiation with 1 or 10μM ABT888 form day 2-6. RNA was extracted at day 7 and gene expression was analyzed. B) 3T3-L1 cells were differentiated and treated with 10μM RBPI-3 (PARGi) for days 1-3. At day 4, whole cell extracts were analyzed by western blotting. C) 3T3-L1 cells were treated with 100nM FK866 and/or 10μM PJ34 during differentiation (day 2-4). Samples were taken at day 5 and analyzed by western blot. D) qPCR analysis of the cells used in C. E) WT or ARTD1$^{-/-}$ MEF cells were differentiated and analyzed at day 7 by western blotting. F) qPCR analysis of the cells used in E.

Figure S3: PPARγ and ARTD1 interact at the PPREs of PPARg target genes. A) 3T3-L1 cells were treated during differentiation with 10μM ABT888 at day 5 and 6

and cells were fixed at day 0 or 7 and Chromatin was precipitated using an anti ARTD1 antibody. B) 3T3-L1 cells were treated daily with 10μM PJ34 starting at day 1. At day 0, 3 or 7, cells were fixed with formaldehyde and chromatin was precipitated with an anti-PAR antibody. Data are mean ± SEM. Values were normalized over beads and over IL6-100 as control gene. Data are mean ± SEM. T-test: *p<0.05, **p<0.01, ***p<0.001.

C) Hek cells were treated with Rosiglitazone (10 μM) for the indicated times and whole cell extracts were analysed for PAR formation.

Figure S4: PAR formation enhances PPARγ dependent gene expression. A) 3T3-L1 cells overexpressing PPARγ2 were treated with 10μM Rosiglitazone for 16 hours and subsequently Luciferase activity was measured. B) Hek cells overexpressing PPARγ2, WT ARTD1, ARTD1 E988K, or Y907A/C908Y or GFP(-) were treated with 1mM H_2O_2 in the presence of catalase inhibitor for 2 hours.

Figure S5: PAR formation controls PPARγ-dependent gene expression by maintaining ligand induced cofactor exchange. A) 3T3-L1 cells were treated daily with 10μM ABT888 starting at day 5. At day 8 the cells were fixed with Formaldehyde and chromatin was precipitated with a p300 antibody. Data are mean ± SEM. n=2. B) PAR formation is required for maintenance of PPARγ-dependent gene expression.

Lehmann et al. *Figure S1*

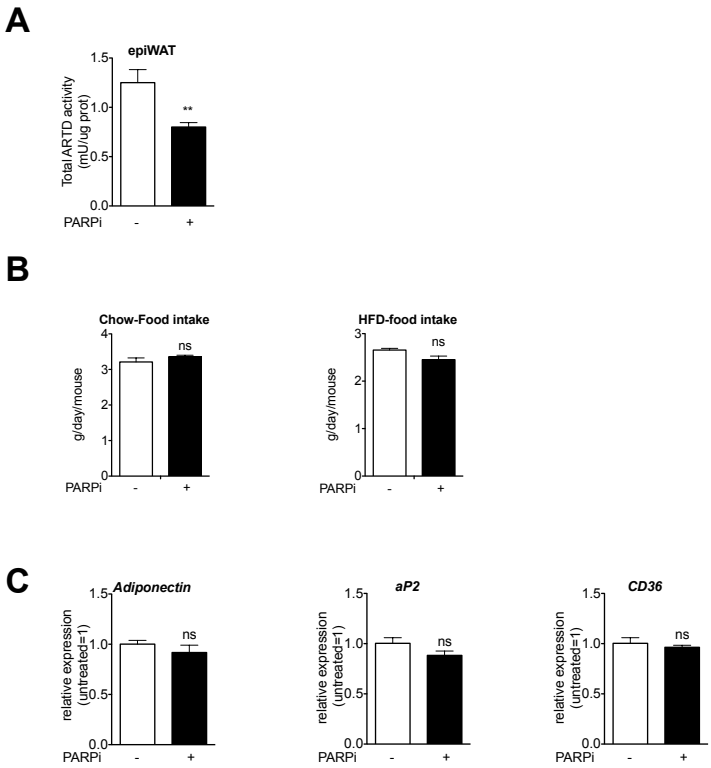

Lehmann et al. *Figure S2*

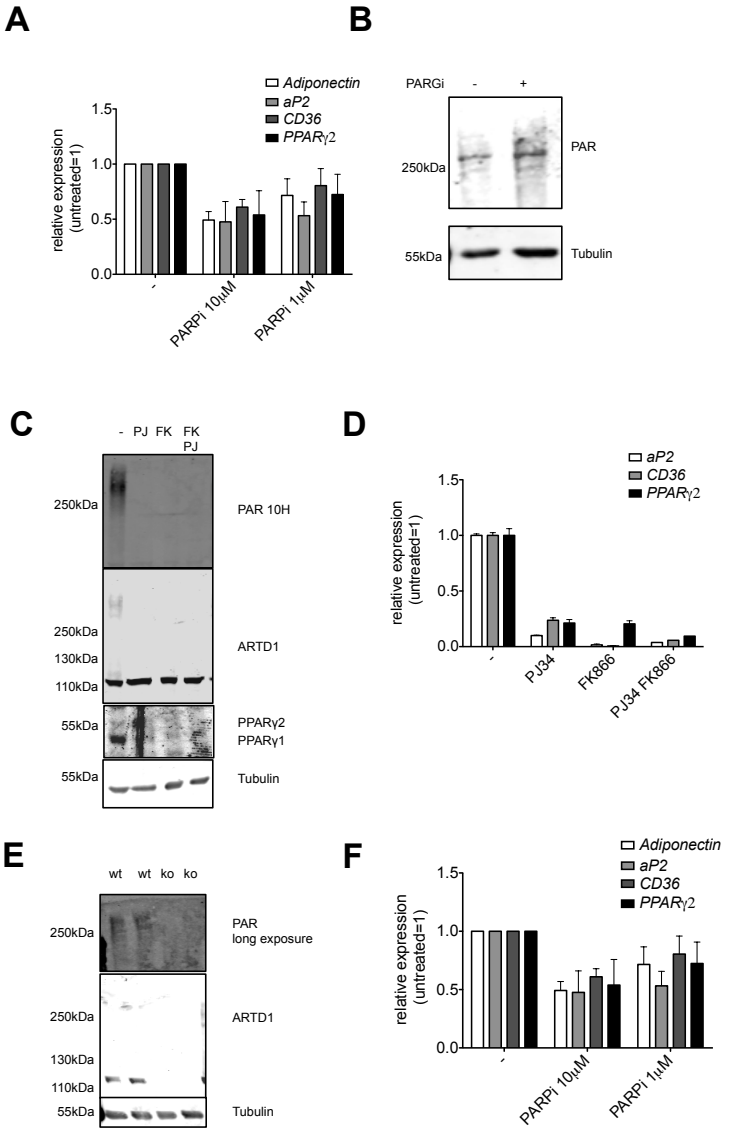

Lehmann et al. *Figure S3*

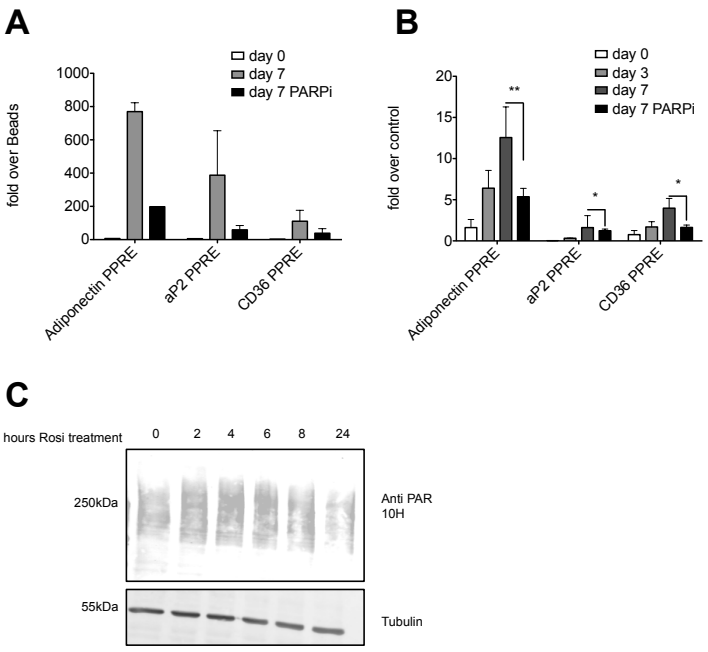

Lehmann et al. *Figure S4*

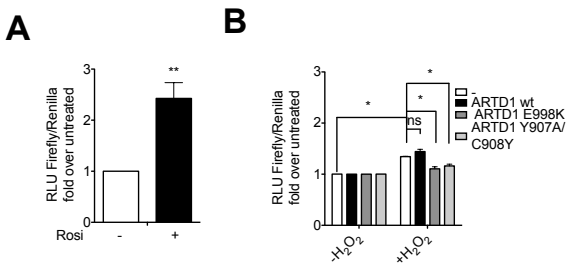

Lehmann et al. *Figure S5*

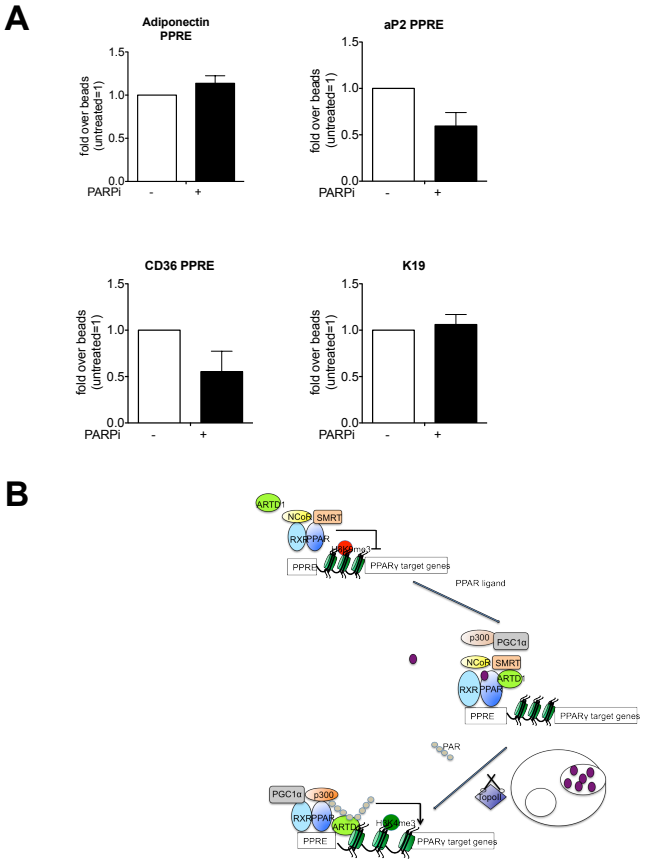

3.3 Unpublished results

3.3.1 Generation of conditional knockout ARTD1$^{-/-}$ mice

In order to investigate the effect of ARTD1 on adipose tissue *in vivo* and to rule out indirect effects of the ARTD1 depletion in other tissues than adipose tissue, which cannot be ruled out with conventional knockout mice, we decided to generate a mouse with a floxed ARTD1 allele. This will be used afterwards to bread an adipocyte specific knockout of ARTD1. A commercially available targeting vector from EUCOMM (European Conditional Mouse Mutagenesis Program) was used to target exon 4 of ARTD1 in ES cells to generate ARTD1$^{fl/fl}$ mice in collaboration with Polygene (Rümlang, Switzerland). The targeting vector contains different functional parts (Fig. 1A). The 5' and 3' homolougs arms are requird for the targeted insertion of the casssete. Additionally, the cassette contains loxP sites that flank exon 4 of the *ARTD1* gene for later Cre-mediated excision. For selection, the vector contains a neomycin resistance gene and a lacZ gene that allows blue/white selection of clones. The selection cassette is flanked by *Flp*-recombinase target (frt) sites, which allows the removal of the cassette upon flippase (Flp)-mediated recombination. Outside of the homologous regions is a diphtheria toxin gene allowing counterselection for random integration of the construct. The targeting construct was transfected into ES cells and upon homologous recombination resulted in an integrated transgene (Fig.1B). To verify the correct integration site, different PCRs were established. PCR 1 (primers GF3 and LAR3) and 2 (primers GR4 and RAF5) amplify a region that contains DNA sequences outside of the selection cassette and extends into the construct and can thus confirm the exact integration site, whereas PCR 3 (primers 1405 and LAR3) confirms only the presence of the selection cassette (Fig. 1C). Both the targeting vector and a commercially available targeted ES clone from EUCOMM, which unforuntately did not generate chimera (data not shown) served as controls allowing the amplification of the expected positive signal. The long range flanking PCRs 1 and 2 amplified a product only when DNA from the EUCOMM cell clones was tested, but not using only the targeting vector or a negtive control (genomic DNA from mouse cells) (Fig. 1D). Serveral transfected ES-cells were analysed for the targeted integration of the cassette (Fig. 1E). A considerably high frequency of over 60% of the tested clones were tested positive for a correct vector integration.

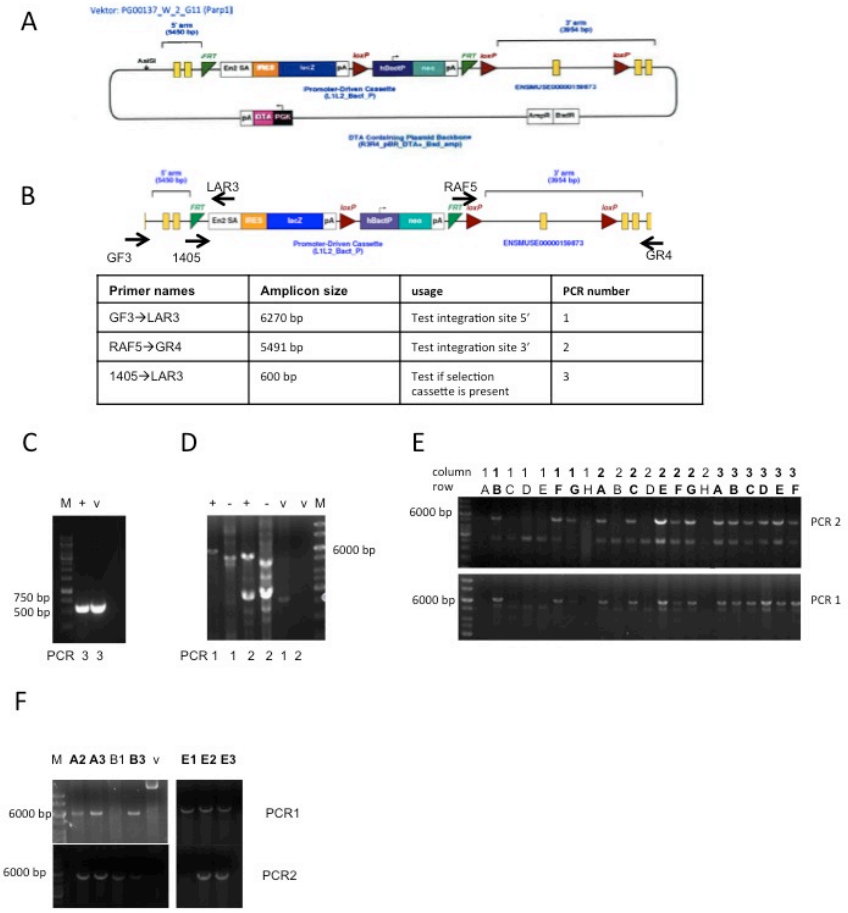

Primer names	Amplicon size	usage	PCR number
GF3→LAR3	6270 bp	Test integration site 5'	1
RAF5→GR4	5491 bp	Test integration site 3'	2
1405→LAR3	600 bp	Test if selection cassette is present	3

Figure 1: Schematic scheme of the targeting vector and validation of ES cell clones for ARTD1$^{fl/+}$

A) The targeting vector containing loxP flanked Exon 4 of ARTD1 and selection cassette for transfected ES cells as well as Diphtheriatoxin for counterselction. Vector was bought from EUCOMM.
B) Schematic illustration of insereted construct and Primers used for characterizing the clones
C) Vector (v) was tested for the presence of the selection cassette (PCR 3). Previously bought and characterized ES-cell clones were used as a positive control (1), Marker (M).
D) PCRs 1 and 2 for insertions were verified with positive control (+), negative control (genomic Raw DNA =-) and vector (v).
E) ES cells were transfected with the vector and selected for the locus of integration. Clones tested positive for the integration at the desired locus are shown in bold.
F) Selected clones were thawed and expanded and reanalysed for the presence of the construct at the right chromosomal location.

Several positive clones were expanded and rechecked for the right integration (Fig. 1F). The targetd ES cells were additionally injected into blastocytes to generate chimeras. Born chimeras are currently being bread with wt C57/BL6 mice to confirm germline transmission. Mice will subsequently be bread further in the C57/BL6 background, since this strain is preferred for metabolic studies [286]. The resulting heterzygous offspring will be crossed inter se. Homozygous ARTD1$^{fl/fl}$ mice will be crossed with mice carrying an inducible Cre-enzyme under the adipose tissue specific Adiponectin promoter. Adiponectin-Cre; ARTD1$^{fl/fl}$ mice will have an exon 4 deletion

of ARTD1 specifically in adipose tissue and will therefore not express a functional protein in WAT.

3.3.2 Browning of wite adipose tissue is associated with PAR formation

The experiments presented in this part were performed in collaboration with Dr. Matthias Rosenwald and Prof. Dr. Christian Wolfrum who provided the mouse material. White adipose tissue (WAT) can be transformed to brown-like adipose tissue by exposure of mice to cold or PPARγ-agonists [160,162,168]. This increase is accompanied by an increase in *UCP-1* expression [154]. To investigate if PAR formation and ARTD1/2 are involved in this process, we treated differentiated adipocytes from day 7 until day 21 with PPARγ-agonist Rosiglitazone and measured *UCP-1* expression. Treatment with Rosiglitazone increased *UCP-1* expression drastically by a factor of about 450, while the co-treatment with the PARP inhibitor ABT888 abrogated this effect (Fig. 2A). Interestingly, ABT888 alone seemed to stimulate *UCP-1* expression in untreated cells, although not to the same extent as Rosiglitazone. These initial expression changes need to be confirmed on the protein levels as the increase on mRNA level in untreated cells might not affect the basal UCP-1 protein levels. Nevertheless, these initial results indicate that PAR formation is involved in Rosiglitazone-induced *UCP-1* expression in 3T3-L1 cells.

Mice kept at 8°C over 0, 1, 4 or 7 days were sacrificed and whole cell extracts of the subcutaneous WAT and BAT was analysed by Westernblot for PAR formation (Fig. 2B). Upon exposure to cold, a distinct band around 55/60 kDa appeared, both in BAT and WAT. This band was stronger in the WAT than in the BAT samples and the band could represent auto-modified ARTD2, which was previously reported to have a minor effect on BAT [282]. Unfortunately, the commercially available antibodies against ARTD2 did not allow the detection of mouse ARTD2 (only human ARTD2). Moreover, a high molecular weight smear around 300 kDa was detected with the anti-PAR antibody which increased in BAT samples from day 1 and 4. These results indicated that PAR formation is induced upon exposure of mice to cold.

To investigate the enzymes mainly involved in PAR anabolism and catabolism, mRNA levels of *ARTD1, ARTD2* and *PARG* were analysed by qPCR (Fig. 2C). *ARTD1* mRNA levels did not change in response to cold exposure. In contrast, A*RTD2* levels increased significantly in BAT and showed a similar trend in

WAT, although this increase was not significant. The expression of *PARG*, the main PAR-metabolizing enzyme, was not changed in BAT, while in WAT there was a slight although non-significant decrease. These results need to be verified on protein levels but indicate that exposure of mice to cold induces *ARTD2* expression in BAT and reduced *PARG* expression in WAT.

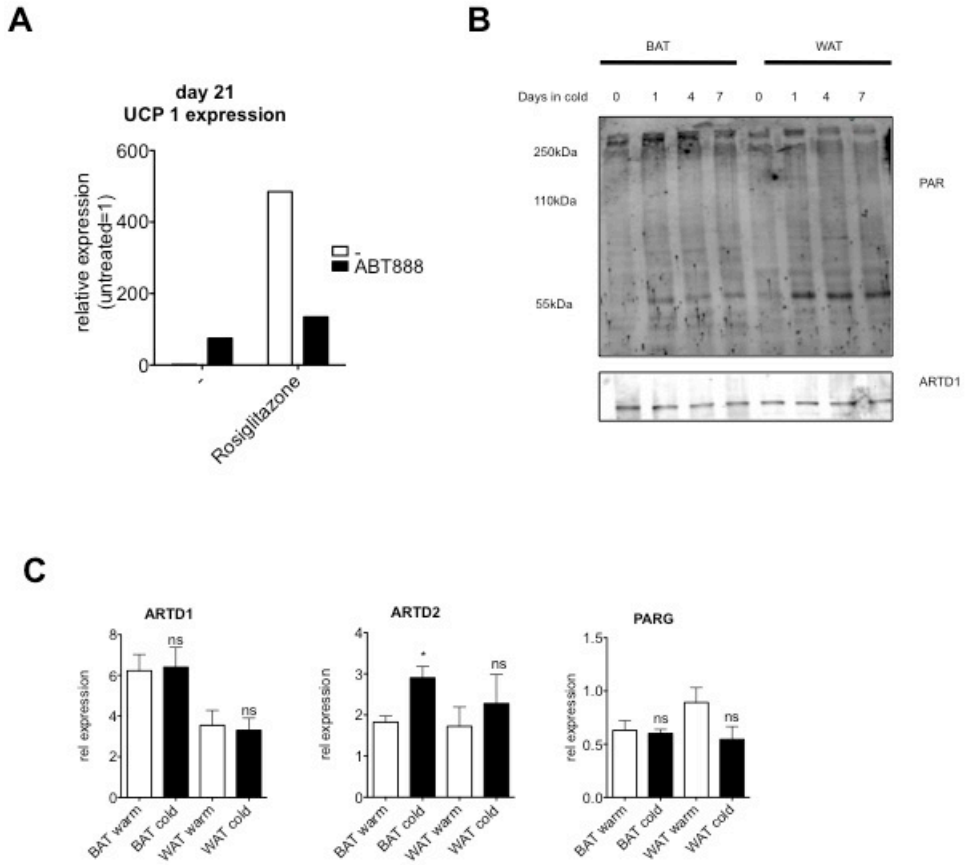

Figure 2: WAT to BAT trans-differentiation is associated with PAR formation

A) Cells at day 7 of differentiation were treated with 1µM Rosiglitazone and 10µM ABT888 every second day until day 21. RNA was isolated and qPCR for UCP1 was performed. The values were normalized to Cyclophilin A expression. n=1

B) C57BL/6N mice were kept in the cold (8°C) for 0-7 days. The subcutaneous white adipose tissue (WAT) and brown adipose tissue (BAT) was isolated and WCE were analysed by WB using antibodies against PAR and ARTD1.

C) C57BL/6N mice were kept in the cold (8°C) for 0-7 days. The subcutaneous white adipose tissue (WAT) and brown adipose tissue (BAT) was subsequently isolated, RNA isolated from the tissues and analysed by qPCR. Values were normalized for 36BP4 expression. Presented are means ±SEM. n=4

In summary, our results indicate that PAR formation is required for PPARγ-agonist induced UCP-1 expression. In addition, PAR formation is induced upon exposure to cold. Whether ARTD1- or ARTD2-mediated PAR formation is required for the trans-differentiation of WAT to BAT will be further investigated by exposing ARTD1$^{-/-}$,

ARTD2$^{-/-}$, and wt mice to cold for several days before analyzing the browning potential of the different genotypes.

3.3.3 Characterization of ARTD3 enzymatic activity

Commonly used PARP inhibitors are not specific for one distinct ARTD member, but most of them target different family members with comparable affinity [287]. In order to develop specific inhibitors, it is important to understand the enzymatic activities and biochemical properties of every single ARTD family member. While ARTD1 and ARTD2 are well studied, ARTD3, which is a target of many of the commonly used drugs, is poorly characterized [287]. Moreover, there are conflicting reports about the enzymatic activity of ARTD3 [18,107,108]. One publication reported poly-ADP-ribosylating activity for ARTD3, whereas others report none or only mono-ADP-ribosylating activity [18,107,108]. To provide additional insights into this biochemical questions, we investigated the ADP-ribosylating activity of ARTD3. ARTD3 from our (CH) or from Caldecott's laboratory (UK) was expressed in insect cells using a baculo-virus system, purified with a nickel-NTA column and their enzymatic activities analysed at different NAD^+ concentrations in the presence or absence of histones (Fig. 3A). ARTD3 from both sources showed only mono- or oligo-ADP-ribosylating activity, as evidenced by the absence of any band-shift of ARTD3, which could only be observed for the ARTD1 sample, which served as positive control. The basal activity of CH-ARTD3 was slightly lower under all tested conditions compared to the UK-ARTD3, which became even more evident when high NAD^+ concentrations were used. In addition, we tested how pH changes (pH range 8 to 9.5) would change the activity of ARTD3 (Fig. 3A). The different tested pHs did not affect ARTD3 enzymatic activity, neither under high, nor under low NAD^+ concentrations.

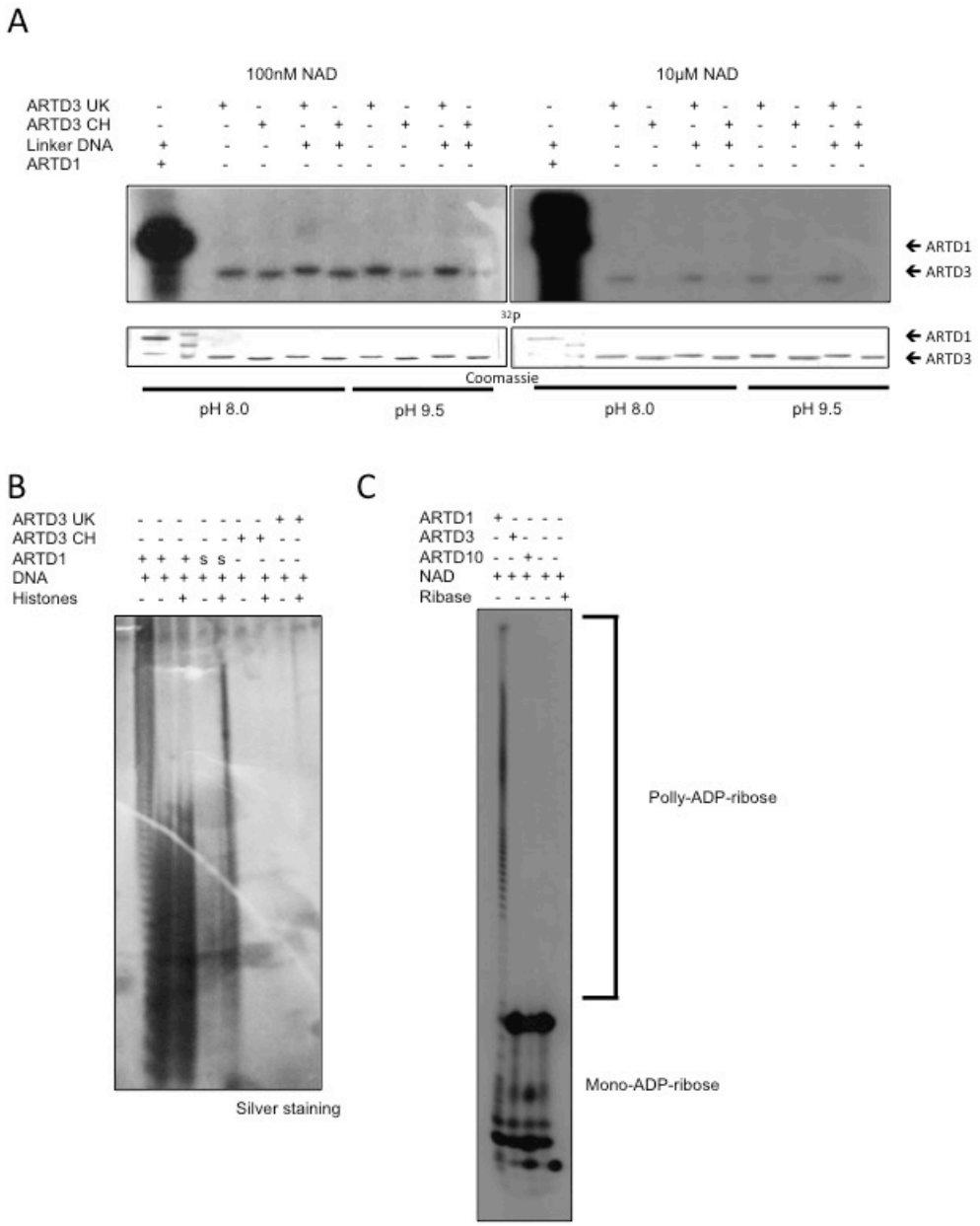

Figure 3: ARTD3 is a mono-ADP-ribosyltransferase

A) *In vitro* radioactive ARTD3 activity assay was performed with 500nM ARTD3 from Hottiger (CH) or Caldecott (UK) laboratories with 100nM or 10µM NAD^+ (^{32}P) and Eco linker in ARTD reaction buffer pH8.0 or 9.5. ARTD1 was used as a positive control. CB= coomassie blot.

B) Product analysis ARTD1, short ARTD1(s) or ARTD3 were incubated with 1 mM NAD^+ in the presence of DNA (cut plasmid DNA) and Histones (H1.4) for 45 mins at 30°C, Polymers were extracted and analysed on a silver gel.

C) Product analysis of ARTD1, short ARTD1(s) or ARTD3. Proteins were incubated with 10 µM ^{32}P labeled NAD^+ in the presence of DNA (cut plasmid DNA) and Histones (H1.4) for 30 mins at 30°C, proteins were digested with Proteinase K and polymers were analysed on a sequencing gel.

To test, whether DNA can activate ARTD3, a short double-stranded (ds) DNA consisting of the EcoRI-motif (8 bp with 2 nucleotides overhand) was used in this assay. ARTD1 was strongly activated by DNA while ARTD3 was not stimulated by

DNA (Fig. 3A). This is in contrast to other studies, which report that DNA is able to stimulate ARTD3 [106,107]. To investigate if the ARTD3 formed product was mono- or oligo-ADP-ribose, product analysis was performed on a silver gel which allows the detection of oligomers consisting of 8 or more ADP-ribose moieties (Fig. 3B). For ARTD1, a ladder of polymers could be detected, which was enhanced upon the addition of histones. For the short form of ARTD1 (aa 524-1014,), which lacks the DNA-binding and the BRCT domain, a similar product was observed [2]. For ARTD3 no signal could be detected, meaning that under the tested experimental conditions no oligomers comprised of more than 7 ADP-riboses were formed. In order to investigate if monomers or smaller oligomers of ADP-ribose were formed by ARTD3, we performed a radioactive product analysis that allows detection of mono- and oligo-ADP-ribose as well (Fig. 3C). As expected, ARTD1 showed a ladder-like pattern of ADP-ribose polymers. For ARTD10, which is a mono-ART, and for ARTD3 only monomers were observed, although for ARTD3 the product was only very weak, indicating that the enzymatic activity of ARTD3 is weak (compared to ARTD1 or 10) and that ARTD3 is a mono-ADP-ribosyltransferase. While a short dsDNA fragment was not able to stimulate ARTD3 (Fig. 3A), other structures such as DNA lesions or hairpins might be able to activate ARTD3. The enzymatic activity of ARTD3 was thus analysed in presence of DNA constructs harboring different structures, some of them containing nicks, gaps, flaps or overhangs (Fig. 4A). Although ARTD1 could be stimulated with intact dsDNA (C) or with dsDNA containing a nick (N), no stimulation was observed for ARTD3 with any of the tested constructs. These results provide evidence that ARTD3 is unlikely activated by DNA.

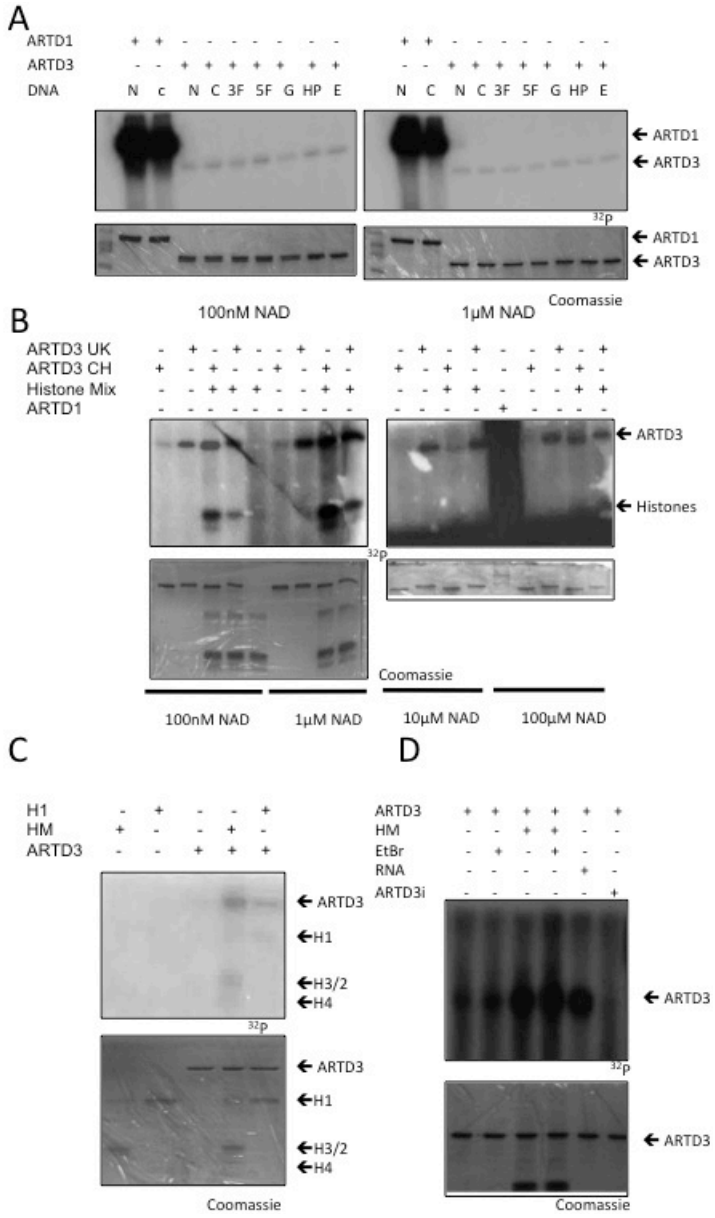

Figure 4: ARTD3 is not activated by DNA, but by Histones and RNA

A) *In vitro* radioactive ARTD3 activity assay was performed with 500nM ARTD3 with 100nM or 1µM, NAD^+ (^{32}P) in ARTD reaction buffer in the presence of different DNAs. ARTD1 was used as a positive control. CB= coomassie blot. N=nick C=control oligo, 3'Flap=3, 5'Flap=5, Gap(G), hairpin (HP) or 8mer EcoLinker (E).

B) *In vitro* radioactive ARTD3 activity assay was performed with 500nM ARTD3 from Hottiger (CH) or Caldecott lab (UK) with 100nM, 1µM, 10µM or 100µM NAD^+ (^{32}P) in ARTD reaction buffer in the presence of the Histone mix (HM). ARTD1 was used as a positive control. CB= coomassie blot

C) *In vitro* radioactive ARTD3 activity assay was performed with 500nM ARTD3 with 1µM NAD^+ (^{32}P) in ARTD reaction buffer in the presence of 1µg histonemix (HM) or H1. CB= coomassie blot

D) *In vitro* radioactive ARTD3 activity assay was performed with 500nM ARTD3 with 1µM NAD^+ (^{32}P) in ARTD reaction buffer in the presence or absence of 10µg Histonemix (HM), 30µM ME0328 (ARTD3 inhibitor=ARTD3i) or 1.5µl KCN RNA and 50µg/ml Ethidiumbromide (EtBr) to inhibit any DNA mediated activation. CB= coomassie blot

Since histones were described to activate ARTD1 *in vitro*, we investigated if histones could potentially also activate ARTD3. Indeed, addition of histones increased the

activity of ARTD3 under all tested conditions (Fig 4B,C,D). In addition to an increased ARTD3 auto-modification upon addition of histones, the ADP-ribosylation of core histones as well as H1 could be observed (Fig 4C). To rule out that this activation by histones was mediated by a contamination with nucleic acids, Ethidiumbromide (EtBr) was supplemented to the reaction (Fig 4D). EtBr was described to intercalate in the DNA and is therefore used as a tool for visualization of DNA but can also be used to clear extracts from contaminating DNA[288,289]. EtBr did not interfere with the ARTD3 stimulation by histones, suggesting that the histones themselves and not a contamination with nucleic acids conveyed the activation.
ARTD1 was recently described to bind to and be activated by RNA [290-293]. We thus investigated the effect of RNA on ARTD3 activity (Fig. 4D). Indeed, pre-incubation of ARTD3 with RNA increased its activity (Fig. 4D). Addition of a specific ARTD3 inhibitor which was developed in collaboration with the Schüler laboratory (see published results) indeed inhibited the detected activity of ARTD3 (Fig. 4D).

Recently ARTD3 was described to activate ARTD1 [108]. However, this study did not consider the activation of ARTD1 by ARTD3 through co-purified nucleic acids (e.g. DNA or RNA). To elucidate this possibility, we tested ARTD3 purified from bacteria or insect cells for the stimulation of ARTD1 purified from insect cells (Fig. 5A). Co-incubation of ARTD3 and ARTD1 led to an increased modification of ARTD1 as well as for ARTD3. This stimulatory effect was best observed when ARTD3 was used in great molar excess to ARTD1 (25:1). Whenever this ratio was changed in favor of ARTD1, the effect became smaller (Fig. 5B, C). When using ARTD1 and ARTD3 at equimolar concentrations no stimulation could be detected, suggesting that only ARTD3 in great excess is able to activate ARTD1. In addition, this effect was only visible under low NAD^+ concentrations (e.g. 100nM NAD^+, Fig. 5D). Under these conditions, auto-modification of ARTD3 was hardly detectable. To investigate, if ARTD3 modifies ARTD1, we took advantage of the inactive ARTD1 Y907A/C908Y mutant (Fig. 5E). While we saw an increased auto-modification of ARTD1 wildtype upon ARTD3 addition, no comparable signal could be detected when the inactive ARTD1 mutant was used, suggesting that the detected signal was due to induced ARTD1 auto-modification rather than trans-modification of ARTD1 by ARTD3. More experiments also including ARTD3 inactive mutants are required to confirm this conclusion.

In order to test if the activation of ARTD1 by ARTD3 was mediated by DNA contamination of ARTD3, we incubated ARTD3 in the reaction mix with either EtBr or DNAseI (Fig. 5G, F). Both treatments abolished the enhanced auto-modification of ARTD1 by ARTD3, suggesting that the stimulation is indeed caused by contaminating DNA. The effect of EtBr was even concentration-dependent (Fig. 5G). We further investigated if addition of EtBr already during the purification of ARTD3 could prevent this artifact. Indeed, supplementing wash buffers with EtBr during the ARTD3 purification abrogated the activation of ARTD1 by ARTD3 (Fig. 5H).

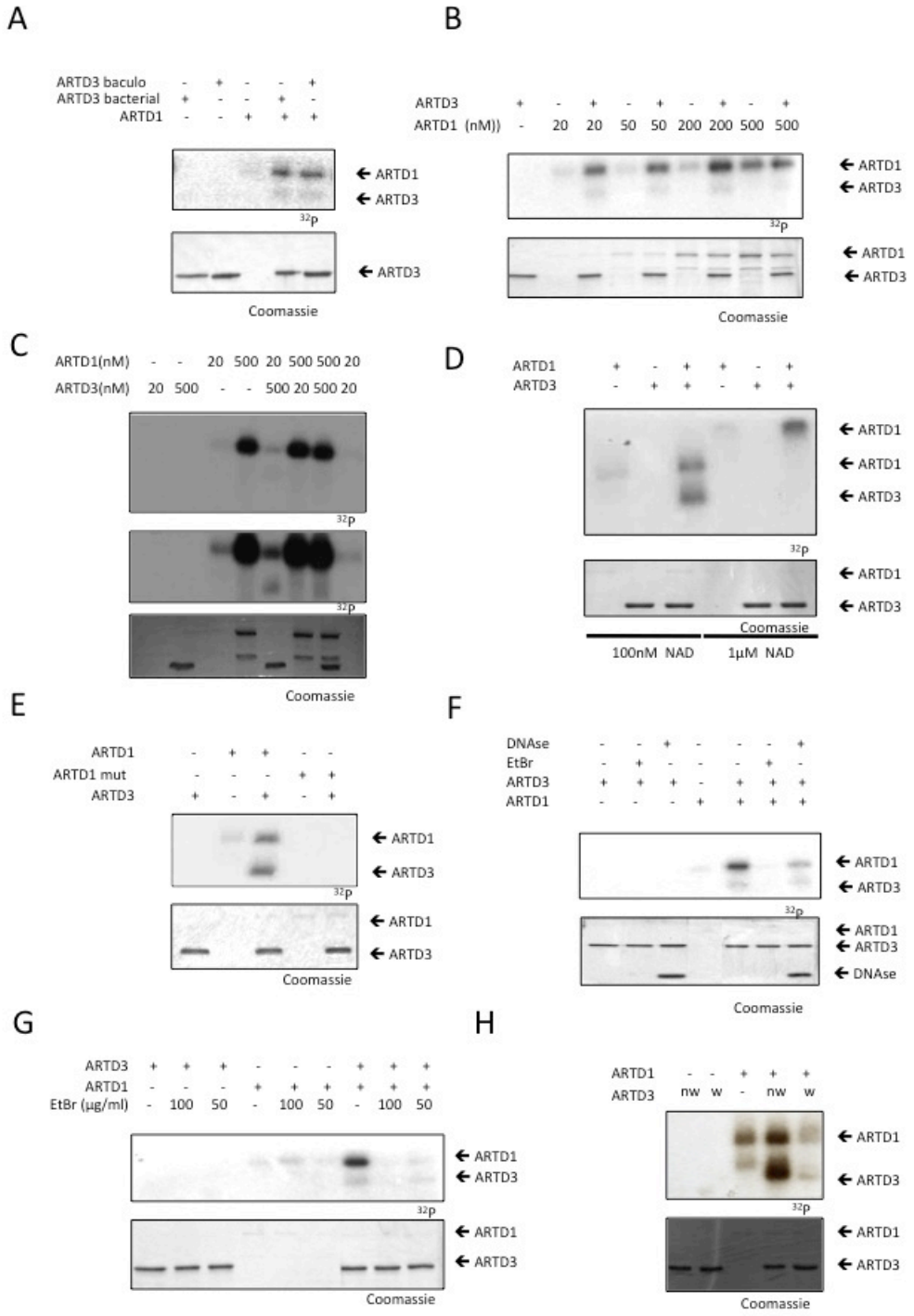

Figure 5: ARTD1 is not modified by ARTD3 and stimulation of ARTD1 by ARTD3 is mediated by DNA contamination

A) *In vitro* radioactive ARTD3 activity assay was performed with 500nM ARTD3 from baculo or bacterial origin and 20nM myc-ARTD1-his with 100nM NAD^+ (^{32}P) in ARTD reaction buffer. CB= coomassie blot

B) *In vitro* radioactive ARTD3 activity assay was performed with 500nM ARTD3 and 20nM, 50nM, 200nM or 500nM myc-ARTD1-his with 100nM NAD^+ (^{32}P) in ARTD reaction buffer. CB= coomassie blot

C) *In vitro* radioactive ARTD3 activity assay was performed with 20 or 500nM ARTD3 and 20nM or 500nM myc-ARTD1-his with 100nM NAD^+ (^{32}P) in ARTD reaction buffer. CB= coomassie blot

D) *In vitro* radioactive ARTD3 activity assay was performed with 500nM ARTD3 and 20nM myc-ARTD1-his with 100nM or 1μM NAD^+ (^{32}P) in ARTD reaction buffer. CB= coomassie blot
E) *In vitro* radioactive ARTD3 activity assay was performed with 500nM ARTD3 and 20nM or myc-ARTD1-his (wt) or inactive Y907A,C908Y mutant (ARTD3mut) with 100nM NAD^+ (^{32}P) in ARTD reaction buffer. CB= coomassie blot
F) *In vitro* radioactive ARTD3 activity assay was performed with 500nM ARTD3 and 20nM myc-ARTD1-his with 100nM NAD^+ (^{32}P) in ARTD reaction buffer. DNA dependent activation of ARTD1 was inhibited by the addition of 100μg/ml Ethidiumbromide (EtBr) or 1 U DNAse1. CB= coomassie blot
G) *In vitro* radioactive ARTD3 activity assay was performed with 500nM ARTD3 and 20nM myc-ARTD1-his with 100nM NAD^+ (^{32}P) in ARTD reaction buffer. DNA dependent activation of ARTD1 was inhibited by the addition of 100 μg/ml or 50μg/ml Ethdiumbromide. CB= coomassie blot
H) *In vitro* radioactive ARTD3 activity assay was performed with 500nM ARTD3 ARTD3 that was either washed with Ethidiumbromide (w) during purification or not washed (nw) and 20nM myc-ARTD1-his with 100nM NAD^+ (^{32}P) in ARTD reaction buffer. CB= coomassie blot

Together, these results identify ARTD3 as a mono-ADP-ribosyltransferase that is activated by RNA and histones. In addition, ARTD3 could modify H1 and core histones. Moreover, we could provide evidence that the recently reported activation of ARTD1 by ARTD3 is most likely due to DNA contamination of the ARTD3 protein.

3.3.4 ARTD1 does not affect sickness behavior syndrome in mice but represses TNFα-dependent clock gene expression

Circadian rhythms are indispensable for homeostasis in various organisms. They are maintained by a complex internal network of proteins [287,294]. In mammals, circadian rhythms are organized in a hierarchical manner. In addition to the master clock in the suprachiasmatic nuclei (SCN) of the anterior hypothalamus that is entrained by light-dark cycles, there are circadian oscillators in many other organs, including the liver [295-303]. The master clock synchronizes all peripheral clocks, which in turn can respond to and regulate various physiological and behavioral processes such as feeding [294,304]. The peripheral clocks can sustain circadian rhythms for a few days without input from the master clock. Under specific circumstances, they can even overrule the central clock. Imposing artificial feeding schedules in rodents for example, can completely uncouple the peripheral clock from the central clock system [296,300]. The timing mechanism in central and peripheral clocks was shown to be comparable and due to technical reasons, most of the studies on clock functions have been performed on peripheral clocks [304,305]. On a molecular level, circadian rhythms are maintained by the two main transcription factors circadian locomotor output cycles kaput (CLOCK)

and BMAL-1 that are rhythmically transcribed [306-309]. There are interacting positive and negative feedback loops that ensure the oscillating gene expression of clock-genes. CLOCK-BMAL1 heterodimers bind to E box enhancers and can activate transcription of their target genes [306,308]. CLOCK-BMAL1 activates the transcription of *period* genes (Per 1-3) and *cryptochrome* genes (Cry 1-2), *Rev-Erbα* and of clock control genes such as *DBP, Tef* and *Hlf.* Cry and Per proteins translocate back into the nucleus, where they suppress *CLOCK-BMAL1* transcription [310-314]. *Rev-Erbα* transcription can be suppressed by Per2 and Rev-Erbα itself suppresses *BMAL1* transcription, leading to oscillating transcription of the latter [314-318]. This central oscillator mechanism directly controls the rhythmic transcription of clock output regulators such as albumin D-element binding protein (*Dbp)*. Dysfunctions of circadian rhythms are implicated in a wide range of diseases such as sleeping disorders and depression [304,319].

Sickness behavior syndrome (SBS) describes symptoms such as fever, fatigue, depression and reduced appetite that are commonly associated with autoimmune and infectious diseases [320]. Many studies show that SBS is induced by cytokines such as interleukin 1 (IL-1) or tumor necrosis factor α (TNFα). Recently, an animal model for SBS in autoimmune diseases, employing stimulating antibodies for CD40, was established [321]. The crosslinking of CD40 by the antibodies activates CD40 expressing cells, mainly dendritic cells, monocytes and macrophages [321-324]. SBS in mice injected with anti-CD40 antibody mimics SBS in humans displaying symptoms such as fatigue and reduced appetite which becomes apparent in different readouts [321]. Mice reduce their activity in both movement through the cage (measured by infrared measurements) and in the use of the freely accessible running wheel. In addition, their body weight decreases tremendously. As a sign of the ongoing inflammatory processes, their spleen increases massively in size. Recently, it was described that TNF impairs the expression of E-box driven genes, and also CD40 antibody induced SBS in the mouse model is entirely dependent on TNF-receptor (TNFR) and results in deregulation of clock genes [325,326]. Another study implicated cold inducible RNA binding protein (CIRBP) in the control of clock gene expression [327]. CIRBP is a RNA-binding protein that can stabilize the transcript and influence its translation by binding to 3' or 5' untranslated regions (UTRs) [327-329]. The expression of *CIRBP* is induced upon mild hypothermia or hypoxia [327-329]. Loss of CIRB reduced the

amplitude of clock gene expression [327]. Moreover, the authors describe a direct binding of CIRBP to mRNAs of clock genes, indicating that it influences their stability.

ARTD1 was described by our group in the food entrainment of the peripheral liver clock to poly-ADP-ribosylate CLOCK thereby interfering with its DNA-binding abilities [279]. We thus investigated whether ARTD1 is involved in SBS by making use of the aforementioned CD40 antibody injection mouse model. wt and ARTD1$^{-/-}$ mice injected with a control (iso) antibody did not show any difference in bodyweight (Fig. 6A). As expected, wt mice treated with an anti-CD40 antibody lost around 10% of their bodyweight within 2 days after injection of the antibody. ARTD1$^{-/-}$ mice showed a similar significant decrease in bodyweight, suggesting that they develop SBS comparable to wt mice in this model. SBS was also evident when measuring locomoter activity using running wheels (Fig. 6B) and infrared activity detection devices (Fig. 6C). Upon CD40 antibody injection, wt mice display a loss in both measurements for locomoter activity [321]. The ARTD1$^{-/-}$ mice displayed a comparable loss in activity in both measurements after the injection of anti CD40 antibody, but not using the control antibody. Consistent with these findings, wt as well as ARTD1$^{-/-}$ mice showed splenomegaly as evidenced by the increase in spleen weight after CD40 antibody injection, indicating an ongoing inflammatory process (Fig. 6D). Together, ARTD1$^{-/-}$ mice displayed symptoms of SBS comparable to wt mice, indicating that ARTD1 is unlikely regulating SBS.

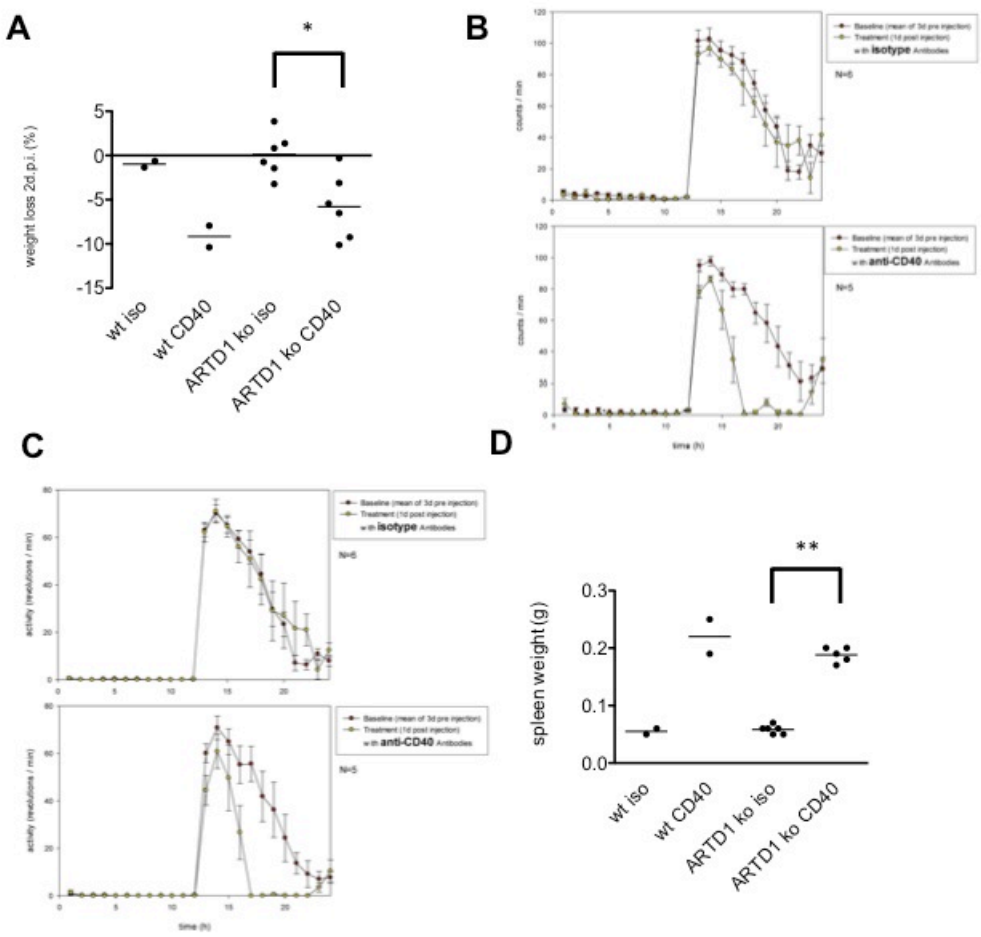

Figure 6: ARTD1-/- mice lose weight, show splenomegaly and decreased activity upon injection of CD40 antibody.

A) Body weight loss two days post injection of CD40 mAb or control IgG2a (iso), is shown as percent of body weight before injection. Wt n=2; ARTD1$^{-/-}$ n=6 shown are single and mean values T-tests: Non-parametric Mann-Whitney test. P values (two-tailed): *<0.05; **<0.005; ***<0.0005.

B) Running wheel (RW) activity of ARTD1 -/- mice was measured for the first day after i.p. injection of CD40 mAb or IgG2a as control. Baselines (red dots) are the mean of three 24 h recordings of day-1, day-2 and day-3 prior to injection of antibodies at day 0. Injection of CD40 or IgG2a control. Mean of 1-h values ± SEM

C) Same as in B but infrared (IR) measurements.

D) Spleen weight two days post induction was measured. Wt n=2; ARTD1$^{-/-}$ n=6 shown are single and mean values T-tests: Non-parametric Mann-Whitney test. P values (two-tailed): *<0.05; **<0.005; ***<0.0005.

In order to analyse the ARTD1 effect on clock gene expression, *CLOCK* mRNA levels were measured in the liver 2 days after injection of the anti-CD40 antibodies. CD40 antibody injection indeed evoked a strong immune response, which was accompanied by an increase of *IL6*, *IL1β* and *TNFα* expression in the liver of ARTD1$^{-/-}$ mice (Fig. 7A). *BMAL1* and *CLOCK* expression was significantly increased, whereas *Per1,3* and *Rev-Erbα* expression was not changed (Fig. 7B). The expression of the clock output genes *Dbp* and *Hlf* was not affected (Fig. 7C).

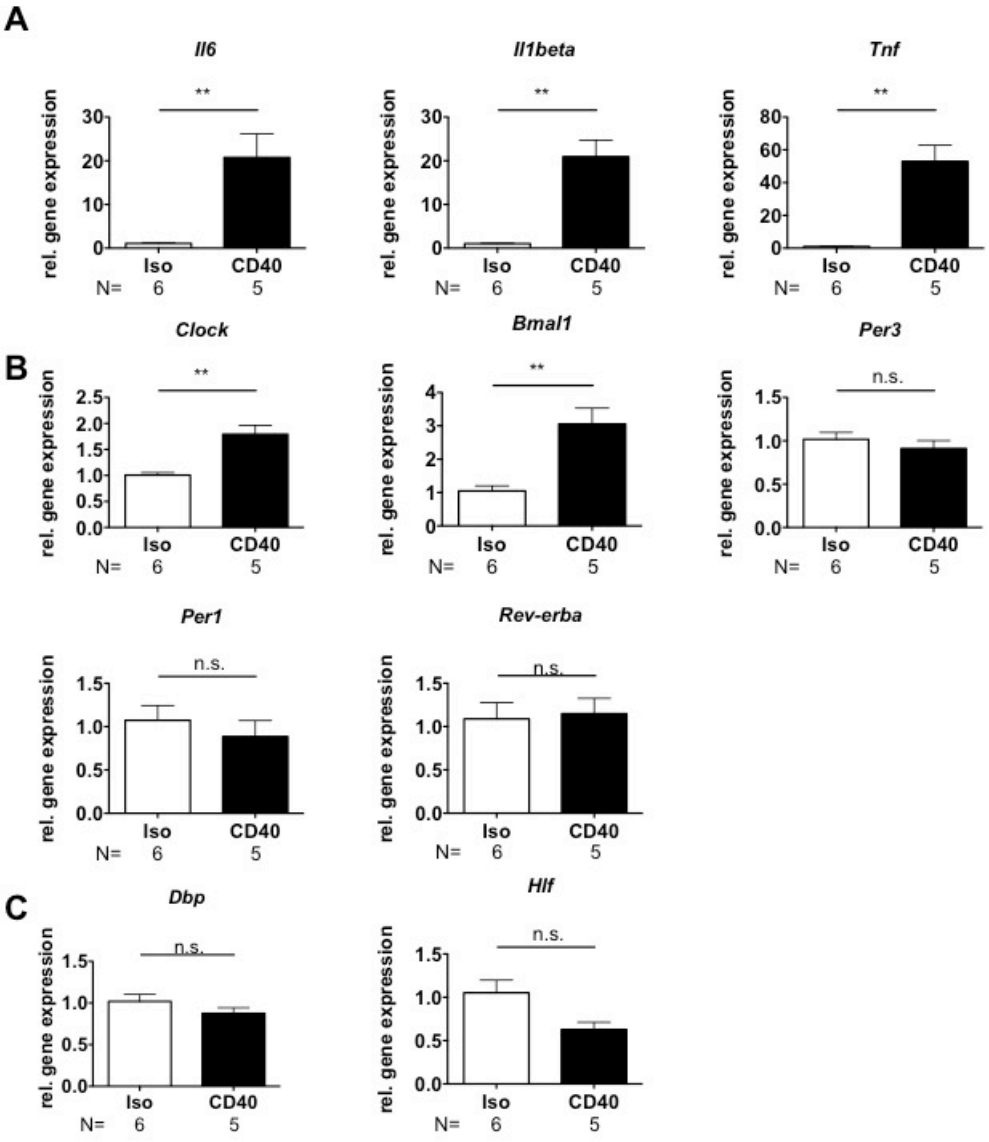

Figure 7: Gene expression in the liver of ARTD1$^{-/-}$ mice is changed upon injection of an anti CD40 antibody.

A) Inflammatory gene expression in mouse liver two days post injection of CD40 or isotype control (iso) antibody, quantified by RT-PCR normalized to 18s rRNA. Values show mean±SEM. T-tests: Non-parametric Mann-Whitney test. P values (two-tailed): *<0.05; **<0.005; ***<0.0005.

B) Same as in A but for basic clock genes

C) Same as in A but for Clock-output genes.

The same experiments with wt mice using anti-CD40 treatment revealed that *CLOCK*, *Per3* and *Rev-Erbα* were down-regulated which resulted in decreased expression of clock output genes *Dbp* and *Hlf* [321]. These results overall suggested that although ARTD1 does not influence locomoter activity, it has an effect on clock gene expression in the liver.

To investigate the effect of ARTD1 on clock gene expression in more detail, we investigated synchronized 3T3 cells treated with TNFα (Fig. 8).

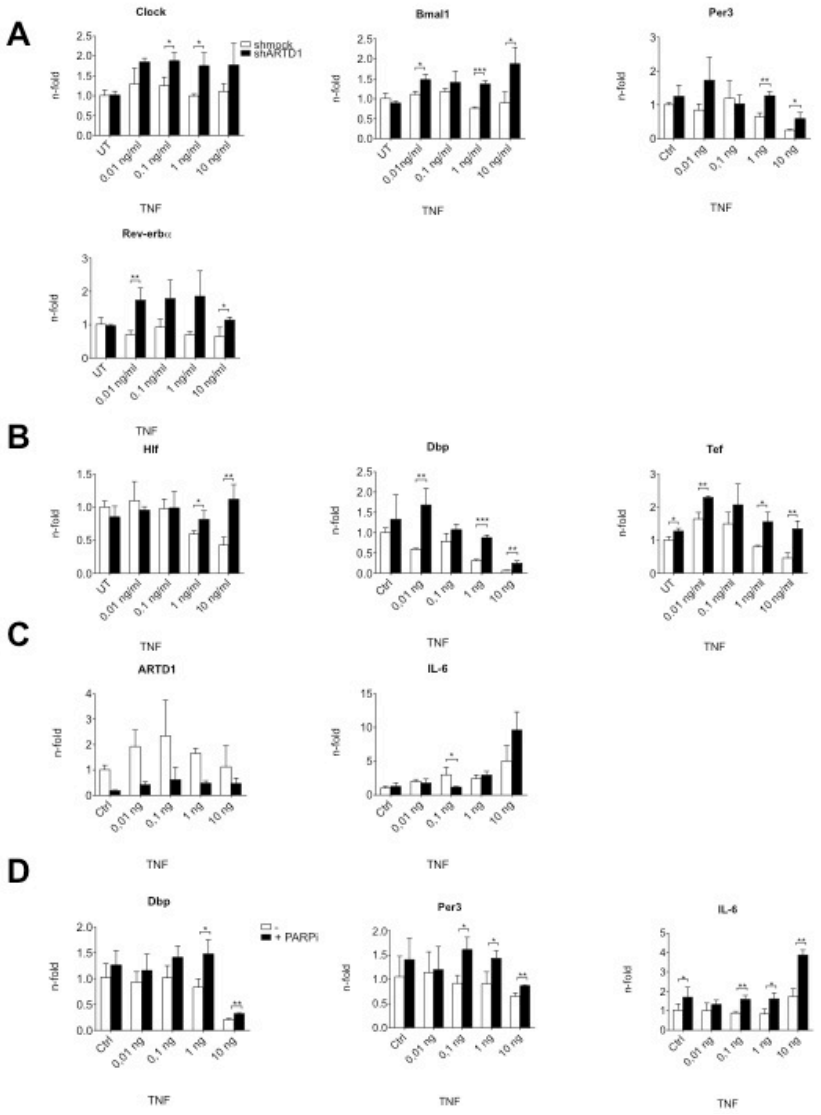

Figure 8: ARTD1 knockdown cells show increased Clock gene expression.

A) Starvation of confluent 3T3 shMock or shARTD1 cells in 1% FCS-containing medium over night followed by 4 hour treatment in 1% FCS with the indicated concentrations of TNFα. RNA was isolated, basic clock gene expression was analysed by qPCR and normalized against *GAPDH* levels. Shown are mean of three technical replicates±SEM.

B) Same as in A but for Clock-output genes

C) Same as in A but for control genes of the inflammatory response and knockdown controls.

D) Same as in A, but starved wildtype cells were preincubated with 10μM PJ434 prior to TNF treatment.

It was earlier described that in response to TNFα stimulation 3T3 cells suppress the expression of clock genes and a similar result was found in mice infused with TNFα [325]. Starved 3T3 cells with reduced ARTD1 protein levels as well as mock control cells were treated with different TNFα concentrations for four hours and clock gene

expression was analysed (Fig. 8). As expected, higher concentrations of TNFα led in to a down-regulation of CLOCK-BMAL1 target genes (such as *Dbp*, *Tef*, *Hlf* and *Per3*) in both shMock and shARTD1 cells. Knockdown of ARTD1 increased *CLOCK-BMAL1* as well as *Per3* and *Rev-erbα* expression under all tested TNFα concentration as well as in unstimulated cells (Fig. 8A). The expression of the tested CLOCK-BMAL1 target genes were upregulated in shARTD1 cells under both unstimulated or TNFα treated conditions (Fig. 8B). To test if ADP-ribosylation was involved in the observed regulation, cells were treated with PARP inhibitor with the TNFα stimulation. Indeed, an up-regulation of *Dbp* and *Per3,* as well as *IL6,* could be observed in inhibitor treated cells (Fig. 8D). These results suggested that ARTD1 and its enzymatic activity act as a repressor for clock gene expression.

In order to confirm that a transient knock-down of ARTD1 would generate the same results, 3T3 cells were transfected with siMock or siARTD1 and the experiment repeated as described above (Fig. 9). As expected, treatment with TNFα decreased clock gene expression in a concentration-dependent manner (Fig. 9A, B). Consistent with the previous experiments, siARTD1 cells showed slightly higher expression of *CLOCK* and *BMAL1,* and a striking increase in their target genes *Per1-3,* as well as the output genes *Dbp, Hlf* and *Tef*, which was already observed under unstimulated conditions (Fig. 9A, B). Also, *IL6* expression was increased in siARTD1 cells, which is consistent with unpublished data from our laboratory (Fig. 9C; unpublished results). To investigate the effect of ARTD1 depletion on *CIRBP* mRNA levels, we measured *CIRBP* expression in the same samples (Fig. 9D). TNFα treatment down-regulated *CIRBP* expression in a concentration dependent manner in both siMock and siARTD1 cells. siARTD1 treated cells showed an increase in *CIRBP* levels in comparison to siMock cells, suggesting that ARTD1 might influence *CIRBP* expression levels which could subsequently stabilize *CLOCK* mRNAs and thus lead to the observed increase in clock gene expression.

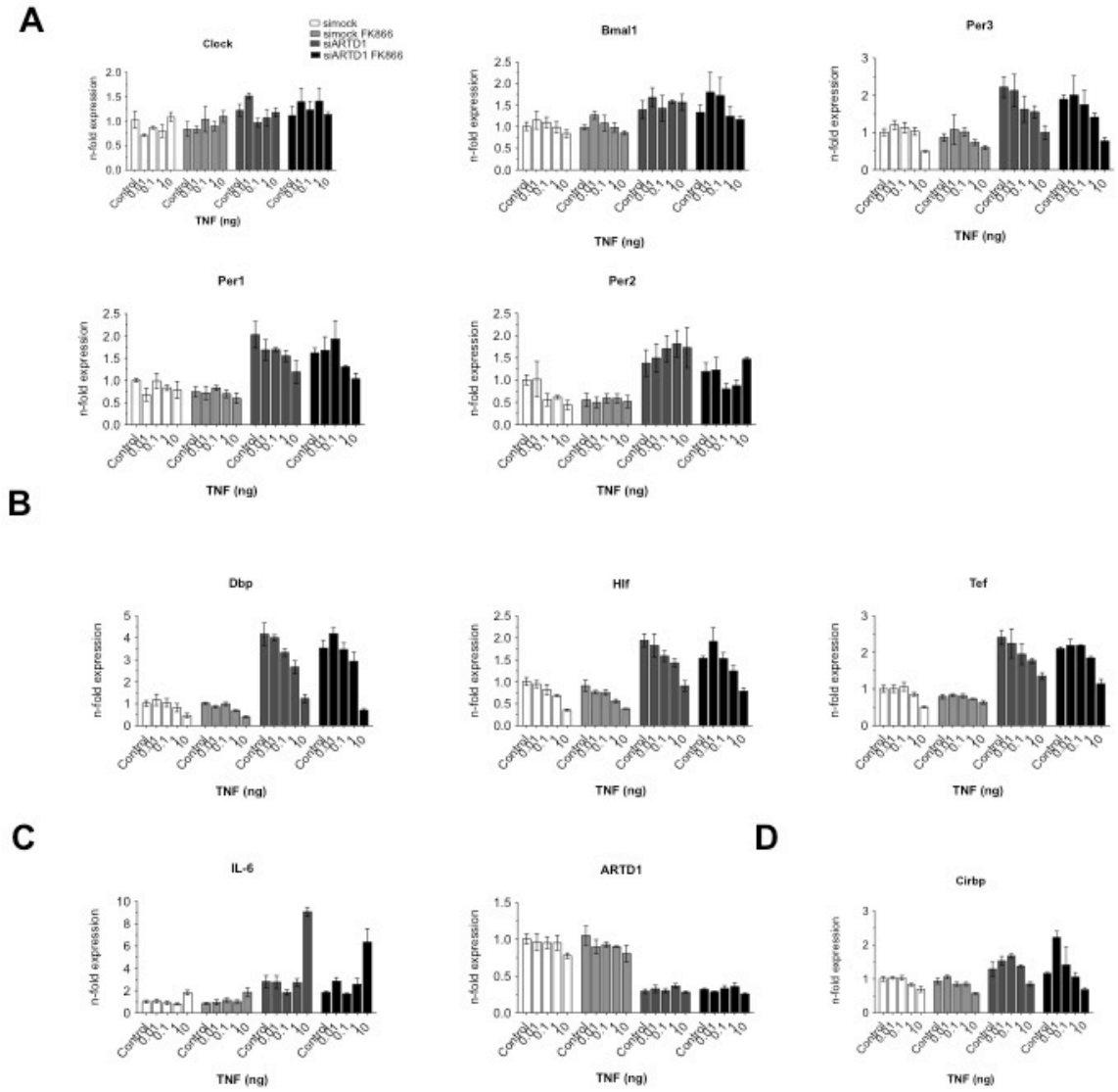

Figure 9: Transient knockdown of ARTD1 increases clock gene expression and CIRBP expression in 3T3 cells independent of FK866.

A) 3T3 cells were transfected with anti-ARTD1 siRNA or with a mock control. 48 hours after the transfection cells were starved overnight in medium containing 1% FCS in the presence or absence of 100nM FK866. Starved cells were treated for 4 hours with the indicated concentrations TNFα in the presence or absence of 100nM FK866 in 1% FCS medium. RNA was isolated, basic cock gene expression was analysed by qPCR and normalized against *GAPDH* levels. Shown are mean of three technical replicates±SEM. Basic clock genes

B) Same as in A but for Clock-output genes

C) Same as in A but for control genes of the inflammatory response and knockdown controls.

D) Same as in A CIRBP expression levels

The observed change in *CLOCK* gene expression upon siARTD1 treatment could be indirectly caused by increased cellular NAD^+ levels due to the lack of ARTD1 as NAD^+ consuming enzyme and the subsequent activation of sirtuins. Experiments were thus repeated in presence of FK866, an inhibitor of niacinamide-phosphoribosyl-transferase (NAMPT) to reduce cellular NAD^+ levels [330]. The addition of FK866 did not change the expression of *CLOCK* or clock output genes

neither in siMOCK nor in siARTD1 cells (Fig. 9A,B), indicating that the cellular NAD^+ levels are less likely to contribute to the observed gene expression changes. Treatment of 3T3 cells with PJ34 (PARP inhibitor) however increased *CLOCK* gene expression (Fig. 8D). The discrepancy between FK866 and PARP inhibitor treatment might indicate that ARTD1 consumes NAD^+ from cellular sources that are not affected by FK866 (e.g. protein-bound NAD^+). Another possibility would be that PJ34 is inhibiting an off-target.

In summary, our results provide evidence that ARTD1 represses clock-gene expression in the liver, which, however, does not affect SBS in mice. In cell culture experiments, we could reproduce an effect of ARTD1 knockdown on clock gene expression. The effect of ARTD1 on gene expression was already observed in cells that were not stimulated with TNFα, but was maintained upon TNFα stimulation. This could indicate an effect of ARTD1 on the chromatin structure at regulatory regions of CLOCK genes. Also, we observed increased expression of *CIRBP* in siARTD1 cells which could indicate that the stabilization of clock genes mRNA might be affected indirectly (data not shown). However, further experiments, such as WB analysis of CIRBP or RNA stability measurements, would be required to determine the exact role of ARTD1 and PAR formation in this context.

3.3.5 Material and methods

Embryonic stem cell genotyping

The targeting vector for tissue specific knockouts for ARTD1 was bought from Eucomm (European Conditional Mouse Mutagenesis Program, Lemförde, Germany, http://www.mousephenotype.org/martsearch_ikmc_project/about/eucomm).

Embryonic stem cells (ESCs) were transfected and DNA isolation was performed by Polygene (Rümlang, Switzerland).

The following primers were used to genotype ESCs:

5'-CACTGAACTGTCTCCTTAGCCAACTCTGC-3'GF3

5'-CTAGGATTCTGTGTCTTGACCATGCACTTG-3' GR4

5'-CACACCTCCCCCTGAACCTGAAAC-3' RAF5

5'-CACAACGGGTTCTTCTGTTAGTCC-3' LAR3 (all sequences from Eucomm)

5'-GCTTCTACTACCTCCCAAGAAAGAGCG-3' 1405

For short PCR fragments GoTaq polymerase was used (Promega, Madison, WI, USA) according to the manufacturer's instructions. For long PCR amplicons, the expand long template PCR system was used (Roche, Basel, Switzerland) employing buffer system 2 according to the manufacturer's instruction. PCR program: 93°C 2:00; (93°C 0:10; 50°C 0:30; 68°C 8:00) x10; increase extension time at 68°C by 0:40 every second cycle until cycle 28; 68°C 07:00; 4°C. For the improved PCR program, the annealing temperature was increased to 60°C. PCR amplicons were analysed on a 1% agarose gel.

Cell culture

3T3 and 3T3-L1 cells were cultivated in Dulbecco's Modified Eagle's Medium (DMEM) (PAA, Pasching, Austria, supplemented with 1% (v/v) Penicillin/Streptavidin and 10% (v/v) fetal calf serum (Gibco, Invitrogen, CA, California, USA). 3T3-L1 cells were differentiated at 80% confluence. For differentiation, the medium was changed after 2 days and induction medium (containing 5µg/ml insulin (I-9278), 0.25mM 3-isobutyl-1-methylxanthine (I-5879) and 0.5µM dexamethasone (D-4902); all from Sigma Aldrich (St. Louis, MO, USA) was added for 3 additional days. From day 5 onwards, the medium was changed every second day to regular DMEM containing (1µg/ml). Rosiglitazone (Sigma Aldrich, St.

Louis, MO, USA) was supplemented at 1μM and ABT888 (Enzo Life Sciences, Farmindale, NY, USA) was added at 10μM every second day starting at day 7. 3T3 cells were plated at 80% confluence. After one day, at 100% confluence, they were starved overnight in DMEM containing 1% FCS and 0.1% Penicillin/Streptavidin in the presence or absence of 100nM FK866 (Sigma Aldrich, St. Louis, MO, USA). Cells were pretreated for 1 hour with 10μM PJ34 (Alexis Biochemicals, San Diego, CA) prior to treatment with recombinant murine TNFα (Sigma Aldrich, St. Louis, MO, USA) at concentrations ranging from 0.01ng to 10ng for 4 hours.

siRNA transfection

15pmol siRNA (Negative control allstars (siMock), mouse siPARP1 #5, Qiagen, Hilden, Germany) were transfected with RNAi MAX lipofectamine (Invitrogen, Carlsbad, CA, USA). 2 days after transfection cells were 100% confluent. Knockdown was verified by qPCR.

RNA isolation and qRT-PCR

Total RNA from 3T3-L1 cells was extracted using TRIzol (Invitrogen, Carlsbad, CA). DNase treatment was performed using the TURBO DNA-freeTM Kit (Life Technologies, Carlsbad, CA, USA). Total RNA from mice tissue for the adipocyte study was isolated with TRIzol. Equal amounts of RNA were reverse transcribed using the High-Capacity cDNA Reverse Transcription kit (Applied Biosystems, Foster City, CA). Quantitative-real-time polymerase chain reactions (qPCR) were performed with SYBR® green SensiMix SYBR Hi-ROX Kit (Bioline Reagents Ltd, London, UK) in a Rotor-Gene Q 2plex HRM System (Qiagen, Hilden, Germany). *Cyclophilin* was chosen as the internal control for normalization after screening several candidate control genes for 3T3-L1 cells. *36BP4* was used for normalization of mice samples. RNA from 3T3 cells was extracted using NucleoSpin - RNA II kit (Macherey-Nagel, Düren, Germany). RNA from mouse tissues harvested for the analysis of clock gene expression was extracted by homogenization of the organ in peqGOLD RNA pure (PeqLab, Erlangen, Germany) according to the manufacturer's instructions. Subsequently, RNA was reverse-transcribed using random hexamers (Fermentas, Waltham, MA, USA) and M-MuLV reverse transcriptase (Roche, Basel, Switzerland). Equal amounts of cDNA were amplified in an ABI 7900 HT detection

system (Applied Biosystems, Foster City, CA, United States) using the TaqMan Universal PCR Master Mix (Applied Biosystems, Foster City, CA, United States). The relative levels of each RNA were calculated by the ΔΔCT method, with *eEF1a1*, *18s rRNA* or *GAPDH* as housekeeping genes.

Mice

For the clock gene analysis, C57BL/6J mice were purchased from RCC Ltd. (Füllinsdorf, Switzerland). ARTD1$^{-/-}$ mice were supplied by our laboratory. Male mice aged between 8–12 weeks were used. Experiments were performed according to Taraborelli and coworkers [321]. Locomotor activity was measured by recording either motor activity in the cages or using freely accessible running wheels. Activity recordings were based on 1 min episodes by using the Chronobiology Kit software (Stanford Software Systems, Santa Cruz, CA, USA). Three days (day-1, -2, -3) preceding injection were averaged and used as baseline activity. At day 0, mice were injected i.p. at Zeitgeber time (ZT)5 with 200µg CD40 mAb (clone FGK4.5; rat IgG2a anti-mouse CD40, BioX Cell, West Lebanon, NH, USA) in 200µl PBS. As an antibody control, 200µg rat IgG2a isotype control (clone 2A3, BioX cell) in 200µl PBS was used. Two days after injection, mice were sacrificed and used for the analysis.

For the adipocyte studies, experiments were performed with young adult (6–9 weeks) male mice kept on an inverted 12h dark/light cycle, fed *ad libitum* chow diet. For the cold stimulation, animals were housed in type II cages with 2 animals per cage. Following acclimatization at 23°C, air temperature was lowered to 8°C for 7 days. Animal experiments were performed according to the regulations of the Cantonal Veterinary Office (Zurich, Switzerland).

Western Blotting

Protein amounts were assessed using the DC Protein Assay (Bio-Rad). 30µg of protein extract was loaded and separated on 7.5% SDS-polyacrylamide gels. Gels were blotted on a PDVF membrane and analysed by using protein specific antibodies and an Odyssey-detection system using fluorescent-dye-coupled 2nd antibodies (LI-COR Biosciences, Cambridge, UK).

Antibodies

Following antibodies were used: From Santa Cruz Biotechnology, Inc (Dallas, TX, USA): PARP1/ARTD1 (H-250, rabbit); From Sigma Aldrich (St. Louis, MO, USA): tubulin (mouse). The PAR 10H (mouse) was provided by Paul O. Hassa (IVBMB, University of Zurich).

***In vitro* ARTD1/3 activity assays**

Recombinant, full-length, his-tagged ARTD1 and ARTD3 proteins were generated in Sf21 cells using the BacPAK system (Clontech). Purification was performed in batch using Ni^{2+}-beads/Nitrobond (Invitrogen). If not stated otherwise, proteins were washed with EtBr-containing wash buffer during purification. 20nM or 500nM HA-ARTD3-his and 20nM, 50nM or 500nM of myc-ARTD1-his were incubated for 10mins at 24°C with 100nM, 1µM, 10µM or 100µM ^{32}P labeled NAD^+ in ARTD reaction buffer (250mM Tris-HCl pH8, 20mM $MgCl_2$, 1.25mM DTT, 5µg/ml P/B/L – proteinase inhibitors) in the presence or absence of 5pmol Eco Linker, or other DNAs, as indicated in the figure legends. For activation by histones either 1µg Histone Mix containing core histones from (Roche, Basel, Switzerland) or 1µg recombinant H1.4 was used. For activation by RNA, 0.75µg of *in vitro* transcribed RNA was used (obtained from Karolin Leger, IVBMB, Zurich, Switzerland). The reactions were stopped by the addition of sample buffer. The samples were seperated on 12% SDS polyacrylamide gels and gels were stained with coomassie, de-stained, and subjected to film exposure. To inhibit DNA-dependent activation, reactions were supplemented with 100µg/ml or 50µg/ml Ethidiumbromide (EtBr, Sigma Aldrich, St. Louis, MO, USA) or preincubated with 1U DNAse I (Roche, Basel, Switzerland) for 15mins at 30°C.

ADP-ribose product analysis

For cold product analysis, a protocol described by Malanga and coworkers was adapted [331]. Briefly, 6µg of ARTD1 and ARTD3 were incubated for 45mins at 30°C in reaction buffer (100mM Tris pH8.0, 10mM $MgCl_2$ and 125mM NaCl) with 1mM NAD^+ and 1µg NHEI-digested CMV-GFP plasmid in the presence or absence of 6µg H1.4. Proteins were precipitated by the addition of BSA and 40% (w/v) ice-cold TCA

on ice. The resulting pellet was washed with ethanol 99.8% and then with ice-cold diethylether. Polymers were detached using 0.5M KOH/10mM EDTA and DNAse I, RNAse A and proteinase K digestion. After extraction with phenol–chloroform–isoamyl alcohol, PAR was precipitated with ethanol overnight. Following centrifugation, PAR was air-dried and resuspended in 50mM Tris pH 7.5 and 10mM EDTA. The polymers were separated on 2M urea 20% acrylamide sequencing gels and visualized by silver staining according to the manufacturer's instructions (Pierce, Thermo Fisher Scientific, Rockford, IL, USA).

For radioactive product analysis, 6µg of ARTD1 and ARTD3 were incubated for 45mins at 30°C in reaction buffer (100mM Tris pH8.0, 10mM $MgCl_2$ and 125mM NaCl) with 10µM NAD^+ and 1µg NHEI-digested CMV-GFP plasmid in the presence or absence of 6µg H1.4. Proteinase K was added to the reactions and was incubated over night at 37°C. Reactions were separated by 10% urea-PAGE at 45W for 90min and exposed to an X-ray film.

4 Discussion and Perspectives

4.1 ARTD1 controls adipocyte differentiation and function

The differentiation of preadipocytes into adipocytes is driven by a tightly regulated cascade of transcription factors. It is accompanied by drastic changes in the chromatin structure and the establishment of so called transcription hotspots that, in addition to the recruitment of several transcription factors, are also characterized by an open and permissive chromatin structure. This permissive chromatin structure is established by cofactors that are recruited by activated transcription factors such as PPARγ and allows high expression of adipocyte-specific genes. In this thesis we identified a role for ARTD1 in adipocyte differentiation. One published paper describes an increase in PAR formation during the late phase of adipogenesis that was mediated by site-specific, topoisomerase II-mediated ds-DNA breaks and was required for PPARγ-dependent gene expression [332]. In another paper, these findings were validated and confirmed *in vivo* using ARTD1$^{-/-}$ mice. Adipogenesis was impaired in adipose derived stromal cells (ASCs) obtained from ARTD1$^{-/-}$ mice [333]. In addition, wt ASCs showed less differentiation when subjected to PARP inhibitor treatment. ARTD1$^{-/-}$ mice showed decreased weight gain on high fat diet, but developed hepatic steatosis. In our newest submitted manuscript, we present data from PARP inhibitor-treated mice strengthening the importance of ADP-ribosylation for adipogenesis *in vivo*. PARP inhibitor treated mice show reduced body weight, fat mass, smaller adipocytes and an altered PPARγ-dependent gene expression. We further investigated the mechanistic details of ARTD1 requirement during adipogenesis. By using different PARP- as well as PARG-inhibitors, we could confirm that PAR formation is required for PPARγ-dependent gene expression and the cofactor exchange at PPREs. In absence of PAR, there was increased recruitment of the corepressor NCOR-1 to PPARγ-target sites while p300 levels were decreased.

Recently, a role of ARTD1-dependent PAR formation in PPARγ-dependent 5-hydroxymethylation of PPREs was described [285]. This model suggests PARylation of a PPARγ-co-activator complex leading to recruitment of TET proteins that induce region-specific demethylation (conversion to hydroxmethly-C). Although presenting a potentially interesting mechanism, a lot of details are still unclear. The authors only

analyse one PPRE of one gene, but it is completely unclear if all PPREs behave the same in this regard. Also, it is unclear which component of the co-activator complex is PARylated. Comparable to our results, the authors observe the requirement of PAR for the recruitment of a cofactor. In contrast, our own analysis of DNA methylation revealed only a slight effect upon PARP inhibitor treatment (data not shown, experiment performed by Süheda Erener, IVBMB, University of Zürich). In addition, inhibition of DNMTs during differentiation led to a decrease in gene expression (data not shown), which suggests that *de novo* methylation is beneficial for adipocyte differentiation. The requirement for global demethylation during adipogenesis is controversial and it is currently unclear if PPARγ and PPARγ ligands are involved in this process [334-337]. Especially in regard of the establishment of transcriptional hotspots during differentiation, it would be interesting to analyse DNA methylation during adipogenesis. This could be done by performing genome wide DNA methylation and hydroxymethylation assays such as methylated DNA Immunoprecipitation (meDIP), hydroxymethylated DNA Immunoprecipitation (hmeDIP) or bisulfite and oxidized bisulfite sequencing [338-341]. A recent study on 5-hydroxymethalyation in 3T3-L1 cells suggests that 5-hydroxymethalyation in 3T3-L1 cells is acquired early during differentiation and maintained throughout differentiation [342]. This dataset could be compared to the sites of hotspot formation and ARTD1 binding.

Adipogenesis is accompanied by the establishment of hotspots that can prime certain DNA sites for the binding of later transcription factors. It would be interesting to analyse the role of ARTD1 in these hotspots. It is unlikely that ARTD1 is involved in the establishment of hotspots, as we observe PAR formation and ARTD1 recruitment to PPREs only in the late phase of adipogenesis. However, it would be interesting to perform a genome wide analysis of ARTD1 binding in undifferentiated and differentiated 3T3-L1 cells (ChIP-Seq). Such experiments would provide evidence, to which genes ARTD1 is recruited and reveal if prior priming by a hotspot is needed for ARTD1 binding. It could be that ARTD1 is important for the maintenance of the late enhanceosome. Shortly after induction of differentiation, more than 22 000 new DHS (DNAse1 hypersensitive regions) are established, of which at least half are gone at day 7 of differentiation [199]. ARTD1 might help to establish whether a hotspot stays in an open chromatin conformation or is closed. Only 33% of all PPARγ-binding sites are remodeled before PPARγ binding [199]. It

could also be that ARTD1 is only needed at these sites and not at those primed by hotspots. Genome wide analyses throughout the differentiation process would help to answer these questions.

PPARγ is a ligand-dependent transcription factor. Ligands described to activate PPARγ include various polyunsaturated fatty acids and derivatives [227,228,230,231,233]. In addition, during adipogenesis, the cells acquire a high lipogenic capacity. Both the expression of enzymes important for de novo fatty acid synthesis as well as for triacylglycerol synthesis, are increased tremendously [237-239]. So although there is increased fatty acid synthesis, these fatty acids are stored in form of triglycerides in lipid droplets [240]. Cellular fatty acids can originate from different sources. They may be taken up as unesterified plasma fatty acids or as fatty acids generated by lipoprotein lipase (LPL)-mediated hydrolysis of chylomicrones in tissue capillaries, or originate from *de novo* synthesis. Fatty acids from all these sources can activate PPAR-mediated gene expression [241,343-345]. However, there remain unanswered questions. The above mentioned papers describe the activation of PPARα and ∂ but not of PPARγ. In addition, it is currently unknown whether fatty acids require esterification to triglycerides and subsequent rehydrolysis (lipolysis) before signal transduction to the nucleus [241]. Therefore it is possible, that these fatty acids need to be released by lipases such as ATGL or hormone sensitive lipase (HSL) in order to activate PPARγ [242,243]. Indeed, HSL deficient mice show less PPARγ activity and smaller adipocytes [243]. ATGL deficient mice showed less PPARα activity, which could be reversed by the treatment with PPARα agonists, indicating a role of ATGL in the generation of endogenous PPAR agonists [241]. It is an intriguing possibility that PAR formation maintains PPARγ- dependent gene expression in the absence of a PPARγ-ligand. Our data indicate that a PPARγ-ligand is needed for initial activation of PPARγ, but once PAR formation is induced, it ensures transcriptional activation of PPARγ-target genes in the absence of a ligand. Consistent with this, we could reverse the inhibition of PPARγ-dependent gene expression due to PARP inhibitors by supplementing cells with an artificial PPARγ-ligand (Rosiglitazone).

BAT has completely different features and functions than WAT [135]. However, PPARγ is also important for the formation of BAT [244,245,346]. It would be thus of great interest to investigate the effect of ARTD1 and PAR formation on the differentiation and function of BAT. As over-activation of PPARγ is connected to increased BAT formation, it is likely that PAR formation is also required in this process [168].

Preliminary results suggest an effect of PAR formation in these processes. Inhibition of PAR formation inhibited the Rosiglitazone-induced increase in *UCP-1* expression. ARTD1$^{-/-}$ mice were described to have an increased BAT and an increased number of mitochondria in their brown adipocytes, whereas ARTD2$^{-/-}$ mice showed no effect on BAT [280]. We plan to further analyse the browning potential of ARTD1$^{-/-}$ and ARTD2$^{-/-}$ mice by exposing them to cold and consecutively measuring their BAT content and quality of the BAT (by histological analysis). This will answer the question if ARTD1 or ARTD2 are required for the browning of adipocytes. However, detailed mechanistic studies need to be performed for example by studying ARTD1 or ARTD2 depletion on the browning of 3T3-L1 cells.

Binding of PPARγ and PPARγ ligand to PPREs has a stimulatory effect on adipogenic gene expression. However, PPARs are also important regulators of the immune system [347]. Ligands for PPARγ and PPARα were shown to have considerable anti-inflammatory activities in different models for inflammatory and autoimmune diseases such as experimental autoimmune encephalomyelitis, inflammatory bowel disease, and arthritis [347-362]. *PPARγ* expression is not restricted to adipocytes but to a lesser extent it is also found in the colon, the retina and in the immune system [363]. Mice with only one copy of *PPARγ* and targeted knockouts for *PPARγ* in macrophages or the intestinal epithelium all showed increased susceptibility to chemically induced colitis [347,364-366]. The suppression of transcription of inflammatory mediators involves both PPARγ-dependent and -independent pathways, which complicates the analysis of experiments and the therapeutic use [367-370]. However, it is well documented, that PPARγ can repress the expression of inflammatory genes by a process that involves protein-protein interactions rather than sequence-specific DNA binding [371]. This process is called transrepression and has been described for PPARγ and NF-κB in macrophages, for example [371,372]. In this context, transrepression is mediated by ligand-dependent SUMOylation of PPARγ, which recruits the latter to NCOR1/HDAC corepressor complexes at inflammatory gene promoters such as inducible nitric oxide synthase (iNOS). This binding inhibits the stimulus (LPS)-induced release of corepressors and maintains the promoter in a repressed state. We showed in this thesis, that PAR formation is required for ligand-induced cofactor exchange and PPARγ-dependent gene expression. It would be interesting to investigate if the transrepression of NF-κB by PPARγ is also dependent on PAR formation. It could be that the dependency on PAR distinguishes the two modes of

action of PPARγ-dependent transrepression and transactivation. This could be investigated in LPS-stimulated macrophages. It would be interesting to analyse NF-κB-dependent gene expression in the presence or absence of PPARγ agonist and PARP inhibitors. In addition, the effect of PARP inhibition on the SUMOylation status of PPARγ could be investigated. It is known that there is a massive crosstalk between different PTMs [373,374]. For example, PARylation was described to be affected by other PTMs such as methylation [19,375]. The involvement of ARTD1 and PAR formation in transrepression is an intriguing possibility, especially because ARTD1 has been implicated as a coregulator of NF-κB [90]. After the induction of the inflammatory response by LPS or streptocozin, various proinflammatory cytokines are down-regulated in ARTD1$^{-/-}$ mice [90,376-383]. This could also be confirmed in *in vitro* models [86-90]. However, the involvement of ARTD1 enzymatic activity remains controversial. Early studies described PARylation of p65 and indicated that this modification suppressed NF-κB-dependent gene expression [384,385]. On the other hand, ARTD1 has also been described to coregulate NF-κB-dependent gene expression independent of its enzymatic activity [86,88-90,382,386]. The importance of PAR formation for the control of NF-κB-dependent gene expression needs to be further investigated and should be extended regarding transrepression by PPARγ.

Roles for ARTD1 in the control of gene expression have been described in different physiological situations [5]. Whether ARTD1 functions as a corepressor or coactivator depends on the transcription factors, cell types and stimuli that are used [5](and unpublished data of our laboratory). In some contexts, ARTD1 is a coactivator [387-390], whereas in others it acts as a corepressor [91,391-393]. In this thesis we show evidence, that in clock-dependent gene expression ARTD1 acts as a repressor, which has also been reported in a previous study where ARTD1 was described to PARylate CLOCK-BMAL thereby interfering with their DNA-binding capacity[279]. In the presented data we observed increased *CIRBP* mRNA expression upon ARTD1 depletion, providing an additional possibility to regulate the stability of certain mRNAs. However, further studies such as confirmation of the increased expression by Westernblot analysis or knockdown of CIRBP and RNA-stability measurements need to be performed to confirm this hypothesis. An important question is how such an abundant protein like ARTD1 can specifically control pathways in different ways. One possibility is that the availability of cofactors such as p300/NCOR, different adaptor molecules, or different posttranslational modifications might be responsible

for the different actions of ARTD1. We know from unpublished results from our lab that different cell lines show different transcriptional responses to the knockdown of ARTD1 and stimulation with LPS or TNFα (Roberta Minotti, IVBMB, University of Zürich). For example, macrophages express more IL6 upon ARTD1 knockdown, whereas mouse lung fibroblast cells show the opposite effect. Interestingly, macrophages also express *PPARγ*. It would therefore be interesting to investigate if the effect of ARTD1 depletion depends on the expression of *PPARγ*.

This aspect is especially interesting in regard of diseases associated with obesity, such as Type II diabetes, cancer or atherosclerosis, where inflammatory aspects are important [146-149]. It would be of great interest to elucidate the role of ARTD1 in the inflammatory component of these diseases. In analogy to our findings it could be that PAR formation maintains PPARγ in an activated state and consequently controls adipocyte genes and suppresses transrepressory activities. It would thus be interesting to test if PPARγ is also associated with PAR at inflammatory genes, for example by ChIP analysis for PAR and PPARγ and ReChIP analysis combining both PAR and PPARγ ChIP. For this thesis, we have analysed the inflammatory gene expression profiles in the liver of ARTD1$^{-/-}$ mice, which showed a reduction for various cytokines such as *IL6*, *IL10* and *IL12* [333]. This could indicate that deletion of ARTD1 indeed abrogates PPARγ-driven gene expression in adipocytes and increases transrepression of inflammatory genes. Also, in this regard it would be interesting to analyse cytokine levels of mice treated with PARP inhibitor. Although controversial, PPARγ was described to be involved in macrophage differentiation [236,394,395]. In ARTD1$^{-/-}$ mice also MPEG1 and Pu.1 were reduced, which are markers for macrophage differentiation [333]. This all suggests that PAR formation controls various functions of PPARγ.

Given the effect of ARTD1 knockout on inflammatory gene expression in the liver, one could hypothesize that these animals show increased glucose tolerance. However, when ARTD1$^{-/-}$ mice were subjected to a glucose tolerance test (GTT), they showed reduced glucose tolerance along with increased insulin secretion [333]. This was likely due to dyslipidemia and excessive lipid accumulation in the liver. Mice on HFD treated with a PARP inhibitor for 18 weeks, however, do not show an accumulation of fat in the liver (data not shown from Eijia Pirinen, EPFL). This suggests that in this process the ARTD1 protein plays a role that is independent of its enzymatic activity.

It would be extremely appealing to investigate this additional role in conditional and tissue specific ARTD1$^{-/-}$ models. In addition, it would be fascinating to investigate the glucose homeostasis in these animals that could likely reveal very different results as compared to the ARTD1$^{-/-}$ mice. Especially because there seems to be no symptoms of NAFLD (non alcoholic fatty liver disease), PARP inhibitors could be assessed as a potential treatment for obesity and associated inflammatory syndromes. It would thus be interesting to test PARP inhibitors in animal models of type II diabetes. ARTD1$^{-/-}$ mice were described to be protected from streptozotocin induced diabetes, which more closely resembles type I diabetes in human [396,397]. The PARP inhibitor PJ34 was tested in a model for type II diabetes in db/db diabetic animals and showed a slight effect on serum glucose concentration [398]. The effect of more specific PARP inhibitors should be tested in a model for type II diabetes and other obesity related disorders.

In addition, it would be interesting to investigate the association of the susceptibility for the development of type II diabetes with mutations in the *ARTD1* or *PARG* genes. This could hint at a role of these proteins in the development of type II diabetes and thus indicate their potential as diagnostic markers for this disease. Interestingly, recent studies about metabolic signatures in type II diabetes revealed a downregulation of NAD^+ levels in type II diabetes patients, which was connected to widespread transcriptional changes [399]. It would thus be captivating to analyse how PARP inhibitor-treatment affects whole metabolic network and homeostasis in mice. Finally, it would be helpful to analyse the transcriptomes of different tissues of PARP inhibitor treated mice to be able to appreciate how PAR formation controls glucose homoeostasis and homeostasis of metabolites.

4.2 ARDT3 is a mono-ART that is activated by histones and RNA and is involved in DNA double strand break repair

The ARTD protein family consists of 18 members that can transfer ADP-ribose to acceptor proteins. ARTDs possess different enzymatic activities and can form either mono- or poly-ADP-ribose. Regarding ARTD3, it is still unclear if it catalyzes mono- or poly-ADP-ribosylation. In the unpublished results we showed that ARTD3 is weakly active and catalyzes only mono-ADP-ribosylation on itself and on target proteins (such as histones). In addition, ARTD3 was activated by RNA and core

histones and ADP-ribosylated the latter as well. Given the distinct functions of ARTD family members and their involvement in different cellular functions, it is extremely important to generate inhibitors that target certain ARTD members specifically. In this thesis, a paper is presented where our collaborators from the group of Prof. Dr. Herwig Schüler developed an inhibitor that specifically targets ARTD3 [400]. We could verify the function of this inhibitor in cells.

Although ARTD3 contains a catalytic domain which is similar to ARTD1, its catalytic activity is significantly lower compared to ARTD1. While a few labs could detect poly-ART activity for ARTD3, others describe no or only mono-ART activity [18,106-108]. A study of human ARTD3 produced in bacteria raised the possibility that this enzyme might be a mono-ART [108]. We provide evidence in this thesis, that also ARTD3 purified from insect cells was only able to transfer ADP-ribose monomers. This is in line with another report of our lab [18]. The PARP domains of ARTD3, ARTD2 and ARTD1 share 35% sequence similarity and their structure is very similar [401-404]. Overall, the NAD^+ binding site and the PARP signature motif are well conserved [402]. The loops surrounding the active site show the most important differences in the catalytic domain that allowing the development of an ARTD3 selective inhibitor [400,402]. ARTD3 even contains a glutamate (Glu^{514}) corresponding to Glu^{988} in ARTD1, which was suggested to convey poly-ART activity [405]. Apparently, the presence or absence of this catalytic glutamate does not distinguish between mono- and poly-ART activity.

It was demonstrated, that the catalytic and WGR domains tightly cooperate with their corresponding amino-terminal domains [18]. This is shown by the fact, that the C-terminal domain of ARTD1, if replacing the corresponding domain in ARTD3 or ARTD2, does not convey poly-ARTD activity. What conveys poly-ART activity is, however, not known yet and it would be intriguing to investigate this question using different ARTD1/3 chimera. It could for example be imagined that the proteins need their own WGR or that only the exchange of a few amino acids surrounding the catalytic core could make a difference. Establishing these chimeras and testing their activity is ongoing in our laboratory. In addition, it would be of great interest to identify the acceptor amino acids that can be modified by ARTD3 in ARTD3 itself (automodification) and in other target proteins (transmodification). Loseva et al. claim that the automodification takes place on glutamates or aspartates, because it is sensitive to hydroxylamine treatment [108]. However, in their hands also ARTD1

modifications were sensitive to this treatment, although ARTD1 was shown to also modify lysine residues [18,19]. The identity of the amino acids targeted by ARTD3 remains to be investigated for example by mass spectrometry approaches.

ARTD1 is strongly activated by DNA, however whether ARTD2 and ARTD3 are activated by DNA remains controversial [2]. Two studies did not observe a stimulation of ARTD3 by DNA [18,108]. In contrast, other studies observed a slight increase in ARTD3 activity upon addition of DNA [106,107]. In our present study employing different DNA constructs to answer this question no activation of ARTD3 by DNA was observed. The three zinc fingers in the N-terminal domain of ARTD1 are required for DNA binding and DNA-dependent activation of ARTD1. However, these are missing in ARTD3 as well as in ARTD2, which is only slightly activated by DNA [18] (and unpublished data from our lab). However, ARTD2 can be activated by RNA through its SAP (SAF/Acinus/PIAS-DNA-binding domain) domain (unpublished data from our lab). Although ARTD3 does not contain a SAP domain, we could show that it is also activated by RNA. ARTD3 does, however, contain a WGR domain that could mediate binding of nucleic acids. For example, the WGR domain was shown to be involved in the binding and activation of ARTD1 to ss-RNA [293]. If the WGR domain conveys the activation of ARTD3 by RNA remains to be investigated by employing mutants lacking this domain.

ARTD3 can modify histone H1 and we could show that it can also modify core histones, a previously unknown substrate for ARTD3 [107,108]. Previously, it was shown that ARTD3 can bind to the histone variants H3C and H2BE in cells, supporting the idea that ARTD3 is activated by histones *in vivo* [108,406]. Interestingly, addition of histones (H1 or core histones) increased ARTD3 auto- and transmodification activity. We excluded the possibility that the activation of ARTD3 could be conveyed by contamination with ds-nucleic acids by supplementing ethidiumbromide to our reactions. However, since binding of EtBr to single-stranded DNA/RNA is relatively poor, it can currently not be ruled out that a contamination of the histones with single-stranded nucleic acid might cause this increase in ARTD3 activity. To test this possibility further experiments including pretreatment of histones with RNAse or DNAse will be performed. It is notable that contradictory results were published by others and obtained by our laboratory regarding ARTD3 enzymatic activity, although sometimes even proteins of the same origin were used. This indicates that exact experimental conditions are critical, that ARTD3 is very labile, or

that some groups work with ARTD3 contaminated with other ARTD members. Further efforts should be invested to resolve these contradictions in order to be able to truly characterize ARTD3.

Several studies have implicated ARTD3 in DNA damage repair [107,114,115,400]. It is however only implicated in the resolution of DSBs, but not SSBs. ARTD3 is needed to resolve γH2Ax foci in an Aprataxin-and-PNK-Like Factor (APLF) and XRCC4/ DNA ligase 4-dependent manner [107]. Rulten and coworkers suggest that ARTD3 binds to double strand breaks (DSB) and recruits APLF and XRCC4/DNA ligase 4, which renders the chromatin permissive for DNA ligation. Based on our results, we however conclude that it is not the DSBs that activate ARTD3, but rather another stimulus. There is ample modification of histones and histone composition (e.g. phosphorylation of the variant H2Ax by ATM, acetylation and ubiquitination of γH2Ax, H2A and H2B) during the response to DNA damage [407,408]. In addition, acetylated histone H4 (H4K8ac) and a transient increase of the histone variant H2A.Z is detected at DSBs [407,409-411]. It is therefore possible that histones exposed upon DNA damage or histone variants such as γH2Ax itself activate ARTD3. It would be interesting to test the activation of ARTD3 and modification of γH2Ax *in vitro* and *in vivo* to test this hypothesis. Given that ARTD3 has a distinct role in DNA damage signaling, the availability of specific inhibitors for ARTD3 is important.

This thesis includes a paper that was published in collaboration with Prof. Dr. Herwig Schüler that describes the development and functionality of ARTD3 specific inhibitors [400]. These inhibitors could be used to characterize the role of ARTD3 in different cellular processes and to evaluate their potential as therapeutic targets. General PARP inhibitors are currently evaluated in clinical trials, as monotherapies or in combination with radiation and other chemotherapeutics, for the treatment of cancer types such as advanced solid tumors and lymphoma, but so far no PARP inhibitor has been approved for clinical use [412-415]. However, all currently tested PARP inhibitors are NAD^+-analogues that do not specifically target ARTD1, but have a considerable inhibitory effect on other ARTD family members such as ARTD1, ARTD3 or ARTD4 [287]. Interestingly, PARP inhibitors seem to have a broader application spectrum. Preclinical studies for treatment of cardiovascular and neurological indications and inhibition of angiogenesis have been performed [380,386,416-420]. It would thus be of significant importance to assign the observed effects to one or more specific ARTD family members. It is an intriguing possibility that ARTD

specific inhibitors, like ARTD3 inhibitors, could be used in some of these indications and help reduce adverse side effect.

References

1 Sims, R. J., 3rd & Reinberg, D. Is there a code embedded in proteins that is based on post-translational modifications? *Nat Rev Mol Cell Biol* **9**, 815-820, (2008).

2 Hassa, P. O. & Hottiger, M. O. The diverse biological roles of mammalian PARPs, a small but powerful family of poly-ADP-ribose polymerases. *Front Biosci* **13**, 3046-3082, (2008).

3 Hassa, P. O., Haenni, S., Elser, M. & Hottiger, M. O. Nuclear ADP-ribosylation reactions in mammalian cells: where are we today and where are we going? *Microbiol Mol Biol Rev* **70**, 789-829, (2006).

4 Kraus, W. Transcriptional control by PARP-1: chromatin modulation, enhancer-binding, coregulation, and insulation. *Curr Opin Cell Biol* **20**, 294-302, (2008).

5 Kraus, W. & Lis, J. PARP goes transcription. *Cell* **113**, 677-683, (2003).

6 Oei, S. L., Keil, C. & Ziegler, M. Poly(ADP-ribosylation) and genomic stability. *Biochem Cell Biol* **83**, 263-269, (2005).

7 Di Girolamo, M., Dani, N., Stilla, A. & Corda, D. Physiological relevance of the endogenous mono(ADP-ribosyl)ation of cellular proteins. *Febs J* **272**, 4565-4575, (2005).

8 Inageda, K., Nishina, H. & Tanuma, S. Mono-ADP-ribosylation of Gs by an eukaryotic arginine-specific ADP-ribosyltransferase stimulates the adenylate cyclase system. *Biochem Biophys Res Commun* **176**, 1014-1019, (1991).

9 Just, I. *et al.* ADP-ribosyltransferase type A from turkey erythrocytes modifies actin at Arg-95 and Arg-372. *Biochemistry* **34**, 326-333, (1995).

10 Lang, A. E. *et al.* Photorhabdus luminescens toxins ADP-ribosylate actin and RhoA to force actin clustering. *Science* **327**, 1139-1142, (2010).

11 Hottiger, M. O., Hassa, P. O., Lüscher, B., Schüler, H. & Koch-Nolte, F. Toward a unified nomenclature for mammalian ADP-ribosyltransferases. *Trends Biochem Sci* **35**, 208-219, (2010).

12 Koch-Nolte, F., Kernstock, S., Mueller-Dieckmann, C., Weiss, M. & Haag, F. Mammalian ADP-ribosyltransferases and ADP-ribosylhydrolases. *Front Biosci* **13**, 6716-6729, (2008).

13 Rosenthal, F. *et al.* Macrodomain-containing proteins are new mono-ADP-ribosylhydrolases. *Nat Struct Mol Biol* **20**, 502-507, (2013).

14 Verheugd, P. *et al.* Regulation of NF-kappaB signalling by the mono-ADP-ribosyltransferase ARTD10. *Nat Commun* **4**, 1683, (2013).

15 Chambon, P., Weill, J. & Mandel, P. Nicotinamide mononucleotide activation of new DNA-dependent polyadenylic acid synthesizing nuclear enzyme. *Biochem Biophys Res Commun* **11**, 39-43, (1963).

16 D'Amours, D., Desnoyers, S., D'Silva, I. & Poirier, G. Poly(ADP-ribosyl)ation reactions in the regulation of nuclear functions. *Biochem J* **342**, 249-268, (1999).

17 Krishnakumar, R. & Kraus, W. The PARP side of the nucleus: Molecular actions, physiological outcomes, and clinical targets. *Mol Cell* **39**, 8-24, (2010).

18 Altmeyer, M., Messner, S., Hassa, P. O., Fey, M. & Hottiger, M. O. Molecular mechanism of poly(ADP-ribosyl)ation by PARP1 and identification of lysine residues as ADP-ribose acceptor sites. *Nucleic Acids Res* **37**, 3723-3738, (2009).

19 Messner, S. *et al.* PARP1 ADP-ribosylates lysine residues of the core histone tails. *Nucleic Acids Res* **38**, 6350-6362, (2010).

20 Tanaka, M., Miwa, M., Hayashi, K., Kubota, K. & Matsushima, T. Separation of oligo(adenosine diphosphate ribose) fractions with various chain lengths and terminal structures. *Biochemistry* **16**, 1485-1489, (1977).

21 Alvarez-Gonzalez, R. & Mendoza-Alvarez, H. Dissection of ADP-ribose polymer synthesis into individual steps of initiation, elongation, and branching. *Biochimie* **77**, 403-407, (1995).

22 Juarez-Salinas, H., Mendoza-Alvarez, H., Levi, V., Jacobson, M. K. & Jacobson, E. L. Simultaneous determination of linear and branched residues in poly(ADP-ribose). *Anal Biochem* **131**, 410-418, (1983).

23 Miwa, M. *et al.* The branching and linear portions of poly(adenosine diphosphate ribose) have the same alpha(1 leads to 2) ribose-ribose linkage. *J Biol Chem* **256**, 2916-2921, (1981).

24 Dani, N. *et al.* Combining affinity purification by ADP-ribose-binding macro domains with mass spectrometry to define the mammalian ADP-ribosyl proteome. *Proc Natl Acad Sci U S A* **106**, 4243-4248, (2009).

25 Jiang, H., Kim, J. H., Frizzell, K. M., Kraus, W. L. & Lin, H. Clickable NAD analogues for labeling substrate proteins of poly(ADP-ribose) polymerases. *J Am Chem Soc* **132**, 9363-9372, (2010).

26 Jungmichel, S. *et al.* Proteome-wide Identification of Poly(ADP-Ribosyl)ation Targets in Different Genotoxic Stress Responses. *Mol Cell* **52**, 272-285, (2013).

27 Kasid, U. N., Halligan, B., Liu, L. F., Dritschilo, A. & Smulson, M. Poly(ADP-ribose)-mediated post-translational modification of chromatin-associated human topoisomerase I. Inhibitory effects on catalytic activity. *J Biol Chem* **264**, 18687-18692, (1989).

28 Scovassi, A. I., Mariani, C., Negroni, M., Negri, C. & Bertazzoni, U. ADP-ribosylation of nonhistone proteins in HeLa cells: modification of DNA topoisomerase II. *Exp Cell Res* **206**, 177-181, (1993).

29 Smith, H. M. & Grosovsky, A. J. PolyADP-ribose-mediated regulation of p53 complexed with topoisomerase I following ionizing radiation. *Carcinogenesis* **20**, 1439-1443, (1999).

30 Simbulan-Rosenthal, C. M., Rosenthal, D. S., Iyer, S., Boulares, A. H. & Smulson, M. E. Transient poly(ADP-ribosyl)ation of nuclear proteins and role of poly(ADP-ribose) polymerase in the early stages of apoptosis. *J Biol Chem* **273**, 13703-13712, (1998).

31 Eki, T. Poly (ADP-ribose) polymerase inhibits DNA replication by human replicative DNA polymerase alpha, delta and epsilon in vitro. *FEBS Lett* **356**, 261-266, (1994).

32 Ord, M. G. & Stocken, L. A. Adenosine diphosphate ribosylated histones. *Biochem J* **161**, 583-592, (1977).

33 Alvarez-Gonzalez, R. & Jacobson, M. K. Characterization of polymers of adenosine diphosphate ribose generated in vitro and in vivo. *Biochemistry* **26**, 3218-3224, (1987).

34 Alvarez-Gonzalez, R. & Althaus, F. R. Poly(ADP-ribose) catabolism in mammalian cells exposed to DNA-damaging agents. *Mutat Res* **218**, 67-74, (1989).

35 Moss, J., Zolkiewska, A. & Okazaki, I. ADP-ribosylarginine hydrolases and ADP-ribosyltransferases. Partners in ADP-ribosylation cycles. *Adv Exp Med Biol* **419**, 25-33, (1997).

36 Oka, S., Kato, J. & Moss, J. Identification and characterization of a mammalian 39-kDa poly(ADP-ribose) glycohydrolase. *J Biol Chem* **281**, 705-713, (2006).

37 Brochu, G. *et al.* Mode of action of poly(ADP-ribose) glycohydrolase. *Biochim Biophys Acta* **1219**, 342-350, (1994).

38 Brochu, G., Shah, G. M. & Poirier, G. G. Purification of poly(ADP-ribose) glycohydrolase and detection of its isoforms by a zymogram following one- or two-dimensional electrophoresis. *Anal Biochem* **218**, 265-272, (1994).

39 Barkauskaite, E. *et al.* Visualization of poly(ADP-ribose) bound to PARG reveals inherent balance between exo- and endo-glycohydrolase activities. *Nat Commun* **4**, 2164, (2013).

40 Barkauskaite, E., Jankevicius, G., Ladurner, A. G., Ahel, I. & Timinszky, G. The recognition and removal of cellular poly(ADP-ribose) signals. *Febs J* **280**, 3491-3507, (2013).

41 Jankevicius, G. *et al.* A family of macrodomain proteins reverses cellular mono-ADP-ribosylation. *Nat Struct Mol Biol* **20**, 508-514, (2013).

42 Sallmann, F. R., Vodenicharov, M. D., Wang, Z. Q. & Poirier, G. G. Characterization of sPARP-1. An alternative product of PARP-1 gene with poly(ADP-ribose) polymerase activity independent of DNA strand breaks. *J Biol Chem* **275**, 15504-15511, (2000).

43 Shieh, W. *et al.* Poly(ADP-ribose) polymerase null mouse cells synthesize ADP-ribose polymers. *J Biol Chem* **273**, 30069-30072, (1998).

44 Amé, J. *et al.* PARP-2, a novel mammalian DNA damage-dependent poly(ADP-ribose) polymerase. *J Biol Chem* **274**, 17860-17868, (1999).

45 Johansson, M. A human poly(ADP-ribose) polymerase gene family (ADPRTL): cDNA cloning of two novel poly(ADP-ribose) polymerase homologues. *Genomics* **57**, 442-445, (1999).

46 Langelier, M.-F., Servent, K., Rogers, E. & Pascal, J. A third zinc-binding domain of human poly(ADP-ribose) polymerase-1 coordinates DNA-dependent enzyme activation. *J Biol Chem* **283**, 4105-4114, (2008).

47 Tao, Z., Gao, P., Hoffman, D. W. & Liu, H. W. Domain C of human poly(ADP-ribose) polymerase-1 is important for enzyme activity and contains a novel zinc-ribbon motif. *Biochemistry* **47**, 5804-5813, (2008).

48 Langelier, M.-F., Ruhl, D., Planck, J., Kraus, W. & Pascal, J. The Zn3 domain of human poly(ADP-ribose) polymerase-1 (PARP-1) functions in both DNA-dependent poly(ADP-ribose) synthesis activity and chromatin compaction. *J Biol Chem* **285**, 18877-18887, (2010).

49 Pion, E. *et al.* DNA-induced dimerization of poly(ADP-ribose) polymerase-1 triggers its activation. *Biochemistry* **44**, 14670-14681, (2005).

50 Mendoza-Alvarez, H. & Alvarez-Gonzalez, R. Poly(ADP-ribose) polymerase is a catalytic dimer and the automodification reaction is intermolecular. *J Biol Chem* **268**, 22575-22580, (1993).

51 Bauer, P. I., Buki, K. G. & Kun, E. Evidence for the participation of histidine residues located in the 56 kDa C-terminal polypeptide domain of ADP-ribosyl transferase in its catalytic activity. *FEBS Lett* **273**, 6-10, (1990).

52 Potaman, V. N., Shlyakhtenko, L. S., Oussatcheva, E. A., Lyubchenko, Y. L. & Soldatenkov, V. A. Specific binding of poly(ADP-ribose) polymerase-1 to cruciform hairpins. *J Mol Biol* **348**, 609-615, (2005).

53 Lonskaya, I. *et al.* Regulation of poly(ADP-ribose) polymerase-1 by DNA structure-specific binding. *J Biol Chem* **280**, 17076-17083, (2005).

54 Soldatenkov, V., Vetcher, A., Duka, T. & Ladame, S. First evidence of a functional interaction between DNA quadruplexes and poly(ADP-ribose) polymerase-1. *ACS Chem Biol* **3**, 214-219, (2008).

55 Shall, S. & de Murcia, G. Poly(ADP-ribose) polymerase-1: what have we learned from the deficient mouse model? *Mutat Res* **460**, 1-15, (2000).

56 Wang, Z. *et al.* Mice lacking ADPRT and poly(ADP-ribosyl)ation develop normally but are susceptible to skin disease. *Genes Dev* **9**, 509-520, (1995).

57 de Murcia, J. M. *et al.* Requirement of poly(ADP-ribose) polymerase in recovery from DNA damage in mice and in cells. *Proc Natl Acad Sci USA* **94**, 7303-7307, (1997).

58 Masutani, M. *et al.* Function of poly(ADP-ribose) polymerase in response to DNA damage: gene-disruption study in mice. *Mol Cell Biochem* **193**, 149-152, (1999).

59 Masutani, M. *et al.* Poly(ADP-ribose) polymerase gene disruption conferred mice resistant to streptozotocin-induced diabetes. *Proc Natl Acad Sci USA* **96**, 2301-2304, (1999).

60 Wang, Z. *et al.* PARP is important for genomic stability but dispensable in apoptosis. *Genes Dev* **11**, 2347-2358, (1997).

61 Shall, S. & Sugimura, T. What is new about ADP-ribosylation? *BioEssays : news and reviews in molecular, cellular and developmental biology* **28**, 97-99, (2006).

62 de Murcia, J. M. *et al.* Functional interaction between PARP-1 and PARP-2 in chromosome stability and embryonic development in mouse. *Embo J* **22**, 2255-2263, (2003).

63 Bouchard, V. J., Rouleau, M. & Poirier, G. G. PARP-1, a determinant of cell survival in response to DNA damage. *Exp Hematol* **31**, 446-454, (2003).

64 Woodhouse, B. C., Dianova, II, Parsons, J. L. & Dianov, G. L. Poly(ADP-ribose) polymerase-1 modulates DNA repair capacity and prevents formation of DNA double strand breaks. *DNA repair* **7**, 932-940, (2008).

65 Dantzer, F. *et al.* Involvement of poly(ADP-ribose) polymerase in base excision repair. *Biochimie* **81**, 69-75, (1999).

66 Malanga, M. & Althaus, F. R. Poly(ADP-ribose) molecules formed during DNA repair in vivo. *J Biol Chem* **269**, 17691-17696, (1994).

67 Malanga, M. & Althaus, F. R. The role of poly(ADP-ribose) in the DNA damage signaling network. *Biochem Cell Biol* **83**, 354-364, (2005).

68 Trucco, C., Oliver, F., de Murcia, G. & Ménissier-de Murcia, J. DNA repair defect in poly(ADP-ribose) polymerase-deficient cell lines. *Nucleic Acids Res* **26**, 2644-2649, (1998).

69 Haince, J. F. *et al.* PARP1-dependent kinetics of recruitment of MRE11 and NBS1 proteins to multiple DNA damage sites. *J Biol Chem* **283**, 1197-1208, (2008).

70 Mortusewicz, O., Ame, J. C., Schreiber, V. & Leonhardt, H. Feedback-regulated poly(ADP-ribosyl)ation by PARP-1 is required for rapid response to DNA damage in living cells. *Nucleic Acids Res* **35**, 7665-7675, (2007).

71 Caldecott, K. W., Aoufouchi, S., Johnson, P. & Shall, S. XRCC1 polypeptide interacts with DNA polymerase beta and possibly poly (ADP-ribose) polymerase, and DNA ligase III is a novel molecular 'nick-sensor' in vitro. *Nucleic Acids Res* **24**, 4387-4394, (1996).

72 Masson, M. *et al.* XRCC1 is specifically associated with poly(ADP-ribose) polymerase and negatively regulates its activity following DNA damage. *Mol Cell Biol* **18**, 3563-3571, (1998).

73 Dantzer, F. *et al.* Base excision repair is impaired in mammalian cells lacking Poly(ADP-ribose) polymerase-1. *Biochemistry* **39**, 7559-7569, (2000).

74 Frouin, I. *et al.* Human proliferating cell nuclear antigen, poly(ADP-ribose) polymerase-1, and p21waf1/cip1. A dynamic exchange of partners. *J Biol Chem* **278**, 39265-39268, (2003).

75 de Murcia, G. *et al.* Modulation of chromatin superstructure induced by poly(ADP-ribose) synthesis and degradation. *J Biol Chem* **261**, 7011-7017, (1986).

76 Kim, M., Mauro, S., Gévry, N., Lis, J. & Kraus, W. NAD+-dependent modulation of chromatin structure and transcription by nucleosome binding properties of PARP-1. *Cell* **119**, 803-814, (2004).

77 Realini, C. A. & Althaus, F. R. Histone shuttling by poly(ADP-ribosylation). *J Biol Chem* **267**, 18858-18865, (1992).

78 Rouleau, M., Aubin, R. A. & Poirier, G. G. Poly(ADP-ribosyl)ated chromatin domains: access granted. *J Cell Sci* **117**, 815-825, (2004).

79 Boulikas, T. DNA strand breaks alter histone ADP-ribosylation. *Proc Natl Acad Sci USA* **86**, 3499-3503, (1989).

80 Stone, P., Lorimer, W. & Kidwell, W. Properties of the complex between histone H1 and poly(ADP-ribose synthesised in HeLa cell nuclei. *Eur J Biochem* **81**, 9-18, (1977).

81 Huletsky, A. *et al.* The effect of poly(ADP-ribosyl)ation on native and H1-depleted chromatin. A role of poly(ADP-ribosyl)ation on core nucleosome structure. *J Biol Chem* **264**, 8878-8886, (1989).

82 Ju, B. G. *et al.* A topoisomerase IIbeta-mediated dsDNA break required for regulated transcription. *Science* **312**, 1798-1802, (2006).

83 Klenova, E. & Ohlsson, R. Poly(ADP-ribosyl)ation and epigenetics. Is CTCF PARt of the plot? *Cell Cycle* **4**, 96-101, (2005).

84 Yu, W. *et al.* Poly(ADP-ribosyl)ation regulates CTCF-dependent chromatin insulation. *Nat Genet* **36**, 1105-1110, (2004).

85 Krishnakumar, R. *et al.* Reciprocal binding of PARP-1 and histone H1 at promoters specifies transcriptional outcomes. *Science* **319**, 819-821, (2008).

86 Hassa, P. O., Buerki, C., Lombardi, C., Imhof, R. & Hottiger, M. O. Transcriptional coactivation of nuclear factor-κB-dependent gene expression by p300 is regulated by poly(ADP)-ribose polymerase-1. *J Biol Chem* **278**, 45145-45153, (2003).

87 Hassa, P. O. *et al.* Acetylation of poly(ADP-ribose) polymerase-1 by p300/CREB-binding protein regulates coactivation of NF-κB-dependent transcription. *J Biol Chem* **280**, 40450-40464, (2005).

88 Hassa, P. O., Covic, M., Hasan, S., Imhof, R. & Hottiger, M. O. The enzymatic and DNA binding activity of PARP-1 are not required for NF-κB coactivator function. *J Biol Chem* **276**, 45588-45597, (2001).

89 Hassa, P. O. & Hottiger, M. O. in *Poly(ADP-Ribosyl)ation* (ed A. Burkle) Ch. 8, (Landes Bioscience, 2004).

90 Hassa, P. O. & Hottiger, M. O. A role of poly (ADP-ribose) polymerase in NF-κB transcriptional activation. *Biol Chem* **380**, 953-959, (1999).

91 Lönn, P. *et al.* PARP-1 attenuates Smad-mediated transcription. *Mol Cell* **40**, 521-532, (2010).

92 Ju, B.-G. *et al.* Activating the PARP-1 sensor component of the groucho/ TLE1 corepressor complex mediates a CaMKinase IIdelta-dependent neurogenic gene activation pathway. *Cell* **119**, 815-829, (2004).

93 Pavri, R. *et al.* PARP-1 determines specificity in a retinoid signaling pathway via direct modulation of mediator. *Mol Cell* **18**, 83-96, (2005).

94 Ju, B. G. & Rosenfeld, M. G. A breaking strategy for topoisomerase IIbeta/PARP-1-dependent regulated transcription. *Cell Cycle* **5**, 2557-2560, (2006).

95 Szyf, M. DNA methylation patterns: an additional level of information? *Biochem Cell Biol* **69**, 764-767, (1991).

96 Chuang, L. S. *et al.* Human DNA-(cytosine-5) methyltransferase-PCNA complex as a target for p21WAF1. *Science* **277**, 1996-2000, (1997).

97 Caiafa, P. & Zampieri, M. DNA methylation and chromatin structure: the puzzling CpG islands. *J Cell Biochem* **94**, 257-265, (2005).

98 Zampieri, M. *et al.* ADP-ribose polymers localized on Ctcf-Parp1-Dnmt1 complex prevent methylation of Ctcf target sites. *Biochem J*, (2011).

99 Caiafa, P. & Zampieri, M. DNA methylation and chromatin structure: the puzzling CpG islands. *J Cell Biochem* **94**, 257-265, (2005).

100 Caiafa, P. & Zlatanova, J. CCCTC-binding factor meets poly(ADP-ribose) polymerase-1. *J Cell Physiol* **219**, 265-270, (2009).

101 Zlatanova, J. & Caiafa, P. CCCTC-binding factor: to loop or to bridge. *Cell Mol Life Sci* **66**, 1647-1660, (2009).

102 Caiafa, P., Guastafierro, T. & Zampieri, M. Epigenetics: poly(ADP-ribosyl)ation of PARP-1 regulates genomic methylation patterns. *Faseb J* **23**, 672-678, (2009).

103 Reale, A., Matteis, G. D., Galleazzi, G., Zampieri, M. & Caiafa, P. Modulation of DNMT1 activity by ADP-ribose polymers. *Oncogene* **24**, 13-19, (2005).

104 Zampieri, M. *et al.* ADP-ribose polymers localized on Ctcf-Parp1-Dnmt1 complex prevent methylation of Ctcf target sites. *Biochem J* **441**, 645-652, (2012).

105 Urbanek, P., Paces, J., Kralova, J., Dvorak, M. & Paces, V. Cloning and expression of PARP-3 (Adprt3) and U3-55k, two genes closely linked on mouse chromosome 9. *Folia biologica* **48**, 182-191, (2002).

106 Augustin, A. *et al.* PARP-3 localizes preferentially to the daughter centriole and interferes with the G1/S cell cycle progression. *J Cell Sci* **116**, 1551-1562, (2003).

107 Rulten, S. L. *et al.* PARP-3 and APLF function together to accelerate nonhomologous end-joining. *Mol Cell* **41**, 33-45, (2011).

108 Loseva, O. *et al.* PARP-3 is a mono-ADP-ribosylase that activates PARP-1 in the absence of DNA. *J Biol Chem* **285**, 8054-8060, (2010).

109 Rouleau, M., El-Alfy, M., Levesque, M. H. & Poirier, G. G. Assessment of PARP-3 distribution in tissues of cynomolgous monkeys. *The journal of histochemistry and cytochemistry : official journal of the Histochemistry Society* **57**, 675-685, (2009).

110 Schreiber, V. *et al.* Poly(ADP-ribose) polymerase-2 (PARP-2) is required for efficient base excision DNA repair in association with PARP-1 and XRCC1. *J Biol Chem* **277**, 23028-23036, (2002).

111 Rouleau, M. *et al.* A key role for poly(ADP-ribose) polymerase 3 in ectodermal specification and neural crest development. *PLoS One* **6**, e15834, (2011).

112 Rouleau, M. *et al.* PARP-3 associates with polycomb group bodies and with components of the DNA damage repair machinery. *J Cell Biochem* **100**, 385-401, (2007).

113 Vyas, S., Chesarone-Cataldo, M., Todorova, T., Huang, Y. H. & Chang, P. A systematic analysis of the PARP protein family identifies new functions critical for cell physiology. *Nat Commun* **4**, 2240, (2013).

114 Boehler, C. *et al.* Poly(ADP-ribose) polymerase 3 (PARP3), a newcomer in cellular response to DNA damage and mitotic progression. *Proc Natl Acad Sci USA* **108**, 2783-2788, (2011).

115 Fenton, A. L., Shirodkar, P., Macrae, C. J., Meng, L. & Koch, C. A. The PARP3- and ATM-dependent phosphorylation of APLF facilitates DNA double-strand break repair. *Nucleic Acids Res* **41**, 4080-4092, (2013).

116 Hatakeyama, K., Nemoto, Y., Ueda, K. & Hayaishi, O. Purification and characterization of poly(ADP-ribose) glycohydrolase. Different modes of action on large and small poly(ADP-ribose). *J Biol Chem* **261**, 14902-14911, (1986).

117 Tanuma, S., Kawashima, K. & Endo, H. Purification and properties of an (ADP-ribose)n glycohydrolase from guinea pig liver nuclei. *J Biol Chem* **261**, 965-969, (1986).

118 Thomassin, H. *et al.* An affinity matrix for the purification of poly(ADP-ribose) glycohydrolase. *Nucleic Acids Res* **18**, 4691-4694, (1990).

119 Uchida, K. *et al.* Preferential degradation of protein-bound (ADP-ribose)n by nuclear poly(ADP-ribose) glycohydrolase from human placenta. *J Biol Chem* **268**, 3194-3200, (1993).

120 Bonicalzi, M. E., Vodenicharov, M., Coulombe, M., Gagne, J. P. & Poirier, G. G. Alteration of poly(ADP-ribose) glycohydrolase nucleocytoplasmic shuttling characteristics upon cleavage by apoptotic proteases. *Biol Cell* **95**, 635-644, (2003).

121 Lin, W., Ame, J. C., Aboul-Ela, N., Jacobson, E. L. & Jacobson, M. K. Isolation and characterization of the cDNA encoding bovine poly(ADP-ribose) glycohydrolase. *J Biol Chem* **272**, 11895-11901, (1997).

122 Meyer, R. G., Meyer-Ficca, M. L., Jacobson, E. L. & Jacobson, M. K. Human poly(ADP-ribose) glycohydrolase (PARG) gene and the common promoter sequence it shares with inner mitochondrial membrane translocase 23 (TIM23). *Gene* **314**, 181-190, (2003).

123 Shimokawa, T. *et al.* Isolation and cloning of rat poly(ADP-ribose) glycohydrolase: presence of a potential nuclear export signal conserved in mammalian orthologs. *Journal of biochemistry* **126**, 748-755, (1999).

124 Concha, II, Figueroa, J., Concha, M. I., Ueda, K. & Burzio, L. O. Intracellular distribution of poly(ADP-ribose) synthetase in rat spermatogenic cells. *Exp Cell Res* **180**, 353-366, (1989).

125 Meyer-Ficca, M. L., Meyer, R. G., Coyle, D. L., Jacobson, E. L. & Jacobson, M. K. Human poly(ADP-ribose) glycohydrolase is expressed in alternative splice variants yielding isoforms that localize to different cell compartments. *Exp Cell Res* **297**, 521-532, (2004).

126 Cortes, U. *et al.* Depletion of the 110-kilodalton isoform of poly(ADP-ribose) glycohydrolase increases sensitivity to genotoxic and endotoxic stress in mice. *Mol Cell Biol* **24**, 7163-7178, (2004).

127 Koh, D. *et al.* Failure to degrade poly(ADP-ribose) causes increased sensitivity to cytotoxicity and early embryonic lethality. *Proc Natl Acad Sci USA* **101**, 17699-17704, (2004).

128 Slade, D. *et al.* The structure and catalytic mechanism of a poly(ADP-ribose) glycohydrolase. *Nature* **477**, 616-620, (2011).

129 Dunstan, M. S. *et al.* Structure and mechanism of a canonical poly(ADP-ribose) glycohydrolase. *Nat Commun* **3**, 878, (2012).

130 Bonicalzi, M. E., Haince, J. F., Droit, A. & Poirier, G. G. Regulation of poly(ADP-ribose) metabolism by poly(ADP-ribose) glycohydrolase: where and when? *Cell Mol Life Sci* **62**, 739-750, (2005).

131 Cuzzocrea, S. & Wang, Z. Q. Role of poly(ADP-ribose) glycohydrolase (PARG) in shock, ischemia and reperfusion. *Pharmacol Res* **52**, 100-108, (2005).

132 Oka, J., Ueda, K., Hayaishi, O., Komura, H. & Nakanishi, K. ADP-ribosyl protein lyase. Purification, properties, and identification of the product. *J Biol Chem* **259**, 986-995, (1984).

133 Perkins, E. *et al.* Novel inhibitors of poly(ADP-ribose) polymerase/PARP1 and PARP2 identified using a cell-based screen in yeast. *Cancer Res* **61**, 4175-4183, (2001).

134 Shaw, H. B. A Contribution to the Study of the Morphology of Adipose Tissue. *Journal of anatomy and physiology* **36**, 1-13, (1901).

135 Church, C., Horowitz, M. & Rodeheffer, M. WAT is a functional adipocyte? *Adipocyte* **1**, 38-45, (2012).

136 Krause, B. R. & Hartman, A. D. Adipose tissue and cholesterol metabolism. *J Lipid Res* **25**, 97-110, (1984).

137 Sethi, J. K. & Vidal-Puig, A. J. Thematic review series: adipocyte biology. Adipose tissue function and plasticity orchestrate nutritional adaptation. *J Lipid Res* **48**, 1253-1262, (2007).

138 Cook, K. S. *et al.* Adipsin: a circulating serine protease homolog secreted by adipose tissue and sciatic nerve. *Science* **237**, 402-405, (1987).

139 Campfield, L. A., Smith, F. J., Guisez, Y., Devos, R. & Burn, P. Recombinant mouse OB protein: evidence for a peripheral signal linking adiposity and central neural networks. *Science* **269**, 546-549, (1995).

140 Halaas, J. L. *et al.* Weight-reducing effects of the plasma protein encoded by the obese gene. *Science* **269**, 543-546, (1995).

141 Pelleymounter, M. A. *et al.* Effects of the obese gene product on body weight regulation in ob/ob mice. *Science* **269**, 540-543, (1995).

142 Schwartz, M. W. *et al.* Specificity of leptin action on elevated blood glucose levels and hypothalamic neuropeptide Y gene expression in ob/ob mice. *Diabetes* **45**, 531-535, (1996).

143 Stephens, T. W. *et al.* The role of neuropeptide Y in the antiobesity action of the obese gene product. *Nature* **377**, 530-532, (1995).

144 Weigle, D. S. *et al.* Recombinant ob protein reduces feeding and body weight in the ob/ob mouse. *J Clin Invest* **96**, 2065-2070, (1995).

145 Zhang, Y. *et al.* Positional cloning of the mouse obese gene and its human homologue. *Nature* **372**, 425-432, (1994).

146 Calle, E. E. & Kaaks, R. Overweight, obesity and cancer: epidemiological evidence and proposed mechanisms. *Nat Rev Cancer* **4**, 579-591, (2004).

147 Calle, E. E. & Thun, M. J. Obesity and cancer. *Oncogene* **23**, 6365-6378, (2004).

148 Schenk, S., Saberi, M. & Olefsky, J. M. Insulin sensitivity: modulation by nutrients and inflammation. *J Clin Invest* **118**, 2992-3002, (2008).

149 Van Gaal, L. F., Mertens, I. L. & De Block, C. E. Mechanisms linking obesity with cardiovascular disease. *Nature* **444**, 875-880, (2006).

150 Cannon, B. & Nedergaard, J. Brown adipose tissue: function and physiological significance. *Physiological reviews* **84**, 277-359, (2004).

151 Cinti, S. The adipose organ. *Prostaglandins, leukotrienes, and essential fatty acids* **73**, 9-15, (2005).

152 Himms-Hagen, J. Nonshivering thermogenesis. *Brain Res Bull* **12**, 151-160, (1984).

153 Nicholls, D. G. & Locke, R. M. Thermogenic mechanisms in brown fat. *Physiological reviews* **64**, 1-64, (1984).

154 Lin, C. S. & Klingenberg, M. Isolation of the uncoupling protein from brown adipose tissue mitochondria. *FEBS Lett* **113**, 299-303, (1980).

155 Dawkins, M. J. & Scopes, J. W. Non-shivering thermogenesis and brown adipose tissue in the human new-born infant. *Nature* **206**, 201-202, (1965).

156 Frontini, A. & Cinti, S. Distribution and development of brown adipocytes in the murine and human adipose organ. *Cell Metab* **11**, 253-256, (2010).

157 Lean, M. E., James, W. P., Jennings, G. & Trayhurn, P. Brown adipose tissue uncoupling protein content in human infants, children and adults. *Clinical science* **71**, 291-297, (1986).

158 Celi, F. S. Brown adipose tissue--when it pays to be inefficient. *The New England journal of medicine* **360**, 1553-1556, (2009).

159 English, J. T., Patel, S. K. & Flanagan, M. J. Association of pheochromocytomas with brown fat tumors. *Radiology* **107**, 279-281, (1973).

160 Huttunen, P., Hirvonen, J. & Kinnula, V. The occurrence of brown adipose tissue in outdoor workers. *European journal of applied physiology and occupational physiology* **46**, 339-345, (1981).

161 Hany, T. F. *et al.* Brown adipose tissue: a factor to consider in symmetrical tracer uptake in the neck and upper chest region. *European journal of nuclear medicine and molecular imaging* **29**, 1393-1398, (2002).

162 Saito, M. *et al.* High incidence of metabolically active brown adipose tissue in healthy adult humans: effects of cold exposure and adiposity. *Diabetes* **58**, 1526-1531, (2009).

163 van Marken Lichtenbelt, W. D. *et al.* Cold-activated brown adipose tissue in healthy men. *The New England journal of medicine* **360**, 1500-1508, (2009).

164 Virtanen, K. A. *et al.* Functional brown adipose tissue in healthy adults. *The New England journal of medicine* **360**, 1518-1525, (2009).

165 Zingaretti, M. C. *et al.* The presence of UCP1 demonstrates that metabolically active adipose tissue in the neck of adult humans truly represents brown adipose tissue. *Faseb J* **23**, 3113-3120, (2009).

166 Cousin, B. *et al.* Occurrence of brown adipocytes in rat white adipose tissue: molecular and morphological characterization. *J Cell Sci* **103 (Pt 4)**, 931-942, (1992).

167 Giralt, M. & Villarroya, F. White, brown, beige/brite: different adipose cells for different functions? *Endocrinology* **154**, 2992-3000, (2013).

168 Petrovic, N. *et al.* Chronic peroxisome proliferator-activated receptor gamma (PPARgamma) activation of epididymally derived white adipocyte cultures reveals a population of thermogenically competent, UCP1-containing adipocytes molecularly distinct from classic brown adipocytes. *J Biol Chem* **285**, 7153-7164, (2010).

169 Seale, P. *et al.* PRDM16 controls a brown fat/skeletal muscle switch. *Nature* **454**, 961-967, (2008).

170 Timmons, J. A. *et al.* Myogenic gene expression signature establishes that brown and white adipocytes originate from distinct cell lineages. *Proc Natl Acad Sci U S A* **104**, 4401-4406, (2007).

171 Ishibashi, J. & Seale, P. Medicine. Beige can be slimming. *Science* **328**, 1113-1114, (2010).

172 Wu, J. *et al.* Beige adipocytes are a distinct type of thermogenic fat cell in mouse and human. *Cell* **150**, 366-376, (2012).

173 Rosenwald, M., Perdikari, A., Rulicke, T. & Wolfrum, C. Bi-directional interconversion of brite and white adipocytes. *Nat Cell Biol* **15**, 659-667, (2013).

174 Trayhurn, P. Endocrine and signalling role of adipose tissue: new perspectives on fat. *Acta physiologica Scandinavica* **184**, 285-293, (2005).

175 Hotamisligil, G. S., Shargill, N. S. & Spiegelman, B. M. Adipose expression of tumor necrosis factor-alpha: direct role in obesity-linked insulin resistance. *Science* **259**, 87-91, (1993).

176 Lau, D. C., Dhillon, B., Yan, H., Szmitko, P. E. & Verma, S. Adipokines: molecular links between obesity and atheroslcerosis. *American journal of physiology. Heart and circulatory physiology* **288**, H2031-2041, (2005).

177 Tran, T. T. & Kahn, C. R. Transplantation of adipose tissue and stem cells: role in metabolism and disease. *Nature reviews. Endocrinology* **6**, 195-213, (2010).

178 Wajchenberg, B. L. Subcutaneous and visceral adipose tissue: their relation to the metabolic syndrome. *Endocr Rev* **21**, 697-738, (2000).

179 Despres, J. P. & Lemieux, I. Abdominal obesity and metabolic syndrome. *Nature* **444**, 881-887, (2006).

180 Despres, J. P. Intra-abdominal obesity: an untreated risk factor for Type 2 diabetes and cardiovascular disease. *J Endocrinol Invest* **29**, 77-82, (2006).

181 Bjorntorp, P. Metabolic implications of body fat distribution. *Diabetes Care* **14**, 1132-1143, (1991).

182 Fain, J. N., Madan, A. K., Hiler, M. L., Cheema, P. & Bahouth, S. W. Comparison of the release of adipokines by adipose tissue, adipose tissue matrix, and adipocytes from visceral and subcutaneous abdominal adipose tissues of obese humans. *Endocrinology* **145**, 2273-2282, (2004).

183 Bruun, J. M. *et al.* Higher production of IL-8 in visceral vs. subcutaneous adipose tissue. Implication of nonadipose cells in adipose tissue. *Am J Physiol Endocrinol Metab* **286**, E8-13, (2004).

184 Zeve, D., Tang, W. & Graff, J. Fighting fat with fat: the expanding field of adipose stem cells. *Cell stem cell* **5**, 472-481, (2009).

185 Bjorntorp, P. Effects of age, sex, and clinical conditions on adipose tissue cellularity in man. *Metabolism: clinical and experimental* **23**, 1091-1102, (1974).

186 Bjorntorp, P. Size, number and function of adipose tissue cells in human obesity. *Hormone and metabolic research = Hormon- und Stoffwechselforschung = Hormones et metabolisme* **Suppl 4**, 77-83, (1974).

187 Hirsch, J. & Batchelor, B. Adipose tissue cellularity in human obesity. *Clinics in endocrinology and metabolism* **5**, 299-311, (1976).

188 Spalding, K. L. *et al.* Dynamics of fat cell turnover in humans. *Nature* **453**, 783-787, (2008).

189 Rodeheffer, M. S., Birsoy, K. & Friedman, J. M. Identification of white adipocyte progenitor cells in vivo. *Cell* **135**, 240-249, (2008).

190 Tang, W. *et al.* White fat progenitor cells reside in the adipose vasculature. *Science* **322**, 583-586, (2008).

191 Farmer, S. R. Transcriptional control of adipocyte formation. *Cell Metab* **4**, 263-273, (2006).

192 Rosen, E. D. & Spiegelman, B. M. Molecular regulation of adipogenesis. *Annual review of cell and developmental biology* **16**, 145-171, (2000).

193 Gesta, S., Tseng, Y. H. & Kahn, C. R. Developmental origin of fat: tracking obesity to its source. *Cell* **131**, 242-256, (2007).

194 Todaro, G. J., Wolman, S. R. & Green, H. Rapid Transformation of Human Fibroblasts with Low Growth Potential into Established Cell Lines by Sv40. *Journal of cellular physiology* **62**, 257-265, (1963).

195 Green, H. & Kehinde, O. An established preadipose cell line and its differentiation in culture. II. Factors affecting the adipose conversion. *Cell* **5**, 19-27, (1975).

196 Green, H. & Meuth, M. An established pre-adipose cell line and its differentiation in culture. *Cell* **3**, 127-133, (1974).

197 Mikkelsen, T. S. *et al.* Comparative epigenomic analysis of murine and human adipogenesis. *Cell* **143**, 156-169, (2010).

198 Steger, D. J. *et al.* Propagation of adipogenic signals through an epigenomic transition state. *Genes Dev* **24**, 1035-1044, (2010).

199 Siersbaek, R. *et al.* Extensive chromatin remodelling and establishment of transcription factor 'hotspots' during early adipogenesis. *Embo J* **30**, 1459-1472, (2011).

200 Lefterova, M. I. & Lazar, M. A. New developments in adipogenesis. *Trends Endocrinol Metab* **20**, 107-114, (2009).

201 Siersbaek, R., Nielsen, R. & Mandrup, S. PPARgamma in adipocyte differentiation and metabolism--novel insights from genome-wide studies. *FEBS Lett* **584**, 3242-3249, (2010).

202 Tontonoz, P. & Spiegelman, B. M. Fat and beyond: the diverse biology of PPARgamma. *Annu Rev Biochem* **77**, 289-312, (2008).

203 Yeh, W. C., Cao, Z., Classon, M. & McKnight, S. L. Cascade regulation of terminal adipocyte differentiation by three members of the C/EBP family of leucine zipper proteins. *Genes Dev* **9**, 168-181, (1995).

204 Salma, N., Xiao, H. & Imbalzano, A. N. Temporal recruitment of CCAAT/enhancer-binding proteins to early and late adipogenic promoters in vivo. *Journal of molecular endocrinology* **36**, 139-151, (2006).

205 Cao, Z., Umek, R. M. & McKnight, S. L. Regulated expression of three C/EBP isoforms during adipose conversion of 3T3-L1 cells. *Genes Dev* **5**, 1538-1552, (1991).

206 Wu, Z., Bucher, N. L. & Farmer, S. R. Induction of peroxisome proliferator-activated receptor gamma during the conversion of 3T3 fibroblasts into adipocytes is mediated by C/EBPbeta, C/EBPdelta, and glucocorticoids. *Mol Cell Biol* **16**, 4128-4136, (1996).

207 Wu, Z., Xie, Y., Bucher, N. L. & Farmer, S. R. Conditional ectopic expression of C/EBP beta in NIH-3T3 cells induces PPAR gamma and stimulates adipogenesis. *Genes Dev* **9**, 2350-2363, (1995).

208 Tanaka, T., Yoshida, N., Kishimoto, T. & Akira, S. Defective adipocyte differentiation in mice lacking the C/EBPbeta and/or C/EBPdelta gene. *Embo J* **16**, 7432-7443, (1997).

209 Freytag, S. O., Paielli, D. L. & Gilbert, J. D. Ectopic expression of the CCAAT/enhancer-binding protein alpha promotes the adipogenic program in a variety of mouse fibroblastic cells. *Genes Dev* **8**, 1654-1663, (1994).

210 Linhart, H. G. *et al.* C/EBPalpha is required for differentiation of white, but not brown, adipose tissue. *Proc Natl Acad Sci U S A* **98**, 12532-12537, (2001).

211 Rosen, E. D. *et al.* C/EBPalpha induces adipogenesis through PPARgamma: a unified pathway. *Genes Dev* **16**, 22-26, (2002).

212 Zuo, Y., Qiang, L. & Farmer, S. R. Activation of CCAAT/enhancer-binding protein (C/EBP) alpha expression by C/EBP beta during adipogenesis requires a peroxisome proliferator-activated receptor-gamma-associated repression of HDAC1 at the C/ebp alpha gene promoter. *J Biol Chem* **281**, 7960-7967, (2006).

213 Wu, Z. *et al.* Cross-regulation of C/EBP alpha and PPAR gamma controls the transcriptional pathway of adipogenesis and insulin sensitivity. *Mol Cell* **3**, 151-158, (1999).

214 Rosen, E. D. & Spiegelman, B. M. Adipocytes as regulators of energy balance and glucose homeostasis. *Nature* **444**, 847-853, (2006).

215 Tontonoz, P. *et al.* Adipocyte-specific transcription factor ARF6 is a heterodimeric complex of two nuclear hormone receptors, PPAR gamma and RXR alpha. *Nucleic Acids Res* **22**, 5628-5634, (1994).

216 Tontonoz, P., Hu, E., Graves, R. A., Budavari, A. I. & Spiegelman, B. M. mPPAR gamma 2: tissue-specific regulator of an adipocyte enhancer. *Genes Dev* **8**, 1224-1234, (1994).

217 Tontonoz, P., Hu, E. & Spiegelman, B. M. Stimulation of adipogenesis in fibroblasts by PPAR gamma 2, a lipid-activated transcription factor. *Cell* **79**, 1147-1156, (1994).

218 Adams, M., Reginato, M. J., Shao, D., Lazar, M. A. & Chatterjee, V. K. Transcriptional activation by peroxisome proliferator-activated receptor gamma is inhibited by phosphorylation at a consensus mitogen-activated protein kinase site. *J Biol Chem* **272**, 5128-5132, (1997).

219 Hu, E., Kim, J. B., Sarraf, P. & Spiegelman, B. M. Inhibition of adipogenesis through MAP kinase-mediated phosphorylation of PPARgamma. *Science* **274**, 2100-2103, (1996).

220 Gelman, L. *et al.* p300 interacts with the N- and C-terminal part of PPARgamma2 in a ligand-independent and -dependent manner, respectively. *J Biol Chem* **274**, 7681-7688, (1999).

221 Grontved, L., Madsen, M. S., Boergesen, M., Roeder, R. G. & Mandrup, S. MED14 tethers mediator to the N-terminal domain of peroxisome proliferator-activated receptor gamma and is required for full transcriptional activity and adipogenesis. *Mol Cell Biol* **30**, 2155-2169, (2010).

222 van Beekum, O. *et al.* The adipogenic acetyltransferase Tip60 targets activation function 1 of peroxisome proliferator-activated receptor gamma. *Endocrinology* **149**, 1840-1849, (2008).

223 Bugge, A., Grontved, L., Aagaard, M. M., Borup, R. & Mandrup, S. The PPARgamma2 A/B-domain plays a gene-specific role in transactivation and cofactor recruitment. *Mol Endocrinol* **23**, 794-808, (2009).

224 Tontonoz, P., Hu, E., Devine, J., Beale, E. G. & Spiegelman, B. M. PPAR gamma 2 regulates adipose expression of the phosphoenolpyruvate carboxykinase gene. *Mol Cell Biol* **15**, 351-357, (1995).

225 Lehmann, J. M. *et al.* An antidiabetic thiazolidinedione is a high affinity ligand for peroxisome proliferator-activated receptor gamma (PPAR gamma). *J Biol Chem* **270**, 12953-12956, (1995).

226 Tzameli, I. *et al.* Regulated production of a peroxisome proliferator-activated receptor-gamma ligand during an early phase of adipocyte differentiation in 3T3-L1 adipocytes. *J Biol Chem* **279**, 36093-36102, (2004).

227 Forman, B. M., Chen, J. & Evans, R. M. Hypolipidemic drugs, polyunsaturated fatty acids, and eicosanoids are ligands for peroxisome proliferator-activated receptors alpha and delta. *Proc Natl Acad Sci U S A* **94**, 4312-4317, (1997).

228 Keller, H. *et al.* Fatty acids and retinoids control lipid metabolism through activation of peroxisome proliferator-activated receptor-retinoid X receptor heterodimers. *Proc Natl Acad Sci U S A* **90**, 2160-2164, (1993).

229 Kliewer, S. A. *et al.* Fatty acids and eicosanoids regulate gene expression through direct interactions with peroxisome proliferator-activated receptors alpha and gamma. *Proc Natl Acad Sci U S A* **94**, 4318-4323, (1997).

230 Krey, G. *et al.* Fatty acids, eicosanoids, and hypolipidemic agents identified as ligands of peroxisome proliferator-activated receptors by coactivator-dependent receptor ligand assay. *Mol Endocrinol* **11**, 779-791, (1997).

231 Houseknecht, K. L., Cole, B. M. & Steele, P. J. Peroxisome proliferator-activated receptor gamma (PPARgamma) and its ligands: a review. *Domestic animal endocrinology* **22**, 1-23, (2002).

232 Forman, B. M. *et al.* 15-Deoxy-delta 12, 14-prostaglandin J2 is a ligand for the adipocyte determination factor PPAR gamma. *Cell* **83**, 803-812, (1995).

233 Kliewer, S. A. *et al.* A prostaglandin J2 metabolite binds peroxisome proliferator-activated receptor gamma and promotes adipocyte differentiation. *Cell* **83**, 813-819, (1995).

234 Schopfer, F. J. *et al.* Nitrolinoleic acid: an endogenous peroxisome proliferator-activated receptor gamma ligand. *Proc Natl Acad Sci U S A* **102**, 2340-2345, (2005).

235 Zhang, C. *et al.* Lysophosphatidic acid induces neointima formation through PPARgamma activation. *J Exp Med* **199**, 763-774, (2004).

236 Nagy, L., Tontonoz, P., Alvarez, J. G., Chen, H. & Evans, R. M. Oxidized LDL regulates macrophage gene expression through ligand activation of PPARgamma. *Cell* **93**, 229-240, (1998).

237 Coleman, P. S., Ewell, A. J. & Good, R. A. Retention of susceptibility to mitogens after direct dansylation of viable human lymphocytes. *Proc Natl Acad Sci U S A* **75**, 3766-3770, (1978).

238 Student, A. K., Hsu, R. Y. & Lane, M. D. Induction of fatty acid synthetase synthesis in differentiating 3T3-L1 preadipocytes. *J Biol Chem* **255**, 4745-4750, (1980).

239 Mackall, J. C., Student, A. K., Polakis, S. E. & Lane, M. D. Induction of lipogenesis during differentiation in a "preadipocyte" cell line. *J Biol Chem* **251**, 6462-6464, (1976).

240 Ducharme, N. A. & Bickel, P. E. Lipid droplets in lipogenesis and lipolysis. *Endocrinology* **149**, 942-949, (2008).

241 Haemmerle, G. *et al.* ATGL-mediated fat catabolism regulates cardiac mitochondrial function via PPAR-alpha and PGC-1. *Nat Med* **17**, 1076-1085, (2011).

242 Zechner, R., Kienesberger, P. C., Haemmerle, G., Zimmermann, R. & Lass, A. Adipose triglyceride lipase and the lipolytic catabolism of cellular fat stores. *J Lipid Res* **50**, 3-21, (2009).

243 Zimmermann, R. *et al.* Decreased fatty acid esterification compensates for the reduced lipolytic activity in hormone-sensitive lipase-deficient white adipose tissue. *J Lipid Res* **44**, 2089-2099, (2003).

244 Barak, Y. *et al.* PPAR gamma is required for placental, cardiac, and adipose tissue development. *Mol Cell* **4**, 585-595, (1999).

245 Rosen, E. D. *et al.* PPAR gamma is required for the differentiation of adipose tissue in vivo and in vitro. *Mol Cell* **4**, 611-617, (1999).

246 Kubota, N. *et al.* PPAR gamma mediates high-fat diet-induced adipocyte hypertrophy and insulin resistance. *Mol Cell* **4**, 597-609, (1999).

247 Miles, P. D., Barak, Y., He, W., Evans, R. M. & Olefsky, J. M. Improved insulin-sensitivity in mice heterozygous for PPAR-gamma deficiency. *J Clin Invest* **105**, 287-292, (2000).

248 Koutnikova, H. *et al.* Compensation by the muscle limits the metabolic consequences of lipodystrophy in PPAR gamma hypomorphic mice. *Proc Natl Acad Sci U S A* **100**, 14457-14462, (2003).

249 He, W. *et al.* Adipose-specific peroxisome proliferator-activated receptor gamma knockout causes insulin resistance in fat and liver but not in muscle. *Proc Natl Acad Sci U S A* **100**, 15712-15717, (2003).

250 Imai, T. *et al.* Peroxisome proliferator-activated receptor gamma is required in mature white and brown adipocytes for their survival in the mouse. *Proc Natl Acad Sci U S A* **101**, 4543-4547, (2004).

251 Jones, J. R. *et al.* Deletion of PPARgamma in adipose tissues of mice protects against high fat diet-induced obesity and insulin resistance. *Proc Natl Acad Sci U S A* **102**, 6207-6212, (2005).

252 Rieusset, J. *et al.* A new selective peroxisome proliferator-activated receptor gamma antagonist with antiobesity and antidiabetic activity. *Mol Endocrinol* **16**, 2628-2644, (2002).

253 Yamauchi, T. *et al.* Inhibition of RXR and PPARgamma ameliorates diet-induced obesity and type 2 diabetes. *J Clin Invest* **108**, 1001-1013, (2001).

254 Medina-Gomez, G. *et al.* PPAR gamma 2 prevents lipotoxicity by controlling adipose tissue expandability and peripheral lipid metabolism. *PLoS Genet* **3**, e64, (2007).

255 Chawla, A. *et al.* A PPAR gamma-LXR-ABCA1 pathway in macrophages is involved in cholesterol efflux and atherogenesis. *Mol Cell* **7**, 161-171, (2001).

256 Escher, P. *et al.* Rat PPARs: quantitative analysis in adult rat tissues and regulation in fasting and refeeding. *Endocrinology* **142**, 4195-4202, (2001).

257 Berger, J. & Moller, D. E. The mechanisms of action of PPARs. *Annu Rev Med* **53**, 409-435, (2002).

258 Fajas, L. *et al.* The organization, promoter analysis, and expression of the human PPARgamma gene. *J Biol Chem* **272**, 18779-18789, (1997).

259 Meirhaeghe, A. *et al.* Characterization of the human, mouse and rat PGC1 beta (peroxisome-proliferator-activated receptor-gamma co-activator 1 beta) gene in vitro and in vivo. *Biochem J* **373**, 155-165, (2003).

260 Meirhaeghe, A. *et al.* A functional polymorphism in a STAT5B site of the human PPAR gamma 3 gene promoter affects height and lipid metabolism in a French population. *Arteriosclerosis, thrombosis, and vascular biology* **23**, 289-294, (2003).

261 Mueller, E. *et al.* Genetic analysis of adipogenesis through peroxisome proliferator-activated receptor gamma isoforms. *J Biol Chem* **277**, 41925-41930, (2002).

262 Zhang, J. *et al.* Selective disruption of PPARgamma 2 impairs the development of adipose tissue and insulin sensitivity. *Proc Natl Acad Sci U S A* **101**, 10703-10708, (2004).

263 McInerney, E. M. *et al.* Determinants of coactivator LXXLL motif specificity in nuclear receptor transcriptional activation. *Genes Dev* **12**, 3357-3368, (1998).

264 Gampe, R. T., Jr. *et al.* Asymmetry in the PPARgamma/RXRalpha crystal structure reveals the molecular basis of heterodimerization among nuclear receptors. *Mol Cell* **5**, 545-555, (2000).

265 Kallenberger, B. C., Love, J. D., Chatterjee, V. K. & Schwabe, J. W. A dynamic mechanism of nuclear receptor activation and its perturbation in a human disease. *Nature structural biology* **10**, 136-140, (2003).

266 Yu, C. *et al.* The nuclear receptor corepressors NCoR and SMRT decrease peroxisome proliferator-activated receptor gamma transcriptional activity and repress 3T3-L1 adipogenesis. *J Biol Chem* **280**, 13600-13605, (2005).

267 Fajas, L. *et al.* The retinoblastoma-histone deacetylase 3 complex inhibits PPARgamma and adipocyte differentiation. *Developmental cell* **3**, 903-910, (2002).

268 Soukas, A., Socci, N. D., Saatkamp, B. D., Novelli, S. & Friedman, J. M. Distinct transcriptional profiles of adipogenesis in vivo and in vitro. *J Biol Chem* **276**, 34167-34174, (2001).

269 Chen, Z., Torrens, J. I., Anand, A., Spiegelman, B. M. & Friedman, J. M. Krox20 stimulates adipogenesis via C/EBPbeta-dependent and -independent mechanisms. *Cell Metab* **1**, 93-106, (2005).

270 Oishi, Y. *et al.* Kruppel-like transcription factor KLF5 is a key regulator of adipocyte differentiation. *Cell Metab* **1**, 27-39, (2005).

271 Kim, J. B. *et al.* Nutritional and insulin regulation of fatty acid synthetase and leptin gene expression through ADD1/SREBP1. *J Clin Invest* **101**, 1-9, (1998).

272 Kim, J. B. & Spiegelman, B. M. ADD1/SREBP1 promotes adipocyte differentiation and gene expression linked to fatty acid metabolism. *Genes Dev* **10**, 1096-1107, (1996).

273 Fajas, L. *et al.* Regulation of peroxisome proliferator-activated receptor gamma expression by adipocyte differentiation and determination factor 1/sterol regulatory element binding protein 1: implications for adipocyte differentiation and metabolism. *Mol Cell Biol* **19**, 5495-5503, (1999).

274 Kim, J. B., Wright, H. M., Wright, M. & Spiegelman, B. M. ADD1/SREBP1 activates PPARgamma through the production of endogenous ligand. *Proc Natl Acad Sci U S A* **95**, 4333-4337, (1998).

275 Cristancho, A. G. & Lazar, M. A. Forming functional fat: a growing understanding of adipocyte differentiation. *Nat Rev Mol Cell Biol* **12**, 722-734, (2011).

276 Siersbaek, R., Nielsen, R. & Mandrup, S. Transcriptional networks and chromatin remodeling controlling adipogenesis. *Trends Endocrinol Metab* **23**, 56-64, (2012).

277 Steger, D. J. & Lazar, M. A. Adipogenic hotspots: where the action is. *Embo J* **30**, 1418-1419, (2011).

278 Bai, P. & Canto, C. The role of PARP-1 and PARP-2 enzymes in metabolic regulation and disease. *Cell Metab* **16**, 290-295, (2012).

279 Asher, G. *et al.* Poly(ADP-ribose) polymerase 1 participates in the phase entrainment of circadian clocks to feeding. *Cell* **142**, 943-953, (2010).
280 Bai, P. *et al.* PARP-1 inhibition increases mitochondrial metabolism through SIRT1 activation. *Cell Metab* **13**, 461-468, (2011).
281 Devalaraja-Narashimha, K. & Padanilam, B. J. PARP1 deficiency exacerbates diet-induced obesity in mice. *The Journal of endocrinology* **205**, 243-252, (2010).
282 Bai, P. *et al.* PARP-2 regulates SIRT1 expression and whole-body energy expenditure. *Cell Metab* **13**, 450-460, (2011).
283 Bai, P. *et al.* Poly(ADP-ribose) polymerase-2 [corrected] controls adipocyte differentiation and adipose tissue function through the regulation of the activity of the retinoid X receptor/peroxisome proliferator-activated receptor-gamma [corrected] heterodimer. *J Biol Chem* **282**, 37738-37746, (2007).
284 Mangerich, A. *et al.* Inflammatory and age-related pathologies in mice with ectopic expression of human PARP-1. *Mechanisms of ageing and development* **131**, 389-404, (2010).
285 Fujiki, K. *et al.* PPARgamma-induced PARylation promotes local DNA demethylation by production of 5-hydroxymethylcytosine. *Nat Commun* **4**, 2262, (2013).
286 Berglund, E. D. *et al.* Glucose metabolism in vivo in four commonly used inbred mouse strains. *Diabetes* **57**, 1790-1799, (2008).
287 Wahlberg, E. *et al.* Family-wide chemical profiling and structural analysis of PARP and tankyrase inhibitors. *Nat Biotechnol* **30**, 283-288, (2012).
288 Lai, J. S. & Herr, W. Ethidium bromide provides a simple tool for identifying genuine DNA-independent protein associations. *Proc Natl Acad Sci U S A* **89**, 6958-6962, (1992).
289 Reinhardt, C. G. & Krugh, T. R. A comparative study of ethidium bromide complexes with dinucleotides and DNA: direct evidence for intercalation and nucleic acid sequence preferences. *Biochemistry* **17**, 4845-4854, (1978).
290 Fakan, S., Leduc, Y., Lamarre, D., Brunet, G. & Poirier, G. G. Immunoelectron microscopical distribution of poly(ADP-ribose)polymerase in the mammalian cell nucleus. *Exp Cell Res* **179**, 517-526, (1988).
291 Guetg, C., Scheifele, F., Rosenthal, F., Hottiger, M. O. & Santoro, R. Inheritance of silent rDNA chromatin is mediated by PARP1 via noncoding RNA. *Mol Cell* **45**, 790-800, (2012).
292 Parent, M. *et al.* Poly(ADP-ribose) polymerase-1 is a negative regulator of HIV-1 transcription through competitive binding to TAR RNA with Tat.positive transcription elongation factor b (p-TEFb) complex. *J Biol Chem* **280**, 448-457, (2005).
293 Huambachano, O., Herrera, F., Rancourt, A. & Satoh, M. S. Double-stranded DNA binding domain of poly(ADP-ribose) polymerase-1 and molecular insight into the regulation of its activity. *J Biol Chem* **286**, 7149-7160, (2011).
294 Schibler, U. & Sassone-Corsi, P. A web of circadian pacemakers. *Cell* **111**, 919-922, (2002).
295 Balsalobre, A., Damiola, F. & Schibler, U. A serum shock induces circadian gene expression in mammalian tissue culture cells. *Cell* **93**, 929-937, (1998).
296 Damiola, F. *et al.* Restricted feeding uncouples circadian oscillators in peripheral tissues from the central pacemaker in the suprachiasmatic nucleus. *Genes Dev* **14**, 2950-2961, (2000).
297 Hamada, T., LeSauter, J., Venuti, J. M. & Silver, R. Expression of Period genes: rhythmic and nonrhythmic compartments of the suprachiasmatic nucleus pacemaker. *J Neurosci* **21**, 7742-7750, (2001).
298 Jagota, A., de la Iglesia, H. O. & Schwartz, W. J. Morning and evening circadian oscillations in the suprachiasmatic nucleus in vitro. *Nat Neurosci* **3**, 372-376, (2000).
299 Low-Zeddies, S. S. & Takahashi, J. S. Chimera analysis of the Clock mutation in mice shows that complex cellular integration determines circadian behavior. *Cell* **105**, 25-42, (2001).
300 Stokkan, K. A., Yamazaki, S., Tei, H., Sakaki, Y. & Menaker, M. Entrainment of the circadian clock in the liver by feeding. *Science* **291**, 490-493, (2001).
301 Welsh, D. K., Logothetis, D. E., Meister, M. & Reppert, S. M. Individual neurons dissociated from rat suprachiasmatic nucleus express independently phased circadian firing rhythms. *Neuron* **14**, 697-706, (1995).
302 Yamazaki, S. *et al.* Resetting central and peripheral circadian oscillators in transgenic rats. *Science* **288**, 682-685, (2000).
303 Zylka, M. J., Shearman, L. P., Weaver, D. R. & Reppert, S. M. Three period homologs in mammals: differential light responses in the suprachiasmatic circadian clock and oscillating transcripts outside of brain. *Neuron* **20**, 1103-1110, (1998).
304 Reppert, S. M. & Weaver, D. R. Coordination of circadian timing in mammals. *Nature* **418**, 935-941, (2002).

305 Yagita, K., Tamanini, F., van Der Horst, G. T. & Okamura, H. Molecular mechanisms of the biological clock in cultured fibroblasts. *Science* **292**, 278-281, (2001).

306 Gekakis, N. *et al.* Role of the CLOCK protein in the mammalian circadian mechanism. *Science* **280**, 1564-1569, (1998).

307 King, D. P. *et al.* Positional cloning of the mouse circadian clock gene. *Cell* **89**, 641-653, (1997).

308 Hogenesch, J. B., Gu, Y. Z., Jain, S. & Bradfield, C. A. The basic-helix-loop-helix-PAS orphan MOP3 forms transcriptionally active complexes with circadian and hypoxia factors. *Proc Natl Acad Sci U S A* **95**, 5474-5479, (1998).

309 Bunger, M. K. *et al.* Mop3 is an essential component of the master circadian pacemaker in mammals. *Cell* **103**, 1009-1017, (2000).

310 Kume, K. *et al.* mCRY1 and mCRY2 are essential components of the negative limb of the circadian clock feedback loop. *Cell* **98**, 193-205, (1999).

311 Vitaterna, M. H. *et al.* Differential regulation of mammalian period genes and circadian rhythmicity by cryptochromes 1 and 2. *Proc Natl Acad Sci U S A* **96**, 12114-12119, (1999).

312 Okamura, H. *et al.* Photic induction of mPer1 and mPer2 in cry-deficient mice lacking a biological clock. *Science* **286**, 2531-2534, (1999).

313 Shearman, L. P., Jin, X., Lee, C., Reppert, S. M. & Weaver, D. R. Targeted disruption of the mPer3 gene: subtle effects on circadian clock function. *Mol Cell Biol* **20**, 6269-6275, (2000).

314 Shearman, L. P. *et al.* Interacting molecular loops in the mammalian circadian clock. *Science* **288**, 1013-1019, (2000).

315 Oishi, K., Fukui, H. & Ishida, N. Rhythmic expression of BMAL1 mRNA is altered in Clock mutant mice: differential regulation in the suprachiasmatic nucleus and peripheral tissues. *Biochem Biophys Res Commun* **268**, 164-171, (2000).

316 Preitner, N. *et al.* The orphan nuclear receptor REV-ERBalpha controls circadian transcription within the positive limb of the mammalian circadian oscillator. *Cell* **110**, 251-260, (2002).

317 Ueda, H. R. *et al.* A transcription factor response element for gene expression during circadian night. *Nature* **418**, 534-539, (2002).

318 Yu, W., Nomura, M. & Ikeda, M. Interactivating feedback loops within the mammalian clock: BMAL1 is negatively autoregulated and upregulated by CRY1, CRY2, and PER2. *Biochem Biophys Res Commun* **290**, 933-941, (2002).

319 Bunney, W. E. & Bunney, B. G. Molecular clock genes in man and lower animals: possible implications for circadian abnormalities in depression. *Neuropsychopharmacology* **22**, 335-345, (2000).

320 Dantzer, R. & Kelley, K. W. Twenty years of research on cytokine-induced sickness behavior. *Brain Behav Immun* **21**, 153-160, (2007).

321 Taraborrelli, C. *et al.* TNFR1 is essential for CD40, but not for lipopolysaccharide-induced sickness behavior and clock gene dysregulation. *Brain Behav Immun* **25**, 434-442, (2011).

322 Danese, S., Sans, M. & Fiocchi, C. The CD40/CD40L costimulatory pathway in inflammatory bowel disease. *Gut* **53**, 1035-1043, (2004).

323 Elgueta, R. *et al.* Molecular mechanism and function of CD40/CD40L engagement in the immune system. *Immunol Rev* **229**, 152-172, (2009).

324 Grewal, I. S. & Flavell, R. A. CD40 and CD154 in cell-mediated immunity. *Annu Rev Immunol* **16**, 111-135, (1998).

325 Cavadini, G. *et al.* TNF-alpha suppresses the expression of clock genes by interfering with E-box-mediated transcription. *Proc Natl Acad Sci U S A* **104**, 12843-12848, (2007).

326 Okada, K. *et al.* Injection of LPS causes transient suppression of biological clock genes in rats. *J Surg Res* **145**, 5-12, (2008).

327 Morf, J. *et al.* Cold-inducible RNA-binding protein modulates circadian gene expression posttranscriptionally. *Science* **338**, 379-383, (2012).

328 Liu, Y. *et al.* Cold-induced RNA-binding proteins regulate circadian gene expression by controlling alternative polyadenylation. *Sci Rep* **3**, 2054, (2013).

329 Fujita, J. Cold shock response in mammalian cells. *J Mol Microbiol Biotechnol* **1**, 243-255, (1999).

330 Hasmann, M. & Schemainda, I. FK866, a highly specific noncompetitive inhibitor of nicotinamide phosphoribosyltransferase, represents a novel mechanism for induction of tumor cell apoptosis. *Cancer Res* **63**, 7436-7442, (2003).

331 Malanga, M., Bachmann, S., Panzeter, P. L., Zweifel, B. & Althaus, F. R. Poly(ADP-ribose) quantification at the femtomole level in mammalian cells. *Anal Biochem* **228**, 245-251, (1995).

332 Erener, S., Hesse, M., Kostadinova, R. & Hottiger, M. O. Poly(ADP-ribose)polymerase-1 (PARP1) controls adipogenic gene expression and adipocyte function. *Mol Endocrinol* **26**, 79-86, (2012).

333 Erener, S. *et al.* ARTD1 deletion causes increased hepatic lipid accumulation in mice fed a high-fat diet and impairs adipocyte function and differentiation. *Faseb J* **26**, 2631-2638, (2012).

334 Sugii, S. & Evans, R. M. Epigenetic codes of PPARgamma in metabolic disease. *FEBS Lett* **585**, 2121-2128, (2011).

335 Fujiki, K., Kano, F., Shiota, K. & Murata, M. Expression of the peroxisome proliferator activated receptor gamma gene is repressed by DNA methylation in visceral adipose tissue of mouse models of diabetes. *BMC Biol* **7**, 38, (2009).

336 Noer, A., Sorensen, A. L., Boquest, A. C. & Collas, P. Stable CpG hypomethylation of adipogenic promoters in freshly isolated, cultured, and differentiated mesenchymal stem cells from adipose tissue. *Mol Biol Cell* **17**, 3543-3556, (2006).

337 Bastos Sales, L. *et al.* Effects of endocrine disrupting chemicals on in vitro global DNA methylation and adipocyte differentiation. *Toxicol In Vitro* **27**, 1634-1643, (2013).

338 Booth, M. J. *et al.* Quantitative sequencing of 5-methylcytosine and 5-hydroxymethylcytosine at single-base resolution. *Science* **336**, 934-937, (2012).

339 Weber, M. *et al.* Chromosome-wide and promoter-specific analyses identify sites of differential DNA methylation in normal and transformed human cells. *Nat Genet* **37**, 853-862, (2005).

340 Williams, K. *et al.* TET1 and hydroxymethylcytosine in transcription and DNA methylation fidelity. *Nature* **473**, 343-348, (2011).

341 Ficz, G. *et al.* Dynamic regulation of 5-hydroxymethylcytosine in mouse ES cells and during differentiation. *Nature* **473**, 398-402, (2011).

342 Serandour, A. A. *et al.* Dynamic hydroxymethylation of deoxyribonucleic acid marks differentiation-associated enhancers. *Nucleic Acids Res* **40**, 8255-8265, (2012).

343 Ziouzenkova, O. *et al.* Dual roles for lipolysis and oxidation in peroxisome proliferation-activator receptor responses to electronegative low density lipoprotein. *J Biol Chem* **278**, 39874-39881, (2003).

344 Ziouzenkova, O. *et al.* Lipolysis of triglyceride-rich lipoproteins generates PPAR ligands: evidence for an antiinflammatory role for lipoprotein lipase. *Proc Natl Acad Sci U S A* **100**, 2730-2735, (2003).

345 Chakravarthy, M. V. *et al.* "New" hepatic fat activates PPARalpha to maintain glucose, lipid, and cholesterol homeostasis. *Cell Metab* **1**, 309-322, (2005).

346 Kelly, L. J. *et al.* Peroxisome proliferator-activated receptors gamma and alpha mediate in vivo regulation of uncoupling protein (UCP-1, UCP-2, UCP-3) gene expression. *Endocrinology* **139**, 4920-4927, (1998).

347 Straus, D. S. & Glass, C. K. Anti-inflammatory actions of PPAR ligands: new insights on cellular and molecular mechanisms. *Trends Immunol* **28**, 551-558, (2007).

348 Lovett-Racke, A. E. *et al.* Peroxisome proliferator-activated receptor alpha agonists as therapy for autoimmune disease. *J Immunol* **172**, 5790-5798, (2004).

349 Dubuquoy, L. *et al.* PPARgamma as a new therapeutic target in inflammatory bowel diseases. *Gut* **55**, 1341-1349, (2006).

350 Cuzzocrea, S. *et al.* Role of endogenous and exogenous ligands for the peroxisome proliferators activated receptors alpha (PPAR-alpha) in the development of inflammatory bowel disease in mice. *Lab Invest* **84**, 1643-1654, (2004).

351 Lee, K. S. *et al.* Modulation of airway remodeling and airway inflammation by peroxisome proliferator-activated receptor gamma in a murine model of toluene diisocyanate-induced asthma. *J Immunol* **177**, 5248-5257, (2006).

352 Kim, S. H. *et al.* Epigallocatechin-3-gallate protects toluene diisocyanate-induced airway inflammation in a murine model of asthma. *FEBS Lett* **580**, 1883-1890, (2006).

353 Belvisi, M. G., Hele, D. J. & Birrell, M. A. Peroxisome proliferator-activated receptor gamma agonists as therapy for chronic airway inflammation. *Eur J Pharmacol* **533**, 101-109, (2006).

354 Delayre-Orthez, C. *et al.* PPARalpha downregulates airway inflammation induced by lipopolysaccharide in the mouse. *Respir Res* **6**, 91, (2005).

355 Cuzzocrea, S. *et al.* Reduction in the evolution of murine type II collagen-induced arthritis by treatment with rosiglitazone, a ligand of the peroxisome proliferator-activated receptor gamma. *Arthritis Rheum* **48**, 3544-3556, (2003).

356 Shiojiri, T. *et al.* PPAR gamma ligands inhibit nitrotyrosine formation and inflammatory mediator expressions in adjuvant-induced rheumatoid arthritis mice. *Eur J Pharmacol* **448**, 231-238, (2002).

357 Okamoto, H. *et al.* Inhibition of NF-kappaB signaling by fenofibrate, a peroxisome proliferator-activated receptor-alpha ligand, presents a therapeutic strategy for rheumatoid arthritis. *Clin Exp Rheumatol* **23**, 323-330, (2005).

358 Cuzzocrea, S. *et al.* Rosiglitazone, a ligand of the peroxisome proliferator-activated receptor-gamma, reduces acute inflammation. *Eur J Pharmacol* **483**, 79-93, (2004).

359 Lo Verme, J. *et al.* The nuclear receptor peroxisome proliferator-activated receptor-alpha mediates the anti-inflammatory actions of palmitoylethanolamide. *Mol Pharmacol* **67**, 15-19, (2005).

360 Oliveira, A. C. *et al.* Antinociceptive and antiedematogenic activities of fenofibrate, an agonist of PPAR alpha, and pioglitazone, an agonist of PPAR gamma. *Eur J Pharmacol* **561**, 194-201, (2007).

361 Ivashchenko, C. Y., Duan, S. Z., Usher, M. G. & Mortensen, R. M. PPAR-gamma knockout in pancreatic epithelial cells abolishes the inhibitory effect of rosiglitazone on caerulein-induced acute pancreatitis. *Am J Physiol Gastrointest Liver Physiol* **293**, G319-326, (2007).

362 Gervois, P. *et al.* Global suppression of IL-6-induced acute phase response gene expression after chronic in vivo treatment with the peroxisome proliferator-activated receptor-alpha activator fenofibrate. *J Biol Chem* **279**, 16154-16160, (2004).

363 Kersten, S., Desvergne, B. & Wahli, W. Roles of PPARs in health and disease. *Nature* **405**, 421-424, (2000).

364 Desreumaux, P. *et al.* Attenuation of colon inflammation through activators of the retinoid X receptor (RXR)/peroxisome proliferator-activated receptor gamma (PPARgamma) heterodimer. A basis for new therapeutic strategies. *J Exp Med* **193**, 827-838, (2001).

365 Shah, Y. M., Morimura, K. & Gonzalez, F. J. Expression of peroxisome proliferator-activated receptor-gamma in macrophage suppresses experimentally induced colitis. *Am J Physiol Gastrointest Liver Physiol* **292**, G657-666, (2007).

366 Adachi, M. *et al.* Peroxisome proliferator activated receptor gamma in colonic epithelial cells protects against experimental inflammatory bowel disease. *Gut* **55**, 1104-1113, (2006).

367 Rossi, A. *et al.* Anti-inflammatory cyclopentenone prostaglandins are direct inhibitors of IkappaB kinase. *Nature* **403**, 103-108, (2000).

368 Straus, D. S. *et al.* 15-deoxy-delta 12,14-prostaglandin J2 inhibits multiple steps in the NF-kappa B signaling pathway. *Proc Natl Acad Sci U S A* **97**, 4844-4849, (2000).

369 Ray, D. M., Akbiyik, F. & Phipps, R. P. The peroxisome proliferator-activated receptor gamma (PPARgamma) ligands 15-deoxy-Delta12,14-prostaglandin J2 and ciglitazone induce human B lymphocyte and B cell lymphoma apoptosis by PPARgamma-independent mechanisms. *J Immunol* **177**, 5068-5076, (2006).

370 Soller, M., Drose, S., Brandt, U., Brune, B. & von Knethen, A. Mechanism of thiazolidinedione-dependent cell death in Jurkat T cells. *Mol Pharmacol* **71**, 1535-1544, (2007).

371 Pascual, G. & Glass, C. K. Nuclear receptors versus inflammation: mechanisms of transrepression. *Trends Endocrinol Metab* **17**, 321-327, (2006).

372 Pascual, G. *et al.* A SUMOylation-dependent pathway mediates transrepression of inflammatory response genes by PPAR-gamma. *Nature* **437**, 759-763, (2005).

373 Kouzarides, T. Chromatin modifications and their function. *Cell* **128**, 693-705, (2007).

374 Hottiger, M. O. ADP-ribosylation of histones by ARTD1: An additional module of the histone code? *FEBS Lett* **585**, 1595-1599, (2011).

375 Kassner, I., Barandun, M., Fey, M., Rosenthal, F. & Hottiger, M. O. Crosstalk between SET7/9-dependent methylation and ARTD1-mediated ADP-ribosylation of histone H1.4. *Epigenetics Chromatin* **6**, 1, (2013).

376 Szabo, C. *et al.* Inhibition of poly (ADP-ribose) synthetase attenuates neutrophil recruitment and exerts antiinflammatory effects. *J Exp Med* **186**, 1041-1049, (1997).

377 Satoh, H., Sato, F., Takami, K. & Szabo, S. New ulcerative colitis model induced by sulfhydryl blockers in rats and the effects of antiinflammatory drugs on the colitis. *Jpn J Pharmacol* **73**, 299-309, (1997).

378 Liaudet, L. *et al.* Activation of poly(ADP-Ribose) polymerase-1 is a central mechanism of lipopolysaccharide-induced acute lung inflammation. *Am J Respir Crit Care Med* **165**, 372-377, (2002).

379 Mabley, J. G. *et al.* Anti-inflammatory effects of a novel, potent inhibitor of poly (ADP-ribose) polymerase. *Inflamm Res* **50**, 561-569, (2001).
380 Soriano, F. G., Pacher, P., Mabley, J., Liaudet, L. & Szabo, C. Rapid reversal of the diabetic endothelial dysfunction by pharmacological inhibition of poly(ADP-ribose) polymerase. *Circ Res* **89**, 684-691, (2001).
381 Szabo, C., Cuzzocrea, S., Zingarelli, B., O'Connor, M. & Salzman, A. L. Endothelial dysfunction in a rat model of endotoxic shock. Importance of the activation of poly (ADP-ribose) synthetase by peroxynitrite. *J Clin Invest* **100**, 723-735, (1997).
382 Ha, H. C., Hester, L. D. & Snyder, S. H. Poly(ADP-ribose) polymerase-1 dependence of stress-induced transcription factors and associated gene expression in glia. *Proc Natl Acad Sci U S A* **99**, 3270-3275, (2002).
383 Cuzzocrea, S. *et al.* Effects of 5-aminoisoquinolinone, a water-soluble, potent inhibitor of the activity of poly (ADP-ribose) polymerase, in a rodent model of lung injury. *Biochem Pharmacol* **63**, 293-304, (2002).
384 Chang, W. J. & Alvarez-Gonzalez, R. The sequence-specific DNA binding of NF-kappa B is reversibly regulated by the automodification reaction of poly (ADP-ribose) polymerase 1. *J Biol Chem* **276**, 47664-47670, (2001).
385 Kameoka, M. *et al.* Evidence for regulation of NF-kappaB by poly(ADP-ribose) polymerase. *Biochem J* **346 Pt 3**, 641-649, (2000).
386 Soriano, F. G., Virag, L. & Szabo, C. Diabetic endothelial dysfunction: role of reactive oxygen and nitrogen species production and poly(ADP-ribose) polymerase activation. *J Mol Med (Berl)* **79**, 437-448, (2001).
387 Anderson, M. G., Scoggin, K. E., Simbulan-Rosenthal, C. M. & Steadman, J. A. Identification of poly(ADP-ribose) polymerase as a transcriptional coactivator of the human T-cell leukemia virus type 1 Tax protein. *J Virol* **74**, 2169-2177, (2000).
388 Cervellera, M. N. & Sala, A. Poly(ADP-ribose) polymerase is a B-MYB coactivator. *J Biol Chem* **275**, 10692-10696, (2000).
389 Nie, J. *et al.* Interaction of Oct-1 and automodification domain of poly(ADP-ribose) synthetase. *FEBS Lett* **424**, 27-32, (1998).
390 Hassa, P. O. & Hottiger, M. O. The functional role of poly(ADP-ribose)polymerase 1 as novel coactivator of NF-κB in inflammatory disorders. *Cell Mol Life Sci* **59**, 1534-1553, (2002).
391 Butler, A. J. & Ordahl, C. P. Poly(ADP-ribose) polymerase binds with transcription enhancer factor 1 to MCAT1 elements to regulate muscle-specific transcription. *Mol Cell Biol* **19**, 296-306, (1999).
392 Miyamoto, T., Kakizawa, T. & Hashizume, K. Inhibition of nuclear receptor signalling by poly(ADP-ribose) polymerase. *Mol Cell Biol* **19**, 2644-2649, (1999).
393 Soldatenkov, V. A. *et al.* Transcriptional repression by binding of poly(ADP-ribose) polymerase to promoter sequences. *J Biol Chem* **277**, 665-670, (2002).
394 Tontonoz, P., Nagy, L., Alvarez, J. G., Thomazy, V. A. & Evans, R. M. PPARgamma promotes monocyte/macrophage differentiation and uptake of oxidized LDL. *Cell* **93**, 241-252, (1998).
395 Ricote, M., Li, A. C., Willson, T. M., Kelly, C. J. & Glass, C. K. The peroxisome proliferator-activated receptor-gamma is a negative regulator of macrophage activation. *Nature* **391**, 79-82, (1998).
396 Pieper, A. A. *et al.* Poly(ADP-ribose) polymerase-deficient mice are protected from streptozotocin-induced diabetes. *Proc Natl Acad Sci U S A* **96**, 3059-3064, (1999).
397 Rerup, C. C. Drugs producing diabetes through damage of the insulin secreting cells. *Pharmacol Rev* **22**, 485-518, (1970).
398 Szabo, C., Biser, A., Benko, R., Bottinger, E. & Susztak, K. Poly(ADP-ribose) polymerase inhibitors ameliorate nephropathy of type 2 diabetic Leprdb/db mice. *Diabetes* **55**, 3004-3012, (2006).
399 Zelezniak, A., Pers, T. H., Soares, S., Patti, M. E. & Patil, K. R. Metabolic network topology reveals transcriptional regulatory signatures of type 2 diabetes. *PLoS Comput Biol* **6**, e1000729, (2010).
400 Lindgren, A. E. *et al.* PARP inhibitor with selectivity toward ADP-ribosyltransferase ARTD3/PARP3. *ACS Chem Biol* **8**, 1698-1703, (2013).
401 Kinoshita, T. *et al.* Inhibitor-induced structural change of the active site of human poly(ADP-ribose) polymerase. *FEBS Lett* **556**, 43-46, (2004).
402 Lehtio, L. *et al.* Structural basis for inhibitor specificity in human poly(ADP-ribose) polymerase-3. *J Med Chem* **52**, 3108-3111, (2009).

403 Oliver, A. W. *et al.* Crystal structure of the catalytic fragment of murine poly(ADP-ribose) polymerase-2. *Nucleic Acids Res* **32**, 456-464, (2004).
404 Ruf, A., Mennissier de Murcia, J., de Murcia, G. & Schulz, G. E. Structure of the catalytic fragment of poly(AD-ribose) polymerase from chicken. *Proc Natl Acad Sci U S A* **93**, 7481-7485, (1996).
405 Kleine, H. *et al.* Substrate-assisted catalysis by PARP10 limits its activity to mono-ADP-ribosylation. *Mol Cell* **32**, 57-69, (2008).
406 Ewing, R. M. *et al.* Large-scale mapping of human protein-protein interactions by mass spectrometry. *Mol Syst Biol* **3**, 89, (2007).
407 van Attikum, H. & Gasser, S. M. Crosstalk between histone modifications during the DNA damage response. *Trends Cell Biol* **19**, 207-217, (2009).
408 Celeste, A. *et al.* Genomic instability in mice lacking histone H2AX. *Science* **296**, 922-927, (2002).
409 Kalocsay, M., Hiller, N. J. & Jentsch, S. Chromosome-wide Rad51 spreading and SUMO-H2A.Z-dependent chromosome fixation in response to a persistent DNA double-strand break. *Mol Cell* **33**, 335-343, (2009).
410 Papamichos-Chronakis, M., Krebs, J. E. & Peterson, C. L. Interplay between Ino80 and Swr1 chromatin remodeling enzymes regulates cell cycle checkpoint adaptation in response to DNA damage. *Genes Dev* **20**, 2437-2449, (2006).
411 Downs, J. A. *et al.* Binding of chromatin-modifying activities to phosphorylated histone H2A at DNA damage sites. *Mol Cell* **16**, 979-990, (2004).
412 Shall, S., Gaymes, T., Farzaneh, F., Curtin, N. & Mufti, G. J. The use of PARP inhibitors in cancer therapy: use as adjuvant with chemotherapy or radiotherapy; use as a single agent in susceptible patients; techniques used to identify susceptible patients. *Methods Mol Biol* **780**, 239-266, (2011).
413 Peralta-Leal, A. *et al.* PARP inhibitors: new partners in the therapy of cancer and inflammatory diseases. *Free Radic Biol Med* **47**, 13-26, (2009).
414 De Vos, M., Schreiber, V. & Dantzer, F. The diverse roles and clinical relevance of PARPs in DNA damage repair: current state of the art. *Biochem Pharmacol* **84**, 137-146, (2012).
415 Orlando, L. *et al.* Poly (ADP-ribose) polymerase (PARP): rationale, preclinical and clinical evidences of its inhibition as breast cancer treatment. *Expert Opin Ther Targets* **16 Suppl 2**, S83-89, (2012).
416 Graziani, G. & Szabo, C. Clinical perspectives of PARP inhibitors. *Pharmacol Res* **52**, 109-118, (2005).
417 Martin-Oliva, D. *et al.* Inhibition of poly(ADP-ribose) polymerase modulates tumor-related gene expression, including hypoxia-inducible factor-1 activation, during skin carcinogenesis. *Cancer Res* **66**, 5744-5756, (2006).
418 Pacher, P. & Szabo, C. Role of poly(ADP-ribose) polymerase 1 (PARP-1) in cardiovascular diseases: the therapeutic potential of PARP inhibitors. *Cardiovasc Drug Rev* **25**, 235-260, (2007).
419 Rajesh, M. *et al.* Pharmacological inhibition of poly(ADP-ribose) polymerase inhibits angiogenesis. *Biochem Biophys Res Commun* **350**, 352-357, (2006).
420 Rajesh, M. *et al.* Poly(ADP-ribose)polymerase inhibition decreases angiogenesis. *Biochem Biophys Res Commun* **350**, 1056-1062, (2006).

Curriculum Vitae

Personal information

Name:	LEHMANN
	(born Hesse)
Surname:	Mareike Katharina Gwendolyn
Address:	Kolbenacker 34, CH – 8052 Zürich
	Phone: +41-774252220
	Email: mareike.hesse@vetbio.uzh.ch
Date of birth:	20th of April 1986
Place of birth:	Siegburg, Germany
Nationality:	German

Education

July 2010 – present — Doctoral Studies in Molecular Biology

- Institute of Veterinary Biochemistry and Molecular Biology, University of Zurich, Switzerland
- Ph.D Program in Molecular Lifescience/LSZGS
- Thesis title: ARTD1 and Poly-ADP-Ribosylation Enhance PPARγ-Dependent Adipogenesis *In Vitro* and *In Vivo*

Oct. 2005 – June 2010 — Academic Studies

- University of Bonn, Germany
- Field of study: Molecular Biomedicine
- Degree: Diplom
- Title of diploma thesis: Identification and characterization of unconventional secretion of Protein Kinase A by microglial cells

Aug. 1996 – June 2005 — Secondary School

- Helmholtz-Gymnasium, Bonn, Germany
- Degree: Allgemeine Hochschulreife

Grants

July 2011	Forschungskredit der Universität Zürich, Ph.D salary for one year
August 2013	Travel reimbursement of the MLS Ph.D program for the Summer School on Nuclear Receptor Signalling in Physiology and Pathophysiology

List of Publications

Lindgren, A.E., Karlberg, T., Thorsell, A.G., **Hesse, M**., Spjut, S., Ekblad, T., Andersson, C.D., Pinto, A.F., Weigelt, J., Hottiger, M.O*., et al.* (2013). PARP inhibitor with selectivity toward ADP-ribosyltransferase ARTD3/PARP3. ACS chemical biology *8*, 1698-1703.

Erener, S., Mirsaidi, A., **Hesse, M**., Tiaden, A.N., Ellingsgaard, H., Kostadinova, R., Donath, M.Y., Richards, P.J., and Hottiger, M.O. (2012b). ARTD1 deletion causes increased hepatic lipid accumulation in mice fed a high-fat diet and impairs adipocyte function and differentiation. FASEB journal : official publication of the Federation of American Societies for Experimental Biology *26*, 2631-2638.

Erener, S., **Hesse, M**., Kostadinova, R., and Hottiger, M.O. (2012a). Poly(ADP-ribose)polymerase-1 (PARP1) controls adipogenic gene expression and adipocyte function. Mol Endocrinol *26*, 79-86.

Alejandre-Alcazar, M.A., Kwapiszewska, G., Reiss, I., Amarie, O.V., Marsh, L.M., Sevilla-Perez, J., Wygrecka, M., Eul, B., Kobrich, S., **Hesse, M**.*, et al.* (2007). Hyperoxia modulates TGF-beta/BMP signaling in a mouse model of bronchopulmonary dysplasia. American journal of physiology Lung cellular and molecular physiology *292*, L537-549.

Acknowledgements

First, I would like to thank Prof. Michael Hottiger for providing the opportunity to work on this project in his lab and for his constant support throughout my PhD. Thanks to Prof. Christian Wolfrum, Prof. Alex Hajnal and Prof. Chrisoph Handschin for valuable discussions and input during my committee meetings. Thanks to Prof. Anne Müller who agreed to participate in my thesis exam. A special thanks to Prof. Matthias Ziegler who agreed to read my thesis as external reviewer.

A special thanks goes to Florian Freimoser who helped with my thesis, my papers and much more and to my collaborators Thomas Birchler, Andreas Müller and Prof. Adriano Fontana from the University of Zürich, Matthias Rosenwald and Prof. Christian Wolfrum from the ETH Zürich, Ali Mirsaidi and PD Peter Richards from the University of Zürich and Eija Pirinen and Prof. Johan Auwerx from EPFL.

I would like to acknowledge all current and former members of the IVBMB and CABMM especially Prof. Ueli Hübscher, the head of our institute, who all helped by providing a very positive working atmosphere.

A special thanks goes to present and former members of the Hottiger group for scientific input and a lot of nice memories. I am grateful to have such good colleagues and friends next to me every day. Thanks to Flo for being my lab neighbor from the beginning and for your constant support. Thanks to Anneli, Giody, Flo and Roby for lab beers, Christmas songs and everything else.

Thanks to my best Zürich friends Dani, Ingrid, Julia, Karo and Roby for your friendship and uncountable nice memories. And of course thanks to my best Bonn friends Chrissi, Kathrin and Tina.

Words cannot tell how much I appreciate the constant love and support of my family, my parents, my sister and brother and my grandparents. I would not be where I am now if it wasn't for all of you.

And most importantly, thanks to Holger who made me feel at home here and who supported me whenever I needed it.